A characterization of the lipid biosynthetic interactome in *Saccharomyces cerevisiae*

by

Brianna L. Greenwood

A thesis submitted in partial fulfillment of the requirements for the degree of

Doctor of Philosophy

Department of Biochemistry

University of Alberta

Abstract

Lipids are integral components of all cells. Lipid molecules form the membrane and control membrane integrity while storage lipids act as a source of energy for the cell. The chemical properties of lipids are determined by the composition of the molecule's acyl chain moieties. Incorporation of unsaturated acyl chains into phospholipids destined for the membrane generates a more fluid membrane, while a more unsaturated acyl chain profile in storage lipids permits lipid droplet biogenesis from the endoplasmic reticulum. In *Saccharomyces cerevisiae*, acyl-CoA is desaturated by the sole ∆9-desaturase Ole1. Ole1 plays an important role in *S. cerevisiae*, as up to 80% of the acyl chains are unsaturated. However, unsaturated acyl-CoA is distributed unevenly within the cell. Certain phospholipids, like phosphatidylethanolamine and phosphatidylcholine, are enriched for unsaturated acyl chains, while other phospholipids like phosphatidylinositol contain more saturated moieties. This indicates that the unsaturated acyl-CoA generated by Ole1 is more available to specific lipid biosynthetic enzymes. The mechanism controlling this specificity has not yet been characterized, but interactions between enzymes in lipid biosynthesis have been identified in other organisms. We propose that interactions between Ole1 and lipid biosynthetic enzymes exist in *S. cerevisiae*, and that these interactions control the incorporation of unsaturated acyl chains into certain lipids and thus regulate the chemical properties of phospholipid and storage lipid. We present herein a set of coimmunoprecipitation and membrane yeast two-hybrid studies that identified novel protein-protein interactions between Ole1 and lipid biosynthetic enzymes. Interactions with the main lysophosphatidic acid acyltransferase in *S. cerevisiae*, Slc1, and the essential CDP-DAG synthase, Cds1, were also discovered, further determining

the composition of the complex we have called the desaturasome. We have more deeply characterized the interaction between Ole1 and the diacylglycerol acyltransferase Dga1 and performed functional studies that suggest a role for the Ole1-Dga1 interaction in control over lipid droplet formation. Finally, we present evidence for the contention that the interaction between Ole1 and Dga1 controls the subcellular localization of the acyltransferase. This research has revealed the composition of a lipid biosynthetic interaction network that may serve to control the incorporation of unsaturated acyl-CoA into phospholipid and storage lipid and thus regulate the membrane fluidity and generation of lipid droplets from the endoplasmic reticulum. Future work should aim to determine whether the composition of the desaturasome differs between subcellular compartments and if these interactions channel lipid. Investigating the role of this lipid synthesizing supercomplex may have implications in metabolic engineering and treatment of lipid dysregulatory disorders in humans.

Preface

This thesis is the original work performed by Brianna L. Greenwood (BLG) under the guidance of Dr. David Stuart (DTS). Jack Moore of the Alberta Proteomics and Mass Spectrometry Facility performed the mass spectrometry in Chapter 2 and provided the written procedure in 2.3.5. Dr. Marek Michalak provided the NMY51 strain used in Chapters 2 and 3, and Dr. Michael Schultz provided the Δ*dga1* strain utilized in Chapter 4. Plasmids used in Chapter 2 were generated by Daniel Huang (DH). The FAME analysis in Chapter 3 was performed by Audric Moses in the Lipidomics Core Facility of the Faculty of Medicine and Dentistry at the University of Alberta.

Chapter 3 was accepted for publication in the Journal of Biological Chemistry in May of 2023. BLG is the primary author and performed the experiments, analyzed the data, wrote the first draft, and edited the manuscript. Zijun Luo (ZL), Tareq Ahmed (TA), and DH generated plasmids for the study and obtained preliminary data. DTS designed the research and edited the manuscript. This manuscript has been adapted to fit the format of the thesis presented.

Acknowledgments

I have to acknowledge the incredible mentorship I have been given by Dr. David Stuart. I came to his lab in 2017 as a student, passionate about science and feeling out of my depth in a graduate program. Dave was patient, building my confidence in myself as a researcher and my critical thinking skills as a scientist. I know that I am graduating from this program as a competent scientist because of the support Dave has given me, and I can't thank him enough.

I want to acknowledge the support given to me by Dr. Bonnie McNeil and Dr. Anagha Krishnan. They not only took the time to show me around the lab and help me get settled but also listened to me when I needed to talk through confusing results or cloning issues. They set me up for success in the lab, and I want to thank them for that.

I thank all the members of the Stuart lab for their friendship over the years. Yuze, Karla, Laura, and Dr. Tabinda Shakeel – you have all made my tenure in the lab a joy. I appreciate each of you, and thank you for your help and input. I've had the honour of supervising some truly excellent undergraduate students over the years. Zijun, Tareq, and Daniel have all made significant contributions to my progress and are owed a huge debt of gratitude from me. Thank you all.

I want to acknowledge the graduate students who have kept me sane throughout my time here. I never would have made it this far without you all.

I owe a huge thank you to my family and friends. You all kept me grounded even when it felt like graduate school and research were taking over my life. Thank you for the company on long runs and the family dinners that fueled them.

I appreciate my committee members, Dr. Joanne Lemieux and Dr. Richard Fahlman, for your support and valuable input into my research plans. Thank you for taking the time out of your busy schedules to listen to my wild ideas and help me turn them into well constructed experiments.

Lastly, I have to acknowledge my partner Cameron. Thank you for listening to me ramble about results for hours on end. Thank you for giving me your input from the structural biology perspective. Thank you for supporting me and encouraging me to do big things, no matter how much they scare me. I owe this all to you. I love you.

Table of Contents

List of tables

Chapter 1

Chapter 2

Chapter 3

Chapter 4

List of figures

Chapter 1

Chapter 2

Chapter 3

Chapter 4

List of abbreviations

3-AT	3-aminotriazole
ACAT	acyl-CoA:cholesterol acyltransferase
Acc1	acetyl-CoA carboxylase
ACL	ATP citrate lyase
Ale1	lysophospholipid acyltransferase
APBS	Adaptive Poisson-Boltzmann Solver
Are1	acyl-CoA:sterol acyltransferase 1
Are2	acyl-CoA:sterol acyltransferase 2
CDP-DAG	cytidine diphosphate diacylglycerol
Cds1	phosphatidate cytidylyltransferase
cER	cortical endoplasmic reticulum
Cho1	CDP-DAG-serine O-phosphatidyltransferase
Cho2	phosphatidylethanolamine N-methyltransferase
CoA	coenzyme A
DAG	diacylglycerol
Dga1	acyl-CoA:diacylglycerol acyltransferase
DGAT	diacylglycerol acyltransferase
DHAP	dihydroxyacetone phosphate
DNA	deoxyribonucleic acid
DTT	dithiothreitol
EDTA	ethylenediaminetetraacetic acid
EGTA	ethylene glycol-bis(β-aminoethyl ether)-N,N,N',N'-tetraacetic acid
Elo1	fatty acid elongase 1
Elo2	fatty acid elongase 2
Elo3	very long chain fatty acid elongase
EMC	ER membrane protein complex
ER	endoplasmic reticulum
ERMES	ER-mitochondria encounter structure
FA	fatty acid
Faa1/4	fatty acyl-CoA synthetase
Fas1/2	fatty acid synthase
FFA	free fatty acid

G3P	glycerol-3-phosphate
GO	gene ontology
GPAT	glycerol-3-phosphate acyltransferase
Gpt2	G-3-P/DHAP acyltransferase
HMG-CoA	3-hydroxy-3-methylglutaryl coenzyme A
Hmg1	HMG-CoA reductase
HRP	horseradish peroxidase
iMYTH	integrated membrane yeast two hybrid
LB	lysogeny broth
LC-MS/MS	liquid chromatography tandem mass spectrometry
LD	lipid droplet
LPA	lysophosphatidic acid
LPAAT	lysophosphatidic acid acyltransferase
LPC	lysophosphatidylcholine
LPE	lysophosphatidylethanolamine
LPL	lysophospholipid
Lro1	phospholipid:diacylglycerol acyltransferase
MAM	mitochondria associated endoplasmic reticulum membrane
MCFA	medium chain fatty acid
MCS	membrane contact site
MDH	malate dehydrogenase
MDH	monodansylpentane, AUTODOT
ME	malic enzyme
MGAT	monoacylglycerol acyltransferase
mNG	mNeonGreen
MYTH	membrane yeast two hybrid
NADPH	nicotinamide adenine dinucleotide phosphate
nER	perinuclear/nuclear endoplasmic reticulum
NL	neutral lipid
OD	optical density
Ole1	stearoyl-CoA Δ9-desaturase
Opi3	phosphatidyl-*N*-methylethanolamine N-methyltransferase
PA	phosphatidic acid
Pah1	phosphatidate phosphatase

PAM	plasma membrane associated endoplasmic reticulum membrane
PC	phosphatidylcholine
PCR	polymerase chain reaction
PE	phosphatidylethanolamine
PEMT	phosphatidylethanolamine methyltransferase
PI	phosphatidylinositol
PIP	phosphatidylinositol phosphate
Pis1	CDP-DAG-inositol 3-phosphatidyltransferase
PL	phospholipid
pLDDT	per-residue confidence score
PM	plasma membrane
PMME	phosphatidyl-*N*-methylethanolamine
PMSF	phenylmethylsulfonyl fluoride
PPI	protein-protein interaction
PS	phosphatidylserine
Psd1	phosphatidylserine decarboxylase
Psd2	phosphatidylserine decarboxylase
PYC	pyruvate carboxylase
SCD	stearoyl-CoA Δ9-desaturase
Sct1	G-3-P/DHAP acyltransferase
SD	synthetic defined
SDS	sodium dodecyl sulfate
SDS-PAGE	sodium dodecyl sulfate-polyacrylamide gel electrophoresis
SE	steryl ester
SFA	saturated fatty acid
SL	storage lipid
Slc1	lysophosphatidic acid acyltransferase
TAG	triacylglycerol
Tris HCl	Tris hydrochloride
UFA	unsaturated fatty acid
VLCFA	very long chain fatty acid
YEPD	yeast extract peptone dextrose, complete yeast medium

Amino acid abbreviations

Ala, A	alanine
Arg, R	arginine
Asn, N	asparagine
Asp, D	aspartate
Cys, C	cysteine
Gln, Q	glutamine
Glu, E	glutamate
Gly, G	glycine
His, H	histidine
Ile, I	isoleucine
Leu, L	leucine
Lys, K	lysine
Met, M	methionine
Phe, F	phenylalanine
Pro, P	proline
Ser, S	serine
Thr, T	threonine
Trp, W	tryptophan
Tyr, Y	tyrosine
Val, V	valine

Chapter 1 – Spatial regulation of lipid synthesis in *Saccharomyces cerevisiae* to control lipidome composition

1.1. Introduction

Lipids are essential for membrane architecture and can be stored within lipid droplets as neutral storage lipid. There are eight classes of lipids in total; fatty acids (FA), glycerolipids, glycerophospholipids, sterol and sterol derivatives, sphingolipids, prenol lipids, glycolipids, and polyketides (1). The three major classes of lipids discussed here are the glycerophospholipids (PLs) found in membranes, the storage glycerolipid triacylglycerol (TAG), and sterols, which can either be found in the membrane or acylated and stored as steryl esters (SEs).

The metabolism of lipids is compartmentalized in eukaryotic organisms. While the cytoplasm is the main location of acyl-CoA synthesis, the modification of acyl chains and assembly into downstream lipids occurs primarily in the endoplasmic reticulum (ER) () (2). The mitochondria and Golgi apparatus also play important roles in the lipid biosynthetic process as the primary locations of cardiolipin and sphingolipid synthesis, two classes of lipids that will not be discussed here but have been reviewed (3, 4). The lipid droplet (LD), an ER-associated organelle, is the site of SE and TAG storage as well as a large amount of TAG synthesis (5). Peroxisomes in yeast are primarily catabolic organelles and are the main location of β-oxidation of FAs, specifically (6). To enable

proper subcellular communication, organelles contact each other via membrane contact sites (MCSs), which are often metabolically active and distinct (7).

The membranes that enclose cells and organelles display enrichment for distinct compositions of phospholipid head groups and degree of saturation of acyl chain tails. This variation in composition reflects the diverse functional requirements imposed on membranes from distinct cellular compartments. This specificity is also observed in the acyl chain saturation status and organization across phospholipid types. While some enzymes in lipid biosynthesis exhibit preference for distinct substrates, the precise composition of the lipidome, distinct compositions of specific cellular compartments, and ability to change in response to environmental and cellular demands cannot be entirely explained by this preference (8, 9). We posit that this phenomenon can be explained in part by interactions between lipid biosynthetic enzymes within certain subcellular compartments that channel lipid precursors to specific fates.

Table 1.1 Localization and phenotype of selected proteins of lipid synthesis.

Protein	Activity	Localization[a]	Phenotype[b]
Acc1	acetyl-CoA carboxylase	cytoplasm	E
Fas1/2	fatty acid synthase	cytoplasm	E
Faa1/4	fatty acyl-CoA synthetase	cytoplasm, LD	NE
Ole1	stearoyl-CoA Δ9-desaturase	ER	E
Elo1	fatty acid elongase	ER	NE
Elo2	fatty acid elongase	ER	SL (Elo3)
Elo3	very long chain fatty acid elongase	ER	SL (Elo2)
Gpt2	G-3-P/DHAP acyltransferase	ER, LD	SL (Sct1)
Sct1	G-3-P/DHAP acyltransferase	ER	SL (Gpt2)
Slc1	lysophosphatidic acid acyltransferase	ER, LD	SL (Ale1)
Ale1	lysophospholipid acyltransferase	ER	SL (Slc1)
Cds1	phosphatidate cytidylyltransferase	ER	E
Pis1	CDP-DAG-inositol 3-phosphatidyltransferase	ER, PAM	E
Cho1	CDP-DAG-serine O-phosphatidyltransferase	ER, MAM, PAM	NE (Etn/Cho auxotroph)
Psd1	phosphatidylserine decarboxylase	mitochondrial inner membrane	SL (Psd2)
Psd2	phosphatidylserine decarboxylase	*trans*-Golgi network, endosome	SL (Psd1)
Cho2	phosphatidylethanolamine N-methyltransferase	ER	NE
Opi3	phosphatidyl-N-methylethanolamine N-methyltransferase	ER	NE
Pah1	phosphatidate phosphatase	nucleus, cytosol, ER	NE
Lro1	phospholipid:diacylglycerol acyltransferase	ER	NE
Dga1	acyl-CoA:diacylglycerol acyltransferase	ER, LD	NE
Are1	acyl-CoA:sterol acyltransferase	ER	NE
Are2	acyl-CoA:sterol acyltransferase	ER	NE

[a] from Saccharomyces Genome Database and (10, 11). LD = lipid droplet, ER = endoplasmic reticulum, PAM = plasma membrane associated ER membrane, MAM = mitochondrial associated ER membrane.
[b] from Saccharomyces Genome Database. E = essential gene, SL = synthetically lethal gene, NE = nonessential gene

1.2. Lipid synthesis is compartmentalized

1.2.1. Acyl-CoA synthesis in the cytoplasm

Phospholipid, triacylglycerol, and sterol ester assembly all require activated fatty acids in the form of acyl-CoA. The *de novo* synthesis of these acyl chains is a complex cytosolic process involving the condensation of acetyl-CoA into chains, with lengths of 16 or 18 carbons being the most common. Briefly, acetyl-CoA is activated to malonyl-CoA by the cytosolic acetyl-CoA carboxylase Acc1 (12), which can then be elongated to saturated acyl-CoA by the fatty acid synthase complex composed of Fas1 and Fas2 (13). As the rate limiting step in FA synthesis, the acetyl-CoA carboxylation rate is under remarkable control by both genetic and biochemical means. Acc1 activity is controlled by regulation of mRNA and protein levels, phosphorylation of the protein, and inhibition from downstream products and substrates from other pathways (14–19). The control of carbon flux through lipid synthesis is also tightly regulated by the subcellular localization of FA synthetic machinery, as Acc1 and Fas1/2 are distributed widely throughout the cytoplasm under growth conditions, but relocate to distinct puncta upon glucose starvation (20). Acyl chains in yeast are primarily made *de novo*, though exogenous fatty acids can also be imported and converted to fatty acyl-CoA via acyl-CoA synthetases (21). The medium to long chain-acyl-CoA synthetases Faa1 and Faa4 are found within the cytosol, though their presence on LDs implicates the two in storage lipid synthesis and lipolysis (2, 22, 23). Faa2 is located on the peroxisome and activates medium chain FAs for peroxisomal β-oxidation, while Fat1 activates VLCFAs and is found both on the LD and peroxisome (2, 24–26). Faa3, meanwhile, is found primarily on the PM and generates long chain acyl-

CoAs (21, 27). The compartmentalization of these FA activating enzymes implies a preference for yeast to incorporate LCFAs and some VLCFAs into storage lipid, while directing MCFAs and some VLCFAs to degradation in the peroxisome. This sense of spatiotemporal control is not only seen in FA synthesis and regulation, but as will be discussed, in the downstream synthesis of lipids as well.

1.2.2. Acyl-CoA modification in the ER

De novo synthesized acyl chains are initially assembled with single carbon-carbon bonds as saturated C16 or C18 acyl-CoA in the cytoplasm but are further modified within the ER (Figure 1.1). A high proportion of these are channeled toward the only desaturase in *Saccharomyces cerevisiae*, Ole1, introducing Δ9 double bonds into acyl chains to create unsaturated acyl-CoA and impart distinct physical and chemical properties to lipids (28, 29). Ole1 is an integral ER membrane protein that acts as a homodimer (2, 30). The introduction of a *cis* double bond in the fatty acyl tail by the desaturase decreases the ability of the tail to pack as readily and thus increases the melting temperature of the acyl chain (31). Incorporation of these unsaturated chains into membrane and storage lipid affects the membrane fluidity of downstream phospholipids and glycerolipids (32–34). Elongation of myristoyl-CoA, palmitoyl-CoA, and palmitoleoyl-CoA by 2-4 carbons is also achieved in the ER by Elo1 (35, 36). Elo1 homologs Elo2 and Elo3 can elongate saturated acyl-CoA to C24 and C26 VLCFA destined for the production of sphingolipids (37). As chain length can also alter the fluidity of membrane phospholipids, there is an important role for the ER in determining membrane fluidity.

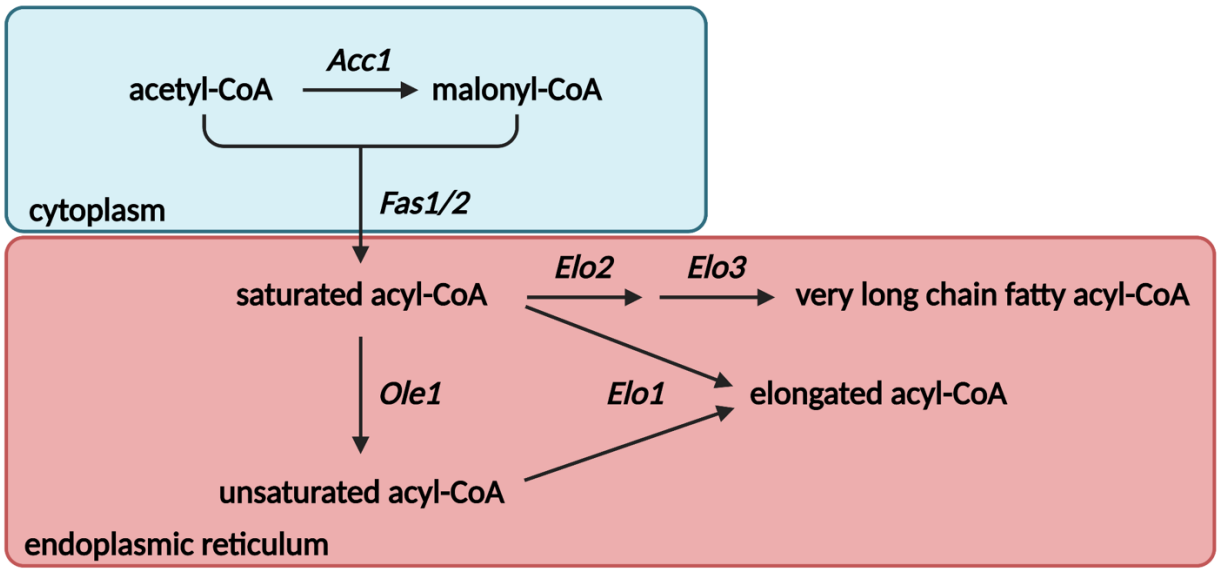

Figure 1.1 **Fatty acyl-CoA synthesis and modification in yeast.** Fatty acyl-CoA synthesis by Acc1 and Fas1/2 occurs in the cytoplasm, while elongation and desaturation of the molecules is accomplished in the ER by Elo1/2/3 and Ole1. Created with BioRender.com.

The saturation status of FAs in yeast is specific and tightly controlled. Over 75% of the cellular fatty acyl chains produced by *Saccharomyces cerevisiae* are unsaturated, demonstrating an important role for Ole1 (38–40). Palmitoleic acid (C16:1) is the most abundant FA produced in yeast, constituting approximately 40% of the FA species (37, 41). Approximately 35% of the FA is oleic acid (C18:1), the other main unsaturated FA produced by *S. cerevisiae* (37, 41). Palmitic acid (C16:0) is a low abundance fatty acid, comprising 15% of the FA species produced (37, 40). Though C18:1 is highly abundant in yeast membranes, stearic acid (C18:0) is relatively rare and makes up less than five percent of FA species (37, 40, 41). Short chain fatty acids (<14 carbons) and VLCFA are not abundant (38, 41). The fatty acid profile is primarily unsaturated across all stages of growth, though there is an increase in saturated fatty acid (SFA) during log phase of growth that prompts an increase in *OLE1* transcription (39, 42). The amount of Ole1 found in the ER is accordingly increased during log phase and decreases as the cells enter

stationary phase (39). The control over the UFA:SFA ratio is achieved by membrane bound transcription factors Mga2 and Spt23, which sense the rigidity of the membrane and increase *OLE1* expression accordingly (43, 44). This control of FA saturation status allows the cell to determine the fluidity of the membrane at the level of individual acyl chains.

1.2.3. Downstream lipid synthesis occurs in the membranes

The production of PLs and TAGs begins with the same pathway in the ER (Figure 1.2). Initially, glycerol-3-phosphate (G3P) is acylated by the glycerol-3-phosphate acyltransferases (GPATs) Sct1 and Gpt2 to produce lysophosphatidic acid (LPA) (8). The lysophosphatidic acid acyltransferases (LPAAT) Slc1 and Ale1 generate phosphatidic acid (PA) via the acylation of the *sn-2* position (9, 45). PA lies at the branch point between two competing pathways and can either be directed to phospholipid synthesis by the CDP-DAG synthase Cds1 or dephosphorylated to produce diacylglycerol (DAG) by Pah1 (46). Once converted to CDP-DAG, the molecule is further modified to phosphatidylinositol (PI) by Pis1 or to phosphatidylserine (PS) by Cho1 (47, 48). PS is decarboxylated to phosphatidylethanolamine (PE) by either the mitochondrially-located Psd1 or the endosomal Psd2, which is then sequentially methylated by the ER proteins Cho2 and Opi3 to phosphatidylcholine (PC) (49–51). This CDP-DAG *de novo* synthesis pathway is the major producer of PE and PC in yeast (52, 53). A parallel pathway for PE and PC synthesis exists, whereby exogenous ethanolamine and choline are converted to CDP-ethanolamine and CDP-choline by cytosolic kinases and ER-bound

cytidylyltransferases. These activated molecules are combined with endogenous DAG to produce PE and PC by the phosphotransferases Ept1 and Cpt1 (54).

The conversion of DAG to TAG also occurs within the ER. DAG can either be acylated by the phospholipid:diacylglycerol acyltransferase Lro1 or the diacylglycerol acyltransferase Dga1. Lro1 scavenges an acyl chain from surrounding PLs to generate TAG and a lysophospholipid (LPL), while Dga1 uses acyl-CoA directly as an acyl donor (55, 56). The TAG generated is stored in LDs within the cells, which are comprised of a neutral lipid core surrounded by a PL monolayer (57). LDs bud from the ER and remain connected in both yeast and mammalian cells (58–60). Sterols are also stored within LDs as sterol esters, which are generated by the acyl-CoA:sterol acyltransferases Are1 and Are2 (61).

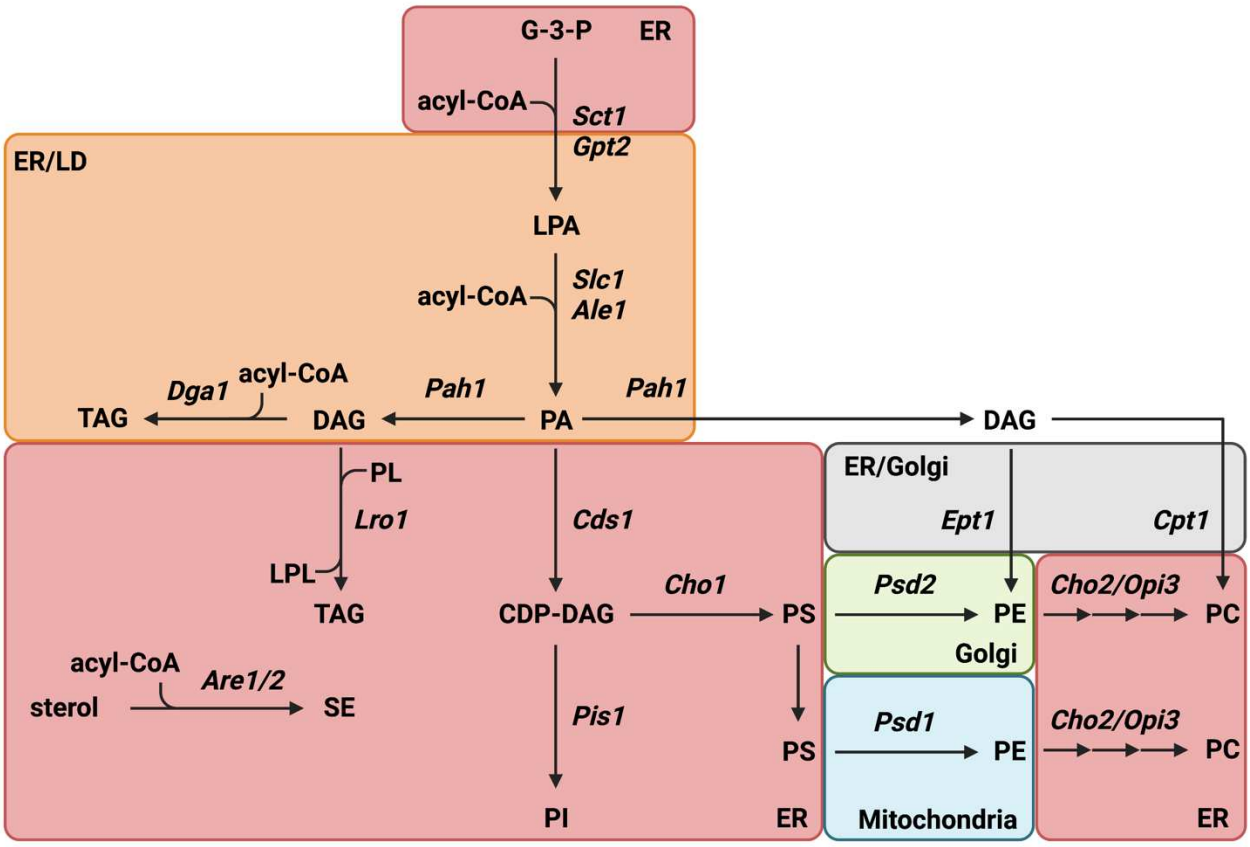

Figure 1.2 **Compartmentalization of major storage lipid and phospholipid synthesis in *Saccharomyces cerevisiae.*** Synthesis of triacylglycerol and the major phospholipids of yeast is compartmentalized between the ER, LD, mitochondria, and Golgi. Sct1 produces LPA in the ER, while Gpt2 is associated with the LD and ER. Slc1 and Ale1 acylate LPA both in the ER and on the surface of the LD, and the resultant PA can either be dephosphorylated to DAG by Pah1 on the LD or ER or converted to CDP-DAG in the ER. DAG acts as the building block primarily for TAG, which is generated by Lro1 in the ER and Dga1 in the ER or LD. DAG can also be converted to PE or PC via the Kennedy pathway. The CDP-DAG produced by Cds1 in the ER cytosolic leaflet can be converted to PI by Pis1 or PS by Cho1, which both reside in the ER. Decarboxylation of PS to PE occurs either in the mitochondria by Psd1 or the TGN by Psd2. Successive methylation of PE by Cho2 and Opi3 in the ER generates PC. Created with BioRender.com.

1.2.4. Phosphatidic acid is generated in the ER

The production of phospholipids begins by acylation of glycerol-3-phosphate to lysophosphatidic acid by a glycerol-3-phosphate acyltransferase (GPAT). In *S. cerevisiae*, there are 2 GPATs both localized to the ER (62). Gpt2, also known as Gat1, and Sct1, sometimes referred to as Gat2, are both *sn-1* acyltransferases with dual substrate specificity for G-3-P and dihydroxyacetone phosphate (8). While deletion mutants of either GPAT are viable, the two genes are synthetic lethal, indicating these are the primary GPATs in yeast (63). Both are integral membrane proteins with multiple proposed transmembrane domains (64, 65). While both GPATs are enriched at the cortical ER associated with the plasma membrane and the nuclear ER (nER), Gpt2 is also found at the LD (2, 45, 62, 66, 67). A deletion of Sct1 mildly reduces GPAT activity *in vivo*, while cells lacking Gpt2 exhibit a dramatic decrease in LPA production, though the proteins are expressed at relatively similar amounts in wild type cells (8, 45, 62). Inhibition of GPAT activity and thus the generation of PA is accomplished by phosphorylation of C-terminal serine residues of both Gpt2 and Sct1 (62, 68–70). As the production of LPA is the rate-limiting step in lipid synthesis, the phosphorylation state of these GPATs regulates carbon flux through lipid synthesis.

Both GPATs can utilize G-3-P and DHAP as acyl acceptors, though Sct1 exhibits a preference for G-3-P over DHAP. *In vitro* analysis revealed that Gpt2 does not have an obvious preference for acyl donor, as the protein can utilize all but C18:0 acyl-CoA, but Sct1 prefers C16:0 and C16:1 over 18-carbon chains (8). However, Sct1 preferentially incorporates C16:0 in LPA *in vivo* and competes with the desaturase for these saturated

acyl chains (69). As the initial step in the glycerolipid synthesis pathway, it seems that Sct1 is generating primarily saturated LPA, while Gpt2 synthesizes unsaturated LPA.

An analysis of PLs in Δ*sct1* and Δ*gpt2* strains demonstrate different downstream roles for the LPA generated by the GPATs, with Sct1 responsible for incorporation of C16:0 in PC and PI and Gpt2 in incorporation of C16:1 in PE (8, 69). Sct1 is also implicated in the synthesis of DAG destined for both acylation to TAG and conversion to PC via the Kennedy pathway (63). Confoundingly, Gpt2 is associated with LDs during late log phase (45, 63, 66). Gpt2 is also enriched at the LD-associated ER upon treatment with oleic acid, and cells lacking the GPAT are more sensitive to fatty acid toxicity induced by the UFA (68). Taken together, it seems that the proteins generate LPA for *de novo* synthesis of differing downstream lipids, with Sct1 incorporating saturated FAs into DAG and PI and Gpt2 generating a more unsaturated LPA profile for PE synthesis.

In *S. cerevisiae*, PA is generated by LPA acyltransferases (LPAATs) encoded by *SLC1* and *ALE1* that constitute a majority of the LPAAT activity. Deletions of either gene alone does not affect yeast growth, while a double mutant is inviable, demonstrating the major roles for these LPAATs in phosphatidic acid production (71). Slc1 is thought to be the main LPAAT in yeast, as a deletion greatly reduces the capacity of a strain to synthesize PA. Ale1 is only responsible for a small portion of the LPAAT activity and shows the ability to utilize a diverse range of lysophospholipids, in contrast to the preference of Slc1 to acylate LPA produced *de novo* (9, 72). Slc1 can be found both in the ER and the LD membranes, while Ale1 localizes to the ER alone (2, 45, 66, 73, 74). Previously, both LPAATs were proposed to be polytopic integral membrane proteins with active sites that face the lumen (64, 75). However, the solved structure of the bacterial

Slc1 ortholog PlsC places the active site in the cytosol and exhibits, rather than multiple transmembrane domains, a monotopic topology with two helices that insert into the membrane bilayer (76, 77). Indeed, this structure agrees with previous topology determined for human LPAAT1 (45, 78). Slc1 taking a monotopic membrane topology would explain the protein's ability to localize to the phospholipid monolayer of the LD.

Prevailing thought held that the two major LPAATs generate similar lipid profiles *in vivo*, though more recent research has discovered that Slc1 and Ale1 incorporate different acyl chains into PA (71, 79). Slc1 is responsible for the incorporation of C18:1 and C14:0 as well as short fatty acyl chains of 10 and 12 carbons into PLs (80). It also more readily generates hetero-acylated PA – i.e. the chain length of the preferred acyl donor is different from the chain length of the *sn-1* acyl chain in LPA (79). Ale1, however, prevents LPC accumulation and plays a major role in reacylation in the Lands cycle (72, 74). The Lands cycle describes the deacylation and reacylation of PC within the membrane and, along with the turnover of other major phospholipid species, contributes to the control of membrane homeostasis (81). These investigations indicate that Slc1 maintains heterogeneity in PA and downstream PL species through *de novo* synthesis, while Ale1 is responsible for incorporating acyl chains of various lengths into lysophospholipid species generated via phospholipid cycling.

1.2.5. Downstream phospholipid synthesis occurs in the ER, mitochondria, and endosome

The phosphatidate cytidylyltransferase Cds1 is the main enzyme responsible for CDP-DAG synthesis (82). A second CDP-DAG synthase, the mitochondrial Tam41,

generates CDP-DAG for cardiolipin synthesis but is not capable of supporting a Cds1 deletion (83). Cds1 is a membrane protein with a predicted six transmembrane helices localizing primarily to the ER membrane but has also been found in the outer and inner nuclear membrane (2, 64, 84). The proposed residues responsible for the CDP-DAG synthase activity mostly face the cytosol of the cell (85). A downregulation of Cds1 greatly increases the total cellular PA, leading to an increase in TAG synthesis and the formation of supersized LDs (86). Reduced CDP-DAG synthase activity also increases the incidence of nuclear lipid droplets (84). The production of CDP-DAG in the cytosolic leaflet of the ER relies on Cds1 in yeast, and thus, the synthase acts as an important regulatory element in controlling flux of PA to PL synthesis.

The essential phosphatidylinositol synthase Pis1 generates PI from CDP-DAG in the ER and inositol-3-phosphate synthesized in the cytosol and is the only way for the cell to produce PI (47). The integral membrane protein has multiple proposed transmembrane helices and can be found in both the ER and Golgi membranes (2, 64, 87, 88). Pis1, similar to Cds1, contains active site residues that face cytosolically (85). This provides a model whereby CDP-DAG is synthesized in the cytosolic leaflet of the ER and is rapidly available, alongside the cytosolic inositol-3-phosphate, for conversion to PI by Pis1.

CDP-DAG can alternatively be directed to PS, PC and PE synthesis by the single phosphatidylserine synthase in *S. cerevisiae*, Cho1 (48, 89). While it is the only enzyme capable of synthesizing PS, the activity of Cho1 is non-essential in the presence of exogenous choline and ethanolamine, as yeast have the ability to make PE and PC through the Kennedy pathway when PS synthesis is attenuated (90). The integral

membrane protein is posited to have six transmembrane domains and localizes to the ER (2, 64). The mitochondrial-associated membrane (MAM), a region of the ER closely associated with mitochondria, contains a remarkable ability to synthesize PS (91, 92). This suggests that a portion of Cho1 molecules is specifically sublocalized within the ER.

The localization of Cho1 to the MAM is important, as the majority of PE within the cell is synthesized by a phosphatidylserine decarboxylase Psd1 located in the inner mitochondrial membrane (93–95). Psd1 generates primarily di-unsaturated PE, though this selectivity is due not to the protein itself but to the mitochondrial localization (96). Psd1 also undergoes autocatalytic cleavage, whereby it is split into an inner mitochondrial membrane anchor and an associated catalytic subunit independent of its localization to the mitochondria (97, 98). A recent study demonstrated the presence of a subpopulation of Psd1 that localizes to the ER, potentially upending the established model of a singly-localized mitochondrial protein (99). Further investigation found that the majority of the wild type protein is found in the mitochondria while functionally impaired forms of Psd1 are primarily dually localized to the ER, which briefly reaffirmed the longstanding contention that the majority of functional protein is found in the mitochondria (100). However, evidence has emerged that the ER-localized Psd1 is actually closely associated with the LD and is functional (101). Though the majority of the protein is found in the mitochondria, this provides new insight into the role of a small subpopulation of Psd1 in LD formation.

A second PSD, Psd2, was initially thought to localize to the Golgi apparatus and vacuole via an N-terminal Golgi retention signal (11, 102, 103). Recent work has shown that the protein actually is maintained in the endosomal system – more precisely, the

trans-Golgi network (11, 104). While Psd1 is the primary synthesizer of PE, Psd2 generates PE principally destined for the vacuole and methylation to PC (11, 95, 105, 106). Strains containing deletions of both Psd1 and Psd2 are still viable with supplementation of choline, but deletion of both PSDs is lethal without ethanolamine and choline supplementation for PE/PC synthesis via the Kennedy pathway (107). Though there are alternate routes to PE and PC synthesis, there remains an essential role for PE biosynthesis by the phosphatidylserine decarboxylase pathway.

The final steps of PC synthesis are performed by Cho2 and Opi3. Cho2 is a phosphatidylethanolamine methyltransferase that converts PE to phosphatidyl-*N*-monomethylethanolamine (PMME), and Opi3 acts as a phospholipid methyltransferase that methylates PMME to PC (51). These are both integral membrane proteins, with Cho2 containing 8 putative transmembrane domains and Opi3 containing anywhere from 3-5 membrane spanning helices (51, 64). Both methyltransferases localize to the ER and neither are essential for cell growth, though a double deletion requires choline supplementation (2, 51, 87). Both *in vivo* and *in vitro* analyses show that both Cho2 and Opi3 preferentially methylate di-C16:1 PE over C16:1/C18:1 PE, independent of the composition of the PE pool (108). The production of PC by PE methylation, as the main source of PC in the cell, has a specificity that reduces the prevalence of hetero-acylated PC species.

1.2.6. TAG synthesis occurs in the ER and LD

The PA generated primarily by Slc1 can be directed to two different fates – phospholipid synthesis or triacylglycerol synthesis. If PA is not converted to CDP-DAG by

Cds1, it is dephosphorylated to DAG by the Mg^{2+}-dependent phosphatidate phosphatase Pah1 (46). Pah1 is a peripheral membrane protein that is soluble when phosphorylated but associates with the ER and LD monolayer via an N-terminal amphipathic helix when dephosphorylated (109, 110). The protein has seven residues that are phosphorylated by Pho85-Pho80, a protein-cyclin kinase complex regulated by cell cycle (111). The dephosphorylation of Pah1 increases both catalytic activity and membrane binding of the protein (111). Indeed, a component of the Pah1 phosphatase complex, Nem1, is found to colocalize with DAG puncta upon LD induction (112). This implicates DAG synthesis as a highly regulated step in the lipid biosynthesis pathway, determining the flux of acyl-CoA between TAG and PL production.

The DAG produced by Pah1 can be converted to TAG and a lysophospholipid by the phospholipid:diacylglycerol acyltransferase Lro1 (55). Lro1 is an integral ER membrane protein with one transmembrane helix and a primarily luminal active site (113). The protein can utilize both PE and PC as acyl donors, scavenging the *sn-2* acyl chain to produce an *sn-1* lysophospholipid and TAG (55, 114). While a deletion of Lro1 does not affect TAG synthesis during stationary phase, there is a marked decrease in TAG production during logarithmic phase without Lro1 (56, 115). The acyltransferase is more abundant during active growth, potentially controlling Lro1's contribution to TAG synthesis during this phase (39). However, the control over Lro1 activity may also be due to localization of the protein. While Lro1 is found widely throughout the perinuclear ER during active growth, it localizes to the nuclear membrane associated with the nucleolus when cells enter post-diauxic shift (116). The protein also colocalizes with concentrated DAG puncta upon LD induction, a process that is reliant on many proteins involved in LD

budding (117). Lro1 activity seems to be reliant on both protein abundance and compartmentalization.

Dga1 is the primary acyl-CoA:diacylglycerol acyltransferase in yeast, catalyzing the terminal step in the production of TAG by acylating DAG using acyl-CoA as a donor (56). Dga1 is orthologous to DGAT2 in humans and other higher eukaryotes, which is responsible for the *de novo* synthesis of TAG (118). A deletion of the diacylglycerol acyltransferase greatly reduces the TAG produced in stationary phase, though it does not abolish TAG production entirely, indicating that Lro1 can take over TAG synthesis to an extent (56, 115). Similar to DGAT2, Dga1 localizes both to the LD phospholipid monolayer and the ER membrane (2, 58). The majority of the protein during active growth is found in the ER; as the cells enter later phases of growth, Dga1 relocates to a predominantly LD localization (58). The migration of the protein from the ER to the LD occurs independent of energy state and ongoing synthesis of the protein (58). The mechanism controlling Dga1 localization is unknown, but it may serve to control activity of the protein as well. While some contend that the protein is more active at the surface of the LD, others assert that Dga1 is more active in the bilayer of the ER (119–121). In fact, work with DGAT2s has shown that while an ER-tethered version of the protein is catalytically active, blocking the migration of the protein to the LD forms smaller LDs (122, 123). This taken together suggests that Lro1 primes the LD from the ER during active growth, while Dga1 transfers to the LD and encourages growth of the organelle.

Previously, Dga1 was suggested to be a polytopic membrane protein with a large luminal loop, but that topology would not allow the protein to transfer to the LD monolayer (124, 125). This topology also conflicts with previous determination of the topology of

murine DGAT2, with two transmembrane helices connected by a short hydrophobic linker (126). The recent development of AlphaFold has allowed a new model of the acyltransferase to be proposed, with a predominantly cytosolic topology and one small hairpin inserting the protein into the membrane, a similar topology to the mammalian DGAT2s (126). The small hydrophobic hairpin of the proposed model is only ~23 Å, which would not fully span the hydrophobic region of the phospholipid bilayer, making Dga1 a monotopic membrane protein with the ability to transfer to a phospholipid monolayer (77, 127). This new model would also place all of the residues found to be catalytically necessary on the cytosolic side of the ER membrane, providing a way for yeast to generate TAG from cytosolic acyl-CoA (124, 126).

1.2.7. SE is generated in the ER and stored in the LD

TAGs are not the only neutral lipid of importance in yeast. *S. cerevisiae* also generates sterol esters (SEs) readily (39). The acylation of sterol to SE is catalyzed by two acyl-CoA:sterol acyltransferases called Are1 and Are2 (61, 128). Both are integral membrane proteins with a proposed nine transmembrane segments located exclusively in the ER membrane (2, 64, 87, 129). While these ACATs have the potential to acylate DAG and contribute to the production of TAG, Dga1 and Lro1 cannot produce SE, making Are1 and Are2 the only SE generating enzymes (115). While a deletion of these genes is not lethal, growth is attenuated when *ARE1* and *ARE2* are deleted, indicating an important mechanism for control of cellular sterol concentration by these ACATs (129). Are1 and Are2 are the only enzymes able to control sterol concentration in the membrane through acylation.

While these two proteins are similar to approximately 43% amino acid similarity, they contribute differently to SE synthesis (61). A deletion of *ARE2* shows a dramatic reduction in SE synthesis and no effect on TAG synthesis, though a deletion of Are1 slightly reduces cellular SE and TAG content in stationary phase (61, 128). This is consistent with the relatively larger amount of Are2 over Are1 in the ER, as well as relatively higher expression and stability of *ARE2* over *ARE1* (129, 130). Interestingly, Are1 primarily acylates ergosterol precursors, sequestering sterol intermediates for quick mobilization when needed (129). The different roles for these ACATs allow for control of sterol concentration during rates of high sterol synthesis and sequestration of sterol intermediates during stalled synthesis.

1.3. Lipids are specifically acylated

Investigation of the yeast lipidome has revealed a precise assembly in the lipid biosynthetic pathway. Though 70-80% of the acyl chains in yeast are unsaturated, the proportion of unsaturated chains found in certain membrane lipid types exceeds that (39). Global analyses of the yeast lipidome from cultures grown with both raffinose and glucose revealed that the majority of PA contains two unsaturated acyl chains, with only a quarter of the species containing one saturated moiety (131, 132). Discordantly, the PS species produced from the majority unsaturated pool of PA are more saturated. Approximately 50% of the PS species contain one unsaturated and one saturated chain, with the other half of the PS di-unsaturated (132). When PE and PC species are analysed, this same enrichment for saturated acyl moieties is not observed – the vast majority of PE and PC in the cell contain two unsaturated acyl chains, with less than 10% of PE and 20% of PC

produced with one saturated chain (131). There is evidence that the saturated acyl chain, when present in these phospholipids, is preferentially incorporated in the *sn-1* position, with a selective enrichment for unsaturated acyl chains in the *sn-2* position acylated by Slc1 (133, 134). Analyses of PE and PC indicate that the molecules produced via the CDP-DAG pathway are enriched for unsaturated acyl chains, while those species produced from Kennedy synthesis or remodelled in the Lands cycle do not retain this specificity (135, 136). Though Psd1 has a demonstrated preference for di-unsaturated PS, this is reliant on the localization of the protein in the mitochondria and is not a feature intrinsic to the protein itself.

The production of PI is even more of an anomaly. While the other simple membrane lipids in the cell contain an overwhelming majority of unsaturated acyl moieties, PI is preferentially enriched for saturated chains. Over 70% of the PI species in the cell contain at least one saturated acyl chain, while 15-25% of the species contain only unsaturated acyl chains, a phenomenon only seen for PI (131, 132). The distribution of the acyl chains in PI is similar to that seen in PS, PE, and PC – the *sn-1* position is the primary location of saturated acyl chains, while the *sn-2* position of the molecule is predominantly unsaturated (133, 137). Psi1, an acyltransferase localized to the ER and LD involved in reacylation of lyso-PI, is essential for the enrichment of C18:0 at the *sn-1* position by replacing C16:1 and C18:1 moieties in newly synthesized PI (80, 137). While Psi1 is necessary for the preferential incorporation of C18:0 seen in PI over other membrane lipids, it is not responsible for the predominance of C16:0 at the *sn-1* position (137). As mentioned, Sct1 has been implicated in PI synthesis and prefers C16:0 acyl chains. Interestingly, Psi1 and Sct1 interact genetically – a deletion of Psi1 suppresses

the slow growth phenotype seen in cells overexpressing Sct1 (69). To this date, no mechanism for the channeling of LPA from Sct1 to PI synthesis has been described.

Storage lipid found within the LD is also preferentially acylated. The majority of TAG species produced by *S. cerevisiae* contain three unsaturated acyl chains, and little to no TAG contain only saturated acyl chains (39, 40, 138). Stereospecific analyses of the glycerolipid species show that TAG, similar to PLs, contain almost exclusively unsaturated fatty acids in the *sn-2* position (138, 139). SE as a whole contain also primarily unsaturated fatty acids in stationary phase, though ergosterol esters in particular contain a majority of unsaturated fatty acids in diauxic phase and an even proportion of UFA:SFA ratio in log and stationary phase (39, 129). The concentration of unsaturated acyl chains in these neutral lipids may aid in LD budding from the ER and promote TAG synthesis; indeed, an active desaturase is required for triglyceride accumulation in the liver of mice, and saturated TAG accumulates within the lipid bilayer more readily than its unsaturated counterpart (140, 141). It is yet unclear what mechanism is channeling unsaturated acyl-CoA to neutral lipid synthesis, but the phenomenon promotes LD emergence from the ER.

1.4. Lipids are specifically distributed

By and large, work has shown that the distribution of PL across membranes is different depending on the subcellular component the membrane originates from. This specificity is seen for distribution of both PL head type and PL acyl chain saturation status. While an alteration of the acyl chain composition changes membrane fluidity, controlling the composition of PLs by head type can influence membrane curvature (Figure 1.3). The

intrinsic shape of a PL molecule (J_s) is defined by the tendency of a membrane made of the PL to curve (142). Lysophospholipids like LPC, LPA, and LPE are conically shaped, thus imparting a positive curvature on monolayer membranes, while PA, PE, and DAG are shaped like an inverted cone, tending towards a negative membrane curvature. PI, PS, and PC do not contain an intrinsic curvature and promote the formation of lipid bilayers (142, 143). There is generally a greater proportion of bilayer forming PS and phosphoinositides in the plasma membrane over the microsomal membranes, with a concomitant decrease in PC in the plasma membrane (41, 144). While the microsomal phospholipids of yeast grown on glucose are composed of 6.4% PS and almost 39% PC, the PM phospholipids contain over 32% PS and only 11.3% PC (41). The mitochondria, however, are supplemented with negatively curved PE and exhibit a decrease in cylindrical PS and PI (10, 41). The LD monolayer is enriched for cylindrical PC as well as conical LPE and LPC, with a decrease in PE (145–148). Proper proportioning of lipids across organelles could serve as a control mechanism for membrane curvature, i.e. allowing for budding of the LD from the ER or folding of mitochondrial cristae.

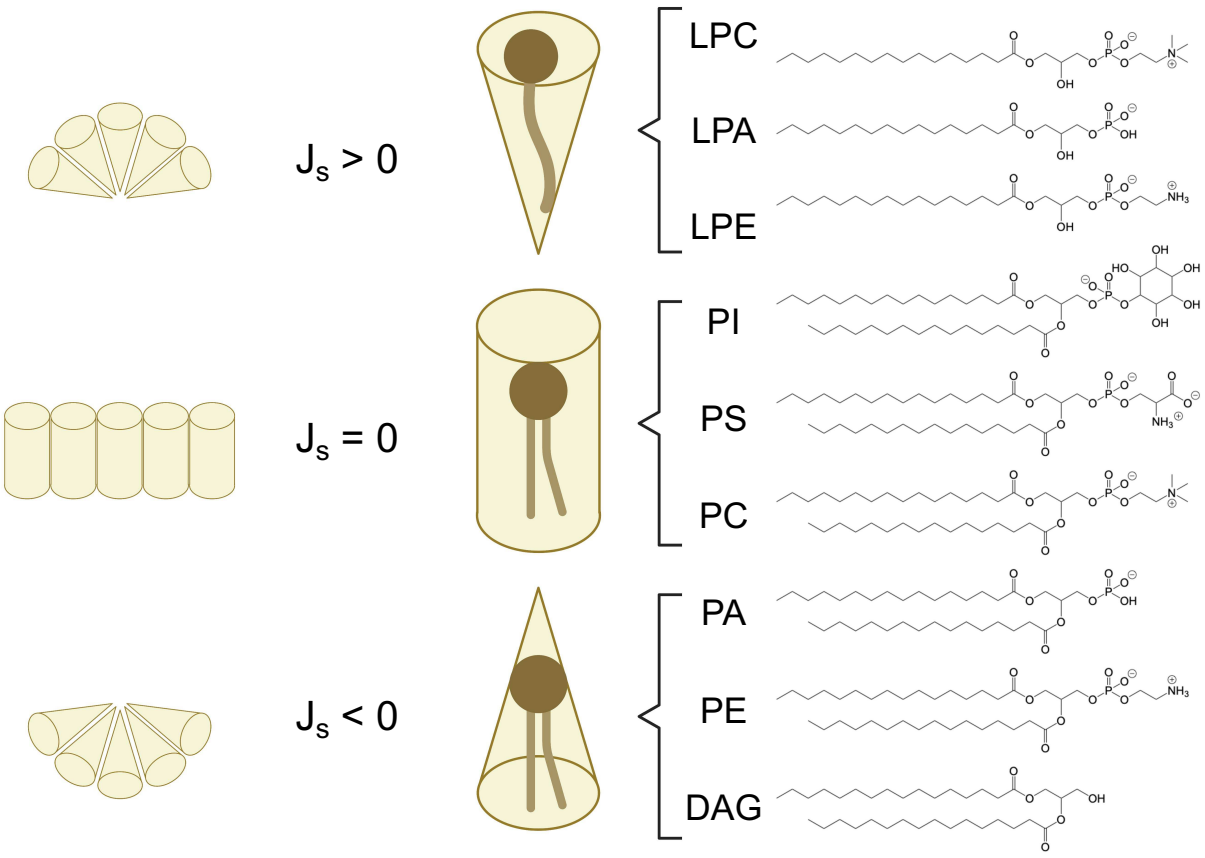

Figure 1.3 **Lipid shape and intrinsic curvature (J_s) impact membrane formation.** Lipids are organized from most positive J_s to most negative. Phospholipids with a positive J_s are conical in nature and impart a positive curvature to membranes. Lipids with a negative J_s are shaped like inverted cones and alternately promote formation of a negatively curved membranes. Conically shaped lipids have little to no intrinsic curvature, and thus promote formation of lipid bilayers. Created with BioRender.com.

Differential distribution of acyl chain composition across organelles is also seen in yeast. The plasma membrane is enriched for SFA across all PL types, not only in the expected PI but in PS and PE as well (132). The opposite is true for LDs; the monolayer surrounding the neutral lipid is preferentially unsaturated in the PS and PE species (132). The differential distribution of phospholipids may reflect the need for the cell to control subcellular membrane composition to allow for different functions of the membranes (149). Indeed, accumulation of unsaturated PL species as well as unsaturated neutral lipid is necessary for proper budding of the LD from the ER (141). Lipid rafts, which are

comprised of sphingolipids, sterol, and saturated PS, are found primarily within the PM and are crucial for proper functioning of ion channels and other essential proteins (150, 151). The partitioning of saturated and unsaturated PLs, then, may serve to ensure proper organelle formation and function within the yeast.

Overall, the unsaturated acyl chains produced by Ole1 are incorporated in the PA pool generated for PC and PE synthesis more readily than the PA pool destined for the PS population at the PM. LPA generated by Sct1 is directed to DAG production and PI synthesis, enriching those lipid molecules for saturated acyl chains. This infers that lipid synthesis is partitioned not only by organelle, but within various subdomains of the ER as well.

1.5. Membrane contact sites are metabolically distinct

As the ER is the main location of phospholipid synthesis, membrane contact sites (MCSs) are essential for proper spatial distribution of lipids throughout the other organelles. These sites allow for crosstalk between compartments of the eukaryotic cell, contain proteins that act as tethers, and are often metabolically distinct from other membranes. MCSs have been identified between the ER and all organelles, but the MCSs of interest to our work are between the ER and the plasma membrane, mitochondria, and LD.

Growth of the plasma membrane is greatly dependant on the rate of lipid synthesis in the ER, linking the PM to the ER functionally. Accordingly, over 40% of the PM is associated with the cortical ER (cER) (152, 153). There are six proteins within three families that maintain these contacts; the tricalbins Tcb1, Tcb2, and Tcb3, the vesicle-

associated membrane proteins Scs2 and Scs22, and the TMEM16 family member Ist2 (144, 154). All six of these tethers are located in the cER, and all contain domains responsible for lipid binding or interact directly with lipid binding proteins (155–158). Efforts to dissect the roles of each protein family in ER-PM tethering have revealed that the tricalbins are responsible for the enrichment of PS at the PM while Ist2 and Scs2/22 regulate homeostasis of PM PIP and PIP_2, lipids essential to proper cell physiology that have recently been reviewed in full (144, 157, 159). These tethers interact with the lipid synthesizing enzymes Ole1 and Pis1, and analysis of the PM associated ER (PAM) revealed a concentration of not only PI synthesis, but PS synthesis as well (Figure 1.4) (10, 144, 160). Localized synthesis of PI and PS and close proximity to potential ER-PM lipid transfer and tether machinery could explain the particular enrichment for these lipids at the PM.

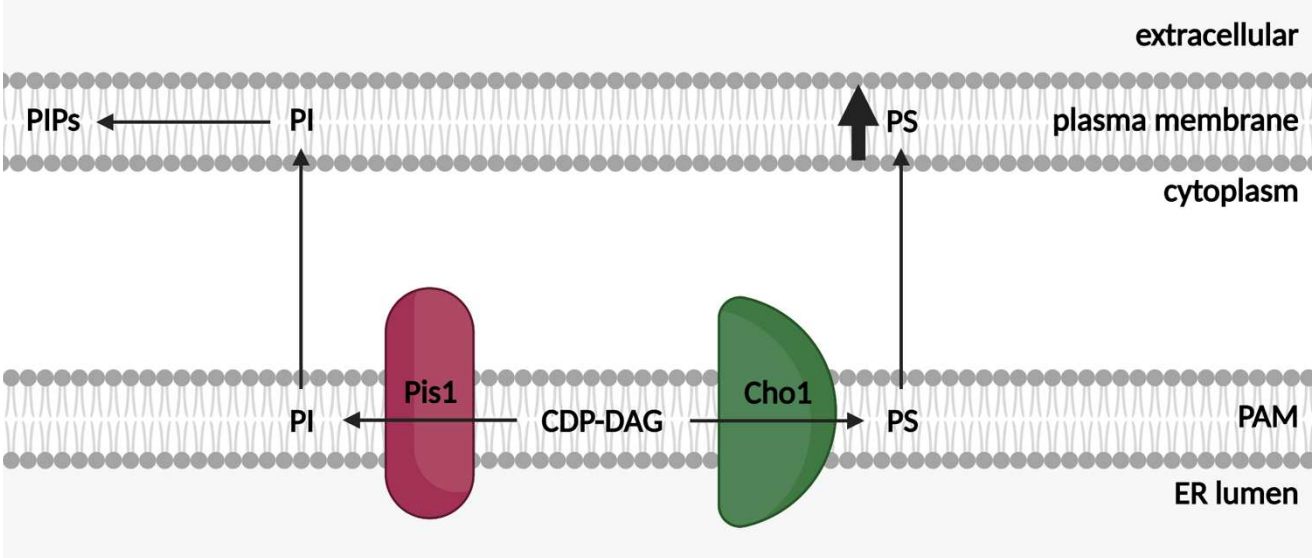

Figure 1.4 **The yeast PM associated ER (PAM) is an active site of phospholipid synthesis**. PI and PS synthase activity is enriched at the PAM. Both phosphoinositides and PS are concentrated within the plasma membrane. Created with BioRender.com.

The mitochondria is also tethered to the ER via the MAM. Though PE synthesis is primarily found in the mitochondria, the precursor PS is generated in the ER and must be transferred to the mitochondrial Psd1. The transfer of these PLs between the two organelles was initially thought to be facilitated by the ER-mitochondria encounter structure (ERMES), which contains four main subunits, three of which have lipid-binding domains (161–163). Others have proposed that ERMES is primarily an ER-mitochondrial tether that facilitates the transfer of phospholipids by other proteins (164). An interaction between the mitochondrial Tom70 and the ER sterol transporter Lam6 has been implicated in sterol transfer, and Lam6 is essential in cells lacking ERMES component Mdm34 (165). The conserved ER membrane protein complex (EMC) is important for transfer of PS to the mitochondria, and cells lacking both the EMC and ERMES complexes are inviable (166). Finally, the lipid transfer protein Vps13 also functions in ER/mitochondria PL transfer, and can compensate for the lack of ERMES components (167, 168). In all, evidence supports multiple mechanisms to transfer lipids between the ER and mitochondria, with ERMES and EMC acting in parallel with lipid transfer proteins (169). The portion of the ER tethered to the mitochondria by these complexes (MAMs) are a site of active lipid synthesis. The Ole1 mammalian ortholog SCD1 is found associated with the MAM and as noted, MAMs are enriched for Cho1 (Figure 1.5) (91, 92, 170). The close proximity of these proteins to the mitochondria could provide a highly unsaturated set of PS molecules to Psd1 for downstream PE synthesis and thus explain the preference of mitochondrially-localized Psd1 for unsaturated PS (96).

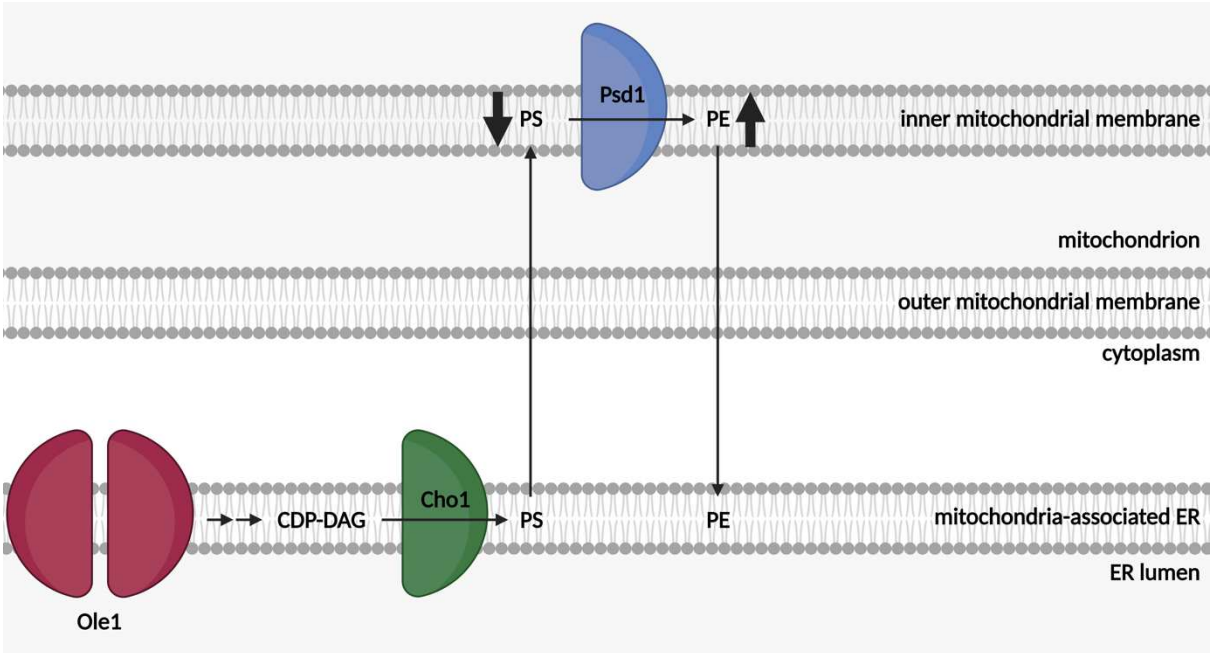

Figure 1.5 **The mitochondria-associated ER (MAM) generates PS for mitochondrial Psd1.** Yeast PS synthase and mammalian stearoyl-CoA desaturase are localized at the MAM. The mitochondrion contains the main PS decarboxylase in the cell, which preferentially generates highly unsaturated PE and enriches the mitochondrion for PE at the expense of PS. Created with BioRender.com.

As discussed earlier, excess acyl-CoA is stored in the LD as sterol ester or triglyceride. Lipid droplets begin between the two leaflets of the perinuclear ER membrane at locations marked by seipin and Nem1 (112, 171). The colocalization of these two proteins allows Nem1 to dephosphorylate Pah1 and increase production of DAG locally (109, 110, 172). Seipin and Nem1 then stimulate the formation of lipid droplets by recruitment of lipid droplet stability proteins as well as Lro1 and Dga1 to the sites of DAG enrichment (112, 173). Recruited Lro1 and Dga1 produce TAG, which accumulates between the leaflets of the ER membrane and forms a lens (59). The lens can then bud into a nascent LD, which is recognized by bona fide LD proteins, allowing the LD to mature (174, 175). The sterol acyltransferases Are1 and Are2 acylate sterols from the ER membrane and generate SE for deposition in the LD (129). Budding of the lipid droplet

from the ER membrane is more reliant on TAG deposition than SE accumulation in the initial neutral lipid lens (176). The rate of LD emergence is also dependent on the incorporation of unsaturated acyl chains into TAG, generating a lipid that packs less readily and a more fluid neutral lipid lens (140, 141, 177). Growth of the mature lipid droplet requires recruitment of neutral lipid synthesizing acyltransferases to the LD phospholipid monolayer from the ER membrane (60, 178, 179).

In yeast, LDs are physically connected to the ER – the lipid monolayer surrounding the LD remains continuous with the ER after budding and almost never detaches (58, 171, 180). The structure of the neutral lipid core includes an inner core comprised of TAG surrounded by shells comprised of primarily SE (5). While LD growth is reliant on localized synthesis of neutral lipid by Gpt2, Slc1, Dga1, and Lro1, the expansion of the PL monolayer surrounding the neutral lipid core necessitates local PL synthesis as well (181, 182). Though Psd1 has been confirmed to be primarily mitochondrially located, localization of the protein to sites of LD synthesis is essential for proper formation of the organelle (Figure 1.6) (101). Interestingly enough, an accumulation of PE in the ER prevents LD budding from the phospholipid bilayer, due to the negative curvature PE imparts on the membrane (183). It has been proposed that a concentration of PE specifically at the bud neck of the LD may be beneficial to promote the negative curvature required of that part of the organelle (97). It is also possible that the PE generated by LD-localized Psd1 is destined for methylation to PC; indeed, proper synthesis of PC is necessary for emergence of the LD in both yeast and Drosophila cells (181, 183). The localized PE could alternatively be used as an acyl donor by Lro1 for TAG generation.

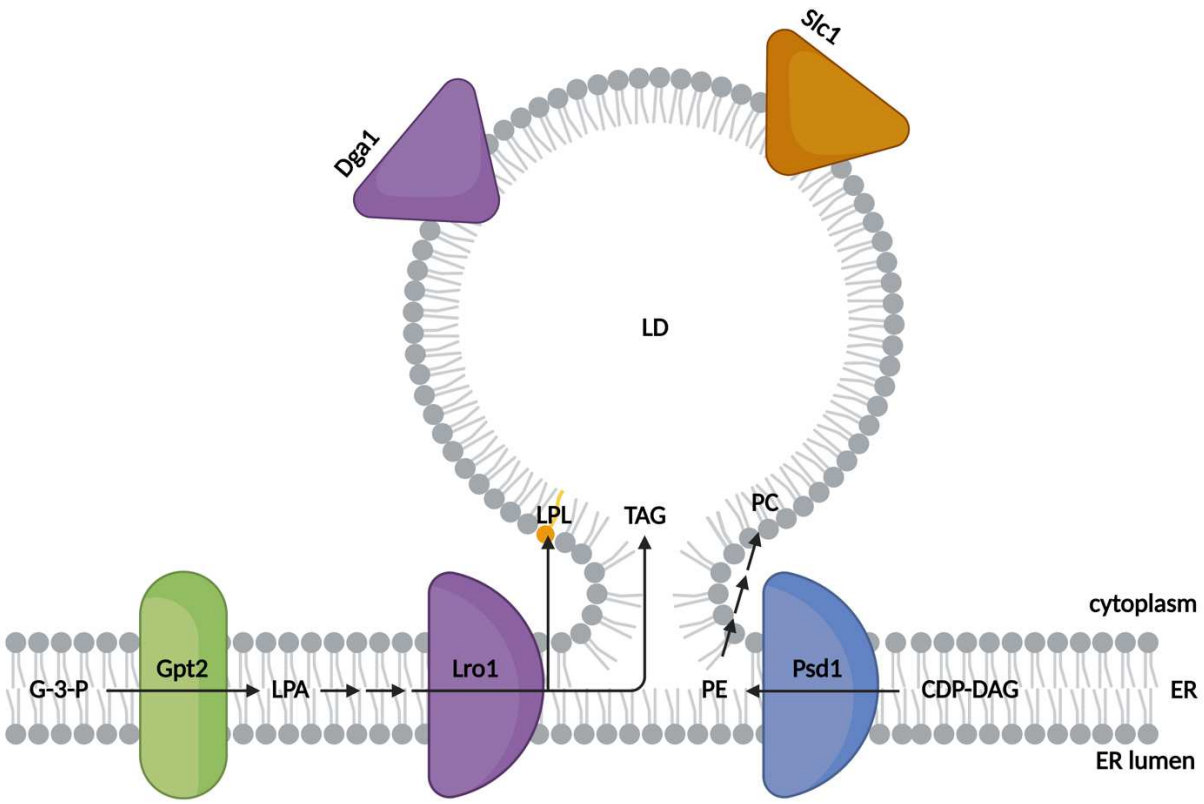

Figure 1.6 **The LD is an active site of both neutral and phospholipid synthesis.** GPAT Gpt2 and LPAAT Slc1, which generate both TAG and phospholipid precursors, have been found on and near the LD. Lro1 produces TAG and a conical lysophospholipid from the ER bilayer, while Dga1 can acylate DAG both in the ER and on the LD surface. Psd1, which is primarily a mitochondrial enzyme, is found at the LD and is important for correct morphology of the organelle. Created with BioRender.com.

1.6. Proteins that synthesize sequential reactions interact in other organisms

The partitioning of differing lipid synthesis enzymes throughout the ER would explain some of the lipidome specificity seen both spatially and temporally within yeast. However, this cannot explain the phenomenon in totality; for instance, Ole1 and Sct1 are both found within the cortical and perinuclear ER and the acyltransferase can use C16:1 in an *in vitro* system, but the unsaturated acyl chains produced by Ole1 are clearly more

readily available to Gpt2 than Sct1. We propose that protein-protein interactions (PPIs) contribute to the control of the lipidome composition. PPIs are physical contacts between the molecular machinery of the cell and are often essential for full efficiency of cellular processes. From the discovery of the first known PPI in 1906 (184), this field has grown greatly and interactions have been implicated in many pathways from gene regulation to branched chain amino acid metabolism (185, 186). Methods to detect protein associations can be structural, computational, or *in vivo* and have been recently reviewed (187). The umbrella of PPIs encompasses everything from obligate complexes like enzymes with multiple subunits that require all interactors to function to transient interacts between proteins that can all act independently (188–190).

Metabolons, in contrast to multi-subunit enzymes, are transient complexes of proteins with low affinity for each other and a highly dynamic nature (191, 192). Metabolons are complexes that permit substrate channeling through protein-protein interactions, which passes intermediates in various pathways to active enzymes of successive pathways. There are multiple ways this may be biologically beneficial; indeed, channeling intermediates can protect cells from toxic compounds, enrich certain substrates, and avoid competing pathways (193). While molecular tunnels directly channel substrates from enzyme to enzyme in obligate complexes, metabolons direct substrates to downstream proteins through local enrichment in a process termed cluster channeling (193). The transient nature of metabolons allows for the regulation of rapid metabolic flux changes, since the dissociation of the complex doesn’t necessitate large amounts of energy or the activity of other regulatory proteins (194). The metabolon, then,

exists as a low-energy step to exert control over the flux of intermediates through competing pathways at various branch points (195).

For a complex to be classified as a metabolon, first, it must be determined that the proteins involved physically interact (192). This can be done through a high-throughput method, such as co-immunoprecipitations or yeast two hybrid assays using a cDNA library, or a directed approach, like yeast two hybrid with specific proteins or fluorescent resonance energy transfer. Often, multiple methods are needed to be used, to remove the chance of false negatives due to the transient nature of the metabolon. To prove the existence of a proposed metabolon, it must be shown that these physical interactions functionally channel substrates (192). While proving that proteins exist in a complex can be of relative ease, proving that these interactions exist to channel substrates is greatly difficult. To date, only a small number of metabolons have been characterized; only three pathways – the oxidative pentose phosphate pathway, glycolysis, and the TCA cycle – contain metabolons in yeast (196–199).

Interactions between proteins that synthesize sequential interactions in lipid biosynthesis pathways have been identified in many organisms. Work in flax has uncovered interactions between acyltransferases that transfer PUFAs between the PC and TAG pathways (200). In mammals, the desaturase and DGAT2 have been found to colocalize within the ER, and an acyl-CoA synthetase and DGAT2 interact to promote LD expansion (123, 170). Perhaps most interesting to this work is an interaction observed between Ole1 and the acyltransferase Gpt2 (201). Indeed, an interaction between Ole1 and Gpt2 that shuttles unsaturated acyl-CoA to LPA synthesis would explain the obvious

inclination for Gpt2 to acylate G-3-P with an unsaturated acyl chain, though it does not obviously prefer unsaturated moieties *in vitro*.

1.7. Concluding remarks

Though acyl-CoA is initially produced as a saturated molecule, the majority of acyl-CoA species generated by *S. cerevisiae* are unsaturated. The major lipids contain 16- or 18-carbon chains, with 26 and 14 carbon fatty acids present as minor species. Incorporation of these types of acyl-CoAs into different lipid classes is tightly controlled *in vivo*. The *sn-2* position of the major PLs PS, PE, and PC is majority unsaturated, while PI contains more saturated acyl chains. These lipids are found in different proportions throughout the subcellular membranes, and the proportion of saturated chains changes across cellular compartment. Both TAG and SE species are enriched for unsaturated moieties, which promotes the biogenesis and maturation of the LD from the ER membrane.

The proteins that synthesize lipids in yeast do not exhibit substrate preferences for unsaturated over saturated lipids when analyzed *in vitro*. However, analysis of the reactions catalyzed *in vivo* reveals an apparent inclination towards specific species of substrate for many of the steps of lipid synthesis. Lipid biosynthetic enzymes are partitioned throughout the cell, though many proteins are found in the main lipid synthesis organelle, the ER.

The mechanisms controlling the specific distribution of unsaturated acyl-CoA across subcellular components and lipid types have not to this date been described in full. We propose that it is created through protein-protein interactions that channel the

unsaturated acyl chains from Ole1 to the enzymes involved in PL and storage lipid synthesis in a manner that is specific to subcellular components. This is in line with recently proposed mechanisms, which postulated that the specificity observed in lipid production could be due to local concentrations of certain substrates and substrate channeling between proteins (202, 203). Careful consideration will need to be taken when investigating whether interactions between the lipid synthesis machinery in yeast exist – it is possible these complexes, instead of obligate complexes, exist transiently within the cell and the composition of the complex differs across membranes. Determination of the lipid interactome has great potential to provide a foundational understanding of lipid channeling in fields from metabolic engineering to human diseases.

1.8. Objectives of this work

This project aimed to decipher a mechanism regulating the de novo synthesis of phospholipid and storage lipid in the yeast *Saccharomyces cerevisiae*. The focus was on identification of the mechanisms that channel lipid species toward specific degrees of unsaturation and how those molecules are directed toward specific fates; i.e. storage as fat or incorporation in membranes. We hypothesized that the specific nature of the lipidome is due to protein-protein interactions channeling acyl-CoA molecules towards membranes or storage as triglyceride. From this work, we propose the existence of a lipid biosynthesis complex that regulates the composition of various lipid species through protein-protein interactions channeling acyl-CoA molecules toward certain fates.

1.9. Organization of the thesis

1.9.1. Chapter 2 – The desaturasome: a multi-protein complex that controls lipid biosynthesis in S. cerevisiae

In chapter 2, we investigated the composition and architecture of the desaturasome, a complex of lipid biosynthetic proteins that interact with the only desaturase in *S. cerevisiae*. This study began with an affinity purification that revealed many proteins from lipid biosynthesis interact with Ole1. A confirmatory membrane yeast-two hybrid (MYTH) study confirmed that proteins from PL and neutral lipid synthesis interact with Ole1. We further elucidated the composition of the desaturasome by demonstrating that the LPAAT Slc1 and CDP-DAG synthase Cds1 interact strongly with the desaturasome constituents as well. This work has begun the determination of the desaturase interactome composition and has given insight into the potential architecture of this complex.

1.9.2. Chapter 3 – Saccharomyces cerevisiae Δ9-desaturase Ole1 forms a supercomplex with Slc1 and Dga1

In chapter 3, we further dissected the interaction between Ole1 and Dga1 as well as Slc1 and Dga1. We determined that a set of charged residues at the C-terminus of Dga1 are essential for the maintenance of the Ole1-Dga1 interaction, but they are not essential for DGAT activity. Functional analysis revealed that the interaction determines number and size of LDs formed without affecting Dga1 activity or TAG synthesis rate.

1.9.3. Chapter 4 – Dga1 mutants lacking strong interactions with Ole1 exhibit altered subcellular localization

In chapter 4, we analyzed the cellular distribution of Dga1 truncations and mutants that lack interaction with the desaturase. We demonstrate that the wild type acyltransferase localizes to the nER and cER, in a fashion that resembles Ole1 distribution. The protein is found on LDs both in active growth and during stationary phase. Dga1 truncations and mutants that exhibited little to no interaction with Ole1 in Chapter 3 do not localize to the nER, but are found readily on the LD. We also demonstrated that the conserved ^{410}DAELKIVG^{418} motif at the C-terminus of Dga1 is likely not an ER retention signal as has been previously proposed. Finally, we show that a deletion of Ole1 does not appear to affect Dga1 localization.

1.9.4. Chapter 5 – Conclusions

In the fifth and final chapter, we discuss the major conclusions that can be drawn from these studies. We conclude with future avenues for desaturasome investigation and the implications this work will have in disease research and metabolic engineering.

Chapter 2 – The desaturasome: a multi-protein complex that channels acyl-CoA to specific fates in *Saccharomyces cerevisiae*

2.1. Summary

Lipids are essential both for integrity of membranes and energy storage in all organisms. The chemical properties of membrane phospholipids and triacylglycerol produced from phosphatidic acid are determined by the composition and organization of their acyl chain components. Unsaturated acyl chains play an important role in maintenance of membrane fluidity through incorporation into phospholipid, while the genesis of lipid droplets relies on unsaturated acyl chain incorporation into triacylglycerol. The cell asserts control over the chemical nature of the lipidome by governing order of assembly. Acyl-CoA is delivered to the enzymes involved in lipid biosynthesis in a specific manner, as demonstrated by both an enrichment for unsaturated acyl chains in phosphatidylcholine and an enrichment for saturated acyl chains in the phosphatidylinositol of *Saccharomyces cerevisiae*. The mechanism allowing this ordered assembly is not yet known, but interactions between lipid synthesizing enzymes have been demonstrated in plants and humans. We propose that these interactions regulate the incorporation of unsaturated acyl chains into phospholipid and triacylglycerol and thus control the composition of membrane and storage lipids. Yeast two-hybrid and coimmunoprecipitation studies have revealed novel protein-protein interactions between Ole1 and enzymes that synthesize storage lipid, phospholipid, and sterol-esters. Notably, Ole1 has been found to interact with the glycerol-3-phosphate acyltransferase Gpt2,

lysophosphatidic acid acyltransferase Slc1, phosphatidate cytidylyltransferase Cds1, phosphatidylinositol synthase Pis1, phosphatidylserine synthase Cho1, phosphatidylethanolamine methyltransferase Cho2, phospholipid:diacylglycerol acyltransferase Lro1, acyl-CoA:diacylglycerol acyltransferase Dga1, and acyl-CoA:sterol acyltransferases Are1 and Are2. The main lysophosphatidic acid acyltransferase in *S. cerevisiae*, Slc1, interacts with the phospholipid synthesizing enzymes Gpt2, Cds1, Pis1, Cho1, and Cho2 as well as the storage lipid synthesizing acyltransferases Lro1, Dga1, Are1, and Are2. Cds1, the essential phosphatidate cytidylyltransferase, interacts with Gpt2, Slc1, Pis1, Cho1, and Cho2, which catalyze phospholipid synthesis. Cds1 also interacts with the neutral lipid synthesizing acyltransferases Lro1, Dga1, Are1, and Are2. This research has determined the composition of an interactome that may exist to regulate the order of acyl chain incorporation into phospholipid, triacylglycerol, and sterol-esters and thus the fluidity of the membrane and the production of lipid droplets. Future research aims to determine exactly how these interactions control lipid synthesis and composition via metabolic flux analysis and gene deletion studies. Investigating this lipid biosynthesis complex will have implications for a wide variety of applied research, from treating lipid dysregulation in humans to biofuel production by microbes.

2.2. Introduction

Lipids are essential for maintenance of membrane integrity and can be stored within lipid droplets as neutral storage lipid. There are eight classes of lipid in total; fatty acids (FA), glycerolipids, glycerophospholipids, sterol and sterol derivatives, sphingolipids, prenol lipids, glycolipids, and polyketides (1). Different classes of lipid serve different purposes in the cell. FA exist primarily as building blocks for lipids, though they can be imported into the peroxisome and degraded through β-oxidation to provide energy (2). Glycerophospholipids, sterols, and sphingolipids are found in the plasma membrane (PM), and their acyl chain composition determines membrane fluidity (3). Glycerolipids and sterol derivatives like sterol esters are stored in lipid droplets and serve as reservoirs for membrane lipid precursors (4, 5).

Fatty acid-derived fatty acyl chains can be either incorporated into storage lipid or membrane lipid, or degraded to be used as energy for the cell (6, 7). The primary source for fatty acyl-CoA in yeast is through de novo synthesis, which occurs in the cytoplasm primarily and is initiated by the carboxylation of acetyl-CoA to malonyl-CoA by acetyl-CoA carboxylase (Acc1). Malonyl-CoA is elongated to a full-length saturated acyl-CoA by the fatty acid synthase complex composed of Fas1 and Fas2. The fatty acyl-CoA produced primarily contain 16 or 18 carbons, though there are 14 carbon and 26 carbon acyl-CoA species produced in small amounts (6). Once the saturated acyl-CoA is released from the FAS complex, the endoplasmic reticulum (ER) localized Δ9-desaturase, Ole1, can capture the acyl-CoA and introduce a double bond in its acyl chain, altering its chemical and physical properties. Almost 80% of the acyl chains produced by *Saccharomyces cerevisiae* are monounsaturated, indicating an important role for Ole1 (8, 9).

The primary lipids of concern for this work are phospholipids, triacylglycerols, and sterol esters. As discussed in 1.2.4, the production of phospholipids (PLs) and triacylglycerols (TAGs) begins with PA synthesis within the ER (Figure 1.2). Glycerol-3-phosphate (G3P) is acylated by the glycerol-3-phosphate acyltransferases (GPATs) Sct1 and Gpt2 to produce lysophosphatidic acid (LPA) (10). The primary lysophosphatidic acid acyltransferase (LPAAT) Slc1 generates phosphatidic acid (PA) via the acylation of the *sn-2* position (11, 12). PA lies at the branch point between two competing pathways and can either be directed to phospholipid synthesis by the CDP-DAG synthase Cds1 or dephosphorylated to produce diacylglycerol (DAG) by Pah1 (Figure 1.2). Once converted to CDP-DAG, the molecule is further modified to phosphatidylinositol (PI) by Pis1 or to phosphatidylserine (PS) by Cho1. PS is decarboxylated to phosphatidylethanolamine (PE) by either the mitochondrial protein Psd1 or the Golgi body-localized Psd2, which is methylated by the ER proteins Cho2 and Opi3 to phosphatidylcholine (PC) (Figure 1.2). PI, PC, and PE are the primary phospholipids of the total cellular membranes, though PA and PS are minor components (13). A parallel pathway for PE and PC synthesis exists, whereby exogenous ethanolamine and choline are converted to CDP-ethanolamine and CDP-choline by cytosolic kinases and ER-bound cytidylyltransferases. These activated molecules are combined with endogenous DAG to produce PE and PC by the phosphotransferases Ept1 and Cpt1 (14). While the Kennedy pathway contributes to intracellular production of PE and PC, the *de novo* CDP-DAG pathway is indispensable and the primary route for PE and PC production (15, 16). As discussed, the phospholipid head and acyl chain compositions of these molecules determine the properties of subcellular membranes (1.4).

The production of the main sterol in yeast, ergosterol, occurs in three modules (17). The first module generates mevalonate from acetyl-CoA. Hmg1/2, the hydroxymethylglutaryl-CoA (HMG-CoA) reductases and final step in mevalonate synthesis, are the rate-limiting enzymes not only for the first module but for the whole of sterol biosynthesis as well (Figure 2.1) (18, 19). Mevalonate synthesis begins in the cytoplasm and completes in the ER (20, 21). The second module, farnesyl pyrophosphate synthesis, occurs in the vacuole and produces an important intermediate in sterol and isoprenoid synthesis (Figure 2.1) (22, 23). The third and final module in ergosterol synthesis produces the intermediates squalene, lanosterol, zymosterol, fecosterol, and episterol in order (Figure 2.1) (24). Zymosterol is the first intermediate distributed widely within the membranes, but lanosterol, fecosterol, and episterol are found in high amounts within the LD (25). Ergosterol, the most abundant sterol, is concentrated in the PM but is also present in the ER, LD, and mitochondrion (13, 26). Proper sterol levels are essential for membrane integrity and thus the control of sterol synthesis is under tight regulation (23, 27–29).

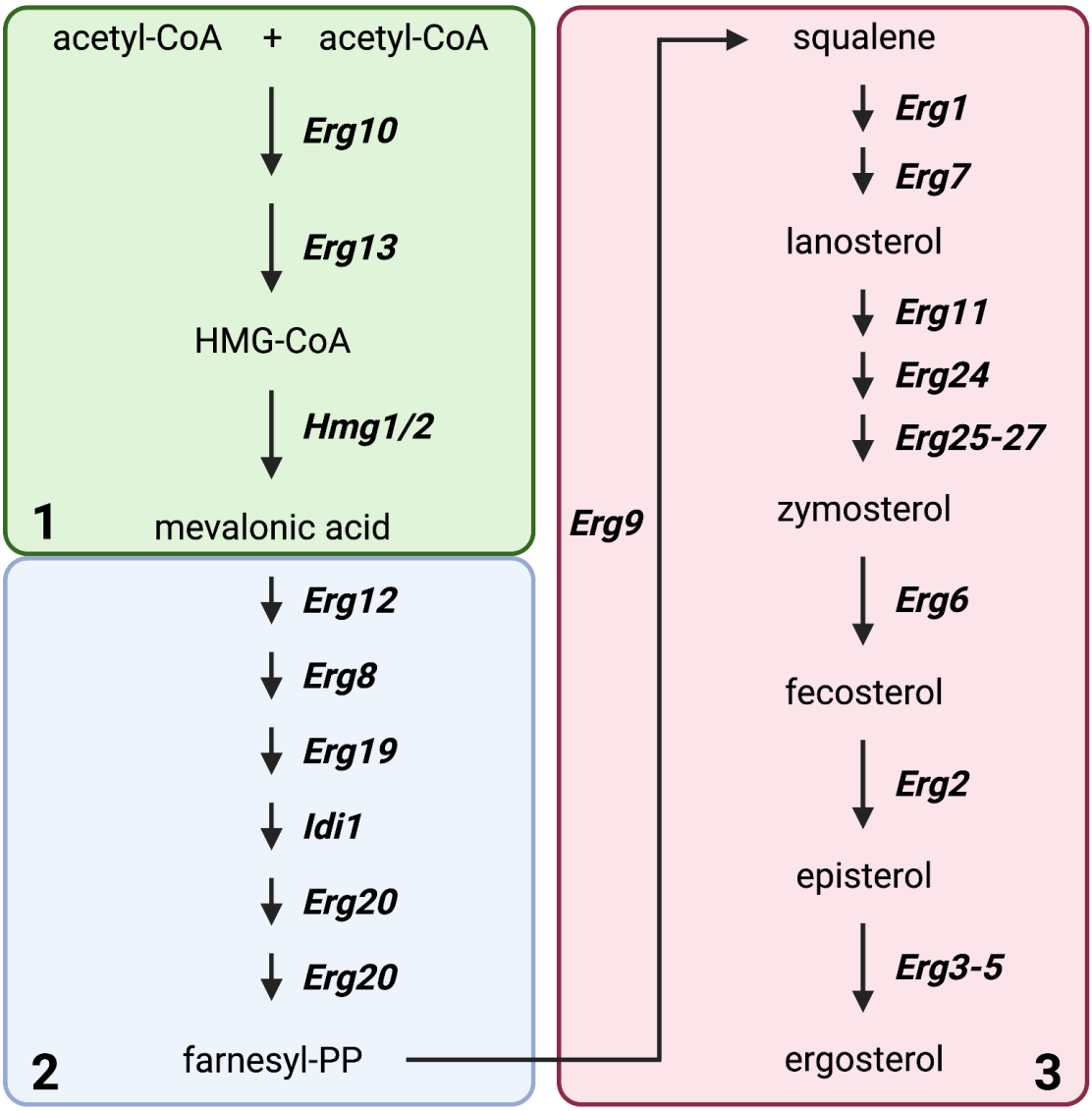

Figure 2.1 **Sterol biosynthesis occurs in three modules.** Module 1 (green) generates mevalonic acid and includes the rate-limiting HMG-CoA reduction to mevalonate. Module 2 (blue) creates farnesyl-PP, and module 3 (red) produces the main sterol ergosterol. Created with BioRender.com.

DAG is acylated both within the ER and the LD. DAG can either be acylated by the phospholipid:diacylglycerol acyltransferase Lro1 or the diacylglycerol acyltransferase Dga1. Lro1 scavenges an acyl chain from surrounding PLs to generate TAG and a lysophospholipid (LPL), while Dga1 uses acyl-CoA directly as an acyl donor (30). The level of sterol within the cell can be controlled via acylation to sterol esters (SEs), which

are generated by the acyl-CoA:sterol acyltransferases Are1 and Are2. Are1 predominantly acylates intermediates in the ergosterol synthesis pathway with a preference for lanosterol, though the protein does contribute minimally to TAG synthesis. Are2 acylates ergosterol only but is the primary sterol acyltransferase within the cell (31). The neutral lipids TAG and SE are primarily stored within the lipid droplet (LD). TAG and SE make up LDs to approximately the same extent, comprising 51% and 44% of the total weight of the organelle, respectively (32).

The lipidome is characteristically dynamic. Analysis of the lipidome across different growth phases in *S. cerevisiae* reveals temporal preference for production of certain lipid classes. During lag phase, after a culture has been diluted from stationary phase but before cellular division begins, the cells are reprogramming lipid metabolism and membrane lipids are actively being synthesized at the expense of storage lipid. During the exponential phase of growth, when cells are still dividing, storage lipid begins to re-accumulate, and finally, during stationary phase when the cells are quiescent, the storage lipid/membrane lipid proportion stabilizes (8, 33). The specificity of intracellular lipid composition is also dependent on temperature of cultivation. At low temperatures, phospholipids are enriched for unsaturated and shorter moieties. When temperature is increased, the opposite effect is seen – phospholipid total length increases, and the number of double bonds in acyl chains decreases (33).

The regulation of genes encoding enzymes in lipid biosynthetic pathways has been characterized and can offer an explanation for the dynamic nature of the lipidome. Genes involved in both *de novo* CDP-DAG based and Kennedy pathway production of PL contain a promoter sequence aptly named the inositol-sensitive upstream activating

element (UAS_{ino}), which downregulates expression in response to exogenous inositol (34). Increased levels of PA in the ER induce expression of genes with the UAS_{ino} promoter element by the sequestration of the Opi1 repressor at the ER (35). Control of membrane fluidity is primarily achieved by transcriptional and post-transcriptional control of the gene encoding the only desaturase in *S. cerevisiae*, *OLE1 (36, 37)*. *OLE1* transcription increases when the ER becomes too rigid via the release of transcription factors Mga2/Spt23 from the ER to the nucleus (38–40). Degradation of the *OLE1* mRNA transcript in response to UFA increase and ERAD-based rapid turnover of Ole1 is also responsible for control of the desaturase activity in the ER (41–43). Analysis of Ole1 levels across the different stages of growth sees an increase in both *OLE1* mRNA and Ole1 protein after a peak in SFA levels at the entry to exponential phase and a marked decrease upon entry into stationary phase (8, 44).

An important characteristic of the lipidome that has increasingly been of interest has been specificity in the composition of individual phospholipid molecules. While 70-80% of acyl chains in *S. cerevisiae* are unsaturated, PE and PC species are preferentially enriched for UFA with ~85% of the acyl chains in late exponential phase containing a double bond (8, 26). In contrast, the PI species contain a large proportion of saturated moieties with a nearly equal UFA:SFA ratio, a trend that persists through all growth phases (8, 26). A small proportion, if any, of the saturated fatty acids are incorporated at the *sn-2* position of these PLs, and the enrichment for UFA in PE and PC is reliant on synthesis through the CDP-DAG pathway (26, 45). While the lipids produced in *S. cerevisiae* contain specificity for the type and position of acyl chain incorporation, there has not been a determination of the mechanism controlling this specificity. We propose

this phenomenon is due to the capture of saturated acyl chains by Ole1, desaturation, and channeling of the substrates to specific fates through protein-protein interactions (PPIs). It has been shown that various enzymes in lipid biosynthetic pathways interact, but an interactome analysis of Ole1 has not yet been reported.

Here, we performed a coimmunoprecipitation of the desaturase Ole1, followed by LC-MS/MS to identify proteins interacting with the Δ9 desaturase. We confirmed these results and further defined the complex with a membrane yeast two hybrid (MYTH) study using Ole1 and other lipid biosynthetic enzymes as bait. We demonstrate that Ole1 interacts *in vivo* with proteins that produce a variety of different classes of lipids in a complex we have called the desaturasome.

2.3. Methods

2.3.1. Strains and Plasmids

The *S. cerevisiae* strain NMY51 was provided by Marek Michalak for the membrane yeast two-hybrid experiments. The *S. cerevisiae* strain W303 was used as the parent for the YBG2 strain. *Escherichia coli* DH5α was used in all cloning steps and to propagate all plasmids. All yeast transformations were completed with the lithium acetate method (46). Strain genotypes available in Table 2.1. All primer sequences can be found in Table 2.2. Vectors used for strain construction and purchased for MYTH are listed in Table 2.3.

Table 2.1 Strains used in this study

Strain name	Parent	Genotype	Reference
W303	-	*MATa {leu2-3,112 trp1-1 can1-100 ura3-1 ade2-1 his3-11,15} [phi+]*	(47)
NMY51	-	*MATa his3Δ200 trp1-901 leu2- 3,112 ade2 LYS2::(lexAop)4-HIS3 ura3Δ::(lexAop)8-LacZ ade2Δ::(lexAop)8-ADE2 GAL4*	Dualsystems
WOMyc	W303	*MATa {leu2-3,112 trp1-1 can1-100 ura3-1 ade2-1 his3-11,15} [phi+] OLE1::13xMyc KanMX*	This study
OLE1-Cub-LexA-VP16	NMY51	*MATa his3Δ200 trp1-901 leu2- 3,112 ade2 LYS2::(lexAop)4-HIS3 ura3Δ::(lexAop)8-LacZ ade2Δ::(lexAop)8-ADE2 GAL4 OLE1-Cub-LexA-VP16 KanMX*	This study
SLC1-Cub-LexA-VP16	NMY51	*MATa his3Δ200 trp1-901 leu2- 3,112 ade2 LYS2::(lexAop)4-HIS3 ura3Δ::(lexAop)8-LacZ ade2Δ::(lexAop)8-ADE2 GAL4 pTMBV4-SLC1*	This study
CDS1-Cub-LexA-VP16	NMY51	*MATa his3Δ200 trp1-901 leu2- 3,112 ade2 LYS2::(lexAop)4-HIS3 ura3Δ::(lexAop)8-LacZ ade2Δ::(lexAop)8-ADE2 GAL4 pTMBV4-CDS1*	This study

Table 2.2 Primers used in this study

Primer name	Primer sequence
3-Cub	CGATAAGAATTCTAATACGACTCACTATAGGG
5-Cub	CGATAAACTAGTATGGAACAAAAACTTATTTCTGAAGAAGATCTGTC GACCATGTCGG
ADH1Ps	GTTCTCGTTCCCTTTCTTCC
ARE1f	GAT GTT CCA GAT TAC GCT GGA TCC ATG ACG GAG ACT AAG GAT TTG TT
ARE1r	ACG GTA TCG ATA AGC TTG ATA TCG AAT TC TCA TAA GGT CAG GTA CAA CGT
ARE2f	GAT GTT CCA GAT TAC GCT GGA TCC ATG GAC AAG AAG AAG GAT CTA CTG
ARE2r	ACG GTA TCG ATA AGC TTG ATA TCG AAT TC TTA GAA TGT CAA GTA CAA CGT ACA CAT
BGCub3-1	CTTAGCACAAGATGTAAGGT
BGO15	TACGACTTGAAGAAATTCTCTC
CDS1f	TACCCATACGATGTTCCAGATTACGCTGGATCCATGTCTGACAACC CTGAGATG
CDS1r	GACGGTATCGATAAGCTTGATATCGAATTCTCAAGAGTGATTGGTC AATGATTT
CHO1f	GAT GTT CCA GAT TAC GCT GGA TCC ATG GTT GAA TCA GAT GAA GAT TTC G
CHO1r	ACG GTA TCG ATA AGC TTG ATA TCG AAT TC CTA TGG CTT TGG AAT TTT CAA GCT
CHO2f	GAT GTT CCA GAT TAC GCT GGA TCC ATG TCC AGT TGT AAA ACC ACT TTG
CHO2r	ACG GTA TCG ATA AGC TTG ATA TCG AAT TC TCA AGC AAG ACT ATC AAG CGT
CUBsr	TGAATGTTGTAATCAGACAGC
CYC1Ts2	CTTTTCGGTTAGAGCGGATG
DGA15	TTACGCTGGATCCATGTCAGGAACATTCAATGATAT
DGA1Nx3	TACGCTGGATCCGAAAGGCATGAGAATAAGTCT
GPT2f	TACCCATACGATGTTCCAGATTACGCTGGATCCATGTCTGCTCCCG CTGCC
GPT2r	GACGGTATCGATAAGCTTGATATCGAATTCTCATTCTTTCTTTTCGT GTTCTCTTTTCTGTCTTACCAG

Primer name	Primer sequence
HMG1f	GAT GTT CCA GAT TAC GCT GGA TCC ATG CCG CCG CTA TTC
HMG1r	ACG GTA TCG ATA AGC TTG ATA TCG AAT TC TTA GGA TTT AAT GCA GGT GAC G
LRO1f	GAT GTT CCA GAT TAC GCT GGA TCC ATG GGC ACA CTG TTT CG
LRO1r	ACG GTA TCG ATA AGC TTG ATA TCG AAT TC TTA CAT TGG GAA GGG CAT CT
Myc3s	AGC TTT TGT TCA CCG TTA
Ole1-Mycf	CTC TGC TAT TAG AAT GGC TAG TAA GAG AGG TGA AAT CTA CGA AAC TGG TAA GTT CTT TCG GAT CCC CGG GTT AAT TAA
Ole1-Mycr	AGC ATG ACT GTG AAA TTT TGA AGA GAT GCA GTA AGC CAT CCC ATA TCT ATT GCT CCA GGG CCG AAT TCG AGC TCG TTT AAA
ole1T3	AGCATGACTGTGAAATTTTGAAGAGATGCAGTAAGCCATCCCATAT CTATTGCTCCAGGGccagatctgtttagcttgc
ole1T5	CTCTGCTATTAGAATGGCTAGTAAGAGAGGTGAAATCTACGAAACT GGTAAGTTCTTTGAACAAAAACTTATTTCTG
PIS1f	GAT GTT CCA GAT TAC GCT GGA TCC ATG AGT TCG AAT TCA ACA CCA GA
PIS1r	ACG GTA TCG ATA AGC TTG ATA TCG AAT TC TCA GTA AGT CTT GTT CTT CTC GTT G
pTMBV4-CDS1f	AGCATAGCAATCTAATCTAAGTTTTCTAG ATG TCT GAC AAC CCT GAG ATG AAA CC
pTMBV4-CDS1r	CGA ATT CCT GCA GAT ATA CCC ATG GAG AGA GTG ATT GGT CAA TGA TTT CTT GGT CA
pTMBV4-SLCf	AGCATAGCAATCTAATCTAAGTTTTCTAGATGAGTGTGATAGGTAG GTTCTT
pTMBV4-SLCr	CGAATTCCTGCAGATATACCCATGGAGATGCATCTTTTTTACAGAT GAACCTT
SCT1f	TACGCTGGATCCCCTGCACCAAAACTCACG
SCT1r	CTACGCATCTCCTTCTTTCCC
SLC1f	TACGCTGGATCCAGTGTGATAGGTAGGTTCTTGTATTACT
SLC1r	GATATCGAATTCTTAATGCATCTTTTTTACAGATGAACCTTC
TEF1Ps	CTTTCGATGACCTCCCATTG

Table 2.3 Plasmids used for strain construction

Plasmid name	*S. cerevisiae* gene	Ori and selection	Source
pTMBV4	Cub-LexA-VP16	2μ LEU2	Dual Systems
pUG6	KanMX6	G418R	Euroscarf
pUG6-CLVt	Cub-LexA-VP16-KanMX6	G418R	This study
pALG5-NubG	ALG5-NubG	CEN/ARS TRP1	Dual Systems
pALG5-NubI	ALG5-NubI	CEN/ARS TRP1	Dual Systems
pADSL-Nx	NubG	CEN/ARS TRP1	Dual Systems
pAG25	NatMX6	ClonNATR	Euroscarf

To generate the *OLE1*-13xMYC (YBG2) strain, the *13xMYC* tag containing the *KanMX6* resistance marker was amplified from the *pFA6a-13Myc-KanMX6* plasmid using the Ole1-Mycf and Ole1-Mycr primers, which contain homology to *OLE1*. The resulting DNA fragment was used to transform W303. Transformants were selected on YEPD agar supplemented with 200 μg/mL geneticin and correct integration of Ole1-13xMyc was confirmed by PCR analysis of genomic DNA using oligonucleotides BGO15 and Myc3s and a western blot against the Myc epitope tag.

To produce the OLE1-Cub-LexA-VP16 strain, the *Cub-LexA-VP16* tag containing the *CYC1* terminator was amplified from plasmid pTMBV4 (Dualsystems Biotech AG, Schlieren, Switzerland) using primers 5-Cub and 3-Cub. The 5' oligonucleotide (5-Cub) included sequence to insert a single Myc epitope and SpeI cleavage site immediately upstream of the Cub sequence. The resulting DNA fragment was digested with SpeI and phosphorylated using T4 polynucleotide kinase prior to ligation with SpeI – EcoRV digested pUG6 (28) resulting in pUG6-CLVt. The *Myc-Cub-LexA-VP16-CYC1t-KanMX*

fragment was amplified from pUG6-CLVt with primers (OLE1t-5, OLE1t-3) containing homology to *OLE1*. This DNA fragment was used to transform NMY51. Transformants were selected on YEPD agar supplemented with 200 µg/mL geneticin and correct integration of *OLE1-Myc-Cub-LexA-VP16* was confirmed by PCR analysis of genomic DNA using oligonucleotides BGO15 and BGCub3-1.

To construct the bait plasmids, *pTMBV4* was digested with XbaI and NcoI. *pTMBV4* contained the 2µ origin of replication, *LEU2* selection marker, *CYC1p*, *CYC1t*, and the *Cub-LexA-VP16* tag. The *SLC1* and *CDS1* genes were amplified from W303 genomic DNA using the primers in Table 2.4, which contained homology to the *pTMBV4* plasmid. *SLC1* and *CDS1* were inserted in frame with *Cub-LexA-VP16* using Gibson isothermal assembly (48). Sequence was confirmed via the Sanger method with primers TEF1Ps and CUBsr. Plasmid *pADSL-Nx* was digested with BamHI and EcoRI. *pADSL-Nx* contained the CEN/ARS origin of replication, *TRP1* selection marker, *ADH1t*, *CYC1t*, and *NubG-HA* tag. Genes encoding the prey plasmids of interest were amplified from W303 genomic DNA using the primers in Table 2.4 and were inserted in frame with *NubG-HA* using Gibson isothermal assembly. All prey plasmids were confirmed by Sanger sequencing prior to use with primers ADH1Ps and CYC1Ts2.

To create the *SLC1*-Cub-LexA-VP16 and *CDS1*-Cub-LexA-VP16 strains, NMY51 cells were transformed with the *pTMBV4-SLC1* or *pTMBV4-CDS1* plasmids. Transformants were selected on media lacking leucine (-leu) and expression of the bait was confirmed by a western blot against the LexA domain of the protein.

Table 2.4 Plasmid construction for interaction analysis by MYTH

Plasmid name	*S. cerevisiae* gene	Primers	Ori and selection
pTMBV4-SLC1	SLC1-Cub-LexA-VP16	pTMBV4-SLC1f, pTMBV4-SLC1r	2μ LEU2
pTMBV4-CDS1	CDS1-Cub-LexA-VP16	pTMBV4-CDS1f, pTMBV4-CDS1r	2μ LEU2
NubG-SCT1	NubG-HA-SCT1	SCT1f, SCT1r	CEN/ARS TRP1
NubG-GPT2	NubG-HA-GPT2	GPT2f, GPT2r	CEN/ARS TRP1
NubG-SLC1	NubG-HA-SLC1	SLC1f, SLC1r	CEN/ARS TRP1
NubG-CDS1	NubG-HA-CDS1	CDS1f, CDS1r	CEN/ARS TRP1
NubG-PIS1	NubG-HA-PIS1	PIS1f, PIS1r	CEN/ARS TRP1
NubG-CHO1	NubG-HA-CHO1	CHO1f, CHO1r	CEN/ARS TRP1
NubG-CHO2	NubG-HA-CHO2	CHO2f, CHO2r	CEN/ARS TRP1
NubG-HMG1	NubG-HA-HMG1	HMG1f, HMG1r	CEN/ARS TRP1
NubG-DGA1	NubG-HA-DGA1	DGA15, DGA1Nx3	CEN/ARS TRP1
NubG-LRO1	NubG-HA-LRO1	LRO1f, LRO1r	CEN/ARS TRP1
NubG-ARE1	NubG-HA-ARE1	ARE1f, ARE1r	CEN/ARS TRP1
NubG-ARE2	NubG-HA-ARE2	ARE2f, ARE2r	CEN/ARS TRP1

2.3.2. Media and Cultivation Conditions

E. coli strains were cultivated in lysogeny broth (LB) containing ampicillin (100 μg/mL) or kanamycin (50 μg/mL) for plasmid maintenance. *S. cerevisiae* strains were propagated on YEPD medium (1% yeast extract, 2% peptone, 2% dextrose) or on synthetic minimal medium (0.17% Yeast Nitrogen Base without amino acids without ammonium sulfate, 0.5% ammonium sulfate, 2% dextrose), supplemented with an amino acid mixture lacking the amino acids or purines as required for selection.

2.3.3. Membrane Isolation

Membranes were isolated from YBG2 cells expressing Ole1-13xMyc and W303. Strains were cultured in YEPD until late logarithmic phase and cells were collected by centrifugation. Cell pellets were resuspended in breaking buffer (100 mM Tris HCl pH 8.5, 5 mM EDTA, 5 mM EGTA, 1 mM PMSF) and lysed by eight passes through Emulsiflex C3 at 20,000 psi (Avestin). The lysate was cleared of cell debris by centrifugation at 2,100 x g for 10 minutes at 4°C. Membranes were isolated from the cleared cell lysate by ultracentrifugation at 105,000 x g for one hour at 4°C. The resulting pellet was resuspended in breaking buffer with 0.5% Triton-X and incubated on ice with gentle agitation for 90 minutes to solubilize the membranes. This was subjected to a second ultracentrifugation at 105,000 x g for one hour at 4°C. The resulting supernatant was labeled the membrane protein fraction and used in the co-immunoprecipitation experiments.

2.3.4. Co-immunoprecipitation

Protein G beads were prepared by crosslinking the anti-Myc primary antibody as previously described (49). Prepared membrane proteins (5-10mg) were added to the beads and incubated for 2 hours at 4°C, with agitation. Membrane proteins from a strain expressing Ole1-Myc were incubated with protein G beads crosslinked to an anti-Myc antibody (Ole1-Myc^{Myc}) and with protein G beads alone (Ole1-Myc^{G}). Membranes from a W303 strain without a myc-tagged Ole1 were incubated with protein G beads crosslinked to an anti-Myc antibody (W303^{Myc}). Beads were washed in breaking buffer with 0.5% Triton-X. Proteins were eluted from the beads by the addition of SDS sample buffer (50

mM Tris-HCl pH 6.8, 2% SDS, 10% glycerol, 1 mM DTT, 12.5 mM EDTA, 0.02% bromophenol blue) and a 10-minute incubation at 85°C.

2.3.5. Mass spectrometry

Samples were electrophoresed on a 1.5 mm 10% polyacrylamide SDS gel and trypsinized in-gel. Samples were reduced (10 mM β-mercaptoethanol in 100 mM bicarbonate) and alkylated (55 mM iodoacetamide in 100 mM bicarbonate). After dehydration enough trypsin (6 ng/µl, Promega Sequencing grade) was added to just cover the gel pieces and the digestion was allowed to proceed overnight (~16 hrs.) at 37°C. Tryptic peptides were first extracted from the gel using 97% water, 2% acetonitrile, 1% formic acid followed by a second extraction using 50% of the first extraction buffer and 50% acetonitrile.

The tryptic peptides were resolved using nano flow HPLC (Easy-nLC 1000, Thermo Scientific) coupled to an Orbitrap Q Exactive mass spectrometer (Thermo Scientific) with an EASY-Spray capillary HPLC column (ES902A, 75 µm x 25 cm, 100 Å, 2 µm, Thermo Scientific). The mass spectrometer was operated in data-dependent acquisition mode with a resolution of 35,000 and *m*/*z* range of 300–1700. The twelve most intense multiply charged ions were sequentially fragmented by using HCD dissociation, and spectra of their fragments were recorded in the orbitrap at a resolution of 17,500; after fragmentation all precursors selected for dissociation were dynamically excluded for 30 s. Data was processed using Proteome Discoverer 1.4 (Thermo Scientific) and the *S. cerevisiae* proteome database was searched using SEQUEST (Thermo Scientific). Search parameters included a strict false discovery rate (FDR) of .01, a relaxed FDR of

.05, a precursor mass tolerance of 10ppm and a fragment mass tolerance of 0.01Da. Peptides were searched with carbamidomethyl cysteine as a static modification and oxidized methionine and deamidated glutamine and asparagine as dynamic modifications.

2.3.6. Mass spectrometry analysis

The proteins detected in the Ole1-Myc^{G} and W303^{Myc} negative controls were excluded and the remaining interactors identified in Ole1-Myc^{Myc} were identified with a minimum of two unique peptides. Background contaminants commonly found in affinity purification experiments and included in the Contaminant Repository for Affinity Purification Mass Spectrometry Data (CRAPome) were removed from analysis (50). The threshold for removal was four – i.e., proteins found contaminating four or more experiments published in the CRAPome were excluded from analysis. GO enrichment analysis was performed using the FunSpec web application with a threshold p-value of 0.01 (51). The ClueGO plugin in Cytoscape was utilized to determine the GO biological processes represented by the proteins copurified with Ole1 (52).

2.3.7. Membrane Yeast Two-Hybrid assay

The Ole1-Cub-LexA-VP16, Slc1-Cub-LexA-VP16, and Cds1-Cub-LexA-VP16 baits were validated by transformation with positive and negative control vectors expressing Alg5-NubI and Alg5-NubG. The concentration of 3-aminotriazole (3-AT) necessary to remove background strain growth on –his medium for the strain expressing both Slc1-Cub-LexA-VP16 and Cds1-Cub-LexA-VP16 was determined to be 5 mM, while

the strain expressing Ole1-Cub-LexA-VP16 required 6 mM 3-AT. The Ole1 bait strain was transformed with the prey plasmids and selected on synthetic minimal agar plates lacking tryptophan (-trp) to maintain the prey vectors. The Slc1 and Cds1 bait strains were transformed with the prey plasmids and selected on synthetic minimal agar plates lacking tryptophan and leucine (-leu -trp) to ensure retention of both the prey and the bait vectors. Interactions between Ole1 and prey were assayed on synthetic minimal agar plates lacking tryptophan and histidine supplemented with 6 mM 3-AT (low stringency) and synthetic minimal agar plates lacking tryptophan, histidine, and adenine supplemented with 6 mM 3-AT (high stringency). Interactions between Slc1 and Cds1 and the various prey were assayed on synthetic minimal agar plates lacking leucine, tryptophan, and histidine, supplemented with 5 mM 3-AT (low stringency) and synthetic minimal agar plates lacking leucine, tryptophan, histidine, and adenine, supplemented with 5 mM 3-AT (high stringency). Spot assays for all strains were performed by spotting cultures serially diluted 1:10 starting from $1.0x10^4$ cells.

LacZ expression was assayed via β-galactosidase assay. Strains were cultured in -trp or -leu -trp liquid media overnight at 30°C with agitation. For the Ole1 bait strain, OD_{600} of the culture was measured and recorded prior to collection of the cells. For the Slc1 and Cds1 bait strains, cells were harvested by centrifugation and resuspended in Z-buffer (60 mM Na_2HPO_4, 40mM NaH_2PO_4, 10 mM KCl, 1 mM $MgSO_4$), and OD_{600} of resuspended cells was measured and recorded. SDS was added to a concentration of 0.01% and cells were lysed by vortexing. Chloroform was added and the mixture was vortexed before adding ortho-Nitrophenyl-β-galactoside (ONPG) at a concentration of 0.72 μg/μL. The reaction mixture was incubated at 37°C until colour development and the reaction was

quenched by addition of Na_2CO_3 to a final concentration of 0.44 M. Reactions were centrifuged to remove cell debris and the colour development was assayed by measuring OD_{420}. β-galactosidase activity was normalized to the positive control, Alg5-NubI.

2.3.8. Statistical analyses

The data are presented as mean values and error bars reflect standard deviation. All n values are indicated in the figure legends. Statistical significance was evaluated by paired, two-tailed t-test. Statistical significance is noted in the text. P values < 0.05 are considered significant.

2.4. Results

2.4.1. Ole1 interacts with enzymes from storage lipid, phospholipid, and sterol synthesis in late logarithmic phase of growth

An immunoprecipitation for Ole1 revealed 101 unique interacting proteins. An analysis of the GO clusters of interactor intracellular location using FunSpec indicated that many of the interactors were located in the ER (GO:0005783, $p \leq 1.00E^{-14}$), and that of the 101 interactors, 84 are membrane proteins (GO:0016020, $p \leq 1.00E^{-14}$) (Table 2.5) (51). Of note, proteins precipitated by Ole1 are also localized to the mitochondrial outer membrane (GO:0005741, $p = 1.19E^{-07}$), plasma membrane (GO:0005886, $p = 1.87E^{-05}$), Golgi apparatus (GO:0005794, $p = 1.89E^{-05}$), and lipid droplet (GO:0005811, $p = 0.0028128$). The percent of the GOterm category associated genes that are identified

interactors can be seen in Table 2.5, % associated genes. Of the total 101 interactors, 33 are essential for survival.

Table 2.5 Ole1 interactors by cellular component as determined by FunSpec.

Category	p-value	# genes identified	% associated genes
endoplasmic reticulum [GO:0005783]	1.00E-14	36	8.7
CDS1 SSH1 YBR287W TSC13 YET3 LCB2 DPL1 GPI17 WBP1 CHO1 ERG4 ALG2 EMP24 ORM1 ERV29 ERG11 MSC7 EPS1 CBR1 OST1 STE24 MCD4 YPT52 ERG3 SEC61 HMG1 PGA3 ERG5 ERG2 SCS7 ALG9 ARE2 PEX11 SEY1 PIS1 DPM1			
membrane [GO:0016020]	1.00E-14	84	5.0
CHS3 CDS1 RFS1 ECM33 PHO88 RIM2 SSH1 YBR287W YCP4 TSC13 SLC1 YET3 YDL119C GGC1 TIM22 LCB2 SEC26 HXT7 GPI17 GNP1 WBP1 RIP1 CHO1 FCY2 FMP10 PMC1 ERG4 ALG2 SEC27 PMR1 EMP24 ORM1 TOM20 CHO2 ERV29 ERG11 HXT1 EPS1 CBR1 AVT7 COA1 OST1 STE24 PTM1 YKL100C MCD4 YPT52 PET10 PTR2 ERG3 CCC1 YPT6 SEC61 TCB3 HMG1 PHO84 PGA3 HXT2 YTA12 HFD1 AIM36 ERG2 YMR221C YHM2 ZRC1 SCS7 RAS2 TOM70 TOM22 ALG9 LYP1 SEC21 TIM23 ARE2 YNR065C YOL092W PEX11 TCB1 VPS21 SEY1 PDR12 PIS1 RHO1 DPM1			
endoplasmic reticulum membrane [GO:0005789]	7.17E-13	26	8.2
CDS1 SSH1 TSC13 YET3 GPI17 WBP1 ALG2 EMP24 ORM1 ERV29 EPS1 CBR1 OST1 STE24 MCD4 ERG3 SEC61 HMG1 PGA3 ERG2 SCS7 ALG9 ARE2 SEY1 PIS1 DPM1			
mitochondrial outer membrane [GO:0005741]	1.19E-07	11	12.0
CHO1 TOM20 CBR1 STE24 HFD1 TOM70 TOM22 VPS21 PIS1 RHO1 DPM1			
plasma membrane [GO:0005886]	1.87E-05	17	4.9
ECM33 HXT7 GNP1 FCY2 HXT1 AVT7 YPT52 PTR2 YPT6 TCB3 PGA3 HXT2 RAS2 LYP1 TCB1 PDR12 RHO1			
Golgi apparatus [GO:0005794]	1.89E-05	13	6.1
SEC26 SEC27 PMR1 EMP24 MTC1 MNN5 PTM1 MCD4 CCC1 YPT6 SEC21 PIS1 RHO1			
COPI vesicle coat [GO:0030126]	0.00018401	3	37.5
SEC26 SEC27 SEC21			
lipid particle [GO:0005811]	0.0028128	4	10.3
SLC1 PET10 HFD1 FAA4			

Analysis of Ole1 interactors by FunSpec is limited in its ability to generate images, so additional analysis of Ole1 interactors was performed using ClueGO in Cytoscape (52). Interactors were identified throughout many different GO biological categories, including the ergosterol biosynthesis and phospholipid biosynthetic processes (Table 2.6). The cellular lipid metabolic process (GO:0044255, $p = 1.13E^{-09}$), transmembrane transport (GO:0055085, $p = 3.90E^{-07}$), and the lipid biosynthetic process (GO: 0008610, $p = 9.28E^{-07}$) were the most significant broad biological processes carried out by the desaturase interactors (Table 2.6, Figure 2.2A). These group into two main categories of biological processes: transport of proteins and organic substances, and lipid metabolism (Figure 2.2A). Of all the proteins identified, 25.7% are involved in the cellular lipid metabolic process, 27.7% are involved in transmembrane transport, and 17.8% are within the lipid biosynthetic process. These make up 8.1%, 5.8%, and 8.6% of the genes within each GOterm, respectively (Table 2.6, % associated genes).

Table 2.6 Ole1 interactors by biological process as determined by ClueGO

Category	p-value	# genes identified	% associated genes
cellular lipid metabolic process [GO:0044255]	1.13E-09	26	8.1
ALG2, ALG9, ARE2, CDS1, CHO1, CHO2, DPL1, DPM1, ERG11, ERG2, ERG3, ERG4, ERG5, FAA4, GPI17, HMG1, LCB2, MCD4, ORM1, PEX11, PIS1, SCS7, SLC1, TCB1, TCB3, TSC13			
transmembrane transport [GO:0055085]	3.90E-07	28	5.8
AVT7, CCC1, FCY2, FMP42, GGC1, GNP1, HEM25, HXT1, HXT2, HXT7, LYP1, PDR12, PHO84, PMC1, PMR1, RIM2, RIP1, SEC61, SSH1, TIM22, TIM23, TOM20, TOM22, TOM70, YBR287W, YPQ1, YTA12, ZRC1			
lipid biosynthetic process [GO:0008610]	9.28E-07	18	8.6
CDS1, CHO1, CHO2, DPM1, ERG11, ERG2, ERG3, ERG4, ERG5, GPI17, HMG1, LCB2, MCD4, ORM1, PIS1, SCS7, SLC1, TSC13			
ergosterol metabolic process [GO:0008204]	8.29E-05	7	21.2
ARE2, ERG11, ERG2, ERG3, ERG4, ERG5, HMG1			
transport [GO:0006810]	1.64E-04	46	3.3
AVT7, CCC1, DPL1, EMP24, ERV29, FAA4, FCY2, FMP42, GGC1, GNP1, HEM25, HXT1, HXT2, HXT7, LYP1, MCD4, PDR12, PGA3, PHO84, PHO88, PMC1, PMR1, PTR2, RAS2, RHO1, RIM2, RIP1, SEC21, SEC26, SEC27, SEC61, SSH1, TIM22, TIM23, TOM20, TOM22, TOM70, VPS21, YBR287W, YET3, YHM2, YPQ1, YPT52, YPT6, YTA12, ZRC1			
organic substance transport [GO:0071702]	2.28E-06	36	3.7
AVT7, DPL1, EMP24, FAA4, FCY2, GGC1, GNP1, HEM25, HXT1, HXT2, HXT7, LYP1, MCD4, PDR12, PGA3, PMR1, PTR2, RAS2, RIM2, SEC21, SEC26, SEC27, SEC61, SSH1, TIM22, TIM23, TOM20, TOM22, TOM70, VPS21, YET3, YHM2, YPQ1, YPT52, YPT6, YTA12			
phospholipid metabolic process [GO:0006644]	2.05E-04	13	8.2
CDS1, CHO1, CHO2, DPL1, DPM1, GPI17, HMG1, MCD4, PIS1, SCS7, SLC1, TCB1, TCB3			
single-organism biosynthetic process [GO:0044711]	5.42E-03	27	3.8
ALG2, ALG9, CDS1, CHO1, CHO2, CHS3, DPM1, ERG11, ERG2, ERG3, ERG4, ERG5, GFA1, GGC1, GPI17, GRS1, HEM25, HMG1, LCB2, MCD4, ORM1, PIS1, RAS2, RHO1, SCS7, SLC1, TSC13			
organic acid transport [GO:0015849]	6.93E-03	7	10.9
AVT7, FAA4, GNP1, HEM25, LYP1, PDR12, YPQ1			

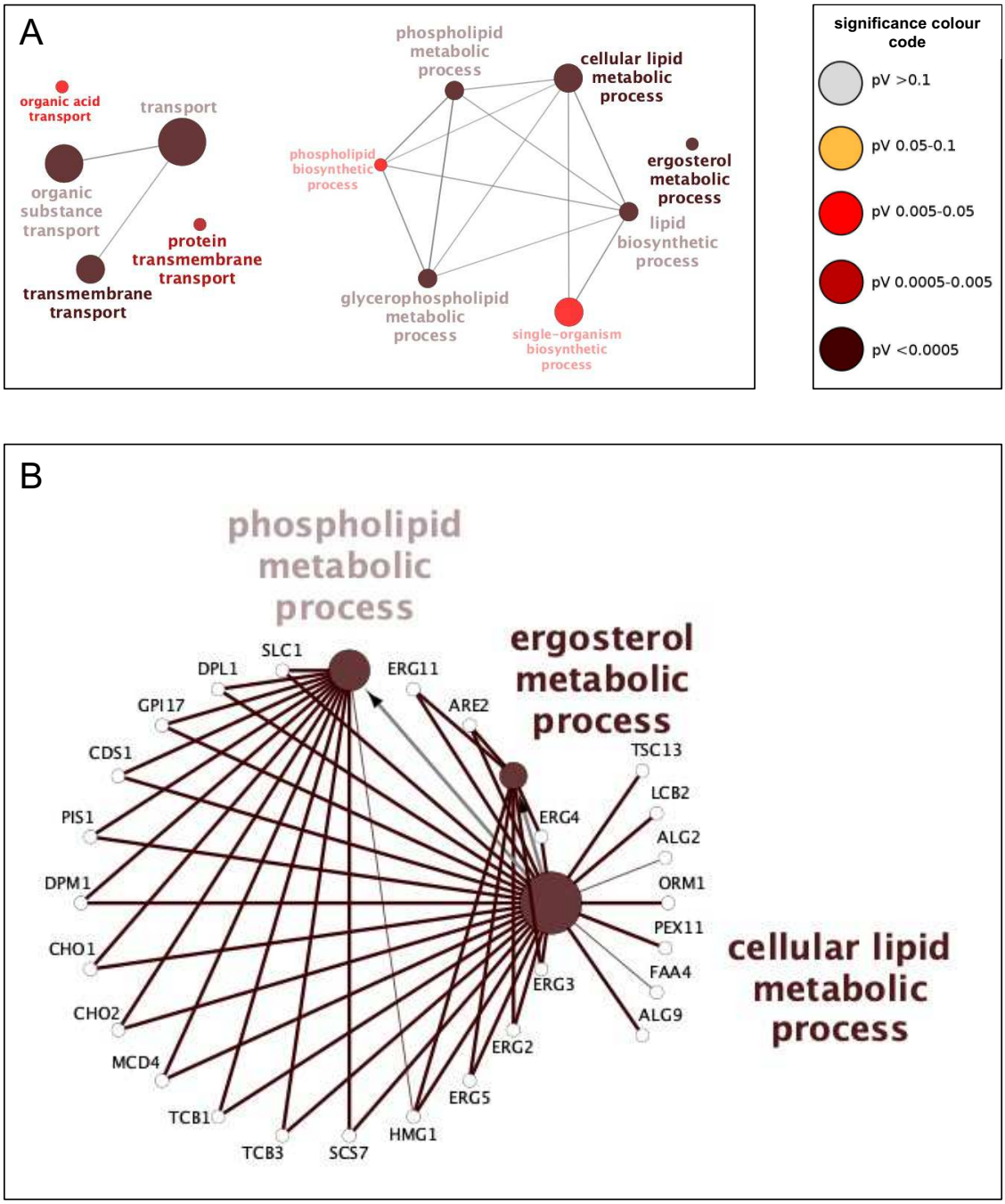

Figure 2.2 **Ole1 interactors act in two main GO biological processes: transport and lipid metabolism.** A. Map of GO biological processes identified by ClueGO analysis of Ole1 interactors. GOterm nodes are coloured according to p-value as in significance colour code insert and sized according to relative number of genes identified in category. Connected nodes are related GOterms. B. Map of interactors from the cellular lipid metabolic, ergosterol metabolic, and phospholipid metabolic processes by gene. GOterm nodes are coloured and sized as in A. Gene nodes are connected to related GO biological processes.

Analysis continued with the proteins of interest in the phospholipid, ergosterol, and cellular lipid metabolic processes (Figure 2.2B, Table 2.7). Twenty-one interactors are involved in lipid anabolic pathways, two are found within lipid catabolic pathways, two are responsible for ER-PM tethering, and one regulates lipid homeostasis. Of the twenty-three metabolic enzymes, only four are known to use fatty acyl-CoA, and of those, three utilize an unsaturated fatty acyl-CoA as a substrate: the acyl-CoA:lysophosphatidic acid acyltransferase Slc1, the acyl-CoA:sterol acyltransferase Are2, and the enoyl reductase Tsc13. The serine palmitoyltransferase component Lcb2 uses the saturated palmitoyl-CoA as a substrate only. One protein, Faa4, generates fatty acyl-CoA that has the potential to be used as a substrate by Ole1. Of the physical interactions with Ole1 found in this study, only interactions with Erg5 and Erg11 have been previously reported in the Saccharomyces Genome Database (SGD) via BioGRID (53–55). Of the proteins involved in PL, TAG, and SE synthesis, we identified Slc1, Cds1, Pis1, Cho1, Cho2, Hmg1, and Are2.

Table 2.7 Ole1 interactors of interest

Pathway	Gene	Protein	Uses acyl-CoA
Lipid anabolism	Slc1	1-acyl-sn-glycerol-3-phosphate acyltransferase	✓
	Gpi17	Subunit of glycosylphosphatidylinositol transamidase	
	Cds1	Phosphatidate cytidylyltransferase	
	Pis1	Phosphatidylinositol synthase	
	Dpm1	Dolichol phosphate mannose (Dol-P-Man) synthase	
	Cho1	Phosphatidylserine synthase	
	Cho2	Phosphatidylethanolamine methyltransferase	
	Mcd4	Mannose-ethanolamine phosphotransferase	
	Scs7	Sphingolipid alpha-hydroxylase	
	Hmg1	HMG-CoA reductase	
	Erg5	C-22 sterol desaturase	
	Erg2	C-8 sterol isomerase	
	Erg3	C-5 sterol desaturase	
	Erg4	C-24(28) sterol reductase	
	Are2	Acyl-CoA:sterol acyltransferase	✓
	Erg11	Lanosterol 14-alpha-demethylase	
	Tsc13	Enoyl reductase	✓
	Lcb2	Component of serine palmitoyltransferase	✓
	Alg2	Glycolipid mannosyltransferase	
	Faa4	Long chain fatty acyl-CoA synthetase	
	Alg9	Dol-P-Man-dependent alpha-1,2 mannosyltransferase	
Lipid catabolism	Dpl1	Dihydrosphingosine phosphate lyase	
	Pex11	Peroxin required for medium-chain fatty acid oxidation	
ER-PM tethering	Tcb1	Lipid-binding ER tricalbin	
	Tcb3	Lipid-binding ER tricalbin	
Lipid homeostasis	Orm1	Subunit of the serine palmitoyltransferase SPOTS complex	

2.4.2. Ole1 interacts closely with enzymes from phospholipid and storage lipid synthesis

Determining the proteins interacting with Ole1 via only affinity purification would miss those proteins transiently interacting with the desaturase or in very low abundance in the cell. Another limitation of AP is the inability to discern between proteins present within the same complex as Ole1 and proteins in close proximity to the desaturase. To determine transient interactions excluded from detection by the AP and to separate co-complexed proteins from physical interactors, we used the membrane yeast two-hybrid method (MYTH). As our interest was in determining interactions between ER-resident Ole1 and proteins in phospholipid and storage lipid production, we chose ER-localized prey from the PL, TAG, and SE pathways.

MYTH is a protein complementation assay that adapts the split-ubiquitin system of PPI analysis for membrane-bound proteins (56, 57). Briefly, a prey protein of interest is tagged with a low affinity mutant (I13G) of the N-terminal half of ubiquitin (NubG). The bait protein is tagged with the C-terminus of ubiquitin (Cub) and a reporter transcription factor (Figure 2.3A). The transcription factor utilized in this study consisted of the *E. coli* DNA-binding protein LexA fused to the VP16 activation domain from the herpes simplex virus. The two halves of the ubiquitin molecule form pseudo-ubiquitin when the two proteins come into proximity. Ubiquitin-specific proteases (UBPs) recognize the pseudo-ubiquitin moiety, cleaving LexA-VP16 and allowing its translocation to the nucleus (Figure 2.3A). The transcription factor activates reporter genes (*HIS3, ADE2, LacZ*), allowing growth on media lacking histidine and adenine and expression of β-galactosidase (58) (Figure 2.3B).

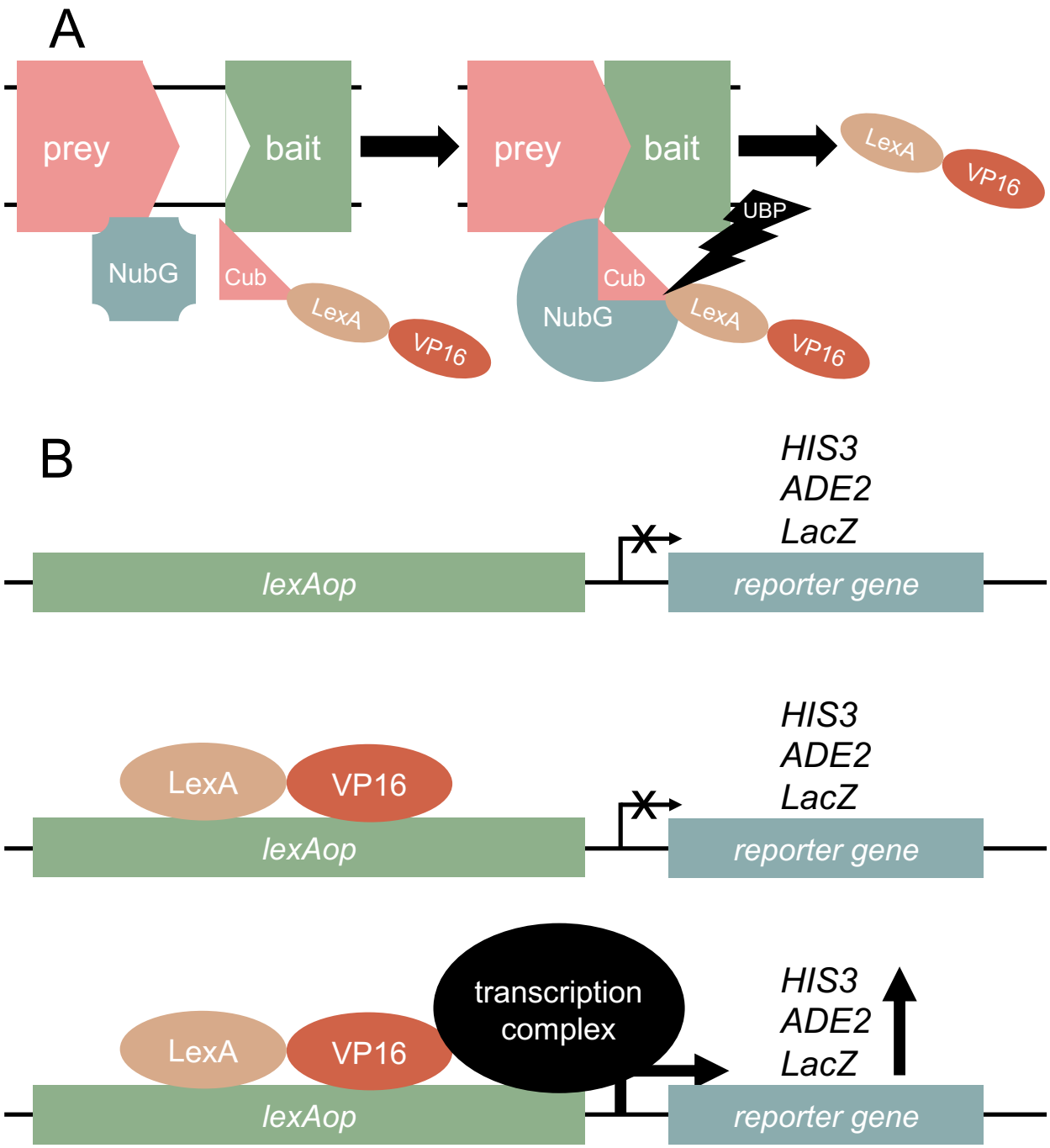

Figure 2.3 **Schematic of the membrane-yeast two hybrid system used in the current study.** A. The prey membrane protein is tagged with NubG and the bait membrane protein is fused to Cub-LexA-VP16. If the two proteins interact, NubG and Cub reconstitute to form pseudo-ubiquitin, which is recognized by UBPs that liberate the transcription factor LexA-VP16. B. Inside the nucleus, the *HIS3*, *ADE2*, and *LacZ* genes are under control of the *lexAop* from *E. coli*. LexA binds *lexAop* and VP16 recruits the transcription complex. The reporter genes are not transcribed without the LexA-VP16 transcription factor and are thus reliant on interaction between the bait and prey proteins in A.

As MYTH is a type of protein-fragment complementation assay reliant on cytosolic UBPs, it is important that both of the tags reside on the cytosolic side of the ER (59). The N-termini of the Slc1, Cds1, Cho2, Hmg1, Are1, and Are2 prey proteins are proposed to be cytosolic, while the N-termini of Pis1, Cho1, Lro1, and Dga1 have all been experimentally determined to be cytosolic (60–63). Ole1 retains a high degree of similarity to the mammalian stearoyl-CoA desaturases (SCD1s) (37). Recently, the structure of the rat SCD1 was solved, demonstrating a dual cytosolic topology of either terminus (64, 65). Consequently, we generated an Ole1 bait protein tagged on the C-terminus and a series of prey proteins tagged on the N-termini. As cells are sensitive to desaturase dosage and will degrade excess Ole1, overexpressing the bait fusion using plasmid-borne MYTH led to high amounts of autoactivation (43). Thus, we introduced the bait tag into the endogenous *OLE1* coding sequence in NMY51, which allowed the fusion to be expressed at native levels and reduced background activation in an integrated MYTH (iMYTH) study. The resulting Ole1 bait strain (YBG1) was transformed with negative and positive control vectors *pALG5-NubG* and *pALG5-NubI* alongside prey constructs expressing the proteins listed in Table 2.4. The Ole1 bait strain coexpressing positive prey protein Alg5-NubI demonstrated rapid growth on both low and high stringency media, while the strain coexpressing negative control Alg5-NubG exhibited no growth (Figure 2.4A). This confirmed that the *HIS3* and *ADE2* reporter genes were transcribed when Ole1-Cub-LexA-VP16 was expressed alongside the positive control prey, indicating an interaction between the two proteins and proper functioning of the system.

Expression of the phospholipid synthesizing enzymes NubG-Gpt2, NubG-Slc1, NubG-Cds1, NubG-Pis1, and NubG-Cho1 alongside Ole1 bait permitted growth on low

and high stringency media (Figure 2.4A). Analysis of the *LacZ* reporter gene activation by β-galactosidase assay confirmed a robust and significant amount of reporter gene expression for these prey constructs over the negative control (p = 3.86E^{-05}, 0.006, 2.48E^{-05}, 0.0011, 0.0094, respectively) (Figure 2.4B). While coexpression of bait Ole1 with preys NubG-Sct1 and NubG-Cho2 did not permit dense growth on selective media, β-galactosidase activity was significantly higher than the negative control (p = 0.003, 0.03, respectively). It is important to mention that Sct1 overexpression in certain strains can reduce growth on plates, limiting the interpretation of the growth data using NubG-Sct1 as prey in this system (66). As the β-galactosidase activity is normalized to the growth of each strain, the *LacZ* activation data is a better indicator of interactions between the prey Sct1 and bait strains. Coexpression of bait Ole1 and prey NubG-Hmg1 did not support growth on selective media or increase *LacZ* activation over the negative control (Figure 2.4). These data indicate that Ole1 interacts with the phospholipid synthesizing proteins Gpt2, Slc1, Cds1, Pis1, and Cho1.

Strains expressing prey from the storage lipid synthesis pathways with Ole1-Cub-LexA-VP16 grew on both low and high stringency plates (Figure 2.4A). Coexpression of NubG-Dga1, NubG-Lro1, NubG-Are1, and NubG-Are2 all significantly increased β-galactosidase activity over the negative control (p = 3.07E^{-08}, 0.0001, 1.81E^{-06}, 1.74E^{-09}, respectively) (Figure 2.4B). The desaturase interacts not only with enzymes from phospholipid synthesis, but the four storage lipid synthesizing acyltransferases as well (Figure 2.5).

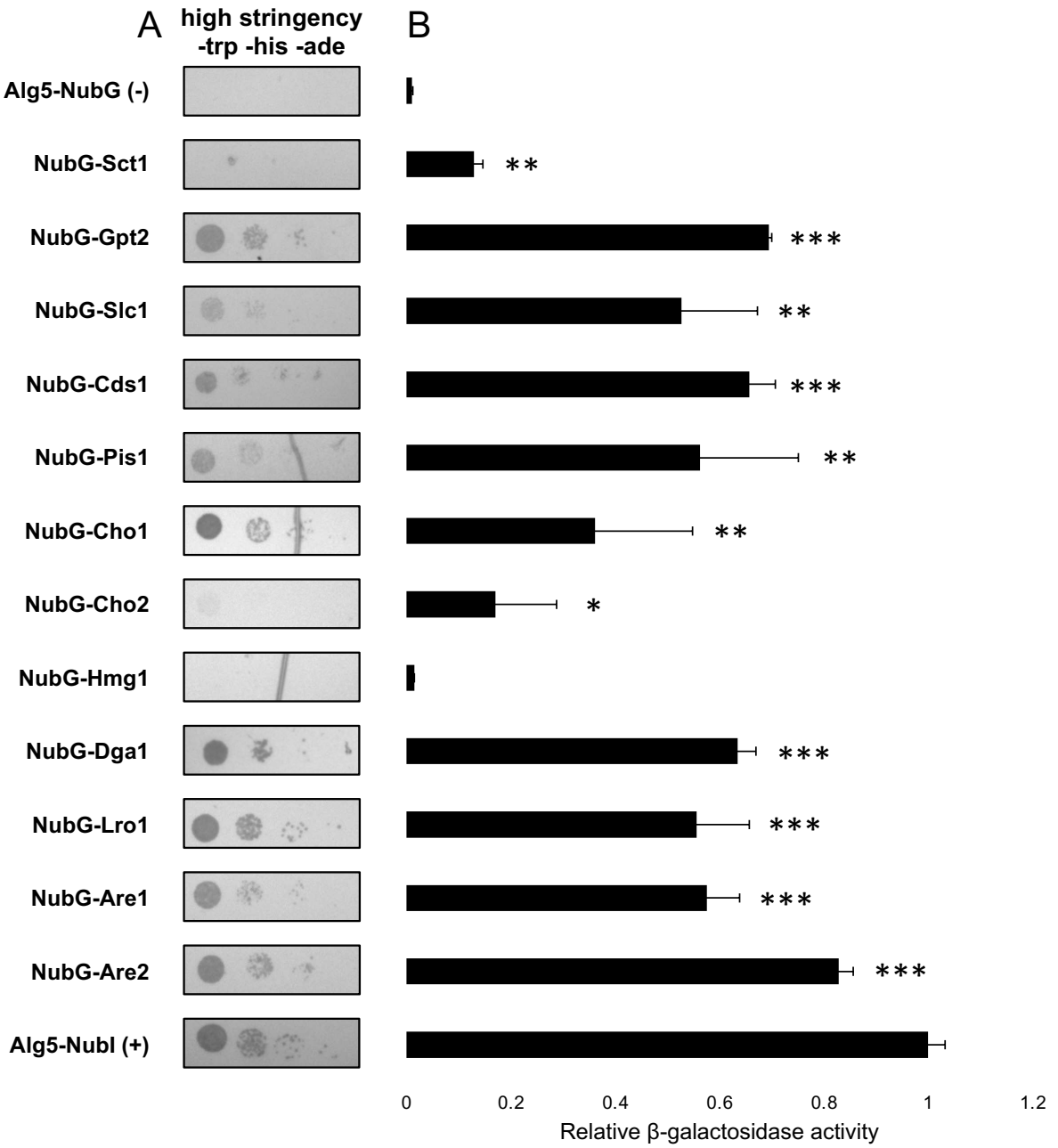

Figure 2.4 **Ole1 interacts with proteins that produce triacylglycerol, sterol ester, and membrane-bound phospholipid.** A. Integrated membrane yeast 2-hybrid assay using a yeast strain expressing endogenously tagged Ole1-Myc-Cub-LexA-VP16 and the indicated constructs. Growth on high stringency (lacking tryptophan, histidine, and adenine, containing 6 mM 3-AT) plates. Images are representative of three separate experiments (n = 3). B. β-galactosidase assay of a yeast strain expressing Ole1-Myc-Cub-LexA-VP16 and the indicated constructs. Each column is representative of three biological replicates (n = 3). Miller units were normalized to the positive control (Alg5-NubI). (* = $p < 0.05$, ** = $p < 0.01$, *** = $p < 0.001$).

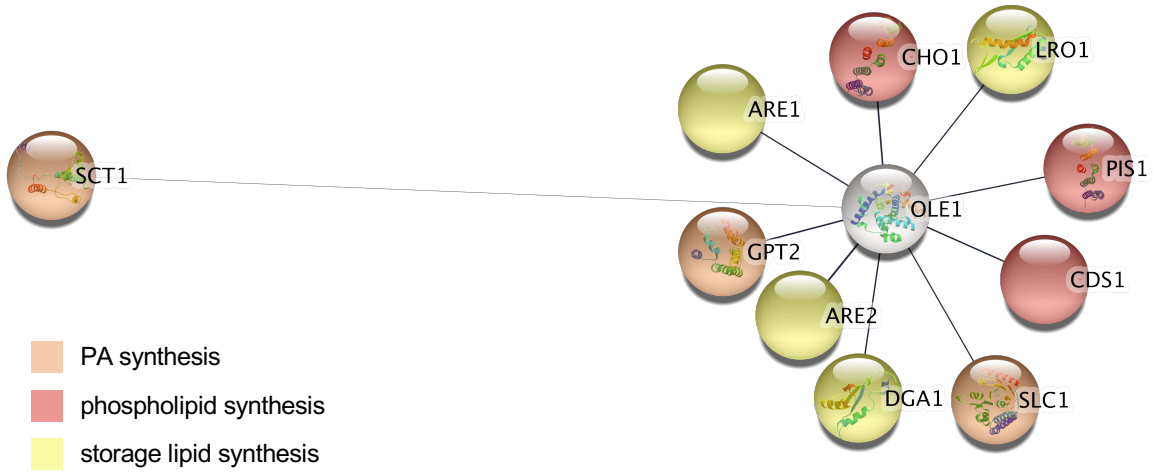

Figure 2.5 **Ole1 interactome network map as determined by iMYTH.** Map of the desaturasome interactions determined by the MYTH assay. Nodes are colored according to synthesis pathway. Edge thickness and length determined by LacZ reporter gene activation as determined by β-galactosidase assay.

2.4.3. Slc1 interacts strongly with phospholipid and storage lipid synthesizing enzymes

The PA generated by Slc1 can either be directed toward phospholipid production by Cds1 or TAG synthesis by Pah1. To gain further insight into the composition of the desaturasome, we chose Slc1 as bait and determined the interactors using the MYTH assay. Coexpression of NubG-Gpt2, NubG-Cds1, NubG-Pis1, NubG-Cho1, and NubG-Cho2 as prey with Slc1-Cub-LexA-VP16 permitted growth on low and high stringency plates, and significantly increased the *LacZ* activation over Alg5-NubG (p = 1.62E^{-06}, 0.00024, 0.00027, 0.00011, 0.001, respectively) (Figure 2.6). NubG-Cds1 and NubG-Cho1 displayed a more robust *LacZ* reporter activation with a β-galactosidase activity at 80% of the positive control, and NubG-Gpt2, NubG-Pis1, and NubG-Cho2 at

approximately 45% of the positive control. Expression of NubG-Sct1 in this system did not permit growth on selective plates but did exhibit a slight increase in β-galactosidase activity when assayed (p = 0.0082). The coexpression of NubG-Hmg1 and Slc1-Cub-LexA-VP16 was not sufficient to allow growth on selective plates or demonstrate a significant increase in β-galactosidase activity over the negative control (Figure 2.6).

Interaction analysis was also performed between Slc1 and the four storage lipid synthesizing acyltransferases. Coexpression of Slc1-Cub-LexA-VP16 with NubG-Dga1, NubG-Lro1, NubG-Are1, and NubG-Are2 supported growth on both low and high stringency selective plates (Figure 2.6A). While all four prey proteins significantly activated the *LacZ* reporter gene (p = $1.54E^{-07}$, 0.0035, 0.014, 0.0012), NubG-Dga1 and NubG-Are2 exhibited a stronger response to coexpression with Slc1-Cub-LexA-VP16 with a β-galactosidase expression nearly at the level of the positive control (91.4% and 102.1% respectively) (Figure 2.6B). The LPAAT Slc1 interacts with both phospholipid and storage lipid synthesizing enzymes (Figure 2.7).

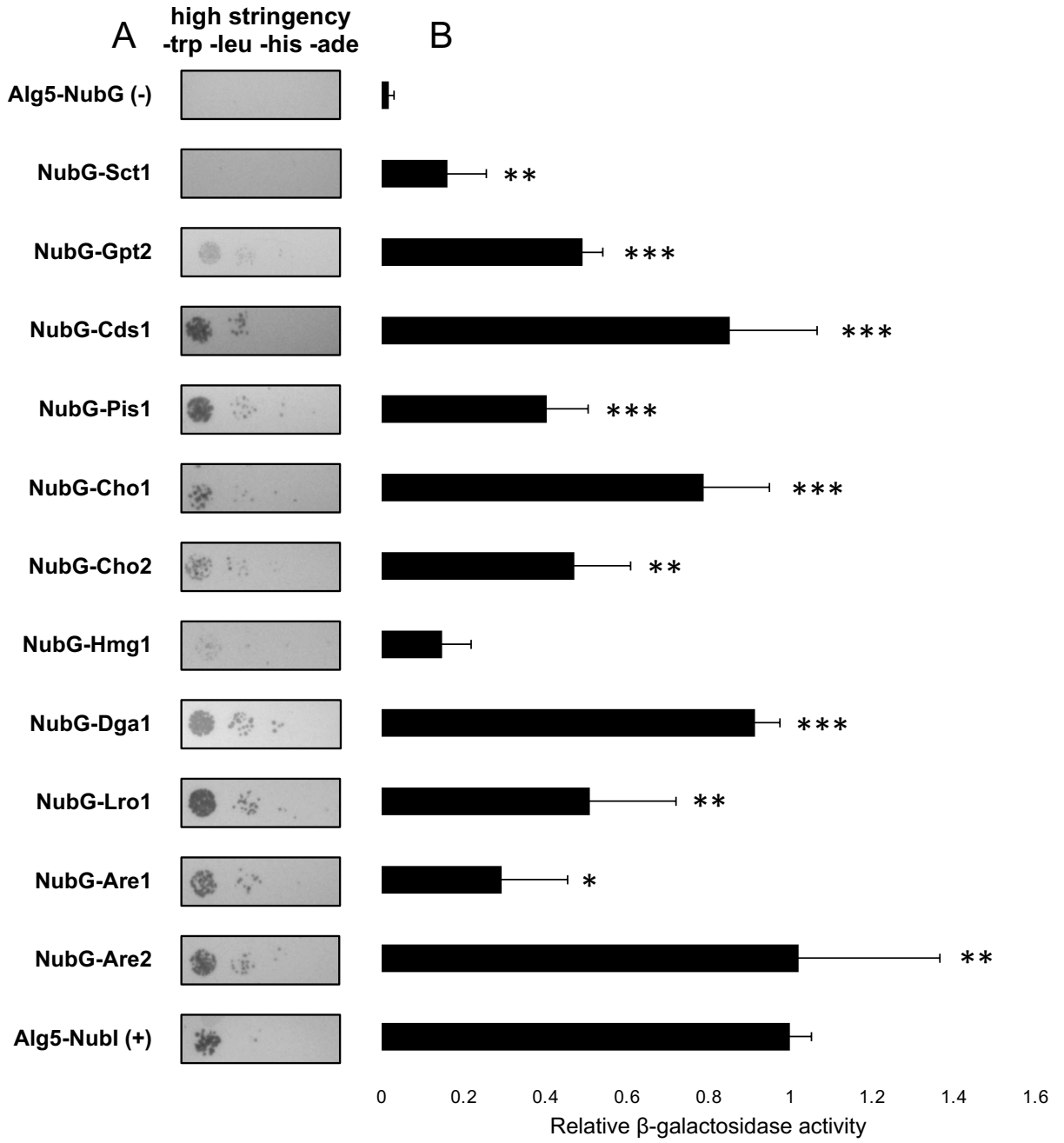

Figure 2.6 **Slc1 interacts with proteins that generate glycerophospholipid, sterol, glycerolipid, and sterol ester.** A. Membrane yeast 2-hybrid assay using a yeast strain expressing Slc1-Cub-LexA-VP16 and the indicated constructs. Growth on high stringency (lacking tryptophan, leucine, histidine, and adenine, containing 5 mM 3-AT) plates. Images are representative of three separate experiments (n = 3). B. β-galactosidase assay of a yeast strain expressing Slc1-Cub-LexA-VP16 and the indicated constructs. Each column is representative of three biological replicates (n = 3). Miller units were normalized to the positive control (Alg5-NubI). (* = $p < 0.05$, ** = $p < 0.01$, *** = $p < 0.001$).

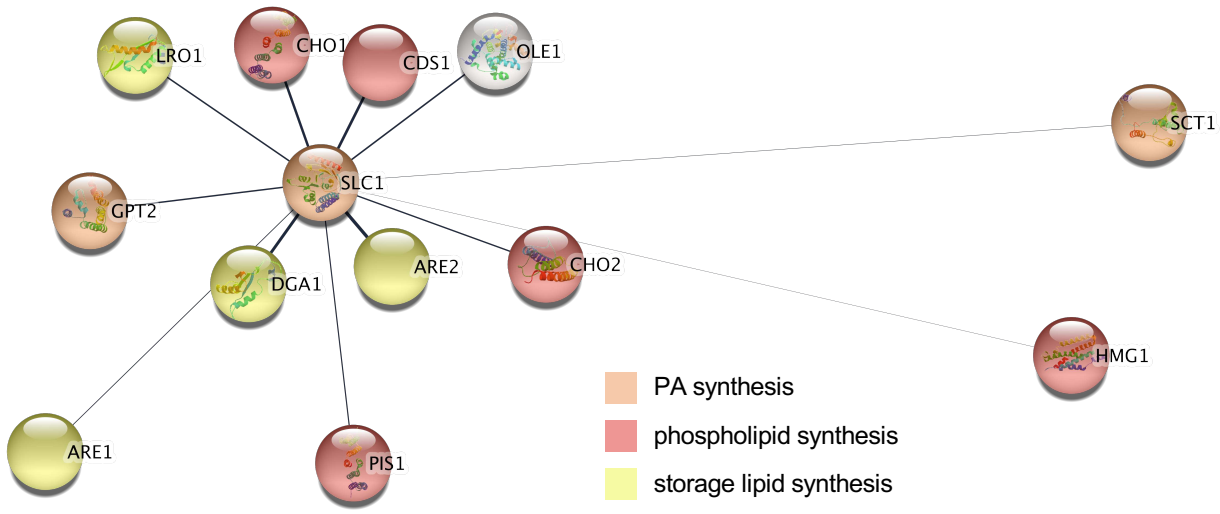

Figure 2.7 **Slc1 interactome network map as determined by iMYTH.** Map of interactions with the main LPAAT Slc1 as determined by the MYTH assay. Nodes are colored according to synthesis pathway. Edge thickness and length determined by LacZ reporter gene activation as determined by β-galactosidase assay.

2.4.4. Cds1 interacts with storage lipid and phospholipid synthesizing enzymes

Contrary to the other bait proteins analyzed, Cds1 generates a precursor specific to phospholipid synthesis. Determining interactors of the protein, which generates CDP-DAG from the branch point substrate PA, could provide a greater understanding into the composition and architecture of the desaturasome within the ER. Coexpression of Cds1-Cub-LexA-VP16 with the prey constructs revealed novel interactors with the CDP-DAG synthase. Of the prey in membrane lipid synthesis, NubG-Gpt2, NubG-Slc1, NubG-Pis1, NubG-Cho1, and NubG-Cho2 were found to interact with Cds1-Cub-LexA-VP16 (Figure 2.8). NubG-Gpt2, NubG-Pis1, and NubG-Cho1 activated the *LacZ* gene significantly, to 77.8%, 75.1%, and 62.4% of the positive control, respectively (p = 2.57E^{-09}, 1.20E^{-05},

2.77E^{-07}). Both strains exhibited robust growth on high stringency media, confirming the interactions seen by β-galactosidase assay (Figure 2.8A). Coexpression of NubG-Slc1 and NubG-Cho2 alongside Cds1-Cub-LexA-VP16 permitted growth on selective media and exhibited significant amounts of β-galactosidase activity over the negative control (p = 0.0093, 5.47E^{-05}, respectively). Though expressing NubG-Hmg1 in this system supported growth on high stringency plates, confirmation of the interaction by assaying *LacZ* activation revealed no significant increase over the negative control. Coexpressing NubG-Sct1 and Cds1-Cub-LexA-VP16 did not support growth on selective media or exhibit any significant β-galactosidase activity (Figure 2.8). Overall, this experiment demonstrated Cds1 interacts with proteins in upstream and downstream lipid synthesis.

An assay of interaction between Cds1-Cub-LexA-VP16 and NubG-Dga1, NubG-Lro1, NubG-Are1, and NubG-Are2 demonstrated that Cds1 interacts strongly with all four acyltransferases. Coexpression of all four prey alongside the Cds1 bait construct supported growth on high stringency plates (Figure 2.8A). The strains containing NubG-Dga1 and NubG-Are1 significantly activated the *LacZ* reporter over the negative control, at 38.2% and 49.5% of the positive control, respectively (p = 5.2E^{-05}, 0.001). The expression of NubG-Lro1 and NubG-Are2 in this system exhibited significant and robust β-galactosidase activity, an activation at 96.2% and 69.3% relative to the positive control (p = 3.8E^{-05}, 0.0004) (Figure 2.8B). We have determined that the CDP-DAG synthase exhibits a set of strong interactions with the acyltransferases that generate neutral lipid (Figure 2.9).

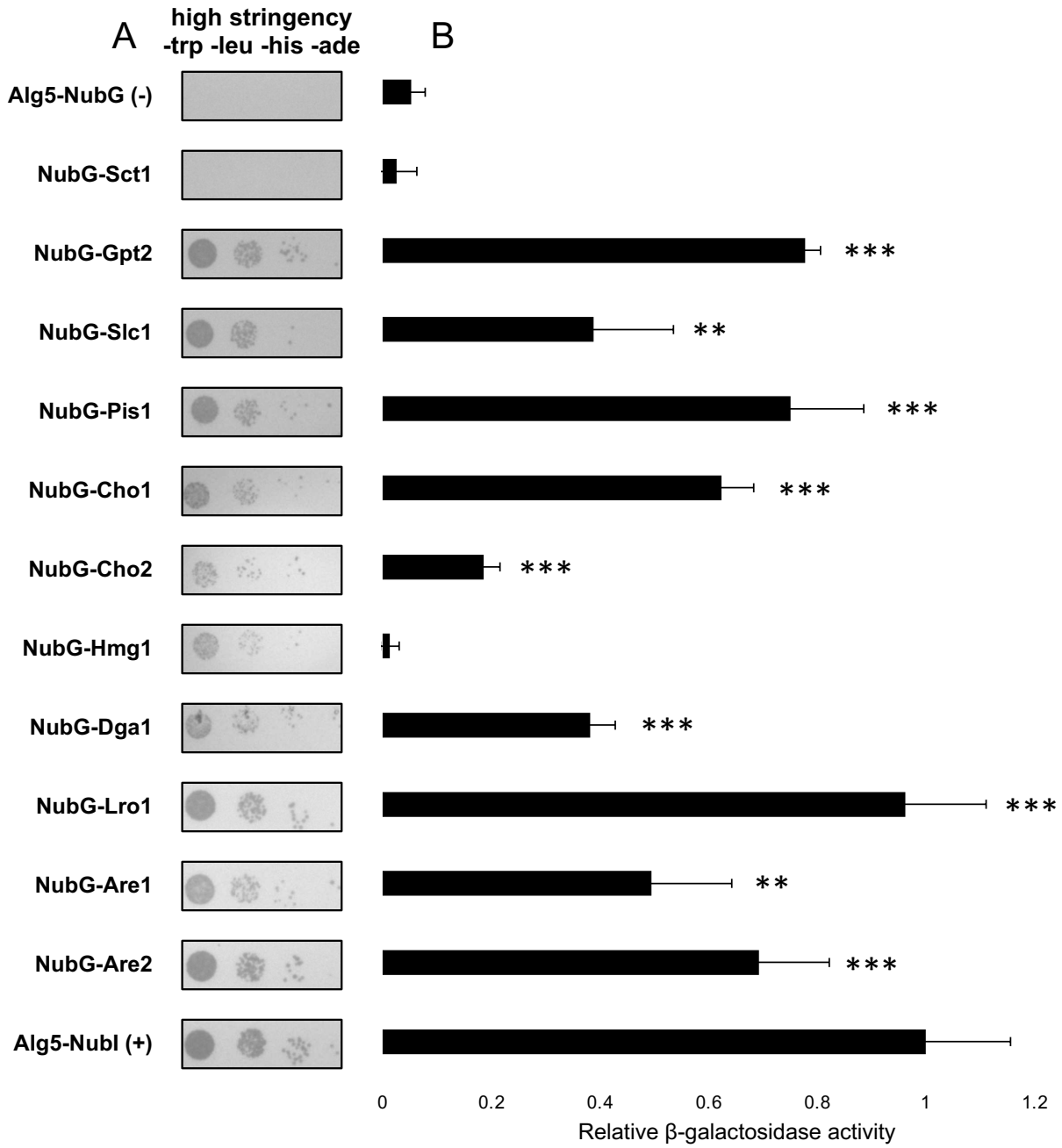

Figure 2.8 **Cds1 interacts with proteins that generate glycerophospholipid, sterol, glycerolipid, and sterol ester.** A. Membrane yeast 2-hybrid assay using a yeast strain expressing Cds1-Cub-LexA-VP16 and the indicated constructs. Growth on high stringency (lacking tryptophan, leucine, histidine, and adenine, containing 5 mM 3-AT) plates. B. β-galactosidase assay of a yeast strain expressing Cds1-Cub-LexA-VP16 and the indicated constructs. Each column is representative of three biological replicates (n = 3). Miller units were normalized to the positive control (Alg5-NubI). (* = $p < 0.05$, ** = $p < 0.01$, *** = $p < 0.001$).

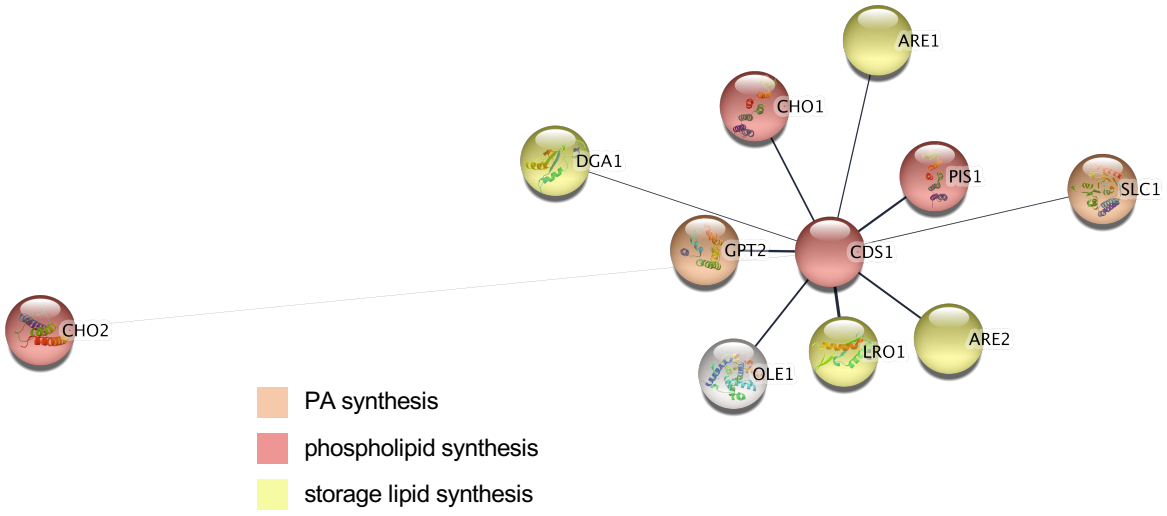

Figure 2.9 **Cds1 interactome network map as determined by iMYTH.** Map of interactions with the essential CDP-DAG synthase Cds1 as determined by the MYTH assay. Nodes are colored according to synthesis pathway. Edge thickness and length determined by LacZ reporter gene activation as determined by β-galactosidase assay.

2.5. Conclusions

This work has begun the process of describing the desaturasome, a complex of lipid biosynthetic enzymes that interact within the cell to generate species selectivity within lipid production. We have demonstrated that the only desaturase in *S. cerevisiae*, Ole1, interacts strongly with acyltransferases that utilize acyl-CoA as a substrate. We have also identified interactions between Ole1 and proteins from both phospholipid and storage lipid biosynthesis that do not use acyl-CoA as a substrate.

Slc1, the main LPAAT in *S. cerevisiae*, interacts strongly with Gpt2, which generates LPA for Slc1, and Cds1, which directs PA to PL synthesis through its conversion to CDP-DAG. It also interacts with proteins in later PL and storage lipid synthesis that do not use PA but use its downstream products. The CDP-DAG synthase

Cds1 interacts strongly with proteins that use CDP-DAG to produce PL, as well as proteins in later PL synthesis. Surprisingly, Cds1 interacts with acyltransferases dedicated to storage lipid synthesis as well. This work has elucidated a protein-protein interaction network in phospholipid and storage lipid synthesis that may explain the selective nature of lipid generation and tight control over lipid flux seen in yeast (Figure 2.10).

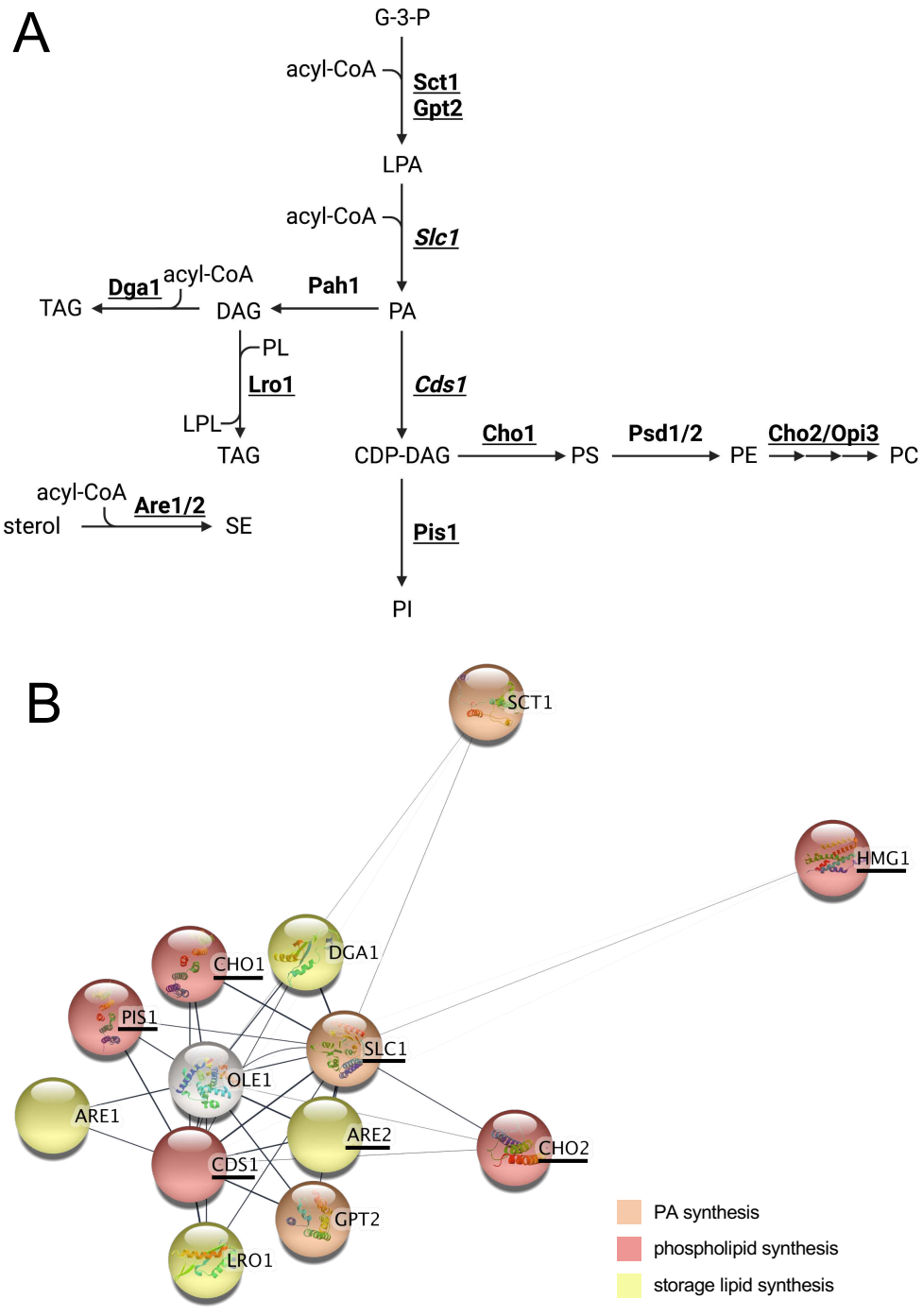

Figure 2.10 **Ole1, Slc1, and Cds1 interact with enzymes responsible for PA, phospholipid, and storage lipid synthesis.** A. Major *de novo* synthesis pathways of PA, PL, and storage lipid in *S. cerevisiae*. Proteins analyzed as prey are underlined. Proteins analyzed as both bait and prey are underlined and italicized. B. Map of the desaturasome interactions determined by the MYTH assay. Nodes are colored according to synthesis pathway. Edge thickness and length determined by LacZ reporter gene activation as determined by β-galactosidase assay. Underlined genes were also identified as Ole1 interactors by affinity purification.

2.5.1. Enzymes catalyzing sequential reactions in the phospholipid biosynthesis pathway interact with one another

Ole1 interacts strongly with the GPAT Gpt2 in a MYTH assay, as previously observed (67). Accordingly, the interaction between Ole1 and the GPAT Sct1 was much weaker by *LacZ* activation. Gpt2, *in vivo*, generates a more unsaturated LPA profile than Sct1, though both GPATs can utilize unsaturated acyl chains (66). The demonstrated difference in interaction between Ole1 and the two GPATs could differentially distribute unsaturated acyl-CoA to Gpt2, explaining this phenomenon. Ole1 also interacted with Slc1 in both methods described here. Slc1, as the primary LPAAT in *S. cerevisiae*, acylates the *sn-2* position of LPA destined for both TAG and phospholipids. As the *sn-2* position is enriched for unsaturated acyl chains in these downstream lipids, this interaction may serve to channel acyl-CoA from Ole1 to Slc1 and control the acyl composition of *de novo* synthesized membrane phospholipids and storage lipid (68, 69).

The GPATs exhibit a similar interaction pattern with Slc1, with Slc1 interacting more strongly with Gpt2 than Sct1 based on *LacZ* activation. Gpt2 and Slc1, as LD-associated enzymes, may serve to generate PA for TAG and phospholipid synthesis at the LD, though it has been shown that Sct1 synthesizes LPA for eventual TAG production. Determination of further downstream interactors of Gpt2 and Slc1 at the LD may reveal whether the PA generated is destined for TAG or PL synthesis.

Slc1 and the CDP-DAG synthase Cds1 interact with each other as well, consistent with a model whereby at least a portion of the PA generated by the LPAAT is directed to CDP-DAG synthesis for phospholipid production. Cds1 interacts strongly with both Pis1 and Cho1, proteins that utilize CDP-DAG to create PI and PS, respectively.

2.5.2. Enzymes synthesizing nonsequential reactions in phospholipid synthesis interact

Through this study, we have identified Ole1, Slc1, and Cds1 interactors that are involved in various types of lipid synthesis. Although this was unsurprising, we discovered interactions between Ole1 and enzymes responsible for later lipid synthesis that do not use acyl-CoA as a substrate. While the MYTH assay differentiates between proteins within close proximity and proteins within the same complex that do not interact with the bait protein, it is not possible to discern between direct interactions and interactions maintained via a bridging interaction partner (57). The interactions seen between Ole1 and non-acyl-CoA utilizing proteins in the MYTH assay may be maintained through a bridging interaction partner. In particular, interactions were detected between Ole1 and Cds1, Cho1, and Pis1 in both methods.

Slc1 interacts strongly with Pis1, Cho1, and Cho2, though the PA generated by the LPAAT must be further processed for use by the interactors. Similarly, Cds1 interacts strongly with Ole1 and Gpt2, two proteins that generate precursors to PA for CDP-DAG synthesis. Taken together, this implies the existence of a lipid biosynthesis complex containing Ole1 and these phospholipid synthesizing enzymes. Indeed, such a complex might explain the tendency for PC generated from PE methylation to contain two unsaturated acyl chains. Future work should determine whether these proteins are all present within the same complex and whether these interactions are sufficient to control PC specificity.

Hmg1, though determined to be an interactor of Ole1 in the AP, was not found to be a strong interactor with Ole1 or any of the bait through the MYTH assay. It is possible

that Hmg1 is present in the desaturasome but not in direct proximity to Ole1, causing the decreased observed signal in MYTH. Alternatively, Hmg1 could have been a false positive in the AP that can be ruled out as an Ole1 interactor due to the combination of techniques used. It is also true that the assay is sensitive to topology of the proteins and termini sidedness. If the N-terminus of Hmg1 is not located in the cytosol as predicted, no interaction signal would be seen (60).

2.5.3. Ole1, Slc1, and Cds1 interact with storage lipid synthesizing enzymes

The only acyltransferase exclusive to storage lipid synthesis identified as an Ole1 interactor by AP was the acyl-CoA:sterol acyltransferase Are2. Investigation of the other acyltransferases with MYTH showed that Ole1 does indeed interact with Lro1, Dga1, and Are1 as well. Though the phospholipid:diacylglycerol acyltransferase Lro1 does not directly use acyl-CoA as an acyl donor, the close proximity of the proteins could enrich unsaturated acyl chains in the phospholipids around Lro1 and thus increase the incorporation of unsaturated acyl chains in TAG. Orthologs of the acyl-CoA:diacylglycerol acyltransferase Dga1 and Ole1 have been shown to colocalize and interact in other systems, but this is the first time an interaction between the proteins has been identified in *S. cerevisiae*. Both TAG and SE are enriched for unsaturated acyl chains, as previously noted, which promotes LD budding from the ER (8, 70). These interactions may serve to channel acyl-CoA from Ole1 to storage lipid and increase fluidity of the neutral lipid core, though future work will need to be done to confirm.

Slc1 also interacts strongly with Lro1, Dga1, and Are2, though the PA produced still requires a conversion to DAG by Pah1 to be available to Lro1 and Dga1. The interaction of the LPAAT with storage lipid synthesizing enzymes is somewhat unsurprising, as the protein is found on and near the storage lipid synthesis and storage organelle, the LD.

A set of novel interactions between the phospholipid synthesizing enzyme Cds1 and the storage lipid synthesis proteins is reported herein as well. This was unexpected, as CDP-DAG is exclusively used to make downstream phospholipid. There is evidence that rapid growth of the LD necessitates a localized concentration of phospholipid production for the LD monolayer (71, 72). In that circumstance, localized CDP-DAG synthesis would promote LD budding and storage lipid synthesis. However, as Cds1 competes with the DAG synthesizing Pah1 for PA, it is possible that these interactions sequester PA from storage lipid synthesis, attenuating LD synthesis. These data imply that, to an extent, Cds1 is present in the same desaturasome as the TAG and SE synthesizing acyltransferases. Whether this colocalization is inhibitory or permissive to TAG and SE synthesis is yet to be determined.

2.5.4. Ole1 interactors are present in specialized ER subdomains

An initial affinity purification for the only desaturase in *S. cerevisiae*, Ole1, revealed many membrane protein interactors. While 35.2% of the proteins are found in the ER, we also identified proteins from other membranes within the cell, namely the mitochondrial outer membrane, plasma membrane, and LD. Ole1 is itself only located within the ER, but it is possible that Ole1 is present at organelle-organelle contact sites.

Indeed, we identified Tcb1 and Tcb3 in the coimmunoprecipitate with Ole1, which are both cortical ER proteins integral to the ER-plasma membrane tether (73). This tether is essential for the enrichment of PS and PE in the plasma membrane seen in wild-type cells, so interactions between lipid synthesizing enzymes and the tether proteins would not be unexpected (74). It has been previously reported that Ole1 and Pis1 interact with ER-PM tethers, and we are reporting herein that Ole1 interacts with Pis1 both by coimmunoprecipitation and MYTH (55, 73). While the close localization of these proteins to the ER-PM contacts would provide PI destined for PIP synthesis in the PM, the close proximity of the two proteins channeling substrates to each other would be contradictory to the decrease in unsaturated acyl chains found in PM-localized PIPs. Importantly, Ole1 was not found to interact strongly with Sct1, which incorporates saturated acyl chains at the *sn-1* position of phospholipids and generates LPA for PI production (66). It should be noted that both techniques employed here are limited in the information provided about subcellular localization of the interactions. Therefore, there is potential that Ole1 interacts with Pis1 in a desaturasome that is not located at the ER-PM contacts. Investigating the composition of lipid biosynthetic complexes found at different subcellular locations may provide insight to this phenomenon.

Ole1 also copurified with proteins found in the outer mitochondrial membrane, Tom20, Tom22, and Tom70. An interaction between Tom70 and the sterol transporter Lam6 is essential for proper sterol transfer between the ER and mitochondria and has been implicated in mitochondrial tethering to the ER (75). Sublocalization of Ole1 has not been reported within the ER, but the human orthologue SCD1 was discovered in mitochondrial associated membranes (MAMs), a portion of the ER in close contact with

the mitochondria (21, 76, 77). MAMs contain the ability to synthesize lipids, PS in particular, and mitochondrially-localized Psd1 demonstrates a specificity for di-unsaturated PS (78). As we discovered, Ole1 interacts strongly with Cho1. The further interaction of the desaturase with a putative ER-mitochondrial tether lends credence to the idea that Ole1 and Cho1 exist in close proximity within the MAM, preferentially generating di-unsaturated PS for mitochondrially-localized Psd1.

The desaturase pulled down four proteins associated with the LD – Slc1, Pet10 (Pln1), Hfd1, and Faa4. We also showed the interaction between Ole1 and the ER-LD proteins Gpt2, Slc1, and Dga1 by MYTH. Though Ole1 itself does not move onto the lipid droplet monolayer, the interactions between the protein and these LD localized enzymes could suggest that a subpopulation of the desaturase is localized to the LD associated ER. As unsaturated acyl chain incorporation into TAG promotes LD budding, such an interaction could be seen as permissive to LD growth and TAG synthesis (70). However, it is also true that LD proteins are found in the ER during certain conditions and their retention in the ER attenuates LD growth (71, 79, 80). There is potential that the interaction with the ER-bound desaturase retain the acyltransferases in the ER and is thus inhibitory to neutral lipid synthesis.

This study has begun the work of identifying the proteins that comprise the desaturasome. This is a step towards understanding the regulation of the specificity of lipid production, but future work should attempt to biochemically confirm whether these interactions are controlling the composition of lipid species. Determining the architecture of the desaturasome and whether the architecture varies by subcellular location within the ER would provide further insight to the regulation of lipid composition.

Chapter 3 – *Saccharomyces cerevisiae* Δ9-desaturase Ole1 forms a supercomplex with Slc1 and Dga1

Brianna L. Greenwood, Zijun Luo, Tareq Ahmed, Daniel Huang, and David T. Stuart

Department of Biochemistry, University of Alberta, Edmonton AB, Canada

Preface

This chapter represents the work accepted for publication in the Journal of Biological Chemistry in May of 2023. BLG is the primary author and performed the experiments, analyzed the data, wrote the first draft, and edited the manuscript. ZL, TA, and DH generated plasmids for the study and obtained preliminary data. DTS designed the research and edited the manuscript. This manuscript has been adapted to fit the format of the thesis presented.

3.1. Summary

Biosynthesis of the various lipid species that compose cellular membranes and lipid droplets depends on the activity of multiple enzymes functioning in coordinated pathways. The flux of intermediates through lipid biosynthetic pathways is regulated to respond to nutritional and environmental demands placed on the cell necessitating that there be extensive flexibility in pathway activity and organization. This flexibility can in part be achieved through the organization of biosynthetic enzymes into metabolon supercomplexes. However, the makeup of such supercomplexes remains unclear. Here, we identified protein-protein interactions between acyltransferases Sct1, Gpt2, Slc1, Dga1 and the ∆9 acyl-CoA desaturase Ole1 in *Saccharomyces cerevisiae*. We further

determined that a subset of these acyltransferases interact with each other without Ole1 acting as a scaffold. We show truncated versions of Dga1 lacking the carboxyl-terminal 20 amino acid residues were non-functional and unable to bind Ole1. Furthermore, charged-to-alanine scanning mutagenesis revealed that a cluster of charged residues near the carboxyl-terminus were required for the interaction with Ole1. Mutation of these charged residues disrupted the interaction between Dga1 and Ole1, but allowed Dga1 to retain catalytic activity and to induce lipid droplet formation. These data support the formation of a complex of acyltransferases involved in lipid biosynthesis that interact with Ole1, the sole acyl-CoA desaturase in *S. cerevisiae* that can channel unsaturated acyl-chains toward phospholipid or triacylglycerol synthesis. This desaturasome complex may provide the architecture that allows for the necessary flux of *de novo* synthesized unsaturated acyl-CoA to phospholipid or triacylglycerol synthesis as demanded by cellular requirements.

3.2. Introduction

The metabolic pathways responsible for the synthesis and assembly of glycerophospholipid species play a key role in establishing cellular membrane structure and controlling energy homeostasis (1). The synthesis of glycerophospholipid species is a complex process starting with the initial carboxylation of acetyl-CoA to malonyl-CoA by acetyl-CoA carboxylase (ACC). Fatty acyl-CoA synthetase (FAS) then catalyzes condensation of acetyl-CoA and malonyl-CoA into saturated acyl-chains with 16 to 18 carbons being the most common (2). In *S. cerevisiae* a high proportion of acyl-CoA undergoes mono-unsaturation catalyzed by the stearoyl-CoA desaturase Ole1 in the endoplasmic reticulum (ER) (3) (Figure 3.1A). Subsequently, saturated and unsaturated acyl-CoA are assembled into a diverse family of glycerophospholipids whose composition, chain length and degree of unsaturation influence membrane properties and structure (4).

The assembly of glycerophospholipids is initiated by glycerophosphate acyltransferases (GPATs) encoded by *GPT2* and *SCT1* that form lysophosphatidic acid (LPA) by adding an acyl chain to glycerol 3-phosphate (5) (Figure 3.1B). This is followed by lysophosphatidic acid acyltransferases (LPAATs) encoded by *SLC1* and *ALE1* that add an acyl chain to the *sn-2* position of LPA to form phosphatidic acid (PA) (6, 7) (Fig. 1B). Slc1 and Ale1 are both found in the ER membrane but only Slc1 localizes to lipid droplets (LDs) (8). Slc1 and Ale1 have an apparent strong preference for C18:1-CoA and this specificity is reflected in the high proportion of phospholipid and neutral lipid species that display C18:1 at the *sn-2* position (9, 10). The PA formed in these reactions can be further modified to CDP-DAG, and acts as precursor to the primary membrane

phospholipids (11). PA can also be subjected to dephosphorylation by phosphatase Pah1 to yield diacylglycerol (DAG) that can act as substrate for diacylglycerol acyltransferases (DGATs) Dga1 and Lro1 to form triacylglycerol (TAG) (12–14) (Figure 3.1B). Dga1 catalyzes the acylation of DAG with acyl-CoA for the synthesis of TAG and is responsible for a large fraction of the TAG synthesized in *S. cerevisiae* (13). Lro1 also forms TAG, but transfers an acyl-chain from an existing phospholipid to DAG rather than utilizing *de novo* synthesized acyl-CoA (14). Dga1 displays localization both in the ER membrane and LDs whereas Lro1 is confined the ER membranes (15). Fatty acyl chains can also be also stored as sterol esters (SE) in reactions catalyzed by Are1 and Are2 (16).

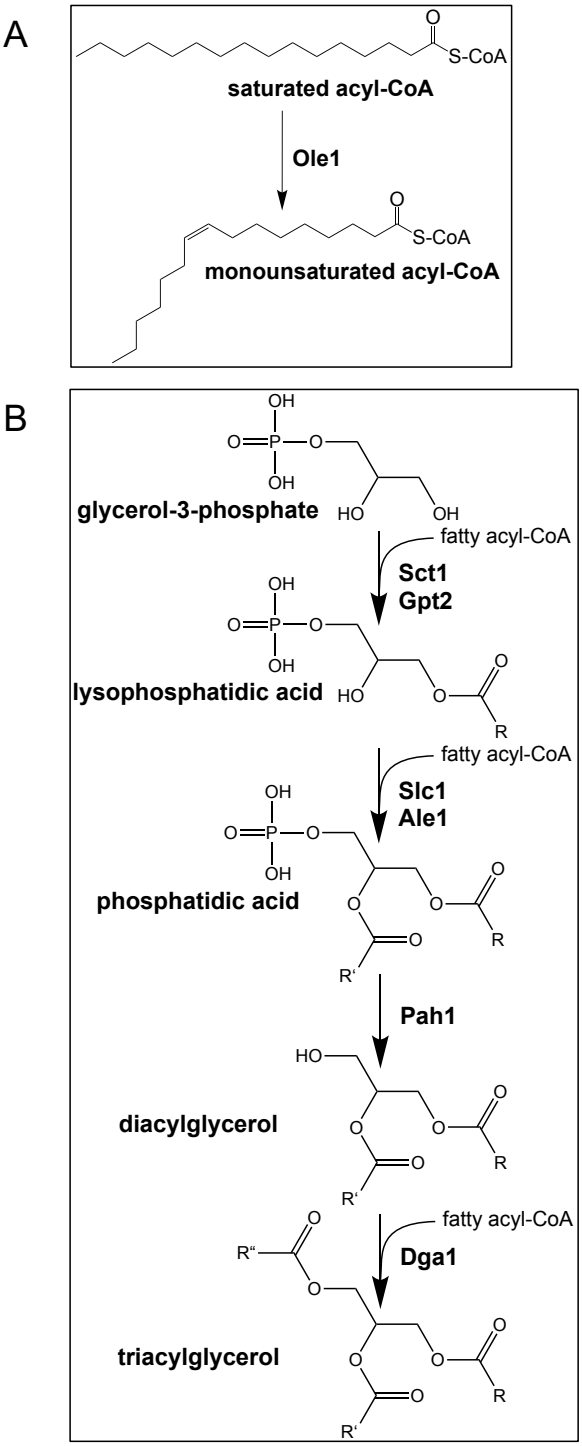

Figure 3.1. **The pathway to triacylglycerol synthesis in *S. cerevisiae*.** A. ∆9 acyl-CoA desaturase Ole1 is required to generate unsaturated acyl-CoA species. B. The pathway to triacylglycerol in *S. cerevisiae*. Enzymes catalyzing the consecutive reactions are shown in bold. Acyltransferases mediate the synthesis of lysophosphatidic acid (LPA) and phosphatidic acid (PA). Dephosphorylation of PA yields diacylglycerol that acts as a substrate for Dgat activities to synthesize triacylglycerol.

Fatty acid biosynthetic pathways can of necessity respond to rapidly changing physiological demands and environmental conditions, yet little is known regarding how they are spatially organized and coordinated to provide this responsiveness. It has been proposed that pathway efficiencies can be optimized through physical interaction between enzymes that act sequentially in a pathway, thus organizing them into metabolons (17). Such organization could promote channeling of intermediates to minimize their diffusion into the cytoplasm or surrounding membrane environments (18). This could provide for precision in the regulation of the flux of intermediates toward specific products through association and dissociation of individual subunits within an enzyme supercomplex (19).There is evidence for the existence of enzyme supercomplexes for lipid biosynthesis assembled through the interaction of FAS with ATP citrate lyase (ACL) and ACC to provide acetyl-CoA and malonyl-CoA substrates and malic enzyme (ME), pyruvate carboxylase (PYC) and malate dehydrogenase (MDH) that provide the NADPH required for FAS to synthesize acyl-chains (20). A soluble TAG synthesizing complex containing LPA acyltransferase, PA phosphatase, DGAT, acyl-acyl carrier protein (ACP) synthetase, and ACP activities was identified in the oleaginous yeast *R. glutinis.* This complex is stabilized by protein-protein interactions and can incorporate acyl-CoA as well as FFA into TAG and its biosynthetic intermediates (21).

Physical interactions have also been demonstrated among acyltransferases and there is an implication that these interactions direct the synthesis of distinct TAG species in several plant models (22–24). Similarly, transfected DGAT2 and MGAT2 display colocalization and physical interaction in a human cell model (25). It is likely that other proteins interact with DGAT2 in this human cell model since cross-linking studies using

both purified membrane fractions and whole cells indicate that DGAT2 exists in a complex that migrates at approximately 650 kDa on polyacrylamide gels, consistent with its being a component of an enzyme supercomplex (25). Thus, lipid biosynthetic pathways assembled into enzyme supercomplexes may be wide-spread but the spatial organization of these complexes and the protein-protein interactions that scaffold them together remain uncharacterized.

Acyl-CoA desaturases play a key role in regulating membrane and storage lipid composition as they introduce double bonds into acyl chains that influence the chemical and physical properties of membrane phospholipids (26). Indeed, in *S. cerevisiae* 75 - 90% of fatty acids are unsaturated and the stearoyl-CoA desaturase encoded by *OLE1* is essential for viability (3, 27). The mouse stearoyl-CoA desaturase SCD1 is not essential but $SCD1^{-/-}$ mice have significantly reduced fat stores (28). Similarly, SCD1 has a role in determining TAG abundance and phospholipid composition in *C. elegans* (29). These observations suggest that stearoyl-CoA desaturase may play a key role in the biosynthesis of membrane phospholipids and TAG that extends beyond its capacity to introduce double bonds into acyl-chains.

Numerous acyl-CoA desaturases including Ole1 have been demonstrated to function as homodimers, and some acyl-CoA desaturases like *A. thaliana* FAD2 and FAD3 form a heterodimer complex to channel oleate to linolenate without allowing a linoleoyl intermediate to be released (30). Owing to the importance of unsaturated acyl-chains in determining the physical properties of membrane phospholipids and the role of stearoyl-CoA desaturase in supplying unsaturated acyl-chains as substrate for acyltransferases, an important question then is: Do acyl-CoA desaturases form physical

complexes with acyltransferases to channel unsaturated acyl chains to specified phospholipid or neutral lipid species? In cultured HeLa cells overexpressed acyl-CoA desaturase SCD1 and acyltransferase DGAT2 colocalize and can be coimmunoprecipitated, consistent with a physical interaction between the two enzymes (31). Additionally, biochemical analysis of microsomal membranes suggests there is channeling of lipid species between oleoylglycerophosphocholine desaturase and monoacylglycerophosphocholine acyltransferase in *Pisum sativum* without intermediate species equilibrating with the bulk membrane pool of phospholipid (32).

In contrast to the extensive biochemical evidence supporting complex formation among enzymes that catalyze lipid biosynthesis there is little structural data to provide information around the protein domains and sequences involved in making protein-protein interactions among these enzymes. The crystal structure of human stearoyl-CoA desaturase SCD1 has been solved but this has not revealed sites of interaction with other enzymes (33). The structure of human acyltransferase DGAT1 revealed that the dimer interface includes transmembrane helices and contacts occurring within the lipid bilayer (34). Although no structural data is available for DGAT2, domains implicated in ER membrane targeting and lipid droplet binding have been elucidated by deletion analysis. However, these studies have yet to reveal how DGAT2 interacts with the triglyceride synthesizing supercomplex it was found to be part of and whether the membrane context influences these interactions (25, 35, 36).

Here we have employed *S. cerevisiae* to investigate the hypothesis that interactions exist among stearoyl-CoA desaturase and acyltransferases responsible for phospholipid and TAG synthesis. We have identified physical interactions between

acyltransferases Slc1 and Dga1 and between both acyltransferases and desaturase Ole1. The interaction between Dga1 and Ole1 requires the carboxyl-terminus of Dga1 required for enzymatic activity. We refer to this desaturase-acyltransferase biosynthetic complex as a desaturasome. Further, we demonstrate physical interaction between Slc1 and Dga1 independent of Ole1. These findings are consistent with the contention that protein-protein interactions among these enzymes can act to channel acyl-CoA toward specific glycerolipid species and may be one mechanism by which control can be imposed over membrane composition and physical properties as well as storage lipid composition.

3.3. Experimental Procedures

3.3.1. Strains and Plasmids

The *Saccharomyces cerevisiae* strain NMY51 (*MATa, his3Δ200, trp1-901, leu2-3,112, ade2, LYS2::(lexAop)4-HIS3,ura3::(lexAop)8-LacZ, ade2::(lexAop)8-ADE2, GAL4*) was provided by Marek Michalak for the membrane yeast two-hybrid experiments. Oligonucleotides and synthetic DNA fragments used in this investigation are listed in Tables 3.1 and 3.2. Plasmids used in this study are listed in Table 3.3. To introduce the Cub-LexA-VP16 tag into the endogenous *OLE1* gene in NMY51 (YBG1), sequence encoding the *Cub-LexA-VP16* tag containing the *CYC1* terminator was amplified from plasmid pTMBV4 (Dualsystems Biotech AG, Schlieren, Switzerland) using primers 5-Cub and 3-Cub. The 5' oligonucleotide (5-Cub) included sequence to insert a single Myc epitope and SpeI cleavage site immediately upstream of the Cub sequence. The resulting

DNA fragment was digested with SpeI and phosphorylated using T4 polynucleotide kinase prior to ligation with SpeI – EcoRV digested pUG6 (37) resulting in pUG6-CLVt. The *MYC-Cub-LexA-VP16-CYC1t-KanMX* fragment was amplified from pUG6-CLVt with primers (OLE1t-5, OLE1t-3) containing homology to *OLE1*. This DNA fragment was used to transform NMY51. Transformants were selected on YEPD agar supplemented with 200 µg/mL geneticin and correct integration of Ole1-Myc-Cub-LexA-VP16 was confirmed by PCR analysis of genomic DNA using oligonucleotides BGO15 and BGCub3-1. YBG3 was derived from NMY51 by deletion of the endogenous *OLE1* gene. The Nat-MX6 gene was amplified from pAG25 (37) using primers Ole1d5 and Ole1d3. The amplified DNA fragment containing homology to *OLE1* was used to transform NMY51 and transformants were selected on YEPD agar supplemented with 100 µg/mL nourseothricin and 0.5% Tween-80. The lack of *OLE1* function was confirmed by PCR analysis of genomic DNA using primers Ole1dsc5 and Ole1dsc3 and lack of growth on YEPD plates supplemented with 100 µg/mL Nourseothricin but lacking Tween-80.

Table 3.1 Primers used in this study

Primer name	Primer sequence
DGA15	TTACGCTGGATCCATGTCAGGAACATTCAATGATAT
DGA1Nx3	TACGCTGGATCCGAAAGGCATGAGAATAAGTCT
DGA1xN3	GCAGAATTGAAGATAGTTGGGGAATTCGATATC
DGA123f	TACGCTGGATCCGAAAGGCATGAGAATAAGTCT
DGA129f	TACGCTGGATCCTCTTTGTCAAGCATCGATAA
DGA137f	TACGCTGGATCCGAACAGACTCTCAAACCACA
212r	GATATCGAATTCTTAGTTACAACCTTCTGTTGCA
240r	GATATCGAATTCTTATAAGTAGTCTCTATACAATGGGATAT
288r	GATATCGAATTCTTATCTTTTGTTTAAAATCAGTTGTGTAC
318r	GATATCGAATTCTTACAGAACATTATAACAGTCCACC
388r	GACGGTATCGATAAGCTTGATATCGAATTCTTATCTTTTCAACTC CGCAATATAC
398r	GACGGTATCGATAAGCTTGATATCGAATTCTTACCCATATTTTTC TCTATTTTCG
DGAD398	ATATCGAATTCTTACCCAACTATCTTCAATTCTGCATCTCTTTTCA ACTCCGCAATATACAAATCATG
DGAD398a	ATATCGAATTCTTACCCAACTATCTTTCTTTTCAACTCCGCAATA TACAAATCATG
DGAD388	ATATCGAATTCTTACCCAACTATCTTCAATTCTGCATCGAAATGA TTAACAACATCATCTGG
S17Df	GACCCTACAGCCGGTATTACC
S17Af	GCCCCTACAGCCGGTATTACC
S17Dr	CGGTAATACCGGCTGTAGGGTCTCCTTCTTCCTT
S17Ar	TAATACCGGCTGTAGGGGCTCCTTCTTCCT
TMBV4SLCf	AGCATAGCAATCTAATCTAAGTTTTCTAGATGAGTGTGATAGGTA GGTTCTT
TMBV4SLCr	CGAATTCCTGCAGATATACCCATGGAGATGCATCTTTTTTACAG ATGAACCTT
SCT1f	TACGCTGGATCCCCTGCACCAAAACTCACG
SCT1r	CTACGCATCTCCTTCTTTCCC
SCT1xNf	TACGCTGGATCCATGCCTGCACCAAAACT
SCT1xNr	TACGCTGGCCgaggcgGCCGCATCTCCTTCTTTCC
SLC1f	TACGCTGGATCCAGTGTGATAGGTAGGTTCTTGTATTACT
SLC1r	GATATCGAATTCTTAATGCATCTTTTTTACAGATGAACCTTC

Primer name	Primer sequence
GPT2f	TACCCATACGATGTTCCAGATTACGCTGGATCCATGTCTGCTCCCCGCTGCC
GPT2r	GACGGTATCGATAAGCTTGATATCGAATTCTCATTCTTTCTTTTCGTGTTCTCTTTTCTGTCTTACCAG
5-Cub	CGATAAACTAGTATGGAACAAAAACTTATTTCTGAAGAAGATCTGTCGACCATGTCGG
3-Cub	CGATAAGAATTCTAATACGACTCACTATAGGG
ole1T5	CTCTGCTATTAGAATGGCTAGTAAGAGAGGTGAAATCTACGAAACTGGTAAGTTCTTTGAACAAAAACTTATTTCTG
ole1T3	AGCATGACTGTGAAATTTTGAAGAGATGCAGTAAGCCATCCCATATCTATTGCTCCAGGGccagatctgtttagcttgc
ole1d3	TTATGGTAGTTGCAGTTTTGTTATTGTAATGTGATACTTAAAAGAACTTACCAGTTTCGTGCATAGGCCACTAGTGGATC
ole1d5	CATAGTAATAGATAGTTGTGGTGATCATATTATAAACAGCACTAAAACATTACAACAAAGCAGCTGAAGCTTCGTACGC
ole1dsc5	ATGCAGCAAATCATCGGCTC
ole1dsc3	AGAGATGCAGTAAGCCATCC
BGO15	TACGACTTGAAGAAATTCTCTC
BGCub3-1	CTTAGCACAAGATGTAAGGT
YI-DGA1pf	CAGGAAACAGCTATGACCATGATTACGCCAATCAACTAAGAGACCGTGGT
DGA1pr	TTATGTGACTGTTCAAACTGTATGC
DGA1p-HAf	CAGAGGCAGAGGCATACAGTTTGAACAGTCACATAAATGCCATACCCATACGATGTTCC
YI-PstCYC1	TACCCGGGGATCCTCTAGAGTCGACCTGCAACCGGCCGCAAATTAAA

Table 3.2 DNA fragments used in this study

Fragment name	Fragment sequence
$DGA1_{KR}$	GATTTCGGTTTGTTGCCATTTAGAGCGCCTATCAATGTTGTTGT TGGAAGGCCTATATACGTTGAAAAGAAAATAACAAATCCGCCA GATGATGTTGTTAATCATTTCCATGATTTGTATATTGCGGAGTT GgcAgctCTATATTACGAAAATAGAGAAAAATATGGGGTACCGGA TGCAGAATTGAAGATAGTTGGGTAAGAATTCgatatcaagcttatcgata ccgtcgacctcgagtcatgtaattag
$DGA1_{REK}$	GATTTCGGTTTGTTGCCATTTAGAGCGCCTATCAATGTTGTTGT TGGAAGGCCTATATACGTTGAAAAGAAAATAACAAATCCGCCA GATGATGTTGTTAATCATTTCCATGATTTGTATATTGCGGAGTT GAAAAGACTATATTACGAAAATgcaGctgccTATGGGGTACCGGA TGCAGAATTGAAGATAGTTGGGTAAGAATTCgatatcaagcttatcgata ccgtcgacctcgagtcatgtaattag
$DGA1_{DEK}$	GATTTCGGTTTGTTGCCATTTAGAGCGCCTATCAATGTTGTTGT TGGAAGGCCTATATACGTTGAAAAGAAAATAACAAATCCGCCA GATGATGTTGTTAATCATTTCCATGATTTGTATATTGCGGAGTT GAAAAGACTATATTACGAAAATAGAGAAAAATATGGGGTACCG GcTGCAGcATTGgctATAGTTGGGTAAGAATTCgatatcaagcttatcgat accgtcgacctcgagtcatgtaattag
$DGA1_{KRDEK}$	GATTTCGGTTTGTTGCCATTTAGAGCGCCTATCAATGTTGTTGT TGGAAGGCCTATATACGTTGAAAAGAAAATAACAAATCCGCCA GATGATGTTGTTAATCATTTCCATGATTTGTATATTGCGGAGTT GgcAgctCTATATTACGAAAATAGAGAAAAATATGGGGTACCGGc TGCAGcATTGgctATAGTTGGGTAAGAATTCgatatcaagcttatcgatac cgtcgacctcgagtcatgtaattag

Table 3.3 Plasmids used in this study

Plasmid Name	*S. cerevisiae* Gene	Ori and selection	Source
pTMBV4	*Cub-LexA-VP16*	*2μ LEU2*	Dual Systems
pADSL-Nx	*NubG*	*CEN/ARS TRP1*	Dual Systems
pADSL-xN	*NubG*	*CEN/ARS TRP1*	Dual Systems
pALG5-NubG	*NubG*	*CEN/ARS TRP1*	Dual Systems
pALG5-NubI	*NubI*	*CEN/ARS TRP1*	Dual Systems
pUG6	*KanMX6*	$G418^R$	Euroscarf
pUG6-CLVt	*Cub-LexA-VP16-KanMX6*	$G418^R$	This study
pAG25	*NatMX6*	$ClonNAT^R$	Euroscarf
pTMBV4-SLC1	*SLC1-Cub-LexA-VP16*	*2μ LEU2*	This study
DGA1-NubG	*DGA1-HA-NubG*	*CEN/ARS TRP1*	This study
NubG-DGA1	*NubG-HA-DGA1*	*CEN/ARS TRP1*	This study
NubG-SCT1	*NubG-HA-SCT1*	*CEN/ARS TRP1*	This study
SCT1-NubG	*SCT1-HA-NubG*	*CEN/ARS TRP1*	This study
NubG-GPT2	*NubG-HA-GPT2*	*CEN/ARS TRP1*	This study
NubG-SLC1	*NubG-HA-SLC1*	*CEN/ARS TRP1*	This study
NubG-DGA1 $_{24-418}$	*NubG-HA-DGA1 $_{24-418}$*	*CEN/ARS TRP1*	This study
NubG-DGA1 $_{30-428}$	*NubG-HA-DGA1 $_{30-428}$*	*CEN/ARS TRP1*	This study
NubG-DGA1 $_{38-418}$	*NubG-HA-DGA1 $_{38-418}$*	*CEN/ARS TRP1*	This study
NubG-DGA1 $_{1-212}$	*NubG-HA-DGA1 $_{1-212}$*	*CEN/ARS TRP1*	This study
NubG-DGA1 $_{1-240}$	*NubG-HA-DGA1 $_{1-240}$*	*CEN/ARS TRP1*	This study
NubG-DGA1 $_{1-288}$	*NubG-HA-DGA1 $_{1-288}$*	*CEN/ARS TRP1*	This study
NubG-DGA1 $_{1-318}$	*NubG-HA-DGA1 $_{1-318}$*	*CEN/ARS TRP1*	This study
NubG-DGA1 $_{1-398}$	*NubG-HA-DGA1 $_{1-398}$*	*CEN/ARS TRP1*	This study
NubG-DGA1 $_{\Delta 388-410}$	*NubG-HA-DGA1 $_{\Delta 388-410}$*	*CEN/ARS TRP1*	This study
NubG-DGA1 $_{\Delta 399-410}$	*NubG-HA-DGA1 $_{\Delta 399-410}$*	*CEN/ARS TRP1*	This study
NubG-DGA1$_{\Delta 399-414}$	*NubG-HA-DGA1$_{\Delta 399-414}$*	*CEN/ARS TRP1*	This study
NubG-DGA1 $_{1-408}$	*NubG-HA-DGA1 $_{1-408}$*	*CEN/ARS TRP1*	This study
NubG-DGA1$_{KR}$	*NubG-HA-DGA1$_{KR}$*	*CEN/ARS TRP1*	This study

NubG-DGA1$_{REK}$	*NubG-HA-DGA1$_{REK}$*	*CEN/ARS TRP1*	This study
NubG-DGA1$_{DEK}$	*NubG-HA-DGA1$_{DEK}$*	*CEN/ARS TRP1*	This study
NubG-DGA1$_{KRDEK}$	*NubG-HA-DGA1$_{KRDEK}$*	*CEN/ARS TRP1*	This study
NubG-DGA1$_{S17A}$	*NubG-HA-DGA1$_{S17A}$*	*CEN/ARS TRP1*	This study
NubG-DGA1$_{S17D}$	*NubG-HA-DGA1$_{S17D}$*	*CEN/ARS TRP1*	This study
Ylp-DGA1	*HA-DGA1*	*Ylp URA3*	This study
Ylp -DGA1 $_{24-418}$	*HA-DGA1 $_{24-418}$*	*Ylp URA3*	This study
Ylp-DGA1 $_{30-428}$	*HA-DGA1 $_{30-428}$*	*Ylp URA3*	This study
Ylp-DGA1 $_{38-418}$	*HA-DGA1 $_{38-418}$*	*Ylp URA3*	This study
Ylp -DGA1 $_{1-212}$	*HA-DGA1 $_{1-212}$*	*Ylp URA3*	This study
Ylp-DGA1 $_{1-240}$	*HA-DGA1 $_{1-240}$*	*Ylp URA3*	This study
Ylp-DGA1 $_{1-288}$	*HA-DGA1 $_{1-288}$*	*Ylp URA3*	This study
Ylp-DGA1 $_{1-318}$	*HA-DGA1 $_{1-318}$*	*Ylp URA3*	This study
Ylp-DGA1 $_{1-398}$	*HA-DGA1 $_{1-398}$*	*Ylp URA3*	This study
Ylp-DGA1 $_{\Delta 388-410}$	*HA-DGA1 $_{\Delta 388-410}$*	*Ylp URA3*	This study
Ylp-DGA1 $_{\Delta 399-410}$	*HA-DGA1 $_{\Delta 399-410}$*	*Ylp URA3*	This study
Ylp-DGA1$_{\Delta 399-414}$	*HA-DGA1$_{\Delta 399-414}$*	*Ylp URA3*	This study
Ylp-DGA1 $_{1-408}$	*HA-DGA1 $_{1-408}$*	*Ylp URA3*	This study
Ylp-DGA1$_{KR}$	*HA-DGA1 $_{K397A, R398A}$*	*Ylp URA3*	This study
Ylp-DGA1$_{REK}$	*HA-DGA1 $_{R404A, E405A, K406A}$*	*Ylp URA3*	This study
Ylp-DGA1$_{DEK}$	*HA-DGA1 $_{D411A, E413A, K415A}$*	*Ylp URA3*	This study
Ylp-DGA1$_{KRDEK}$	*HA-DGA1 $_{K397A, R398A, D411A, E413A, K415A}$*	*Ylp URA3*	This study
Ylp-DGA1$_{S17A}$	*HA-DGA1 $_{S17A}$*	*Ylp URA3*	This study
Ylp-DGA1$_{S17D}$	*HA-DGA1 $_{S17D}$*	*Ylp URA3*	This study

To produce the *SLC1*-Cub-LexA-VP16 fusion, the *SLC1* coding sequence was amplified from W303 genomic DNA using primers pTMBV4-SLC1f and pTMBV4-SLC1r and inserted into pTMBV4 plasmid in frame with the Cub-LexA-VP16 tag using Gibson isothermal assembly (38). Correct assembly of pTMBV4-SLC1 was confirmed by sequencing. The NubG fusions used for two-hybrid testing were constructed using

plasmids pADSL-Nx and pADSL-xN digested with BamHI and EcoRI. *DGA1* and *DGA1* variants amplified with truncations of the 5'- and 3'- sequences from W303 genomic DNA were inserted in frame with *NubG-HA* (Table 3.3). For production of the pADSL-NubG-HA-*SLC1* plasmid, the *SLC1* open reading frame was amplified from *S. cerevisiae* genomic DNA using primers SLC1f and SLC1r and inserted in frame with *NubG-HA*. For production of the pADSL-NubG-HA-*SCT1* and pADSL-NubG-HA-*GPT2* vectors, *SCT1* and *GPT2* coding sequences were amplified from *S. cerevisiae* genomic DNA using primer pairs SCT1f - SCT1r and GPT2f - GPT2r. The resulting DNA fragments were inserted in frame with *NubG-HA*. To create the pADSL-SCT1-HA-NubG construct, *SCT1* was amplified from *S. cerevisiae* genomic DNA using primers SCT1xNf and SCT1xNr. and ligated in to a BamHI – SfiI digested pADSL-xN in frame with *HA-NubG*.

$DGA1_{S17A}$ and $DGA1_{S17D}$ were generated by splice overlap PCR using oligonucleotides S17Af/S17Ar and S17Df/S17Dr. Dga1 carboxyl-terminal truncations were generated by PCR amplification using of *DGA1* coding sequence using oligonucleotides 212, 240, 288, 318, 388, 398. Similarly amino terminal truncations were generated by amplification of DGA1 with primers DGA1-23f, DGA1-29f, and DGA1-37f. In-frame internal deletions Δ399-410, Δ399-414, and Δ389-410 were generated using oligonucleotides DGAD398, DGAD398a, DGAD388. Charged-to-alanine mutations in DGA1 were generated using synthetic DNA fragments (Table 3.2). Each DNA fragment was assembled with StuI/EcoRI digested pADSL-NubG-HA-DGA1. All DNA constructs were confirmed by DNA sequencing.

The W303 derived H1246 (*MAT*α *are1*-Δ::*HIS3 are2*-Δ::*LEU2 dga1*-Δ::*KanMX4 lro1*-Δ::*TRP1 ADE2 ura3*) (39) was obtained from Dr. Randall Weselake for the fatty acid

toxicity analysis. The *DGA1* variants used for functional testing were placed under the regulation of the native *DGA1* promoter in integrating vector YIplac211. The promoter was amplified from W303 genomic DNA with a forward primer containing homology to the Pst1 cut site on YIplac211 (YI-DGA1pf, DGA1pr), and the HA-*DGA1* variants were amplified from the respective pADSL-NubG-HA-*DGA1* plasmids (Table 3.3) using a forward primer for *DGA1* with homology to the *DGA1* promoter and a reverse primer for *CYC1t* with homology to the PstI cut site on YIplac211 (DGA1p-HAf, YI-PSTCYC1). The promoter and *DGA1* truncations were inserted into the vector by Gibson isothermal assembly to produce the YIplac211-*DGA1* variants. These were digested with EcoRV to direct integration at the *URA3* locus and used to transform H1246. All yeast transformations were completed with the lithium acetate method (40). *Escherichia coli* DH5α was used in all cloning steps and for routine propagation of all plasmids.

3.3.2. Medium and cultivation conditions

E. coli strains were cultivated in lysogeny broth (LB) containing ampicillin (100 µg/mL) or kanamycin (50 µg/mL) as needed for plasmid maintenance. Yeast strains were propagated on YEPD medium (1% yeast extract, 2% peptone, 2% dextrose) or on synthetic defined medium (0.17% Yeast Nitrogen Base without amino acids without ammonium sulfate, 0.5% ammonium sulfate, 2% dextrose, supplemented with an amino acid mixture lacking the amino acids or purines as required for selection). YEPD or synthetic defined medium containing dextrose was supplemented with unsaturated fatty acids as noted.

3.3.3. Membrane Yeast Two-Hybrid assay

Interaction between specific proteins was tested using the Membrane Yeast Two-Hybrid test essentially as described (41). The reporter strains NMY51 and YBG1 (OLE1-Cub-LexA-VP16) were validated by transformation with positive and negative control vectors expressing Alg5-NubI and Alg5-NubG. The concentration of 3-aminotriazole (3-AT) necessary to remove background strain growth on medium lacking histidine was determined to be 6 mM. YBG1 harbouring the integrated *OLE1* bait was transformed with the prey plasmids and selected on synthetic minimal agar plates lacking tryptophan (-trp) to ensure retention of the vectors. Plasmid borne bait and prey pairs were tested in NMY51 by transformation of both plasmids and selection on medium lacking both tryptophan and leucine (-trp -leu). In both cases interaction was assayed on synthetic minimal agar plates lacking tryptophan and histidine, and adenine, supplemented with 6 mM 3-AT. Spot assays were performed by spotting cultures serially diluted 1:10 starting from $1.0x10^4$ cells.

LacZ expression was assayed by β-galactosidase assay. Strains were cultured in -trp or -trp -leu liquid media overnight at 30°C with agitation. The culture density was determined based on optical density at 600 nm (OD_{600}) and 1 mL of each culture was harvested by centrifugation. The cell pellets were resuspended in 500 µL Z-buffer (60 mM Na_2HPO_4, 40 mM NaH_2PO_4, 10 mM KCl, 1 mM $MgSO_4$) and 50 µL 0.1% SDS by vortexing. 100 µL of chloroform was added and the mixture was vortexed for 15 seconds before adding 100 µL of 4 mg/mL ortho-Nitrophenyl-β-galactoside (ONPG). The reaction mixture was incubated at 37°C until colour development and then quenched by addition of 500 µL 1M Na_2CO_3. Reactions were centrifuged to remove cell debris and the colour

development was assayed by measuring OD_{420}. β-galactosidase activity is presented as the mean of three independent colonies normalized either to the positive control, Alg5-NubI or to the full-length NubG-Dga1 as indicated. Significance was determined using a two-tailed t-test assuming equal variance.

3.3.4. Protein extraction and western blotting

Expression of all prey proteins was confirmed by western blot. Proteins were extracted from the NYM51 strain expressing the indicated prey or bait protein by bead beating in trichloroacetic acid as described (42) and equivalent volumes of protein were resolved using 10% SDS-PAGE. Proteins were electro-transferred to polyvinylidene difluoride membranes. The prey constructs were detected using anti-HA monoclonal antibody HA.11 clone 16B12 mouse ascites fluid and goat anti-mouse conjugated to horseradish peroxidase (HRP) secondary antibody. Cdk1 was used to determine relative amounts of protein loaded and was detected with an anti-PSTAIR antibody (P7962 Sigma-Aldrich) and goat anti-mouse HRP secondary antibody. The relative band densities of the NubG-Dga1 variants were quantified using BioRad Image Lab analysis software. The Ole1-Cub-LexA-VP16 and Slc1-Cub-LexA-VP16 fusions were detected with a rabbit polyclonal anti-LexA primary antibody (06-719 EMD Millipore) and goat anti-rabbit HRP secondary antibody.

3.3.5. Fatty acid toxicity assay

Fatty acid tolerance studies were performed both on agar-containing plates and in liquid medium. Synthetic minimal agar plates and liquid media lacking uracil (-ura) and

containing 0.05% ethyl acetate and 0.5mM of the indicated fatty acid were used. For the plate-based fatty acid toxicity assays, cultures were inoculated from a single colony and allowed to grow overnight in -ura media. Cultures were spotted to the selective medium plates starting from 1.0 $x10^4$ cells, diluted 1:10 serially. Images were obtained following 48 hours of incubation at 30°C. Fatty acid toxicity was assayed in liquid culture by inoculating cultures into SD medium lacking uracil from a single colony and growing overnight. Cultures were normalized to OD_{600} 0.05 in 1 mL of the indicated media and assayed in triplicate using biological replicates. Cells were cultured in a 2 mL deep well plate for 30hrs, using a plate shaker shaking at 900 rpm at 30°C. Samples were taken every 6 hours and analyzed on a Spectra Max M3, using the respective media as a blank.

3.3.6. Lipid analysis

TAG accumulation was assayed by TLC analysis of total cellular lipid species on silica gel plates stained by Coomassie Blue as previously described (43). TAG species visualized on TLC plates were quantified using Image J. Total cellular lipid accumulation was further corroborated by whole cell staining with Nile red as previously described (43). FAME analysis was performed by gas chromatography with an Agilent 6890 GC instrument equipped with flame ionization detector as previously described (44).

3.3.7. Confocal microscopy

Strains were cultured in YEPD medium at 30°C overnight. Cells were diluted into fresh YEPD supplemented with 100 µg/mL adenine at an OD_{600} of 0.2 and cultured for the indicated time periods. Cultures for LD visualization were stained for 10 minutes in

the dark using BODIPY 493/503 at a concentration of 50 µg/mL. All samples were washed in PBS and immobilized on 2% agarose pads prior to imaging. Images were collected on a Yokagawa CSU-X1 microscope using the GFP laser and filter, a Hamamatsu EMCCD (C9100-13) camera, and Perkin Elmer Volocity software. Images were analysed using Fiji and LD number and size were determined with the ALDQ plugin (45). LD number and size were quantified from at least 100 cells.

3.3.8. Statistical analysis

The data are presented as mean values and error bars reflect standard deviation. All n values are indicated in the figure legends. Statistical significance was evaluated by paired, two-tailed t-test. Differences in lipid droplet number were tested by one-way ANOVA performed with MATlab. Statistical significance is depicted in figures or noted in the figure legends (* represents $p<0.05$, ** $p<0.01$, *** $p<0.001$). Box and whisker plots to display data were constructed using BoxplotR.

3.4. Results

3.4.1. Δ9 desaturase Ole1 interacts with acyltransferases Sct1, Gpt2, Slc1 and Dga1

Ole1 is a central component in the *de novo* synthesis of phospholipids and triacylglycerol by acting as the source of unsaturated acyl-CoA that can be distributed to acyltransferases. We applied a split ubiquitin strategy to test for *in vivo* interactions between Ole1 and acyltransferase enzymes that have roles in glycerolipid biosynthesis.

Ole1 displays 60% similarity to the rat stearoyl-CoA desaturase (3). The structure of the rat enzyme has been solved and the topology of stearoyl-CoA desaturase in rat orients both the amino and carboxyl termini toward the cytosol, with the active site also positioned facing the cytosol (46). On this basis we introduced the Cub-LexA-VP16 tag to the carboxyl end of Ole1. When a plasmid borne Ole1-Cub-LexA-VP16 fusion was introduced into the reporter strain NMY51 the construct induced activation of the reporter genes independent of any binding partner. We hypothesized that the strong autoactivation might have occurred owing to degradation of the tagged version of Ole1 since cells are sensitive to Ole1 dosage (47). This limitation was overcome by employing an integrated membrane yeast two-hybrid (iMYTH) assay by introducing a DNA sequence encoding a Myc-Cub-LexA-VP16 tag into the endogenous chromosomal *OLE1* in the reporter strain NMY51. This Ole1 "bait" strain (YBG1) was subsequently transformed with negative and positive control vectors (pALG5-NubG, pALG5-NubI), in addition to plasmids harbouring the coding sequences for acyltransferases *SCT1, GPT2, SLC1*, and *DGA1* fused to the amino-terminus of ubiquitin (Figure 3.2A). The *OLE1* bait strain harbouring positive control pALG5-NubI displayed growth as expected on selective medium, whereas the negative control pALG5-NubG did not activate the *HIS3* and *ADE2* reporter genes and no growth could be observed on the selective medium (Figure 3.2A). Expression of NubG-Gpt2, NubG-Slc1 and NubG-Dga1 fusions activated the *HIS3* and *ADE2* reporter genes, permitting growth under selection conditions (Figure 3.2A). The NubG-Sct1 fusion displayed weaker growth on the selective plates but was detectable above the negative control. In contrast, when the NubG tag was fused to the carboxyl-terminus of Sct1 (Sct1-NubG) and the carboxyl-terminus of Dga1 (Dga1-NubG), no growth was observed on the

selective medium (Figure 3.2A). Expression of the *LacZ* reporter gene was consistent with the extent of cell growth observable on the selective medium showing that the NubG-Sct1, NubG-Gpt2, NubG-Slc1, and NubG-Dga1 fusions all induced a significant increase in expression of β-galactosidase activity over the negative control Alg5-NubG (Figure 3.2B). Expression of NubG-Sct1 increased activity twice that of the negative control (p = 0.003). NubG-Slc1 expression in YBG1 increased β-galactosidase activity nine-fold over the negative control (p = 0.006), while NubG-Dga1 expression in YBG1 increased activity eleven-fold ($p << 0.005$). Expression of the NubG-tagged acyltransferases in the NYM51 strain was confirmed by western blot analysis of whole cell lysates (Figure 3.5). These observations provide the first demonstration that acyltransferases Sct1, Gpt2, Slc1 and Dga1 interact with Δ9 desaturase Ole1 *in vivo*.

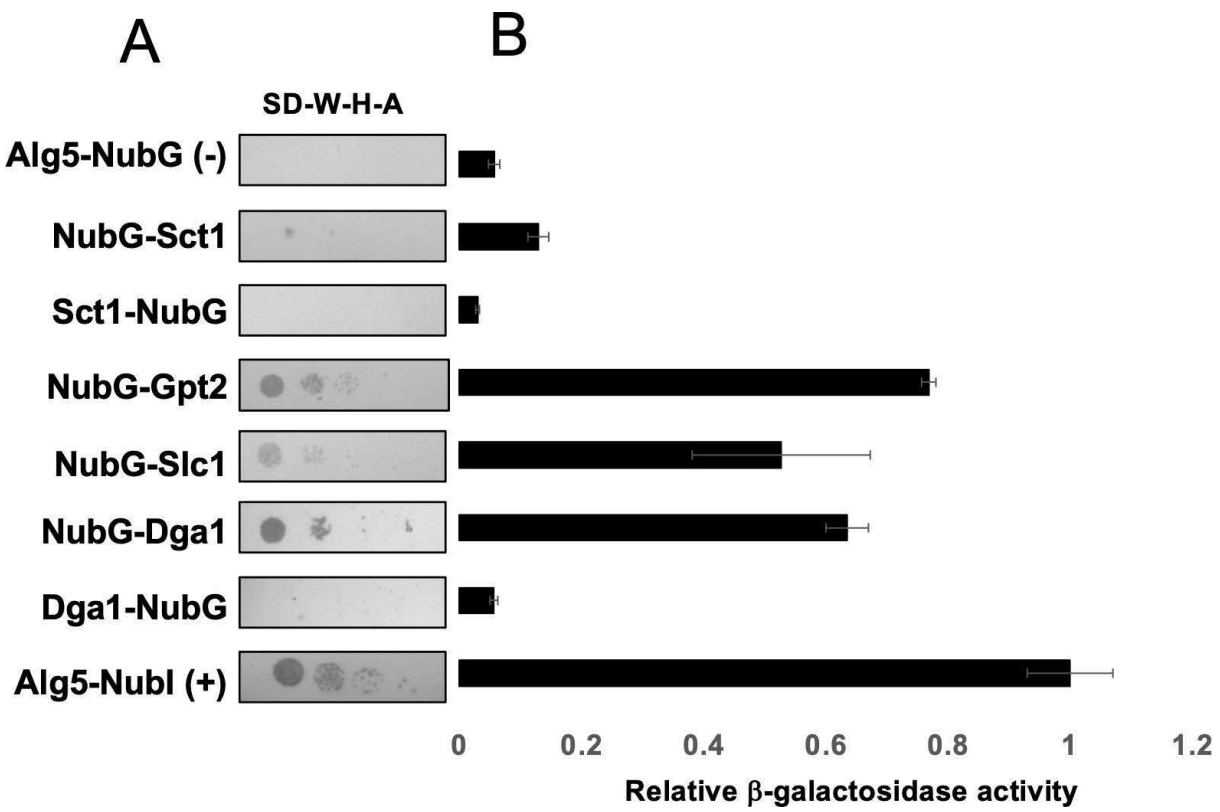

Figure 3.2. **∆9 acyl-CoA desaturase Ole1 interacts with acyltransferases.** A. Integrated membrane yeast 2-hybrid assay using a yeast strain expressing an endogenously tagged Ole1-Myc-C_{ub}-LexA-VP16 as "bait" and the indicated NubG fusions as "prey". Growth on selective medium plates is representative of three separate experiments (n = 3). Synthetic defined medium lacking tryptophan, histidine and adenine (SD-W-H-A) was used for the growth test. B. β-galactosidase activity in Miller units assayed from cell extracts. Each column represents the mean of three biological replicates (n = 3). Activities were normalized to the positive control (*pALG5-NubI*). Error bars reflect standard deviation.

3.4.2. Slc1 interacts with Dga1

Following the observation that Ole1 interacts with acyltransferases Sct1, Gpt2, Slc1 and Dga1, we were interested in determining whether the acyltransferases interacted with one another as an acyltransferase interactome has been demonstrated to in *Linum usitatissimum* (22). A reporter strain harbouring *SLC1*-Cub-LexA-VP16 as "bait" (YBG2) was transformed with negative and positive control vectors (p*ALG5*-NubG, p*ALG5*-NubI),

in addition to acyltransferase fusions, pNubG-*SCT1*, p*SCT1*-NubG, pNubG-*GPT2*, and pNubG-*DGA1*. The Slc1 bait strain containing the positive control prey plasmid p*ALG5*-NubI displayed growth on selective medium whereas the negative control p*ALG5*-NubG displayed no growth as expected (Figure 3.3A). Both of the NubG-Gpt2 and NubG-Dga1 fusions in combination with the *SLC1*-Cub-LexA-VP16 fusion activated the *HIS3* and *ADE2* reporter genes allowing growth on the selective medium (Figure 3.3A). Neither of the NubG-*SCT1* or *SCT1*-NubG fusions were able to induce robust growth when paired with the *SLC1*-Cub-LexA-VP16 fusion (Figure 3.3A). However, when interaction stringency was investigated with a β-galactosidase activity assay, the NubG-*SCT1* fusion in combination with *SLC1*-Cub-LexA-VP16 exhibited three times greater β-galactosidase activity than the negative control ($p = 0.008$), while expression of NubG-Gpt2 and NubG-Dga1 increased β-galactosidase activity almost 10-fold and 17-fold respectively over Alg5-NubG ($p << 0.005$). These data indicate that the *S. cerevisiae* acyltransferases, Sct1, Gpt2, and Dga1 interact with Slc1 as well as with Ole1 *in vivo*.

To gain further insight into the organization of the acyltransferase-desaturase interactions we extended this investigation to test whether the Slc1 and Dga1 could interact with one-another independent of Ole1. The *OLE1* coding sequence was deleted from the reporter strain NMY51 to yield *ole1*::NatMX6 (YGB3). This strain was maintained on medium supplemented with unsaturated fatty acids to support viability and plasmids encoding *SLC1*-Cub-LexA-VP16 and NubG-*DGA1* were installed in the strain. The *ole1* deletion mutant displayed growth on the selective medium indicating that Slc1 and Dga1 fusions were able to interact with one another in the absence of Ole1 (Figure 3.3C, D).

Thus, while Slc1 and Dga1 do both interact with Ole1 they also interact with one another and Ole1 is not required as a scaffold for this interaction.

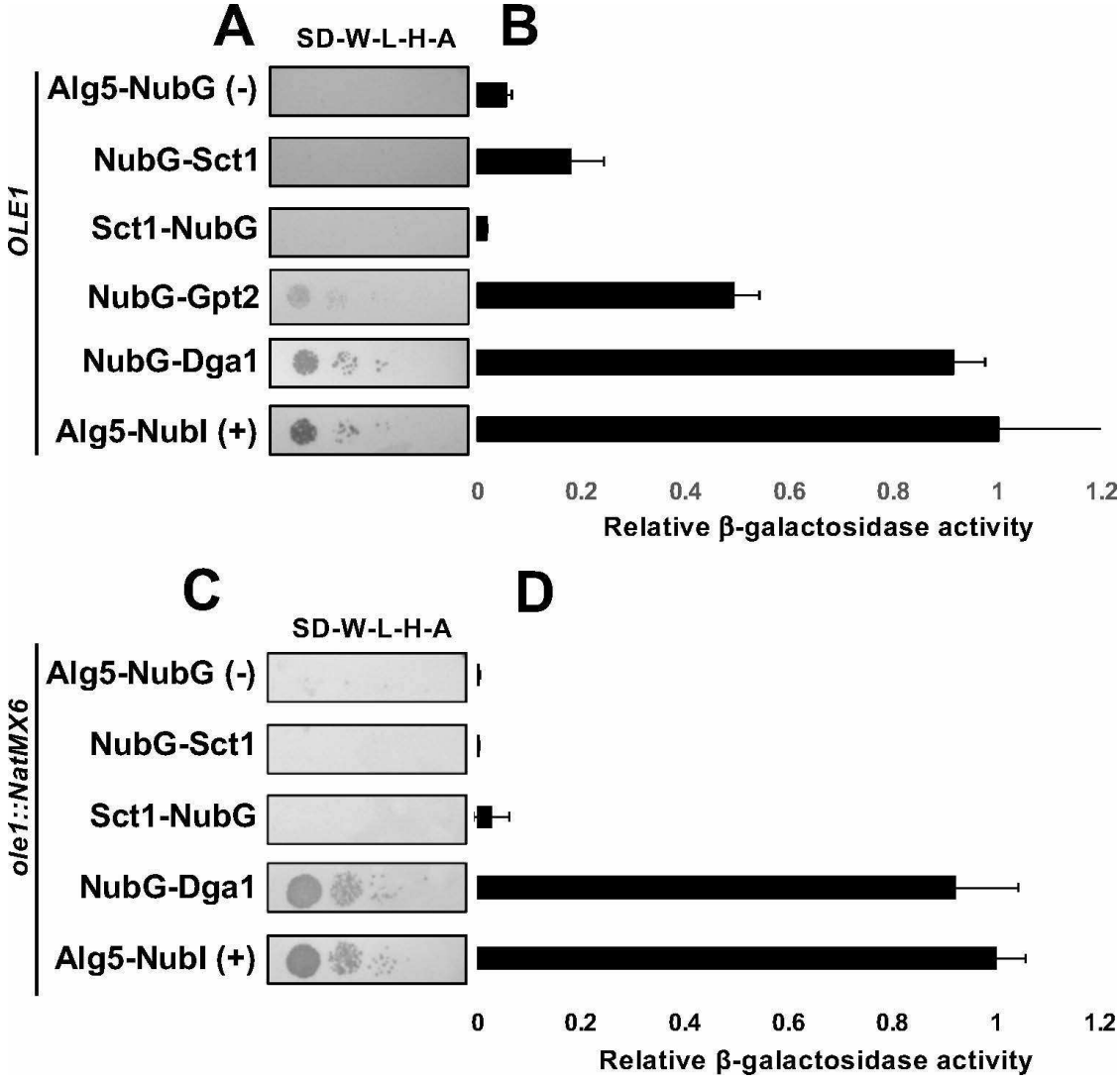

Figure 3.3. **Acyltransferase Slc1 interacts with Dga1.** A. Integrated membrane yeast two-hybrid assay using a yeast strain expressing Slc1-C_{ub}-LexA-VP16 as bait and the indicated NubG fusions as "prey". Growth on selective medium plates is representative of three separate experiments (n = 3). Synthetic defined medium lacking tryptophan, leucine, histidine and adenine (SD-W-L-H-A) was used for the growth test. B. β-galactosidase activity in Miller Units assayed from cell extracts. Each column represents the mean of three biological replicates (n = 3). Activities were normalized to the positive control (pALG5-NubI). Error bars reflect standard deviation. C. Integrated membrane yeast 2-hybrid assay using a Δ*ole1* strain expressing Slc1-C_{ub}-LexA-VP16 as bait and the indicated NubG fusions as "prey". Growth on selective medium plates (SD-W-L-H-A) supplemented with 0.5% Tween-80 and 0.05% oleate is representative of three separate experiments (n = 3). D. β-galactosidase activity in Miller units assayed from Δ*ole1* cell extracts. Each column represents the mean of three biological replicates (n = 3). Activities were normalized to the positive control (pALG5-NubI). Error bars reflect standard deviation.

3.4.3. The carboxyl terminus of Dga1 is required for its interaction with Ole1

Protein-protein interactions between integral membrane proteins can be complex relationships influenced by both the protein partners and the lipid bilayer environment and composition. To further investigate our novel observation that Dga1 interacts with Ole1 in the ER membrane we performed a mutagenic analysis of Dga1 to determine if a specific domain of Dga1 responsible for maintaining the interaction with Ole1 could be identified. Topological analysis of Dga1 indicates that the amino and carboxyl-termini are oriented to the cytosolic side of the ER membrane (48). We initiated a mutagenic analysis by generating truncations of the amino and carboxyl termini of Dga1 and fusing the truncations in frame with NubG to determine if they were capable of interacting with the integrated Ole1-Cub-LexA-VP16 bait in YBG1 (Figure 3.4A). The amino-terminal 36 amino acids residues of Dga1 have been implicated in regulation of the enzyme's activity (49). Deletion of Dga1 amino acids 1-29 had no significant effect on interaction of Dga1 with Ole1 as evaluated by growth of the strains on selective medium and quantitative β-galactosidase activity (Figure 3.4B). Consistent with this finding, we also observed that mutation of Ser^{17}, a residue that is phosphorylated *in vivo* but with no ascribed function (50), to either non-phosphorylatable Ala^{17} or the phosphomimetic Asp^{17} had no detectable effect on the Ole1-Dga1 interaction as measured by growth of the cells on selective medium or quantitative β-galactosidase activity (Figure 3.4B). Further deletion of amino acids 1-37 (NubG-$Dga1_{38-418}$) caused a significant reduction in β-galactosidase activity to about 67% of the full-length Dga1 ($p = 0.015$) (Figure 3.4B).

A truncation that deleted amino acids 319 - 418, predicted to form a carboxyl-terminal cytosolic domain (NubG-Dga1$_{1-318}$), resulted in a loss of interaction with Ole1 based upon a reduction of growth observed on selective medium and the near complete elimination of β-galactosidase activity (Figure 3.4B). Further deletions from the carboxy-terminus (NubG-Dga1$_{1-240}$, NubG-Dga1$_{1-288}$) showed no further reduction in the interaction based on β-galactosidase assay (Figure 3.4B). A shorter truncation of the last twenty amino acids of the carboxy-terminal cytosolic domain of Dga1 (NubG-Dga1$_{1-398}$) also abolished the interaction with Ole1, demonstrated by a loss of growth on selective medium and a decrease in β-galactosidase activity (Figure 3.4B). A Dga1 variant lacking the final ten amino acids (NubG-Dga1$_{1-408}$) supported more extensive growth on selective medium and increased β-galactosidase activity consistent with this truncated variant displaying interaction with Ole1 (Figure 3.4B). NubG-Dga1$_{1-408}$ induced ~200% more β-galactosidase activity that did NubG-Dga1$_{1-398}$ suggesting that residues 398-418 might play an important role in the interaction of Dga1 and Ole1 (Figure 3.4B).

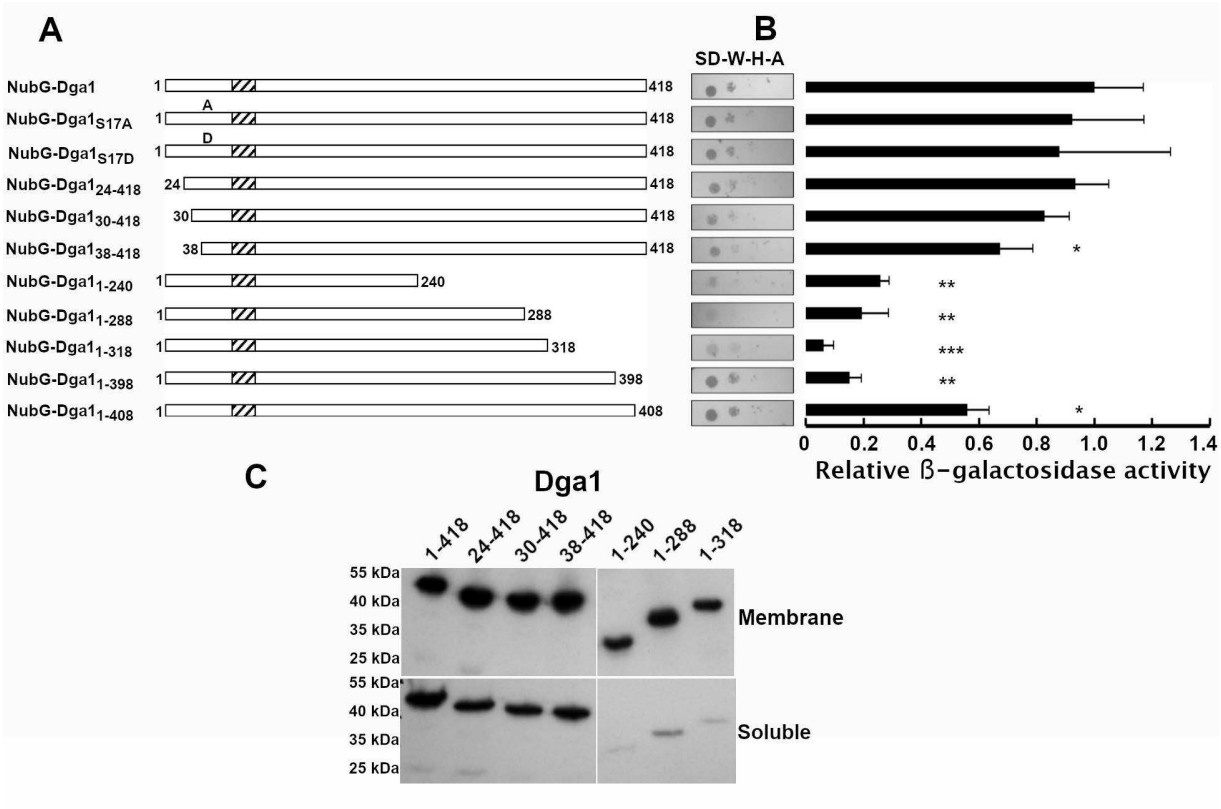

Figure 3.4. **Truncation of the Dga1 carboxyl-terminus disrupts the interaction with Ole1.** A. Schematic map of the Dga1 truncations tested, the dashed box represents the predicted transmembrane domain. B. Integrated membrane yeast two-hybrid assay using a yeast strain expressing Ole1-Myc-C_{ub}-LexA-VP16 as "bait" and the indicated constructs fused to NubG as "prey". Growth on selective medium plates is representative of three independent experiments. Synthetic defined medium lacking tryptophan, histidine and adenine (SD-W-H-A) was used for the growth test. Bars represent β-galactosidase assay of a yeast strain expressing Ole1-Myc-C_{ub}-LexA-VP16 and the indicated NubG-Dga1 variants. Each column is representative of three biological replicates (n = 3). Miller units were normalized to the NubG-full-length Dga1 fusion. Asterisks (*) denote significantly different *LacZ* activity from NubG-Dga1 by Student's t-test, (* = $p < 0.05$, ** = $p < 0.01$, *** = $p < 0.001$). Error bars reflect standard deviation. C. Western blot analysis of the proportion of Dga1 found in the membrane (upper panel) and soluble (lower panel) fractions. The Dga1 variants are indicated at the top of each lane. The migration of molecular weight markers (kDa) is indicated to the left of each panel.

The ability of Dga1 truncations to bind Ole1 and activate the reporter genes in the two-hybrid assay are dependent upon their expression and localization to the ER membrane. Expression and localization of the Dga1 variants was tested by western blot

analysis and subcellular fractionation. Probing whole cell lysates with anti-HA antibodies revealed that the NubG fusion to full-length Dga1 and all of the amino- and carboxyl-terminal truncations from $Dga1_{24-418}$ to $Dga1_{1-318}$ were expressed (Figure 3.5). To confirm that the Dga1 variants were being correctly localized in membranes, whole cell extracts were subjected to centrifugation at 104,000 x *g* for one hour, and samples of the soluble fraction and pelleted membrane fraction were assayed for Dga1 by western blot. Comparison of western blots indicates that over 60% of $Dga1_{24-418}$, $Dga1_{30-418}$ and $Dga1_{38-418}$ were present in the pellet fraction consistent with membrane localization (Figure 3.4C). The Dga1 carboxy-terminal truncations $Dga1_{1-240}$, $Dga1_{1-288}$ and $Dga1_{1-318}$ all display predominant localization to the membrane fraction (Figure 3.4C).

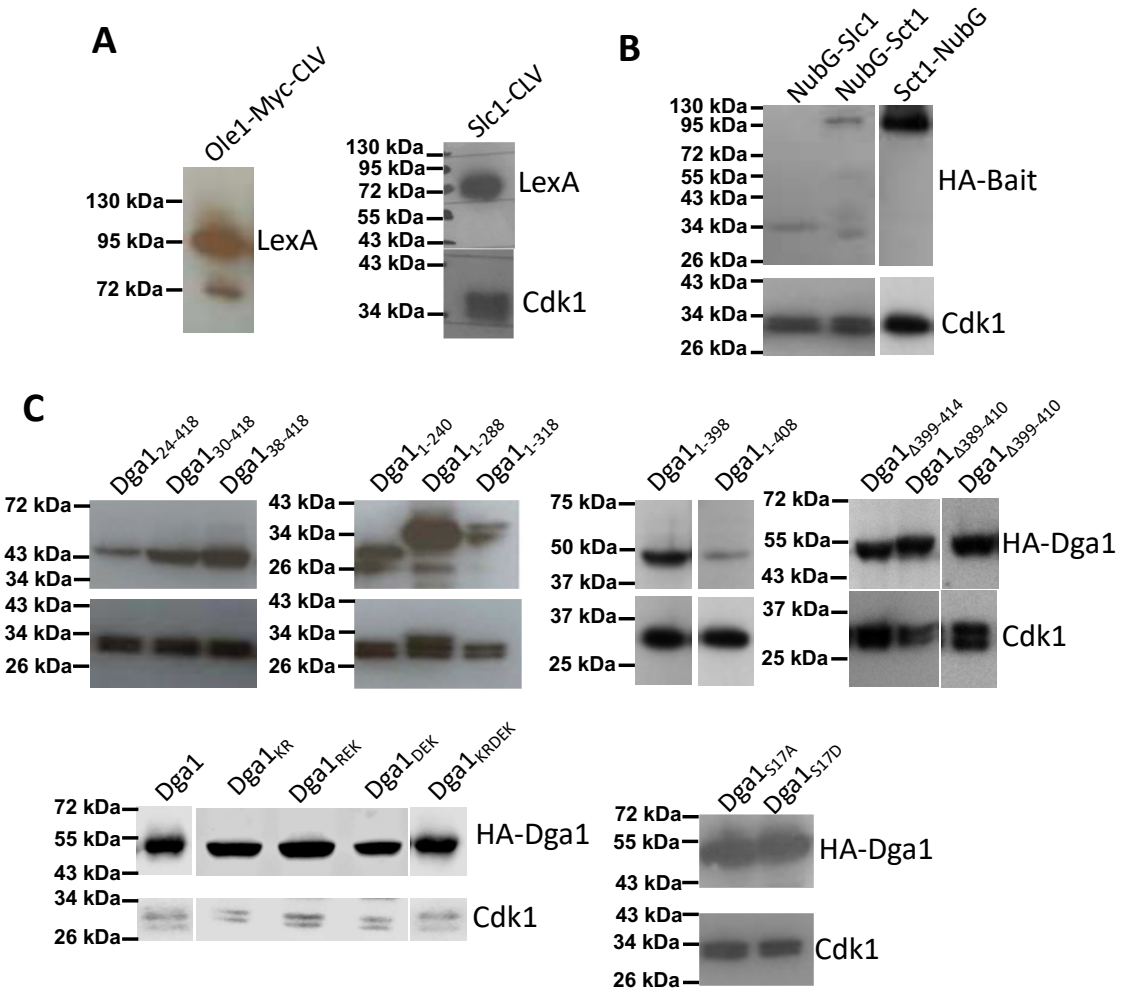

Figure 3.5 **Western blot confirmation of bait and prey protein expression for two-hybrid testing.** A. Ole1 and Slc1 fused to the C-terminus of ubiquitin- LexA-VP16 were detected with an antibody against recognizing LexA. The blots were subsequently probed for Cdk1 with an antibody recognizing the PSTAIRE motif as a loading control. ”Prey” proteins Dga1, Dga1 variants, Slc1, and Sct1 fused to NubG were visualized by probing blots with an antibody recognizing the HA epitope.

3.4.4. Charged residues at the carboxyl-terminus of Dga1 are important for the Ole1-Dga1 interaction

The carboxyl-terminus of Dga1 is essential for the catalytic activity of the enzyme, deletion of residues 413 - 418 result in a near complete loss of activity despite Dga1 being

retained in the ER (48). Dga1 lacks a traditional ER retention or retrieval signal at its carboxyl-terminus, while it is possible that the small truncations at the carboxyl-terminus inhibit localization this is unlikely as deletion of residues 413 - 418 do not reduce its retention in membranes (48). To determine whether the conserved DAELKIVG or KIVG motifs at the carboxyl-terminus were important for maintaining the interaction between Dga1 and Ole1, in-frame deletions of residues 389 - 410, 399 - 410 and 399 - 414 were generated (Figure 3.6A). Each version of Dga1 with these small in-frame internal deletions was assayed for interaction with Ole1. In each case expression of the mutant version of *DGA1* allowed weak but detectable growth on the selective medium plates (Figure 3.6B). The ∆389-410, ∆399-410, ∆399-414 Dga1 deletions activated the *LacZ* reporter gene to a significantly lesser degree than full length-Dga1 inducing β-galactosidase activity to less than 20% of that induced by full-length NubG-Dga1 fusion (Figure 3.6B). Indeed the β-galactosidase activity driven by the internal deletion variants is similar to the larger $Dga1_{1-398}$ truncation (Figure 3.4B). These observations implied that mutations in Dga1 residues from 398 - 411 are sufficient to disrupt the interaction of Dga1 with Ole1.

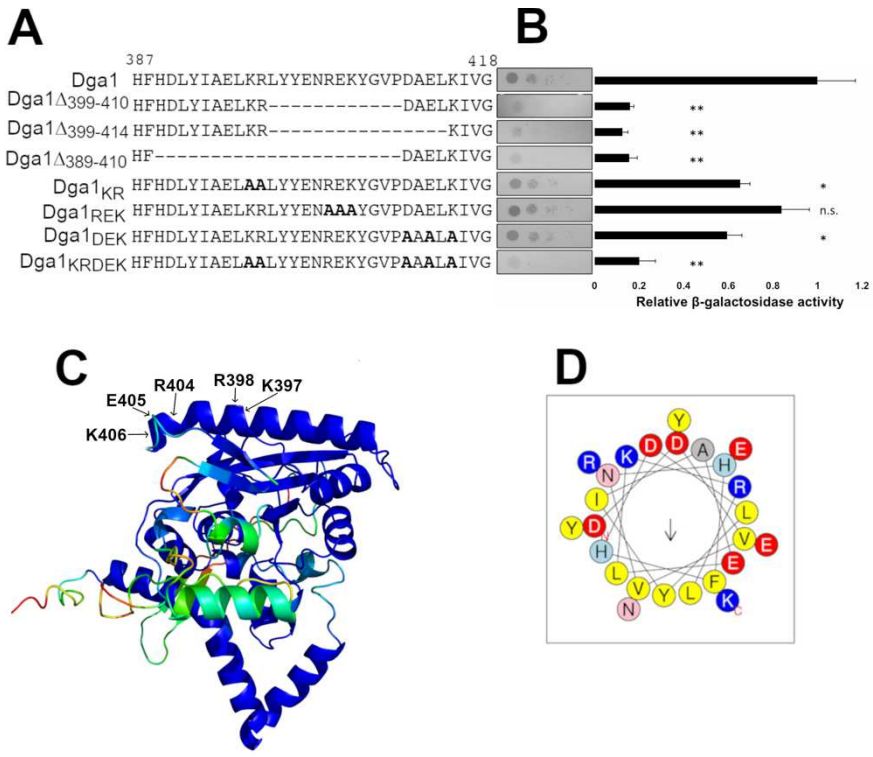

Figure 3.6. **Charged residues at the carboxyl-terminus of Dga1 are important for interaction between Ole1 and Dga1.** A. Sequences of carboxyl-terminal Dga1 mutants. Dashed lines indicate deleted sequences. Bold A indicates replacement of a charged residue with alanine. B. Integrated membrane yeast two-hybrid assay using a yeast strain expressing Ole1-Myc-C_{ub}-LexA-VP16 and the indicated NubG-Dga1 variants. Growth on selective medium plates is representative of three independent experiments. Filled bars represent β-galactosidase activity in Miller units from extracts of the yeast strain expressing Ole1-Myc-C_{ub}-LexA-VP16 and the indicated NubG-Dga1 fusions. Each column is representative of three biological replicates (n = 3). Miller units were normalized to the NubG-full-length Dga1 fusion. Asterisks (*) denote significantly different *LacZ* activity from NubG-Dga1 by Student's t-test, (* = $p < 0.01$, ** = $p < 0.001$, n.s. = not significant). Error bars reflect standard deviation. C. AlphaFold predicted structure of Dga1, colours represent confidence of the predicted model. Residues in the carboxyl-terminal helix mutated from charged-to-alanine are indicated with arrows. D. HeliQuest plot of Dga1 carboxy-terminal helix, from Asp^{382} to Lys^{406}. Negatively charged residues shown in red, positively charged residues shown in blue, polar residues shown in pink and light blue, and nonpolar residues shown in yellow.

The carboxy-terminal 20 amino acids of Dga1 feature several short segments that include charged residues. To determine if these charged segments might be important for the interaction of Dga1 with Ole1 we performed charged-to-alanine scanning

mutagenesis. The residues chosen for this alanine scanning experiment are shown on the AlphaFold generated model where it can be seen that they cluster on a surface predicted to be exposed to the cytoplasm (Figure 3.6C). The helix in the model contains Asp^{382} to Lys^{406} and is amphipathic in nature (Figure 3.6C, 3.6D). The predicted surface of this segment of Dga1 contains a series of charged residues, including Lys^{397}, Arg^{398}, Arg^{404}, Glu^{405}, and Lys^{406}. The more hydrophobic face of this helix is oriented toward the predicted hydrophobic core of Dga1 and the highly conserved motif ^{288}R*X*GF*X*(K/R)*X*A*XXX*G*XXX*(L/ V)VP*XXX*FG(E/Q)^{311} (Figure 3.6C) which is essential for DGAT activity (35, 48). When tested for interaction with Ole1 in the membrane two-hybrid system Dga1 $R^{404}A$, $E^{405}A$, $K^{406}A$ (NubG-$Dga1_{REK}$) displayed growth on selective medium and β-galactosidase activity that was not significantly different from wild-type Dga1 (Figure 3.6B). In this assay both of the mutants Dga1 $K^{397}A$, $R^{398}A$ (NubG-$Dga1_{KR}$) and Dga1 $D^{411}A$, $E^{413}A$, $K^{415}A$ (NubG-$Dga1_{DEK}$) displayed reduced growth on selective medium relative to wild-type Dga1 (Figure 3.6B). Similarly, both mutants displayed a significant reduction in β-galactosidase activity to about 60% of that induced by wildtype Dga1 (p = 0.006, p = 0.012 respectively) (Figure 3.6B). Combining these mutations in NubG-Dga1 $K^{397}A$, $R^{398}A$, $D^{411}A$, $E^{413}A$, $K^{415}A$ (NubG-$Dga1_{KRDEK}$) resulted in a discernable reduction in growth on selective medium and a significant decrease in β-galactosidase activity to a level similar to that displayed by deleting the last twenty amino acids of Dga1 (p = 0.004) (Figure 3.6B). These data are consistent with the contention that the charged clusters in the carboxy-terminal 20 amino acids residues of Dga1 play a role in allowing the interaction of Dga1 and Ole1 *in vivo*.

3.4.5. Interaction of Dga1 with Slc1 displays sequence requirements distinct from those required for Ole1

Dga1 displays interactions with both the ∆9 desaturase Ole1 and acyltransferase Slc1. We were interested in investigating whether Dga1 bound to Slc1 through a similar sequence domain to that required for binding to Ole1. This was tested by performing a membrane two-hybrid test using the *SLC1*-Cub-LexA-VP16 fusion as "bait" for the NubG-Dga1 variants. Similar to the result observed with Ole1 as bait, the amino-terminal Dga1 truncations up to amino acid 37 displayed effective interaction with Slc1 based upon the reporter strains growth on selective medium and β-galactosidase activity similar to the full-length Dga1 (Figure 3.7A,B). In contrast, truncations of the carboxyl-terminal residues resulted in a reduction in the growth of the reporter strain on selective medium (Figure 3.7A). These strains all displayed a reduction of β-galactosidase activity to levels 20 - 40% of that measured in reporter strains expressing the full-length NubG-Dga1 fusion (Figure 3.7B). The reduction in binding to Slc1 displayed by the carboxyl-terminal truncations of Dga1 displays a similar pattern to that observed when binding to Ole1 was tested but expression of the β-galactosidase reporter gene was reduced to a greater extent in the Ole1 binding test than observed in the Slc1 binding test.

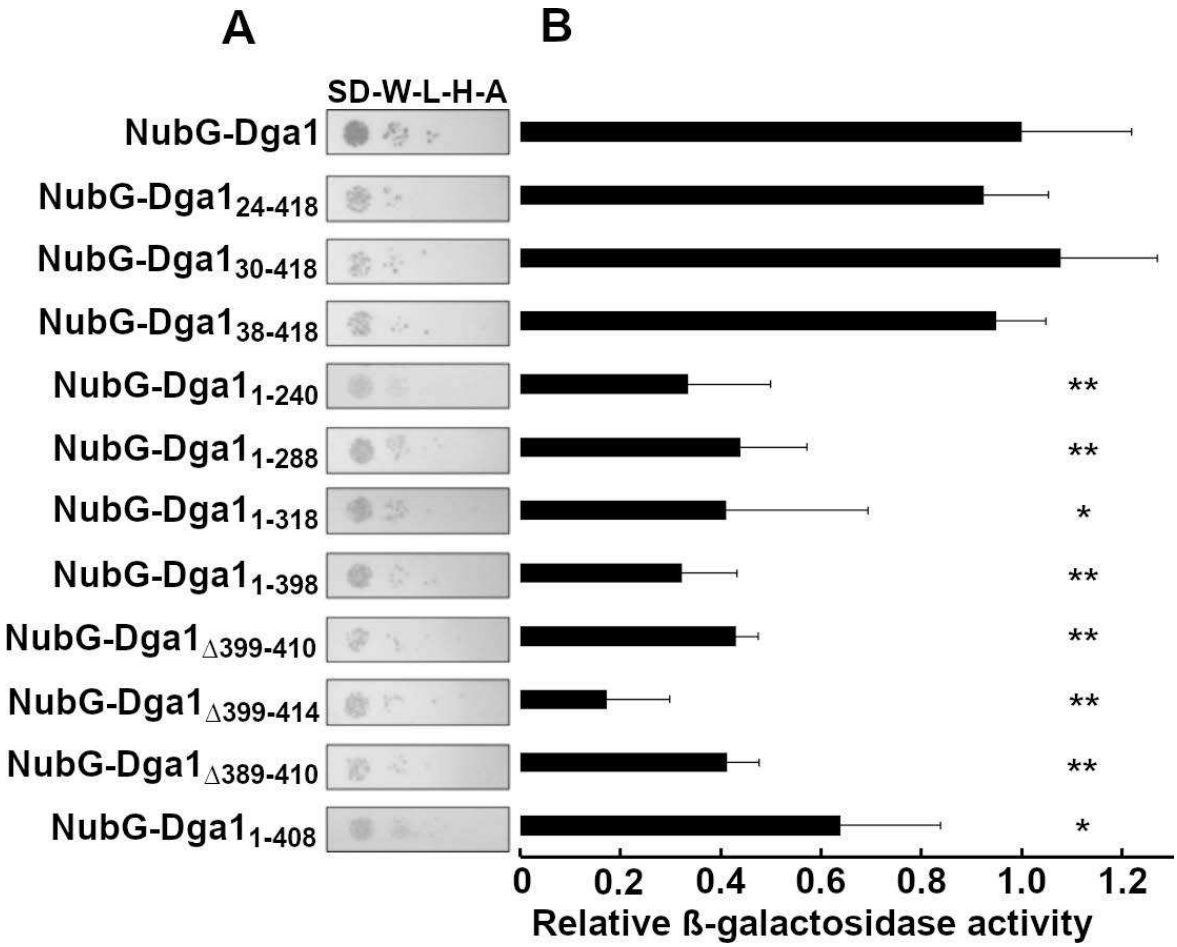

Figure 3.7. **Slc1 interacts with a truncated Dga1.** A. Membrane yeast two-hybrid assay using a yeast strain expressing Slc1-C_{ub}-LexA-VP16 as "bait" and the indicated NubG-Dga1 fusions as "prey". Growth on selective medium is representative of three independent experiments. Synthetic defined medium lacking tryptophan, leucine, histidine and adenine (SD-W-L-H-A) was used for the growth test. B. β-galactosidase activity in Miller units assayed from whole cell extracts assay of NMY51 expressing Slc1-C_{ub}-LexA-VP16 and the indicated NubG-Dga1 fusions. Each column is representative of three biological replicates (n = 3). Miller units were normalized to the full-length NubG-Dga1 fusion. Asterisks (*) denote significantly different *LacZ* activity from NubG-Dga1 by Student's t-test, (* = $p < 0.05$, ** = $p < 0.01$ *** = $p<0.001$). Error bars reflect standard deviation.

3.4.6. Dga1 charged-to-alanine mutants are defective in Ole1 binding but retain acyltransferase function

Dga1 activity is not essential and triglyceride synthesis is not a required activity for *S. cerevisiae* (39). However, acyltransferase activity does become important when cells are challenged with unsaturated free fatty acids (51). In the absence of acyltransferases Are1, Are2, Dga1, and Lro1, fatty acids become toxic to *S. cerevisiae* as displayed by the inability of H1246 cells that lack Are1, Are2, Dga1 and Lro1 to grow in the presence of 0.5mM oleic or palmitoleic acid (Figure 3.8, ΔDgat). Growth on this medium is restored by expression of full-length Dga1 presumably owing to its ability to sequester the unsaturated fatty acids into triacylglycerol (Figure 3.8, Dga1). The truncated versions of Dga1 were tested to determine whether they had sufficient activity to rescue growth of the H1246 strain on medium supplemented with unsaturated fatty acids. All of the amino-terminal truncations could rescue growth in the presence of either oleic acid or palmitoleic acid, suggesting that they were active (Figure 3.8). This observation supports the previous finding suggesting these truncated versions were properly localized to the ER membrane (Figure 3.4C). In contrast, deletion of any amount of the carboxyl-terminus of Dga1 eliminated fatty acid tolerance, suggesting that these variants of Dga1 are nonfunctional (Figure 3.8). The correlation between Dga1 function and ability to interact with Ole1 was further tested by challenging H1246 strains expressing the Dga1 charged-to-alanine mutants with fatty acid supplemented medium. Interestingly, H1246 cells expressing the alanine scanning mutants including $Dga1_{KRDEK}$ that was defective in Ole1 binding, were all able to grow on fatty acid supplemented medium similar to cells

expressing full-length Dga1, indicating that these Dga1 variants are functional and able to incorporate fatty acids into TAG (Figure 3.8).

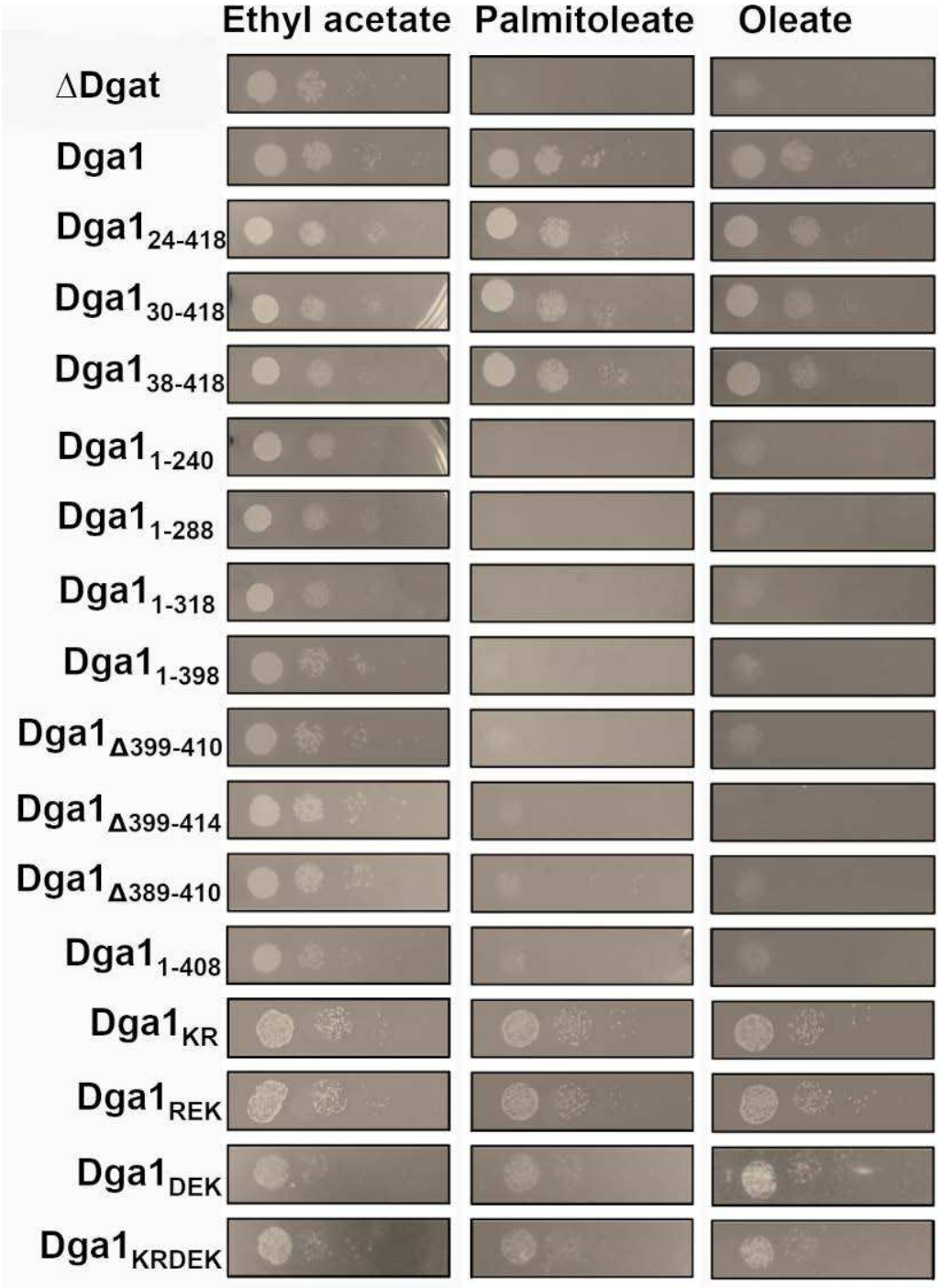

Figure 3.8. **Dga1 charged-to alanine variants are functional.** Fatty acid toxicity assay using medium supplemented with ethyl acetate (0.05%), palmitoleate (0.5 mM), or oleate (0.5 mM). The strain H1246 (*are1 are2 lro1 dga1*) harboured an empty vector (ΔDgat) or the indicated variants of *DGA1*. Strains were allowed to grow for 2 days at 30°C before imaging.

The primary function of Dga1 is TAG synthesis leading to lipid droplet formation in *S. cerevisiae*. Microscopic analysis of *are1 are2 lro1 DGA1*$_{30\text{-}418}$ strains stained with BODIPY demonstrated that lipid droplets could be readily visualized (Figure 3.9A). There did not appear to be any difference in the size or number of lipid droplets per cell detected in *DGA1*$_{30\text{-}418}$ when compared to full length *DGA1* (Figure 3.9A). In contrast, staining H1246 expressing *DGA1*$_{1\text{-}408}$ with BODIPY did not reveal any lipid droplet formation, only diffuse staining could be detected (Figure 3.9A). Lipid droplets could be detected in H1246 strains expressing the Dga1$_{KR}$, Dga1$_{DEK,}$ Dga1$_{REK,}$ or Dga1$_{KRDEK}$ charged to alanine variants consistent with those variants being functional (Figure 3.9A). This indicates that the charged-to-alanine mutations do not disrupt Dga1 catalytic activity but rather have a specific effect on the ability to bind Ole1. These observations also indicate that the ability of Dga1 to bind Ole1 is not essential for Dga1 function and LD formation when unsaturated fatty acids are exogenously supplied. However, further analysis of BODIPY stained cells revealed that Dga1$_{KRDEK}$ expressing cells accumulated fewer lipid droplets during early exponential growth than did cells expressing full-length Dga1 (Figure 3.9B). In contrast, Dga1$_{KRDEK}$ expressing cells accumulated more LDs when the cells approached early stationary phase (Figure 3.9B). Quantification of lipid droplet size from confocal microscopy images revealed that although Dga1$_{KRDEK}$ strains accumulated more lipid droplets per cell, those lipid droplets were smaller during both exponential growth (0.123±0.064 μm^2 vs 0.158±0.059 μm^2) and in early stationary phase (0.152±0.060 μm^2 vs 0.171±0.053 μm^2) than those in cells expressing Dga1 (Figure 3.9C).

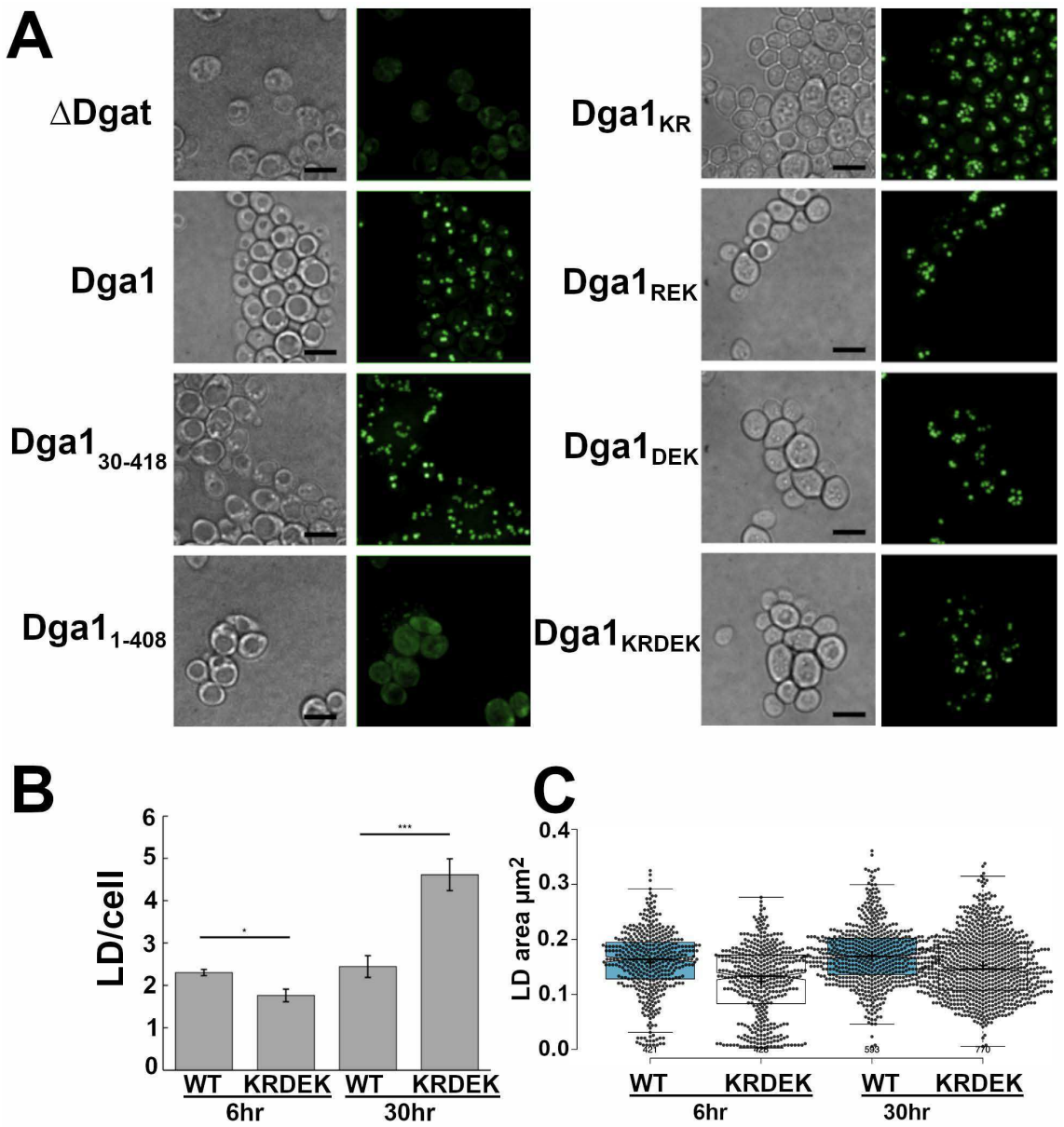

Figure 3.9. **Lipid droplet formation is altered by carboxyl-terminal mutations in Dga1.** A. Cultures of H1246 harbouring the indicated HA-Dga1 variants were grown to stationary-phase, stained with BODIPY 493/503 and visualized by microscopic examination under white light (DIC) or epifluorescence. The micrometer marker bar in the DIC images represents 10 µm. Fluorescence images are Z projections of whole cells. B. Lipid droplets visualized by microscopy were quantified in H1246 strains expressing DGA1 (WT) or the charged-to-alanine mutant DGA1$_{KRDEK}$ (KRDEK) at the indicated times. Bars indicate the mean from counting LDs detected in cells of each strain at each time point WT 6hr n = 166, KRDEK 6 hr n = 188, WT 30 hr n = 224, KRDEK 30 hr n = 167. Error bars reflect standard deviation. C. LD size was quantitated with the ALDQ Fiji plug in method and data reflect mean size µm^2 displayed as box and whisker plots for cells counted at each time point. WT 6 hr n = 421, 30 hr n = 593. KRDEK 6 hr n = 426, 30 hr n = 770.

To determine whether the TAG accumulation was affected by the charged to alanine mutations introduced into Dga1 we compared the amount of TAG in *are1 are2 lro1 DGA1* and *are1 are2 lro1 DGA1*$_{KRDEK}$ strains from active growth. Quantification of TAG species separated by thin layer chromatography indicated that there was no difference between the strains (Figure 3.10). Additionally, analysis of FAMEs from the two strains indicated that the C16/C18 ratio, 1.16 for Dga1 vs 1.13 for Dga1$_{KRDEK}$, was unaffected by the mutations. Additionally, the difference in the ratio of unsaturated to saturated acyl-chains (UFA/SFA) 5.51±0.01 vs 4.97±0.18 for Dga1 and Dga1$_{KRDEK}$ respectively, did not display a statistically significant difference.

These observations are consistent with the notion that compromising the interaction between Dga1 and Ole1 does not prevent the synthesis of TAG but may be disruptive to some aspects of lipid droplet formation and expansion.

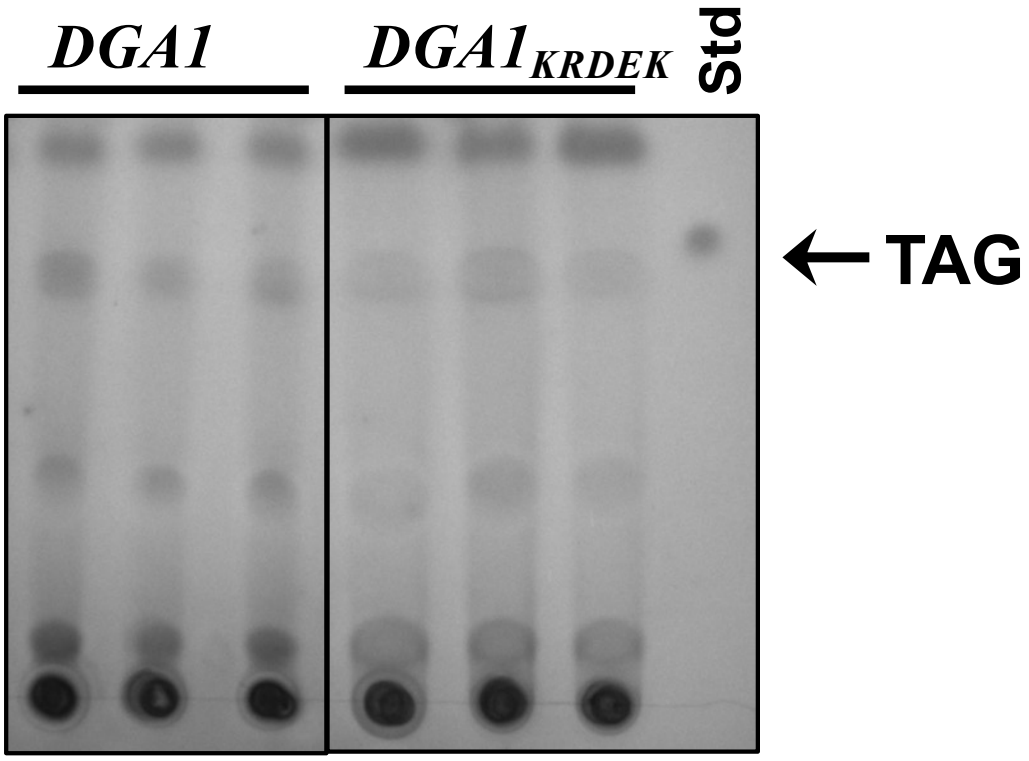

Figure 3.10. **TLC of *are1 are2 lro1 DGA1* or *are1 are2 lro1 DGA1*$_{KRDEK}$ total cellular lipids at the active growth phase.** Total yeast lipids were extracted from triplicate samples of the indicated strains and visualized by staining with Coomassie Blue (43). The position of TAG based on mobility of the tristearin standard (Std) and absence of a spot in *are1 are2 lro1 dga1* samples is indicated by the arrow.

3.5. Discussion

Through the application of targeted MYTH assays this investigation has revealed previously unrecognized interactions between the ∆9 acyl-CoA desaturase Ole1 and acyltransferases Sct1, Gpt2, Slc1 and Dga1. The interaction of these enzymes that all have roles in the synthesis of phospholipid and TAG suggests the possibility of a metabolon or enzyme supercomplex organization that could provide the benefits of substrate channeling to increase pathway flux in glycerophospholipid biosynthesis as well

as facilitate control over intermediates that could disrupt membrane function should they accumulate inappropriately. Cross-linking experiments with human cell cultures have provided support for the contention that acyltransferases DGAT2 and MGAT2 reside in a high molecular weight complex that likely includes SCD1 but the organization of this complex has yet to be investigated (25). A benefit of the MYTH assay applied in this study is that a positive signal demands close physical interaction of the tested proteins and co-complex formation is not sufficient (41). Positive interactions were also detected between acyltransferases Gpt2 - Slc1 and Slc1 - Dga1 consistent with the presence of an acyltransferase interactome among enzymes involved in the synthesis of phospholipids and TAG in *S. cerevisiae*.

Physical interaction between Dga1 and Ole1 has not been previously reported in *S. cerevisiae*. There is however precedent for this interaction as the orthologs of *DGA1* and *OLE1* in human cells and *C. elegans* (DGAT2, SCD1) have been demonstrated to colocalize and human DGAT2 and SCD1 can be co-immunoprecipitated (31). Dga1 shuttles between the ER and LD dependent upon the growth stage of the cells (52, 53). This likely creates at least two distinct pools of Dga1 since Ole1 is present only in the ER. Similarly, human cells display two separate pools of DGAT2, one localized in the ER and one associated with LDs (35). The role of Dga1 at LDs is clearly to promote TAG synthesis and storage in the LD. It is less clear what function Dga1 serves while interacting with Ole1 in the ER membrane. Investigations in *C. elegans* indicate that retaining DGAT2 in the ER allows for LD initiation but fails to support LD expansion (54). This may imply that DGAT activity in the ER is necessary to initiate LD formation but further expansion of the LD requires that DGAT activity be able to segregate from the ER to the LD membrane

structures. It is notable that the second *S. cerevisiae* DGAT, Lro1, can support initiation of LD biogenesis but does not segregate to LDs to support their expansion leading to reduced LD formation in stationary phase strains lacking Dga1 (55).

∆9 desaturase Ole1 has a central role in the synthesis of phospholipids and TAG. Acyl chains are synthesized *de novo* as saturated chains by the FAS complex and formation of mono-unsaturated chains is dependent on Ole1 activity. Thus, a significant portion of newly synthesized acyl-CoA is destined to become substrate for Ole1. LD initiation is dependent upon incorporation of unsaturated acyl-chains into DAG and TAG (56). Thus, linking Dga1 to Ole1 may be a means to efficiently influence LD initiation as this places Dga1 in close proximity to both the source of *de novo* synthesized mono-unsaturated acyl chains and the sites of LD formation. This also positions Dga1 to rapidly move onto the monolayer membrane of growing LDs. We also find that the LPAAT Slc1 interacts with Ole1 which could potentially create complexes including Slc1-Ole1-Dga1 that would be able to supply PA and DAG as well as unsaturated acyl-CoA for TAG synthesis. Dga1 and Slc1 can also interact with one-another independent of Ole1 consistent with the presence of these two enzymes in the LD surface where they can promote TAG accumulation in the LD.

Interaction of Ole1 with Slc1 may be a means by which unsaturated acyl chains can be directed toward phospholipid synthesis in rapidly proliferating cells. The degree of unsaturation in membrane phospholipids is a critical determinant of membrane properties including membrane fluidity and domain structures that influence functionality of membrane embedded proteins. Interaction of Slc1 with Ole1 may also form a complex to receive LPA generated by GPATs Sct1 and Gpt2. A physical interaction between Ole1

and Gpt2 has previously been demonstrated by co-immunoprecipitation (57). Our observation that Sct1 and Gpt2 display interaction with Ole1 provides further support for this contention. Placing Sct1, Gpt2 and Slc1 in close proximity may aid in channeling acyl-CoA to synthesize PA species that can be further processed to yield the major membrane phospholipids.

Mutational analysis of Dga1 revealed that the carboxyl-terminus, predicted to form a cytosolic domain, is required for association with Ole1 but not for membrane localization. Truncations and in-frame internal deletions support a model indicating that interaction with Ole1 is mediated by sequences between Leu^{396} to Gly^{408}. The final ten amino acids, residues 408 - 418 of Dga1 are required for catalytic activity and their deletion reduced but did not eliminate binding to Ole1. The segment from L^{396} to K^{415} encodes a several of clusters of charged residues. Mutation of Lys^{397}, Arg^{398}, Asp^{411}, Glu^{413}, and Lys^{415} to alanine leads to a near complete ablation of interaction with Ole1. Although we cannot state with confidence that $Dga1_{KRDEK}$ has wild-type levels of enzymatic activity it does retain catalytic activity and function based on the ability to rescue fatty acid induced toxicity and promote formation of LDs, thus the loss of interaction with Ole1 is not due to global misfolding or mislocalization.

Although there is no experimentally derived structure for Dga1 the proposal that the carboxyl-terminal domain of Dga1 provides a surface for interaction with Ole1 is consistent with the AlphaFold model that places the charged residues Lys^{397}, Arg^{398}, Asp^{411}, Glu^{413}, and Lys^{415} on an alpha-helix structure arranged on the surface oriented away from the core of Dga1 in a position suitable to make contacts with other proteins. Our data provide no mechanistic information for how the carboxyl-terminus of Dga1

interacts with Ole1. While the charge of the helix surface may be responsible for the interaction, we cannot discount a specific structure formed by this domain being responsible or even the possibility that post-translational modification of carboxyl-terminal residues is responsible. Modification to the carboxyl-terminal amino acids of Dga1 has not been reported but Dga1 is subject to regulation by ER-associated degradation (58). The sequences that target Dga1 for destabilization have not been identified but lysine residues in the carboxyl-terminus of mammalian DGAT2 are ubiquitinated to trigger DGAT2 destruction and mutation of those residues to alanine stabilize DGAT2 (59).

The *DGA1*$_{KRDEK}$ mutant has reduced ability to interact with Ole1 but is active in the production of TAG and can channel exogenous fatty acids into TAG stored in LDs thus preventing lipotoxicity in response to exogenous unsaturated fatty acids. In comparison with an *are1 are2 lro1 DGA1* strain the *are1 are2 lro1 DGA1*$_{KRDEK}$ cells produce fewer detectable LDs and they are smaller during early exponential growth. Untethering Dga1 from Ole1 may disrupt or destabilize the localization of Dga1 to sites of LD initiation and the channeling of endogenously produced unsaturated acyl-CoA to DAG leading to delayed initiation and growth of LDs.

In contrast, as cells approach quiescence the *DGA1*$_{KRDEK}$ strain displays more LDs than the *DGA1* strain but they are smaller. This is a puzzling observation and may reflect our limited understanding of LD biogenesis. One possibility is that this reflects reduced efficiency in channeling unsaturated acyl-CoA to sites of LD growth but since unsaturated acyl-CoA continues to accumulate, ER membrane associated Dga1$_{KRDEK}$ would continue to participate in TAG production, leading to the formation of more LDs. A more trivial explanation that we cannot categorically eliminate is that a minor reduction in Dga1

activity caused by the charged-to-alanine mutations combined with the loss of Ole1 binding may be responsible for the alteration in LD initiation and growth. In the absence of further experimental data the mechanism responsible for this observation remains conjecture since the alterations to Dga1 may influence other as yet undetected functions or protein interactions that may lead to disruption of LD initiation or biogenesis.

The interactions we detect between Ole1 and acyltransferases may also be a reflection of the importance of directing lipid species to appropriate fates and the potential for toxicity caused by ER accumulation of DAG (55). Even though the loss of all DGAT activities is not lethal to *S. cerevisiae* it does result in alteration in membrane structure and function owing to the accumulation of DAG in the ER (55). Placing Dga1 in close proximity to Ole1 may be a means to capture any overflow DAG and unsaturated acyl-CoA to avoid accumulation in the ER membrane. Indeed, increased Ole1 activity yielding increased unsaturated acyl-CoA or a reduction in Cds1 activity yielding decreased flux of unsaturated acyl-CoA to phospholipids leads to an increase in LD formation (60). Cells with reduced capacity for TAG synthesis and LD formation are very sensitive to increased Ole1 or reduced Cds1 activity (60). Thus, reversibly tethering Dga1 to Ole1 in the ER may create a pathway to allow rapid response to excess accumulation of DAG and unsaturated acyl-CoA, channeling these into neutral lipid storage in LDs.

Acknowledgements

We thank Dr. Marek Michalak for the gift of plasmids and yeast strains used in this investigation. Confocal microscopy experiments were performed at the University of Alberta Faculty of Medicine & Dentistry Cell Imaging Core, RRID:SCR_019200, which receives financial support from the Faculty of Medicine & Dentistry, the Department of Medical Microbiology and Immunology, the University Hospital Foundation, and Canada Foundation for Innovation (CFI). Lipid analysis was performed at the University of Alberta Faculty of Medicine & Dentistry Lipidomics Core, RRID:SCR_019176, which receives financial support from the Faculty of Medicine & Dentistry, Canada Foundation for Innovation (CFI) and Natural Sciences and Engineering Research Council of Canada (NSERC) awards to contributing investigators. This work was supported in part by funding from NSERC Discovery grant RGPIN 2021-02898 and the Agriculture Agrifoods Canada AgSci BioCluster.

References

1. Tehlivets, O., Scheuringer, K., and Kohlwein, S. D. (2007) Fatty acid synthesis and elongation in yeast. *Biochim. Biophys. Acta - Mol. Cell Biol. Lipids*. **1771**, 255–270
2. Wagner, S., and Paltauf, F. (1994) Generation of glycerophospholipid molecular species in the yeast *Saccharomyces cerevisiae*. Fatty acid pattern of phospholipid classes and selective acyl turnover at *sn-1* and *sn-2* positions. *Yeast*. **10**, 1429–1437
3. Stukey, J. E., McDonough, V. M., and Martin, C. E. (1990) The OLE1 Gene of *Saccharomyces cerevisiae* Encodes the delta9 Fatty Acid Desaturase and Can Be Functionally Replaced by the Rat Stearoyl-CoA Desaturase Gene. *J. Biol. Chem.* **265**, 20144–20149
4. Nagle, J. F., and Tristram-Nagle, S. (2000) Structure of lipid bilayers. *Biochim. Biophys. Acta*. **1469**, 159–195
5. Zheng, Z., and Zou, J. (2001) The Initial Step of the Glycerolipid Pathway. *J. Biol. Chem.* **276**, 41710–41716
6. Benghezal, M., Roubaty, C., Veepuri, V., Knudsen, J., and Conzelmann, A. (2007) SLC1 and SLC4 Encode Partially Redundant Acyl-Coenzyme A 1-Acylglycerol-3-phosphate O-Acyltransferases of Budding Yeast. *J. Biol. Chem.* **282**, 30845–30855
7. Riekhof, W. R., Wu, J., Jones, J. L., and Voelker, D. R. (2007) Identification and Characterization of the Major Lysophosphatidylethanolamine Acyltransferase in *Saccharomyces cerevisiae*. *J. Biol. Chem.* **282**, 28344–28352
8. Athenstaedt, K., and Daum, G. (1997) Biosynthesis of phosphatidic acid in lipid particles and endoplasmic reticulum of *Saccharomyces cerevisiae*. *J. Bacteriol.* **179**, 7611–7616
9. Jain, S., Stanford, N., Bhagwat, N., Seiler, B., Costanzo, M., Boone, C., and Oelkers, P. (2007) Identification of a Novel Lysophospholipid Acyltransferase in *Saccharomyces cerevisiae*. *J. Biol. Chem.* **282**, 30562–30569
10. Ejsing, C. S., Sampaio, J. L., Surendranath, V., Duchoslav, E., Ekroos, K., Klemm, R. W., Simons, K., and Shevchenko, A. (2009) Global analysis of the yeast lipidome by quantitative shotgun mass spectrometry. *Proc. Natl. Acad. Sci.* **106**, 2136–2141
11. Carman, G. M., and Henry, S. A. (1999) Phospholipid biosynthesis in the yeast *Saccharomyces cerevisiae* and interrelationship with other metabolic processes. *Prog. Lipid Res.* **38**, 361–399
12. Han, G.-S., Wu, W.-I., and Carman, G. M. (2006) The *Saccharomyces cerevisiae* Lipin Homolog Is a Mg2+-dependent Phosphatidate Phosphatase Enzyme*. *J. Biol. Chem.* **281**, 9210–9218
13. Oelkers, P., Cromley, D., Padamsee, M., Billheimer, J. T., and Sturley, S. L. (2002) The DGA1 Gene Determines a Second Triglyceride Synthetic Pathway in Yeast. *J. Biol. Chem.* **277**, 8877–8881
14. Dahlqvist, A., Ståhl, U., Lenman, M., Banas, A., Lee, M., Sandager, L., Ronne, H., and Stymne, S. (2000) Phospholipid:diacylglycerol acyltransferase: An enzyme that catalyzes the acyl-CoA-independent formation of triacylglycerol in yeast and plants. *Proc. Natl. Acad. Sci.* **97**, 6487–6492

15. Sorger, D., and Daum, G. (2002) Synthesis of Triacylglycerols by the Acyl-Coenzyme A:Diacyl-Glycerol Acyltransferase Dga1p in Lipid Particles of the Yeast *Saccharomyces cerevisiae*. *J. Bacteriol.* **184**, 519–524
16. Yang, H., Bard, M., Bruner, D. A., Gleeson, A., Deckelbaum, R. J., Aljinovic, G., Pohl, T. M., Rothstein, R., and Sturley, S. L. (1996) Sterol Esterification in Yeast: A Two-Gene Process. *Science*. **272**, 1353–1356
17. Srere, P. A. (1987) Complexes of sequential metabolic enzymes. *Annu. Rev. Biochem.* **56**, 89–124
18. Wheeldon, I., Minteer, S. D., Banta, S., Barton, S. C., Atanassov, P., and Sigman, M. (2016) Substrate channelling as an approach to cascade reactions. *Nat. Chem.* **8**, 299–309
19. Sweetlove, L. J., and Fernie, A. R. (2018) The role of dynamic enzyme assemblies and substrate channelling in metabolic regulation. *Nat. Commun.* **9**, 2136
20. Shuib, S., Ibrahim, I., Mackeen, M. M., Ratledge, C., and Hamid, A. A. (2018) First evidence for a multienzyme complex of lipid biosynthesis pathway enzymes in *Cunninghamella bainieri*. *Sci. Rep.* **8**, 3077
21. Gangar, A., Karande, A. A., and Rajasekharan, R. (2001) Isolation and Localization of a Cytosolic 10 S Triacylglycerol Biosynthetic Multienzyme Complex from Oleaginous Yeast. *J. Biol. Chem.* **276**, 10290–10298
22. Xu, Y., Caldo, K. M. P., Jayawardhane, K., Ozga, J. A., Weselake, R. J., and Chen, G. (2019) A transferase interactome that may facilitate channeling of polyunsaturated fatty acid moieties from phosphatidylcholine to triacylglycerol. *J. Biol. Chem.* **294**, 14838–14844
23. Regmi, A., Shockey, J., Kotapati, H. K., and Bates, P. D. (2020) Oil-Producing Metabolons Containing DGAT1 Use Separate Substrate Pools from those Containing DGAT2 or PDAT1[OPEN]. *Plant Physiol.* **184**, 720–737
24. Shockey, J., Regmi, A., Cotton, K., Adhikari, N., Browse, J., and Bates, P. D. (2016) Identification of Arabidopsis GPAT9 (At5g60620) as an Essential Gene Involved in Triacylglycerol Biosynthesis1[OPEN]. *Plant Physiol.* **170**, 163–179
25. Jin, Y., McFie, P. J., Banman, S. L., Brandt, C., and Stone, S. J. (2014) Diacylglycerol Acyltransferase-2 (DGAT2) and Monoacylglycerol Acyltransferase-2 (MGAT2) Interact to Promote Triacylglycerol Synthesis. *J. Biol. Chem.* **289**, 28237–28248
26. Renne, M. F., and de Kroon, A. I. P. M. (2018) The role of phospholipid molecular species in determining the physical properties of yeast membranes. *FEBS Lett.* **592**, 1330–1345
27. Czabany, T., Wagner, A., Zweytick, D., Lohner, K., Leitner, E., Ingolic, E., and Daum, G. (2008) Structural and Biochemical Properties of Lipid Particles from the Yeast *Saccharomyces cerevisiae*. *J. Biol. Chem.* **283**, 17065–17074
28. Ntambi, J. M., Miyazaki, M., Stoehr, J. P., Lan, H., Kendziorski, C. M., Yandell, B. S., Song, Y., Cohen, P., Friedman, J. M., and Attie, A. D. (2002) Loss of stearoyl–CoA desaturase-1 function protects mice against adiposity. *Proc. Natl. Acad. Sci. U. S. A.* **99**, 11482–11486

29. Shi, X., Li, J., Zou, X., Greggain, J., Rødkær, S. V., Færgeman, N. J., Liang, B., and Watts, J. L. (2013) Regulation of lipid droplet size and phospholipid composition by stearoyl-CoA desaturase. *J. Lipid Res.* **54**, 2504–2514
30. Lou, Y., Schwender, J., and Shanklin, J. (2014) FAD2 and FAD3 Desaturases Form Heterodimers That Facilitate Metabolic Channeling *in vivo*. *J. Biol. Chem.* **289**, 17996–18007
31. Man, W. C., Miyazaki, M., Chu, K., and Ntambi, J. (2006) Colocalization of SCD1 and DGAT2: implying preference for endogenous monounsaturated fatty acids in triglyceride synthesis. *J. Lipid Res.* **47**, 1928–1939
32. Murphy, D. J., Mukherjee, K. D., and Woodrow, I. E. (1984) Functional association of a monoacylglycerophosphocholine acyltransferase and the oleoylglycerophosphocholine desaturase in microsomes from developing leaves. *Eur. J. Biochem.* **139**, 373–379
33. Bai, Y., McCoy, J. G., Levin, E. J., Sobrado, P., Rajashankar, K. R., Fox, B. G., and Zhou, M. (2015) X-ray structure of a mammalian stearoyl-CoA desaturase. *Nature*. **524**, 252–256
34. Wang, L., Qian, H., Nian, Y., Han, Y., Ren, Z., Zhang, H., Hu, L., Prasad, B. V. V., Laganowsky, A., Yan, N., and Zhou, M. (2020) Structure and mechanism of human diacylglycerol O-acyltransferase-1. *Nature*. **581**, 329–332
35. McFie, P. J., Banman, S. L., Kary, S., and Stone, S. J. (2011) Murine Diacylglycerol Acyltransferase-2 (DGAT2) Can Catalyze Triacylglycerol Synthesis and Promote Lipid Droplet Formation Independent of Its Localization to the Endoplasmic Reticulum. *J. Biol. Chem.* **286**, 28235–28246
36. McFie, P. J., Banman, S. L., and Stone, S. J. (2018) Diacylglycerol acyltransferase-2 contains a c-terminal sequence that interacts with lipid droplets. *Biochim. Biophys. Acta BBA - Mol. Cell Biol. Lipids*. **1863**, 1068–1081
37. Güldener, U., Heck, S., Fielder, T., Beinhauer, J., and Hegemann, J. H. (1996) A new efficient gene disruption cassette for repeated use in budding yeast. *Nucleic Acids Res.* **24**, 2519–2524
38. Gibson, D. G., Young, L., Chuang, R.-Y., Venter, J. C., Hutchison, C. A., and Smith, H. O. (2009) Enzymatic assembly of DNA molecules up to several hundred kilobases. *Nat. Methods*. **6**, 343–345
39. Sandager, L., Gustavsson, M. H., Ståhl, U., Dahlqvist, A., Wiberg, E., Banas, A., Lenman, M., Ronne, H., and Stymne, S. (2002) Storage Lipid Synthesis Is Non-essential in Yeast. *J. Biol. Chem.* **277**, 6478–6482
40. Gietz, R. D., and Schiestl, R. H. (1991) Applications of high efficiency lithium acetate transformation of intact yeast cells using single-stranded nucleic acids as carrier. *Yeast*. **7**, 253–263
41. Stagljar, I., Korostensky, C., Johnsson, N., and te Heeson, S. (1998) A genetic system based on split-ubiquitin for the analysis of interactions between membrane proteins *in vivo*. *Proc. Natl. Acad. Sci.* **95**, 5187–5192

42. Foiani, M., Marini, F., Gamba, D., Lucchini, G., and Plevani, P. (1994) The B subunit of the DNA polymerase alpha-primase complex in *Saccharomyces cerevisiae* executes an essential function at the initial stage of DNA replication. *Mol. Cell. Biol.* **14**, 923–933
43. Siloto, R. M. P., Truksa, M., He, X., McKeon, T., and Weselake, R. J. (2009) Simple Methods to Detect Triacylglycerol Biosynthesis in a Yeast-Based Recombinant System. *Lipids*. **44**, 963–973
44. McNeil, B. A., and Stuart, D. T. (2018) Optimization of C16 and C18 fatty alcohol production by an engineered strain of *Lipomyces starkeyi*. *J. Ind. Microbiol. Biotechnol.* **45**, 1–14
45. Exner, T., Beretta, C. A., Gao, Q., Afting, C., Romero-Brey, I., Bartenschlager, R., Fehring, L., Poppelreuther, M., and Füllekrug, J. (2019) Lipid droplet quantification based on iterative image processing. *J. Lipid Res.* **60**, 1333–1344
46. Man, W. C., Miyazaki, M., Chu, K., and Ntambi, J. M. (2006) Membrane Topology of Mouse Stearoyl-CoA Desaturase 1. *J. Biol. Chem.* **281**, 1251–1260
47. Braun, S. (2002) Role of the ubiquitin-selective CDC48UFD1/NPL4 chaperone (segregase) in ERAD of OLE1 and other substrates. *EMBO J.* **21**, 615–621
48. Liu, Q., Siloto, R. M. P., Snyder, C. L., and Weselake, R. J. (2011) Functional and Topological Analysis of Yeast Acyl-CoA:Diacylglycerol Acyltransferase 2, an Endoplasmic Reticulum Enzyme Essential for Triacylglycerol Biosynthesis. *J. Biol. Chem.* **286**, 13115–13126
49. Kamisaka, Y., Tomita, N., Kimura, K., Kainou, K., and Uemura, H. (2007) *DGA1* (diacylglycerol acyltransferase gene) overexpression and leucine biosynthesis significantly increase lipid accumulation in the Δ *snf2* disruptant of *Saccharomyces cerevisiae*. *Biochem. J.* **408**, 61–68
50. Albuquerque, C. P., Smolka, M. B., Payne, S. H., Bafna, V., Eng, J., and Zhou, H. (2008) A Multidimensional Chromatography Technology for In-depth Phosphoproteome Analysis. *Mol. Cell. Proteomics MCP*. **7**, 1389–1396
51. Pan, X., Siloto, R. M. P., Wickramarathna, A. D., Mietkiewska, E., and Weselake, R. J. (2013) Identification of a Pair of Phospholipid:Diacylglycerol Acyltransferases from Developing Flax (*Linum usitatissimum L.*) Seed Catalyzing the Selective Production of Trilinolenin. *J. Biol. Chem.* **288**, 24173–24188
52. Choudhary, V., El Atab, O., Mizzon, G., Prinz, W. A., and Schneiter, R. (2020) Seipin and Nem1 establish discrete ER subdomains to initiate yeast lipid droplet biogenesis. *J. Cell Biol.* **219**, e201910177
53. Markgraf, D. F., Klemm, R. W., Junker, M., Hannibal-Bach, H. K., Ejsing, C. S., and Rapoport, T. A. (2014) An ER Protein Functionally Couples Neutral Lipid Metabolism on Lipid Droplets to Membrane Lipid Synthesis in the ER. *Cell Rep.* **6**, 44–55
54. Xu, N., Zhang, S. O., Cole, R. A., McKinney, S. A., Guo, F., Haas, J. T., Bobba, S., Farese, R. V., and Mak, H. Y. (2012) The FATP1–DGAT2 complex facilitates lipid droplet expansion at the ER–lipid droplet interface. *J. Cell Biol.* **198**, 895–911

55. Petschnigg, J., Wolinski, H., Kolb, D., Zellnig, G., Kurat, C. F., Natter, K., and Kohlwein, S. D. (2009) Good Fat, Essential Cellular Requirements for Triacylglycerol Synthesis to Maintain Membrane Homeostasis in Yeast. *J. Biol. Chem.* **284**, 30981–30993
56. Zoni, V., Khaddaj, R., Campomanes, P., Thiam, A. R., Schneiter, R., and Vanni, S. (2021) Pre-existing bilayer stresses modulate triglyceride accumulation in the ER versus lipid droplets. *eLife*. **10**, e62886
57. Shabits, B. N. (2017) *Proteomic analysis of yeast membranes enriched in acyltransferases Gpt2p and Sct1p provides insight into their roles and regulation*. Ph.D. thesis, University of Calgary
58. Ruggiano, A., Mora, G., Buxó, L., and Carvalho, P. (2016) Spatial control of lipid droplet proteins by the ERAD ubiquitin ligase Doa10. *EMBO J.* **35**, 1644–1655
59. Brandt, C., McFie, P. J., and Stone, S. J. (2016) Diacylglycerol acyltransferase-2 and monoacylglycerol acyltransferase-2 are ubiquitinated proteins that are degraded by the 26S proteasome. *Biochem. J.* **473**, 3621–3637
60. Romanauska, A., and Köhler, A. (2021) Reprogrammed lipid metabolism protects inner nuclear membrane against unsaturated fat. *Dev. Cell*. **56**, 2562-2578.e3

Chapter 4 – Dga1 mutants lacking strong interactions with Ole1 exhibit altered subcellular localization

4.1. Introduction

4.1.1. Lipid droplet emergence and growth from the ER

Triacylglycerol (TAG) and sterol ester (SE) synthesized by the cell is stored within the lipid droplet (LD). The LD is comprised of an inner neutral lipid core surrounded by a phospholipid (PL) monolayer that is continuous with the endoplasmic reticulum (ER) (1–3). LDs begin as ER subdomains containing seipin and diacylglycerol (DAG), which recruit TAG synthases Lro1 and Dga1 (4). These acyltransferases deposit neutral lipid between the two PL leaflets of the ER in a structure known as a neutral lipid lens (Figure 4.1) (5, 6). Lipid lens coalescence is reliant on accumulation of TAG more so than SE (7). The lens then grows to a nascent LD via the deposition of neutral lipid, emerging from the ER toward the cytoplasm in a process requiring recruitment of membrane-shaping proteins and the production of lysophospholipids (LPLs) that favor a positive membrane curvature (Figure 4.1) (4, 5, 8, 9). A mature and fully emerged LD is covered by a LD monolayer continuous with the cytosolic leaflet of the ER which permits translocation of perilipins and lipid biosynthetic enzymes (4, 10). Proper expansion of the mature LD is reliant on recruitment of fatty acyl-CoA synthases, GPATs, LPAATs, and DGATs to the PL monolayer (11, 12).

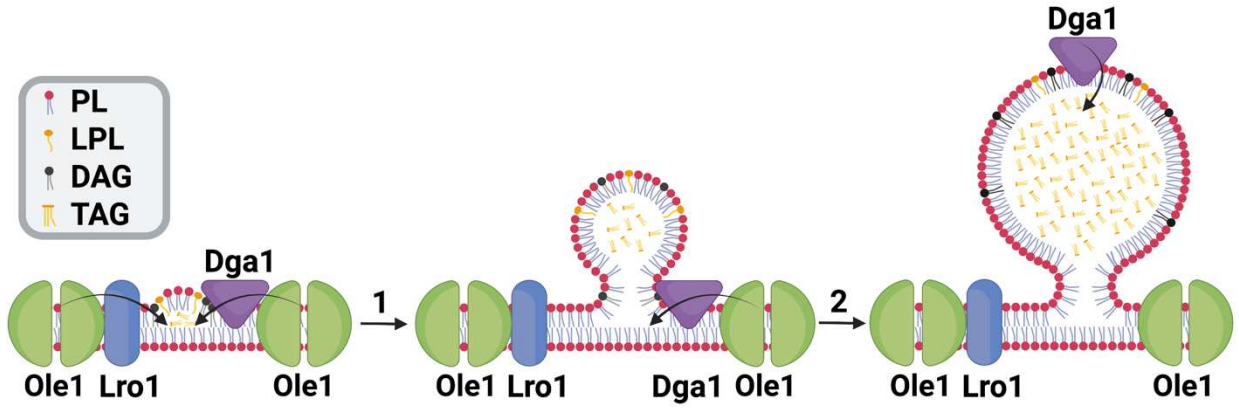

Figure 4.1 **TAG synthesis at the LD budding site**. LD budding from the ER begins by the recruitment of Lro1 and Dga1 to sites of high DAG concentration and membrane shaping proteins (not pictured). Neutral lipid lenses form via the accumulation of TAG between the two leaflets of the ER. Lysophospholipids produced by Lro1 promote cytosolic budding of the nascent LD (arrow 1). LD proteins like Dga1 are recruited to the PL monolayer of a mature LD (arrow 2). On the LD, Dga1 synthesizes TAG and promotes LD expansion. Created with BioRender.com.

LDs and their composite neutral lipid maintain membrane homeostasis and mediation of LD growth is essential (13–15). The organelles store lipid that can be mobilized to support membrane biogenesis via lipolysis by SE hydrolases and TAG lipases or lipophagy in bulk (16–18). LDs also sequester free fatty acids (FFAs) and DAG to buffer lipotoxicity and prevent ER stress (13, 15, 19). In *Saccharomyces cerevisiae*, synthesis of neutral lipid and LD formation are not vital processes, but bulk TAG synthesis is essential in mice (20, 21). While LD formation is necessary for proper lipid homeostasis, unregulated lipid accumulation is associated with nonalcoholic fatty liver disease (NAFLD), dyslipidemia, and diabetes (22). Dissection of the mechanisms controlling LD growth will provide a better understanding of how to address disorders of lipid dysregulation.

4.1.2. TAG synthesis in yeast and mammals

As accumulation of TAG is important to the initial stages of LD formation, we are interested in the TAG biosynthetic pathway. In both yeast and mammalian cells, the generation of TAG can occur both in the ER and on the surface of the LD. In *S. cerevisiae*, ER-localized TAG synthesis is catalyzed by two acyltransferases, Lro1 and Dga1. In humans, TAG is also generated in the ER by two separate proteins, DGAT1 and DGAT2. In contrast, the acylation of DAG to TAG on the LD surface is due exclusively to Dga1 in *S. cerevisiae* and DGAT2 in mammals.

The ER-bound phospholipid:diacylglycerol acyltransferase in *S. cerevisiae*, Lro1, contains a primarily ER-luminal active site and is responsible for the majority of TAG generation during active growth (20, 23, 24). The protein catalyzes the acyl-CoA independent acylation of TAG by scavenging the *sn-2* acyl chain from a pre-existing PL, generating TAG and an LPL (25). DGAT1 is a mammalian membrane-bound O-acyltransferase that is similarly restrained within the ER by its nine transmembrane helices (26, 27). Though both Lro1 and DGAT1 are ER-restricted, they differ in topology and substrate preference. The active site of DGAT1 faces both the luminal and cytosolic sides of the ER, and the protein uses an acyl-CoA as an acyl donor (28–30).

The acyl-CoA diacylglycerol acyltransferase Dga1 is found in both the ER and LD membranes and is essential for TAG synthesis in stationary phase (24, 31, 32). DGAT2, the mammalian ortholog of Dga1, is found both in the ER and in the LD membranes as well (33–35). The transfer of these proteins from the ER to the LD is essential for bulk TAG deposition and LD growth, as an ER-bound DGAT2 generates small LDs *in vivo* while displaying comparable activity to native DGAT2 *in vitro* (11, 35). LDs produced by

Lro1 and DGAT1 are similarly attenuated in size (12, 13). As the LD monolayer contains DAG, the promotion of LD growth by the transfer of TAG synthases to the monolayer may be due to a simple question of access to substrate (33, 36). However, the LD monolayer also contains lipid biosynthetic proteins Slc1, the main LPAAT in *S. cerevisiae*, FATP1, a *Caenorhabditis elegans* acyl-CoA synthetase, and MGAT2, a mammalian monoacylglycerol acyltransferase (11, 37, 38). All three proteins interact with the DGAT2 homolog of their respective organism, potentially channeling lipid to TAG synthesis on the LD and promoting expansion of the organelle (11, 38). ER-localized TAG synthesis by Lro1 and DGAT1 is sufficient to initiate LD synthesis, but transfer of Dga1 and DGAT2 to the LD surface is necessary for LD growth.

Desaturase activity impacts LD expansion as well, as an active desaturase is required for TAG accumulation in hepatocytes (39). Reduced *OLE1* expression caused by deletion of transcription factors responsible for *OLE1* transcription in *S. cerevisiae* also significantly decreases LD size and TAG synthesis (40). This LD growth attenuation may be due to the aforementioned need for the fluidity provided by unsaturated acyl chain incorporation into TAG to promote LD budding from the ER (41). Furthermore, desaturase activity and TAG synthase activity are both genetically and physically linked. In mouse hepatocytes, DGAT2 activity is associated with expression of *Fasn* and *Scd1*, two genes responsible for *de novo* lipogenesis and desaturation (42). Previous work demonstrated an interaction between DGAT2 and the human desaturase SCD1, while we determined that Dga1 and Ole1 contain an orthologous interaction (43, 3.4.1). Our work demonstrates that a disruption of this interaction alters LD number and size, suggesting that the colocalization of these two proteins may be essential for proper LD formation (3.4.6). This

interaction may serve to channel *de novo* unsaturated acyl-CoA to Dga1/DGAT2, which would promote LD budding from the ER via accumulation of a population of more fluid TAG. However, Ole1 is an integral membrane protein with multiple transmembrane helices that is only found within the ER (44, 45). As Dga1/DGAT2 movement from the ER to the LD is essential for LD growth, this interaction may retain the acyltransferase in the ER and inhibit LD expansion. Determining the effect of the diacylglycerol acyltransferase – desaturase interaction on LD initiation and growth will provide a deeper understanding of the regulation of LD synthesis.

4.1.3. A model for Dga1 as a monotopic membrane protein

Analysis of mammalian DGAT2s has revealed conserved residues essential for diacylglycerol acyltransferase function. Dga1 contains multiple regions corresponding to highly conserved motifs in DGAT2s; namely, ^{129}YFP^{131}, ^{193}HPHG^{196}, and the so-called GGE Block (^{268}GGARE^{272}) (46, 47). In Dga1, the YFP and HPHG motifs are essential for activity, while in mouse DGAT2, the second histidine in the HPHG motif has been identified as the catalytic residue (48, 49). The role of the GGE block in DGAT activity has not been elucidated, though the di-glycine and glutamate in the block are 3 of only 16 fully conserved residues in DGAT2s (47).

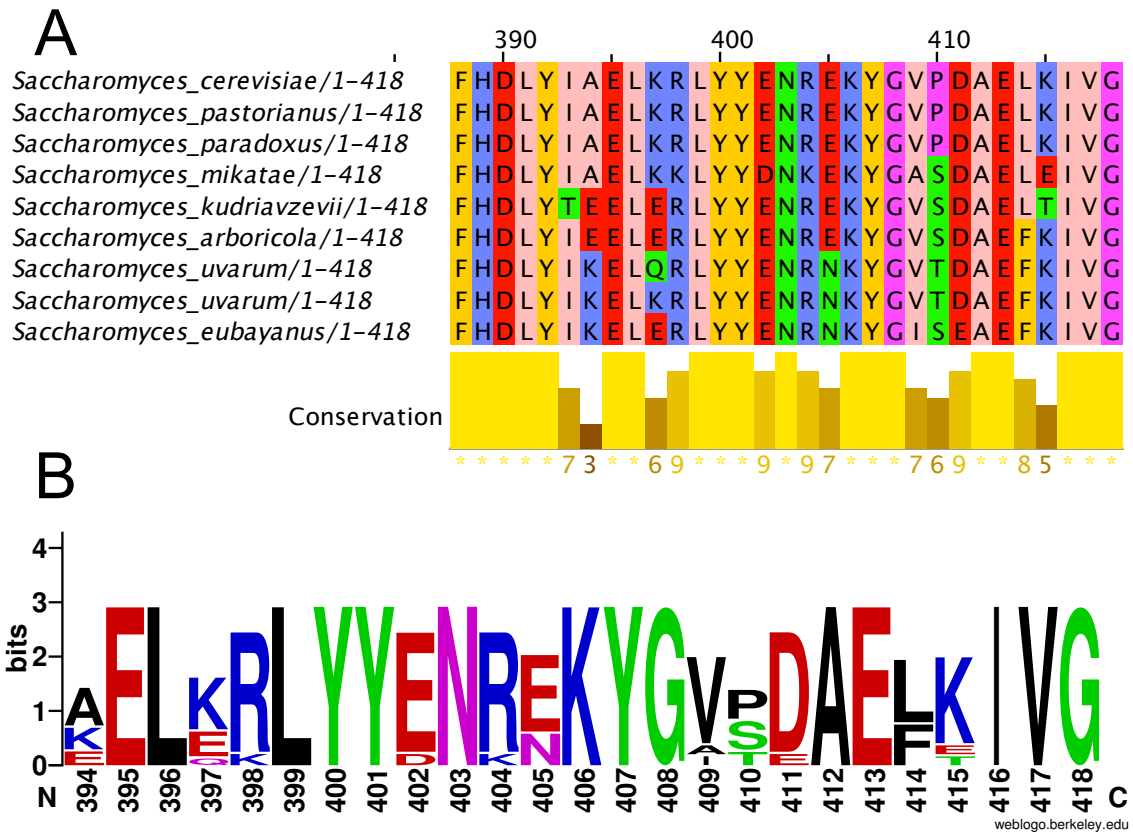

Figure 4.2 **The Dga1 carboxyl terminus is highly conserved**. A. Multiple sequence alignment of selected *Saccharomyces* Dga1. Hydrophobic residues = light pink, aromatic residues = orange, negatively charged residues = red, positively charged residues = blue, hydrophilic residues = green, proline/glycine = magenta. Light yellow indicates high conservation, brown indicates low conservation. Numbers correspond to number of Dga1 polypeptides with residue conservation. * = total conservation. Visualized with Jalview 2. B. WebLogo of Dga1 carboxyl terminus from all proteins identified by NCBI blastp as in 4.2.3. Polar residues = green, basic residues = blue, acidic residues = red, hydrophobic residues = black, asparagine/glutamine = magenta.

The carboxyl terminus of Dga1, ^{411}DAELKIVG^{418}, is highly conserved throughout the *Saccharomyces* genus (Figure 4.2). Though it does not contain a traditional di-lysine ER retrieval motif, it resembles the carboxyl-terminus from the *Vernicia fordii* DGAT2, in which LKLEI serves to retain DGAT2 in the ER (50). The impact of this motif on the subcellular localization of Dga1 is yet to be understood, but a truncation of five residues from the carboxyl-terminus virtually abolished DGAT activity both *in vivo* and *in vitro* when

combined with a carboxyl-terminal epitope tag. While a carboxyl-terminal tag on the full-length protein reduced *in vivo* TAG production by more than half, the *in vitro* DGAT activity was reduced by only 20% (48). We have confirmed the catalytic importance of the carboxyl-terminus with both functional and fatty acid toxicity studies. Interestingly, a carboxyl-terminally tagged Dga1 did not interact with Ole1 in a MYTH assay, while an amino-terminally tagged version of the full-length protein interacted strongly (3.4.1). Our dissection of this interaction implicated Lys^{397}, Arg^{398}, Asp^{411}, Glu^{413}, and Lys^{415} in maintenance of the acyltransferase-desaturase interaction. These observations taken together implicates the carboxyl-terminal end of Dga1 in acyltransferase activity and colocalization with Ole1.

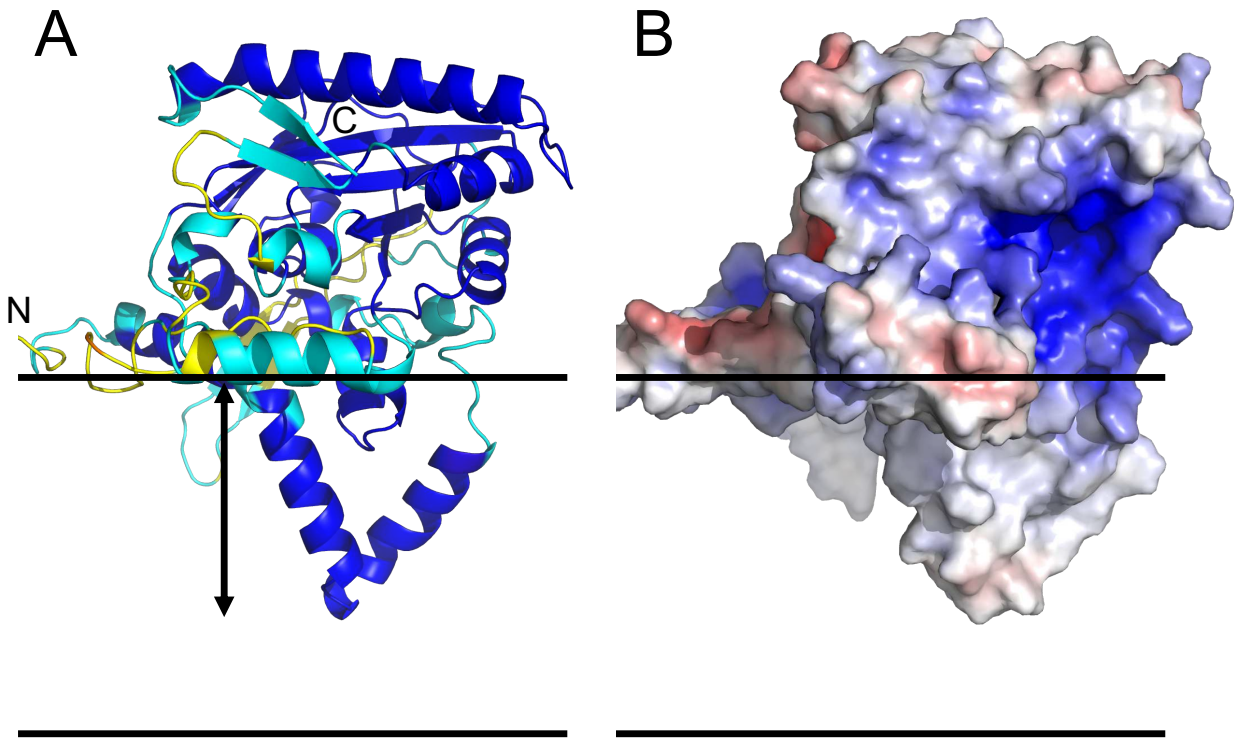

Figure 4.3 **High confidence AlphaFold model of Dga1 (Q08650).** A. Proposed model of Dga1. Amino (N) and carboxyl (C) termini are as indicated. Model is coloured according to the AlphaFold per-residue confidence score (pLDDT) as follows: Very high (pLDDT > 90) = blue, confident (90 > pLDDT > 70) = cyan, low (70 > pLDDT > 50) = yellow, very low (pLDDT < 50) = orange. Amino-terminal region trimmed at Glu^{46} for visualization. Black lines represent the phospholipid bilayer. Black arrow indicates measured depth of kinked helix. B. Protein contact potential for the Dga1 model as determined by the Pymol Adaptive Poisson-Boltzmann Solver (APBS) Electrostatics plugin. Negatively charged regions shown in red, positively charged regions shown in blue, neutral regions shown in white.

The recent development of AlphaFold has provided researchers with a new lens to view Dga1 and DGAT2 structure. The high confidence model of Dga1 proposed by AlphaFold consists of a large soluble domain and one kinked hydrophobic helix descending to a depth of approximately 23 Å from the body of the protein (Figure 4.3A). This is consistent with the experimentally determined topology of MmDGAT2, which contains a soluble catalytic domain facing the cytosol and one small membrane region (Figure 4.3A) (30, 49). Both MmDGAT2 and Dga1 are integral to the membrane, and the

kinked helix in the model would indeed allow integration into the hydrophobic core of the phospholipid bilayer (Figure 4.3B) (48, 49). However, the measured depth of 23 Å does not fully span the hydrophobic core of the membrane, which can range from 30 Å – 38 Å depending on membrane composition (51, 52). This model thus classifies Dga1 as an integral monotopic membrane protein, a topology that allows proteins to move freely between the ER phospholipid bilayer and the LD phospholipid monolayer.

The structure of DGAT2s has not yet been experimentally determined, but the use of AlphaFold has provided a structural prediction that aligns with the current experimental evidence for the protein. A comparison of the model against the PDB using a Dali query reveals that the predicted structure of Dga1 greatly resembles that of PlsC with a Z-score of 12.5 and an RMSD of 3.3 Å over 197 Cα atoms (PDB 5KYM). PlsC is an LPAAT from *Thermotoga maritima* and is classified as a monotopic membrane protein. The LPAAT structure exhibits a predominant cleft containing the catalytic histidine (53). The catalytic histidine of Dga1 (His^{195}) is modeled in a similar cleft that would be accessible to DAG and acyl-CoA. Importantly, the HsDGAT2 model contains an analogous active site pocket with sufficient residues and geometry to bind a DGAT2 specific inhibitor but not a DGAT1 inhibitor (54). The Dga1 model also places Glu^{272} of the highly conserved GGE block in close proximity to His^{195}, which would allow for proton abstraction of the catalytic histidine in a mechanism similar to DGAT1 (26). Taken together, this data supports the new proposed AlphaFold model of the DGAT2s as an accurate structure prediction of the protein and categorizes the acyltransferase as a monotopic membrane protein. This classification of Dga1 and the other DGAT2s as monotopic membrane proteins would explain the ability of the protein to transfer from ER bilayer to LD monolayer.

DGAT2 transfer to the LD monolayer is essential for LD growth, making the study of the mechanisms controlling transfer essential to a deeper understanding of TAG synthesis regulation. The association of DGAT2 with LDs has been extensively characterized by the Stone lab (27, 34, 35, 55). Initial work demonstrated that the proposed transmembrane domain within the amino-terminal half of the protein was not solely responsible for DGAT2 membrane localization. This transmembrane domain ($MmDGAT2_{66-115}$) permits association with the ER, but it does not target the protein to the LD monolayer (34, 35). An independent region of the protein, a proposed amphipathic helix ($MmDGAT2_{293-312}$), is essential for the subcellular localization to LDs (55). This portion of the protein also contains three lysine residues. Accordingly, a lysine-less DGAT2 does not localize to the LD though it does retain activity (56).

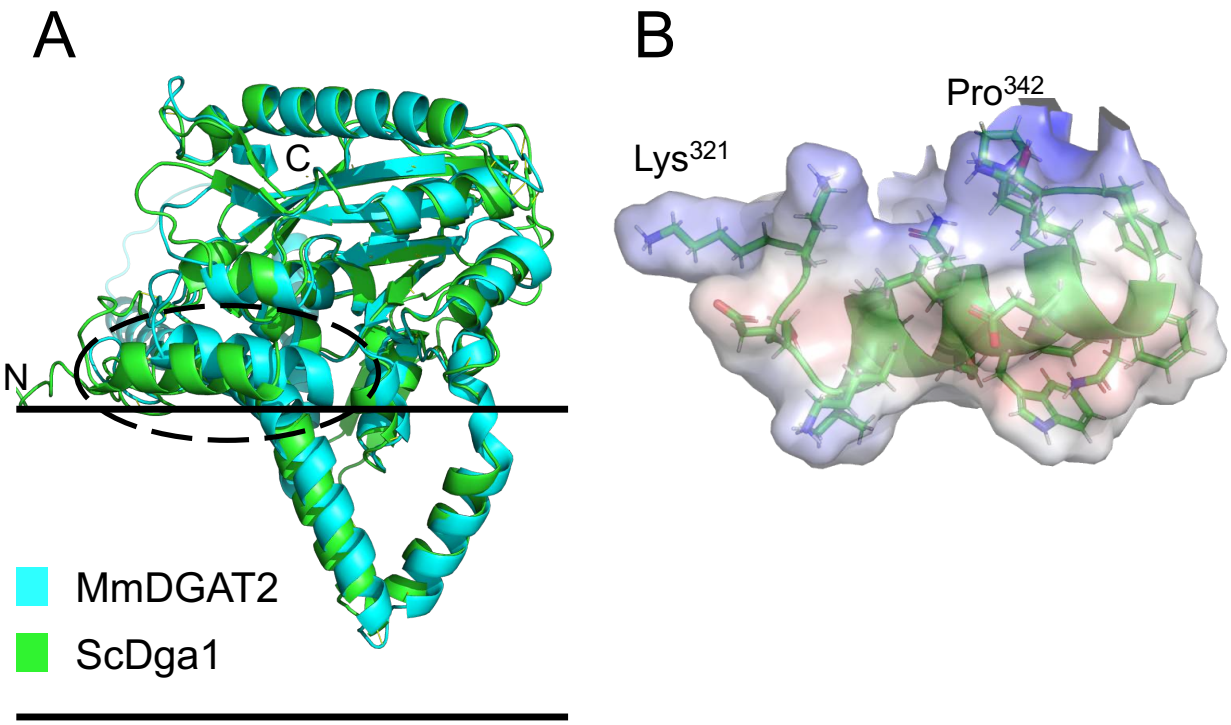

Figure 4.4 **Dga1 contains a similar region to the MmDGAT2 (Q9DCV3) LD targeting domain (MmDGAT2$_{293-312}$).** A. Alignment of the MmDGAT2 (cyan) and ScDga1 (green) models as determined by AlphaFold. Dashed circled encompasses MmDGAT2 LD targeting domain (MmDGAT2$_{293-312}$) and corresponding region of Dga1 (Dga1$_{321-342}$). N and C termini are as marked. Amino-terminal region trimmed for visualization. Black lines represent the phospholipid bilayer. B. Protein contact potential for Dga1$_{321-342}$ as determined by the Pymol APBS Electrostatics plugin. Lys^{321} and Pro^{342} as marked. Surface coloured as follows: negatively charged regions shown in red, positively charged regions shown in blue, neutral regions shown in white. Sidechain residues coloured as follows: C = green, H = white, N = blue, O = red.

The AlphaFold model of MmDGAT2 proposes a similar topology to the Dga1 model (Figure 4.4A). It also positions the LD targeting domain of MmDGAT2 on the external region of the protein near the putative membrane binding region (Figure 4.4A, dashed circle) (55). Amphipathic helices with large hydrophobic residues have been shown to bind phospholipid packing defects that are found readily on the surface of the LD, and the AlphaFold proposed location of this helix makes it available for LD monolayer recognition (57). Dga1 contains a similar helix (Dga1$_{321-342}$) (Figure 4.4A). Surface electrostatics of

the helix show a hydrophobic face with large aromatic residues, and a basic face with four lysine residues (Figure 4.4B). Though Dga1 has a similar region in the structural model, determination of its role in Dga1 LD targeting has not yet been determined.

The carboxyl-terminus of DGAT2 also contains a set of six lysine residues (Lys^{346}, Lys^{353}, Lys^{368}, Lys^{374}, and Lys^{376}) that serve as ubiquitination sites and promote ER-associated degradation of the acyltransferase (56). Dga1 contains two lysine residues that align with these known ubiquitination sites (Lys^{375} and Lys^{406}) and five lysine residues total in the carboxyl-terminus (Lys^{375}, Lys^{376}, Lys^{397}, Lys^{406}, and Lys^{415}). The residues on Dga1 that control degradation of the protein have not been yet identified, but the acyltransferase is also an ERAD substrate that is ubiquitinated by the Doa10 complex and degraded by the proteasome (58). In both mammalian and *S. cerevisiae* cells, the retention of ERAD substrates within the ER increases degradation as the transfer of these proteins to the LD prevents proteasomal access (56, 58). Both access of the carboxyl-terminal Dga1 lysine residues to the ubiquitin ligase complex within the ER and transfer of the protein between the LD and ER serves to control the amount of diacylglycerol acyltransferase within the cell.

We have analyzed Dga1 localization within *S. cerevisiae* using confocal microscopy. This is the first analysis of localization of Dga1 expressed under the regulation of its native promoter and without modification by a carboxyl-terminal tag that inhibits the catalytic activity of the protein. We report herein that Dga1 localizes both to LDs and the ER during active growth and stationary phase. We demonstrate that $Dga1_{321-342}$ is essential for LD localization and the proposed ER-retention signal (^{411}DAELKIVG^{418}) is not solely responsible for ER retention. Finally, we demonstrate that acyltransferase

mutants lacking an interaction with Ole1 exhibit altered subcellular localization across phases of growth, and Dga1 displays a similar distribution pattern to the desaturase.

4.2. Methods

4.2.1. Strains and Plasmids

The *S. cerevisiae* strains BY4741 Δ*dga1* and W303 were used as the parents for the imaged strains. BY4741 Δ*dga1* was a gift from Michael Schultz. *Escherichia coli* DH5α was used in all cloning steps and to propagate all plasmids. All yeast transformations were completed with the lithium acetate method (59). All strain genotypes can be found in Table 4.1. Primer sequences used to generate the strains are listed in Table 4.2.

Table 4.1 Strains used in study

Strain name	Parent	Genotype	Reference
W303	-	*MATa {leu2-3,112 trp1-1 can1-100 ura3-1 ade2-1 his3-11,15} [phi+]*	(60)
Δdga1	BY4741	*MATa his3Δ1 leu2Δ0 met15Δ0 ura3Δ0 dga1Δ::KanMX*	Open Biosystems
Δdga1Δtrp1	BY4741	*MATa his3Δ1 leu2Δ0 met15Δ0 ura3Δ0 dga1Δ::KanMX trp1Δ::NatMX6*	This study
mNeonGreen-DGA1 Δdga1Δtrp1	BY4741	*MATa his3Δ1 leu2Δ0 met15Δ0 ura3Δ0 dga1Δ::KanMX trp1Δ::NatMX6 [pDGA1::mNeonGreen-DGA1 URA3]*	This study
mNeonGreen-DGA1 1-318 Δdga1Δtrp1	BY4741	*MATa his3Δ1 leu2Δ0 met15Δ0 ura3Δ0 dga1Δ::KanMX trp1Δ::NatMX6 [pDGA1::mNeonGreen-DGA1 1-318 URA3]*	This study
mNeonGreen-DGA1 1-398 Δdga1Δtrp1	BY4741	*MATa his3Δ1 leu2Δ0 met15Δ0 ura3Δ0 dga1Δ::KanMX trp1Δ::NatMX6 [pDGA1::mNeonGreen-DGA1 1-398 URA3]*	This study
mNeonGreen-DGA1 Δ389-410 Δdga1Δtrp1	BY4741	*MATa his3Δ1 leu2Δ0 met15Δ0 ura3Δ0 dga1Δ::KanMX trp1Δ::NatMX6 [pDGA1::mNeonGreen-DGA1 Δ389-410 URA3]*	This study
mNeonGreen-DGA1 1-408 Δdga1Δtrp1	BY4741	*MATa his3Δ1 leu2Δ0 met15Δ0 ura3Δ0 dga1Δ::KanMX trp1Δ::NatMX6 [pDGA1::mNeonGreen-DGA1 1-408 URA3]*	This study
mNeonGreen-DGA1 KR Δdga1Δtrp1	BY4741	*MATa his3Δ1 leu2Δ0 met15Δ0 ura3Δ0 dga1Δ::KanMX trp1Δ::NatMX6 [pDGA1::mNeonGreen-DGA1 KR URA3]*	This study
mNeonGreen-DGA1 REK Δdga1Δtrp1	BY4741	*MATa his3Δ1 leu2Δ0 met15Δ0 ura3Δ0 dga1Δ::KanMX trp1Δ::NatMX6 [pDGA1::mNeonGreen-DGA1 REK URA3]*	This study
mNeonGreen-DGA1 DEK Δdga1Δtrp1	BY4741	*MATa his3Δ1 leu2Δ0 met15Δ0 ura3Δ0 dga1Δ::KanMX trp1Δ::NatMX6 [pDGA1::mNeonGreen-DGA1 DEK URA3]*	This study
mNeonGreen-DGA1 KRDEK Δdga1Δtrp1	BY4741	*MATa his3Δ1 leu2Δ0 met15Δ0 ura3Δ0 dga1Δ::KanMX trp1Δ::NatMX6*	This study

Strain name	Parent	Genotype	Reference
		[pDGA1::mNeonGreen-DGA1 KRDEK URA3]	
mNeonGreen-DGA1 SS-mCherry-HDEL Δdga1Δtrp1	BY4741	*MATa his3Δ1 leu2Δ0 met15Δ0 ura3Δ0 dga1Δ::KanMX trp1Δ::NatMX6 [pDGA1::mNeonGreen-DGA1 URA3] [pTPI1::mCherry-HDEL TRP1*	This study
OLE1-mCherry	W303	*MATa {leu2-3,112 trp1-1 can1-100 ura3-1 ade2-1 his3-11,15} [phi+] OLE1::mCherry hphMX6*	This study
OLE1-mCherry Δdga1	W303	*MATa {leu2-3,112 trp1-1 can1-100 ura3-1 ade2-1 his3-11,15} [phi+] OLE1::mCherry hphMX6 dga1Δ::bleMX6*	This study
OLE1-mCherry mNeonGreen-DGA1 Δdga1	W303	*MATa {leu2-3,112 trp1-1 can1-100 ura3-1 ade2-1 his3-11,15} [phi+] OLE1::mCherry hphMX6 dga1Δ::bleMX6*	This study
Δole1Δdga1	W303	*MATa {leu2-3,112 trp1-1 can1-100 ura3-1 ade2-1 his3-11,15} [phi+] ole1Δ::NatMX6 dga1Δ::KanMX*	This study
mNeonGreen-DGA1 Δole1Δdga1	W303	*MATa {leu2-3,112 trp1-1 can1-100 ura3-1 ade2-1 his3-11,15} [phi+] ole1Δ::NatMX6 dga1Δ::KanMX [pDGA1::mNeonGreen-DGA1 URA3]*	This study

Table 4.2 Sequences of primers used in study

Primer	Primer sequence
5DGA1s	ATCCCAGATCACGTTTGTTCCAT
BGO15	TACGACTTGAAGAAATTCTCTC
CYC1Ts2	CTTTTCGGTTAGAGCGGATG
dga1KO3	CACTAAAAAATCCTTATTTATTCTAACATATTTTGTGTTTTCCAATGA ATTCATTAGCCACTAGTGGATCTGATATCACC
dga1KO5	CACATACACTTACATATACATAAGGAAACGCAGAGGCATACAGTTT GAACAGTCACATAATTCGTACGCTGCAGGTCGAC
mCherry_s	CCCTCCATGTGCACCTTGA
Ole1d3	TTATGGTAGTTGCAGTTTTGTTATTGTAATGTGATACTTAAAAGAAC TTACCAGTTTCGT**GCATAGGCCACTAGTGGATC**
Ole1d5	CATAGTAATAGATAGTTGTGGTGATCATATTATAAACAGCACTAAAA CATTACAACAAAG**CAGCTGAAGCTTCGTACGC**
ole1dsc3	AGAGATGCAGTAAGCCATCC
ole1dsc5	ATGCAGCAAATCATCGGCTC
OmC3	GTG AAA TTT TGA AGA GAT GCA GTA AGC CAT CCC ATA TCT ATT GCT CCA GGG CC ATGGCGGCGTTAGTATCGAATCGACA
OmC5	CTC TGC TAT TAG AAT GGC TAG TAA GAG AGG TGA AAT CTA CGA AAC TGG TAA GTT CTT T ATG GTG AGC AAG GGC GAG GAG
TEFs	GGACAATTCAACGCGTCTGTGA
trp1KO3	CTATTTCTTAGCATTTTTGACGAAATTTGCTATTTTGTTAGAGTCTTT TACACCATTTGTCGACTCACTA
trp1KO5	ATGTCTGTTATTAATTTCACAGGTAGTTCTGGTCCATTGGTGAAAGT TTGCGGCTTGCAGAAGCTTCGTACGCTGCAGG

To generate *Δdga1Δtrp1*, *NatMX6* was amplified from pAG25 using primers containing homology to *TRP1* (trp1KO5, trp1KO3) and transformed into BY4741 Δdga1. Transformants were selected on YEPD supplemented with 100 µg/mL nourseothricin and *TRP1* deletion was confirmed by lack of growth on SD lacking tryptophan. To produce the plasmids containing *mNeonGreen-DGA1* and *mNeonGreen-DGA1* mutants, a *S. cerevisiae* codon-optimized *mNeonGreen* sequence was ordered from Invitrogen. The sequence contained homology to the *DGA1* promoter to the 5' of *mNeonGreen* and

homology to the *DGA1* coding sequence to the 3' of *mNeonGreen* (Figure 4.5). Integrating YIplac211 plasmids containing *DGA1* under control of the *DGA1* native promoter with the *CYC1* terminator were digested with AleI and BstXI and the *mNeonGreen* sequence was inserted in frame with *DGA1* using Gibson isothermal assembly, confirmed by Sanger sequencing (Table 4.3). The *mNeonGreen-DGA1* constructs were digested with PstI to direct integration at the *DGA1* promoter, *Δdga1Δtrp1* was transformed with the linearized plasmid, and strains were selected by growth on SD media lacking uracil. ZJOM90 carrying ER marker *SS-mCherry-HDEL* was inserted into the genome as previously described and transformants were selected for by growth on SD media lacking tryptophan (61). Plasmids are listed in Table 4.3.

TCAAAGCAGACCAGTACTTCCACCGCATTTCTGTACTTAACCAAGCACGACAGTGGTCTATCAGG
CTTGGATCTTTCACTACACTTCCGCCAAAGTTTTTTTTTTTTCCTGTTTATCCCAGATCACGTTT
GTTCCATTAAGGAGGTTTACTATCATCTCATTTCCATTTACACATACACTTACATATACATAAGG
AAACGCAGAGGCATACAGTTTGAACAGTCACATAAATGGTTTCAAAGGGTGAAGAAGATAACATG
GCTAGCCTGCCTGCTACCCATGAGTTACATATATTCGGTTCTATTAACGGTGTTGACTTCGACAT
GGTCGGTCAGGGGACGGGAAACCCTAACGACGGTTATGAGGAACTAAACCTGAAGTCAACGAAAG
GAGACCTTCAGTTTTCACCTTGGATATTAGTGCCACACATAGGGTACGGTTTCCATCAGTACTTA
CCGTACCCGGATGGGATGTCCCCATTCCAGGCGGCCATGGTAGATGGTTCCGGTTATCAAGTACA
TAGAACTATGCAGTTCGAAGACGGGGCTAGCTTGACTGTAAACTACAGATATACATACGAAGGCT
CTCATATCAAGGGTGAGGCGCAAGTGAAGGGCACGGGCTTTCCGGCGGACGGACCTGTTATGACC
AACTCACTGACTGCTGCTGATTGGTGCAGGTCAAAGAAAACGTATCCTAACGACAAGACAATTAT
TTCCACATTCAAGTGGTCATATACTACAGGTAACGGCAAAAGGTACAGATCAACGGCGAGAACTA
CATACACTTTTGCGAAACCCATGGCGGCAAACTATCTGAAGAACCAACCCATGTATGTTTTCAGA
AAAACTGAGCTAAAGCACAGTAAAACTGAACTGAATTTTAAGGAGTGGCAAAAGGCGTTTACCGA
CGTGATGGGAATGGATGAACTTTACAAGGGATCCATGTCAGGAACATTCAATGATATTAGGAGAA
GGAAAAAGGAAGAAGGAAGCCCTACAGCCGGTATTACCGAAAGGCATGAGAATAAGTCTTTGTCA
AGCATCGATAAAAGAGAACAGACTCTCAAACCACAACTAGAGTCATGCTGTCCATTGGCGACCCC
TTTTGAAAGAAGGTTACAAACTCTGGCTGTAGCATGGCACACTTCTTCATTTGTACTCTTCTCCA
TATTTACGTTATTTGCAATCTCGACACCAGCACTGTGGGTTCTTGCTATTCCATATATGATTTAT
TTTTTTTTCGATAGGTCTC

Figure 4.5 **Sequence of mNeonGreen fragment codon-optimized for *S. cerevisiae*.** Purple = *DGA1p* homology, green = *mNeonGreen*, black = BamHI cut site, orange = *DGA1* homology.

Table 4.3 Plasmids used in study

Plasmid Name	*S. cerevisiae* Gene	Ori and selection	Source
pAG25	NatMX6	ClonNATR	(62), Euroscarf
Ylp-DGA1	HA-DGA1	Ylp URA3	Chapter 3
Ylp-DGA1$_{1\text{-}318}$	HA-DGA1$_{1\text{-}318}$	Ylp URA3	Chapter 3
Ylp-DGA1$_{1\text{-}398}$	HA-DGA1$_{1\text{-}398}$	Ylp URA3	Chapter 3
Ylp-DGA1$_{\Delta 388\text{-}410}$	HA-DGA1$_{\Delta 388\text{-}410}$	Ylp URA3	Chapter 3
Ylp-DGA1$_{1\text{-}408}$	HA-DGA1$_{1\text{-}408}$	Ylp URA3	Chapter 3
Ylp-DGA1$_{KR}$	HA-DGA1$_{K397A,\ R398A}$	Ylp URA3	Chapter 3
Ylp-DGA1$_{REK}$	HA-DGA1$_{R404A,\ E405A,\ K406A}$	Ylp URA3	Chapter 3
Ylp-DGA1$_{DEK}$	HA-DGA1$_{D411A,\ E413A,\ K415A}$	Ylp URA3	Chapter 3
Ylp-DGA1$_{KRDEK}$	HA-DGA1$_{K397A,\ R398A,\ D411A,\ E413A,\ K415A}$	Ylp URA3	Chapter 3
Ylp-mNG-DGA1	mNeonGreen-DGA1	Ylp URA3	This study
Ylp-mNG-DGA1$_{1\text{-}318}$	mNeonGreen-DGA1$_{1\text{-}318}$	Ylp URA3	This study
Ylp-mNG-DGA1$_{1\text{-}398}$	mNeonGreen-DGA1$_{1\text{-}398}$	Ylp URA3	This study
Ylp-mNG-DGA1$_{\Delta 388\text{-}410}$	mNeonGreen-DGA1$_{\Delta 388\text{-}410}$	Ylp URA3	This study
Ylp-mNG-DGA1$_{1\text{-}408}$	mNeonGreen-DGA1$_{1\text{-}408}$	Ylp URA3	This study
Ylp-mNG-DGA1$_{KR}$	mNeonGreen-DGA1$_{K397A,\ R398A}$	Ylp URA3	This study
Ylp-mNG-DGA1$_{REK}$	mNeonGreen-DGA1$_{R404A,\ E405A,\ K406A}$	Ylp URA3	This study
Ylp-mNG-DGA1$_{DEK}$	mNeonGreen-DGA1$_{D411A,\ E413A,\ K415A}$	Ylp URA3	This study
Ylp-mNG-DGA1$_{KRDEK}$	mNeonGreen-DGA1$_{K397A,\ R398A,\ D411A,\ E413A,\ K415A}$	Ylp URA3	This study
ZJOM90	SS-mCherry-HDEL	Ylp TRP1	(61)
pBS35	mCherry-hphMX6	HygR	(63)
pUG66	bleMX6	BleoR	(64)

To construct a strain bearing native levels of Ole1-mCherry, *mCherry-hphMX6* was amplified from pBS35 with primers containing homology to *OLE1* (OmC5, OmC3) and transformed into W303. Transformants were selected on YEPD supplemented with 200 µg/mL hygromycin and confirmed by PCR analysis using mCherry_s and BGO15. To

create *Δdga1* Ole1-mCherry, *bleMX6* was amplified from pUG66 with dga1KO5 and dga1KO3 and transformed into W303 Ole1-mCherry. Selection was performed on YEPD supplemented with 100 µg/mL zeocin and confirmed by PCR analysis with 5DGA1s and TEFs. The resultant strain was transformed with the *YIplac211-mNeonGreen-DGA1* plasmid as described.

To generate the *Δole1Δdga1* strain, *natMX6* was amplified from pAG25 using primers containing homology to *OLE1* (Ole1d3, Ole1d5) and W303 was transformed. Transformants were selected for on YEPD agar supplemented with 100 µg/mL nourseothricin and 0.5% Tween-80. The deletion of *OLE1* was confirmed by PCR analysis using Ole1dsc5 and Ole1dsc3 and lack of growth on YEPD plates containing with 100 µg/mL nourseothricin but lacking Tween-80 supplementation. The resultant *Δole1* strain was maintained with addition of C16:1 and Tween-80 to the media. Further deletion of *DGA1* was performed using *kanMX6* amplified from pUG6 with the dga1KO5 and dga1KO3 primers. Selection was performed on YEPD agar supplemented with 200 µg/mL geneticin and *DGA1* deletion was confirmed as above. The resultant strain was transformed with the *YIplac211-mNeonGreen-DGA1* plasmid as described.

4.2.2. Media and Cultivation Conditions

E. coli strains were cultivated in lysogeny broth (LB) containing ampicillin (100 µg/mL) for plasmid maintenance. Yeast strains were propagated on YEPD medium (1% yeast extract, 2% peptone, 2% dextrose) or on synthetic minimal medium (0.17% Yeast Nitrogen Base without amino acids without ammonium sulfate, 0.5% ammonium sulfate,

2% dextrose), supplemented with an amino acid mixture lacking the amino acids or purines as required for selection.

4.2.3. Sequence analysis

The Dga1 sequence from the S288C strain of *S. cerevisiae* was used as the reference sequence in a BLAST search using the NCBI blastp suite. Sequences for Dga1, Dga1-like proteins, and hypothetical proteins from the *Saccharomyces* genus with at least 85% sequence identity were kept in the analysis. The consensus sequence logo was generated using WebLogo and sequence alignment was visualized with Jalview 2 (65, 66).

4.2.4. Confocal microscopy

Indicated strains were cultured in YEPD medium at 30^{o}C overnight. Cells were diluted into fresh YEPD medium supplemented with 100 µg/mL adenine at an OD_{600} of 0.2 and grown for the indicated timepoints (exponential phase = 6 hours, stationary phase = 30 hours). Cultures for LD visualization were stained for 10 minutes in the dark using monodansylpentane (MDH) at a concentration of 0.1 µM. All samples were washed in PBS prior to imaging and immobilized on 2% agarose pads. Image stacks with a step size of 0.5 µm were collected on a Yokagawa CSU-X1 microscope using the DAPI, GFP, and RFP lasers and filters, a Hamamatsu EMCCD (C9100-13) camera, and Volocity software (Perkin Elmer). FIJI/Image was used to analyze images and adjust brightness and contrast (67). Both Z-projections and single plane images are shown as noted in the figure legends. ER localization was scored manually from at least 200 cells.

4.2.5. Statistical analysis

The data are presented as mean values and error bars reflect standard deviation. All n values are indicated in the figure legend. Statistical significance was evaluated by paired, two-tailed t-test. Statistical significance is noted in the text. P values < 0.05 are considered significant.

4.3. Results

4.3.1. Dga1 localizes to the nER, cER, and LD during active growth and stationary phase

Previous analyses of Dga1 localization have been performed using overexpressed protein or an inactive carboxyl-terminally tagged protein. To determine if native levels of the protein localize in the same pattern as the overexpressed protein, we generated a strain containing an amino-terminally fluorescently tagged Dga1 under the control of the native promoter. To retain native expression of the protein in the strains, the fluorescently tagged protein is the only Dga1 present. We chose the bright, monomeric fluorescent marker mNeonGreen as the protein is in low abundance (68).

Analysis of the localization of mNeonGreen-Dga1 reveals that both during exponential phase and stationary phase, the protein is found encircling the LDs (Figure 4.6A). During active growth, the ratio of mNeonGreen-Dga1 on the LD to lipid stain is much higher than when cells switch to stationary phase (Figure 4.6B). This may reflect a higher amount of protein on the LD surface during active growth, or a higher amount of

lipid accumulation during stationary phase. In both circumstances, the amount of protein on the LD is high enough to detect readily.

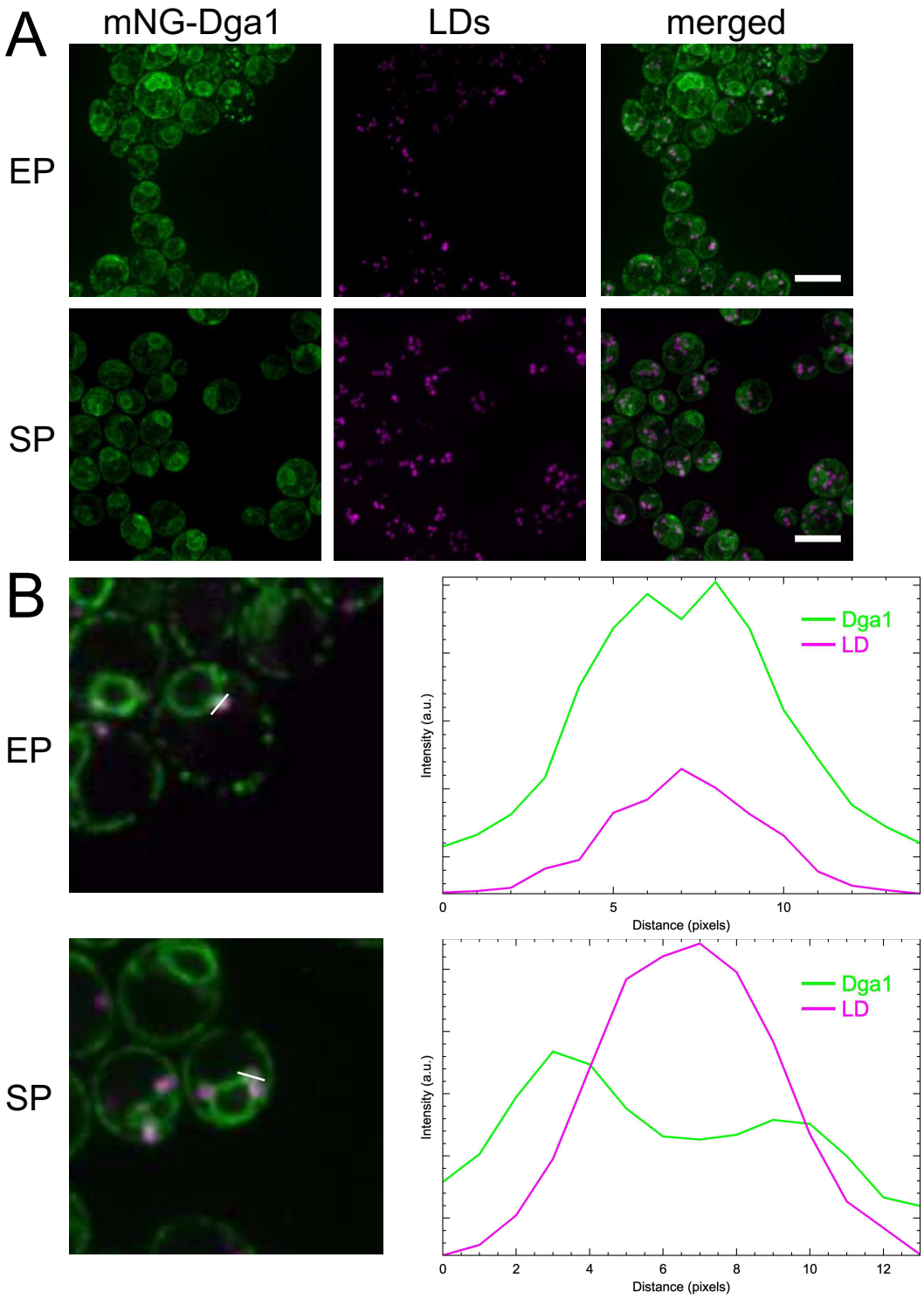

Figure 4.6 **Dga1 localizes to the LD during active growth and stationary phase.** A. Z-projections of cells expressing mNeonGreen-Dga1 (green) and treated with LD stain MDH (magenta). Images are artificially coloured for visibility by colourblind individuals. Scale bar is 10 µm. EP = exponential phase, SP = stationary phase. B. Individual planes from A. Graphs show fluorescence intensity from both mNeonGreen-Dga1 and MDH along the indicated white line.

The acyltransferase is also found in a subcellular localization pattern that resembles the ER; analysis of a strain coexpressing mNeonGreen-Dga1 and an ER marker confirms that, indeed, mNeonGreen-Dga1 is found within the nER and cER during active growth (Figure 4.7). Importantly, the ER marker is not found encircling the LDs as mNeonGreen-Dga1 does. This agrees with the current model of Dga1 LD localization, where the protein is present on the LD monolayer and not on an ER structure circling the LD (32).

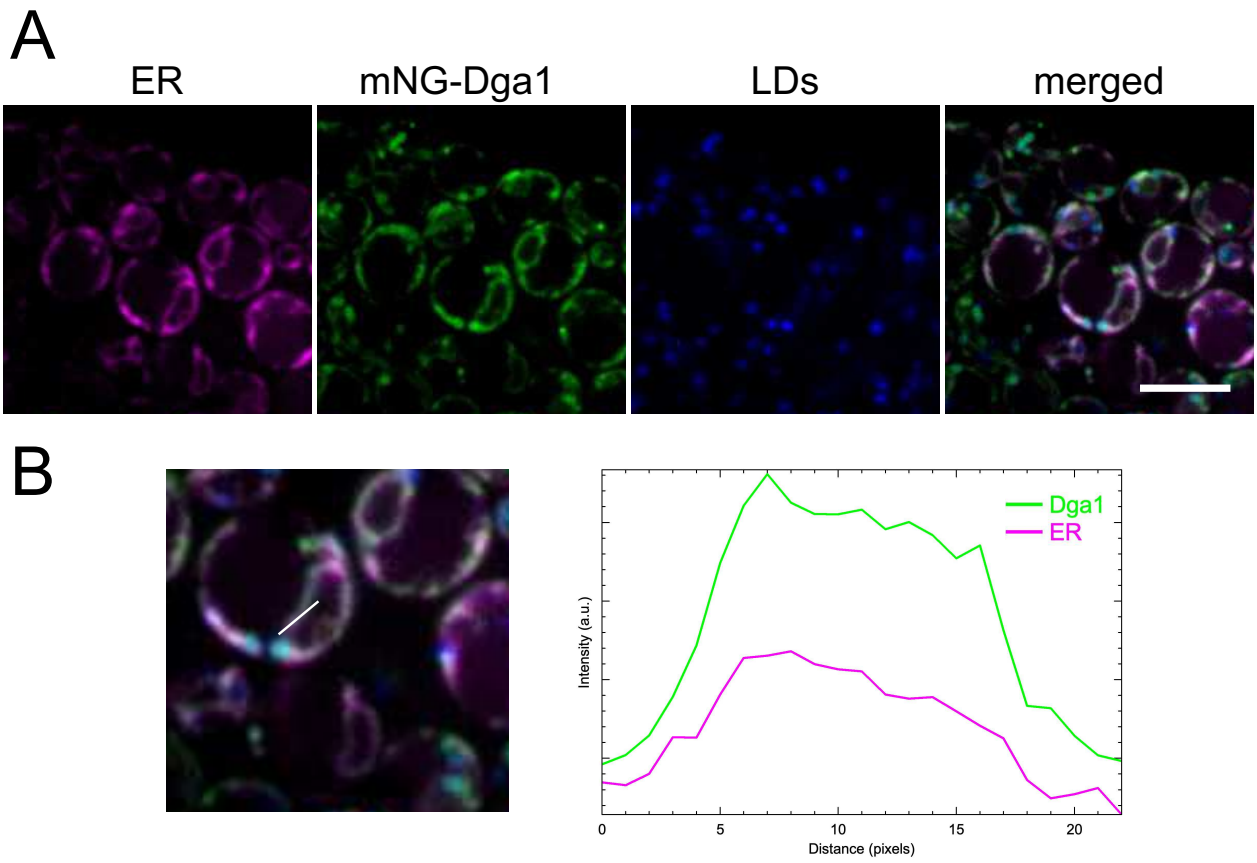

Figure 4.7 **Dga1 localizes to the ER during active growth.** A. Individual slices from cells expressing mCherry-ss-HDEL as an ER marker (magenta) and mNeonGreen-Dga1 (green), treated with LD stain MDH (blue). Scale bar is 10 μm. B. Graph shows fluorescence intensity from both mNeonGreen-Dga1 and the ER marker along the indicated white line.

4.3.2. ER localization of Dga1 truncation mutants is altered during active growth

As carboxyl-terminal truncations of Dga1 abolish acyltransferase activity and reduce the Ole1-Dga1 interaction, we were next interested in the impact of carboxyl-terminal truncations on Dga1 localization. The truncations dissected the different roles of the carboxyl-terminal regions and are depicted in Figure 4.8. While mNeonGreen-Dga1 localizes to the lipid droplets and nER quite readily during active growth, a truncation of the last 100 amino acids of the protein (mNeonGreen-Dga1$_{1\text{-}318}$) localizes in a punctate fashion within the cER. The truncation, which no longer contains the putative LD binding domain discovered in MmDGAT2 (Dga1$_{321\text{-}342}$) (55), is not found circling the LD at all (Figure 4.9). A truncation of only the last twenty residues (mNeonGreen-Dga1$_{1\text{-}398}$), however, reveals that the protein is readily able to localize to the LD. mNeonGreen-Dga1$_{1\text{-}398}$ also accumulates in a punctate pattern within the cER, though little to no protein is found in the nER during active growth (Figure 4.9).

As the last eight residues were proposed to be an ER retention signal, we analyzed the subcellular distribution of mNeonGreen-Dga1$_{\Delta 389\text{-}410}$, which retains the conserved ^{411}DAELKIVG^{418}, a putative ER retention signal (50, 69). This construct displayed a similar localization pattern to mNeonGreen-Dga1$_{1\text{-}398}$, with a punctate cER distribution, strong LD localization, and little nER signal. Interestingly, a deletion of the last ten residues (mNeonGreen-Dga1$_{1\text{-}408}$), which completely removes the conserved ^{411}DAELKIVG^{418}, exhibits a distribution that more readily resembles the wildtype mNeonGreen-Dga1. mNeonGreen-Dga1$_{1\text{-}408}$ is found localized to the nER, is distributed widely throughout the cER, and is readily found on the surface of LDs (Figure 4.9). While

this truncation lacks the highly conserved carboxyl-terminus of Dga1, rendering it inactive, we previously showed it retains interaction with Ole1 to a lesser extent. In contrast, the three truncations that exhibit little interaction with Ole1 also exhibit little nER localization and a more punctate cER distribution.

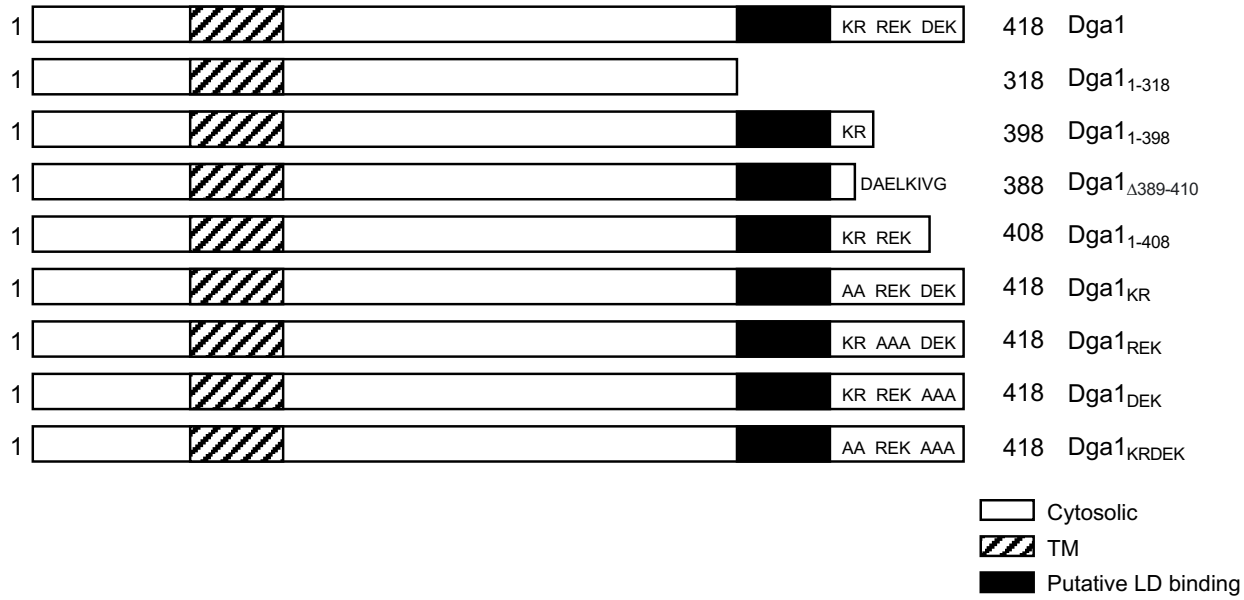

Figure 4.8 **Schematic of Dga1 truncation and mutant constructs used in this study.** Dga1 contains the putative DGAT2 LD binding domain and all charged residues that maintain the Ole1-Dga1 interaction. $Dga1_{1\text{-}318}$ lacks both the LD binding domain and the carboxyl-terminus, which is essential for catalytic activity of the protein. $Dga1_{1\text{-}398}$ retains the potential LD binding domain, but lacks the carboxyl-terminal residues essential for the Ole1-Dga1 interaction and DGAT activity. $Dga1_{\Delta 389\text{-}410}$ contains the LD binding region and the conserved ^{411}DAELKIVG^{418}, though it lacks interaction with Ole1 and acyltransferase activity. $Dga1_{1\text{-}408}$ retains some of the residues essential for interaction with Ole1, but does not retain activity. $Dga1_{KR}$, $Dga1_{REK}$, $Dga1_{DEK}$, and $Dga1_{KRDEK}$ are catalytically active mutants with the indicated mutations. $Dga1_{KR}$ and $Dga1_{DEK}$ interact with Ole1, albeit less strongly than $Dga1_{REK}$ or Dga1. $Dga1_{KRDEK}$ does not interact with Ole1.

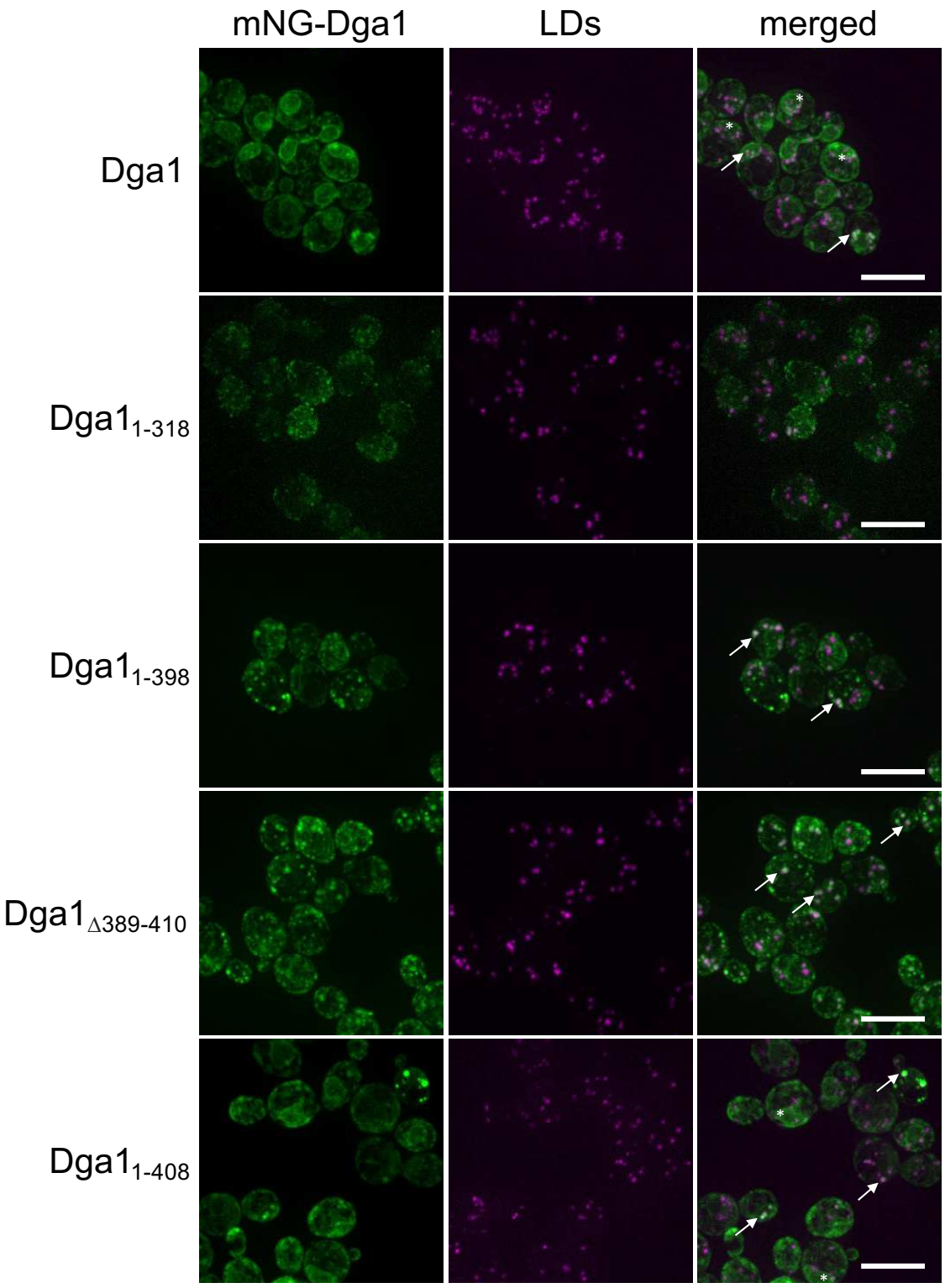

Figure 4.9 **Carboxyl-terminal truncations of Dga1 exhibit a reduced ER localization during active growth.** Z-projections of cells expressing indicated mNeonGreen-Dga1 truncations (mNG-Dga1, green) and treated with LD stain MDH (LDs, magenta) after 6 hours of growth. White arrows indicate mNeonGreen-Dga1 encircled LDs. White asterisks denote clear nER localization. Scale bar is 10 μm.

4.3.3. Alanine mutant exhibits reduced ER distribution during log phase of growth

While carboxyl-terminal truncations of Dga1 abolish activity of the protein and could additionally affect protein folding, alanine mutants of the Dga1 carboxyl-terminus retain acyltransferase activity and thus are attractive candidates to determine the role of Ole1-Dga1 interaction on Dga1 localization. We analyzed the localization of these four mutants during active growth in the same manner as the truncations (Figure 4.10). mNeonGreen-Dga1$_{KR}$, mNeonGreen-Dga1$_{REK}$, and mNeonGreen-Dga1$_{DEK}$ all exhibited very similar patterns of localization to mNeonGreen-Dga1 and mNeonGreen-Dga1$_{1-408}$ (Figure 4.9, Figure 4.10). The acyltransferase mutants are found widely throughout the nER, with localization to the cER and LDs. The alanine mutant that no longer interacts with Ole1, mNeonGreen-Dga1$_{KRDEK}$, exhibits a localization pattern resembling the distribution of mNeonGreen-Dga1$_{1-398}$. The protein is rarely found continuously throughout the nER but is readily found encircling LDs. The primary difference between the mNeonGreen-Dga1$_{KRDEK}$ mutant and the mNeonGreen-Dga1$_{1-398}$ truncation localization is the cER distribution. While the truncation is concentrated in bright puncta throughout the cER along the cell periphery, the mutant puncta are much less distinct. The primary place of mNeonGreen-Dga1$_{KRDEK}$ subcellular distribution appears to be the LD (Figure 4.10).

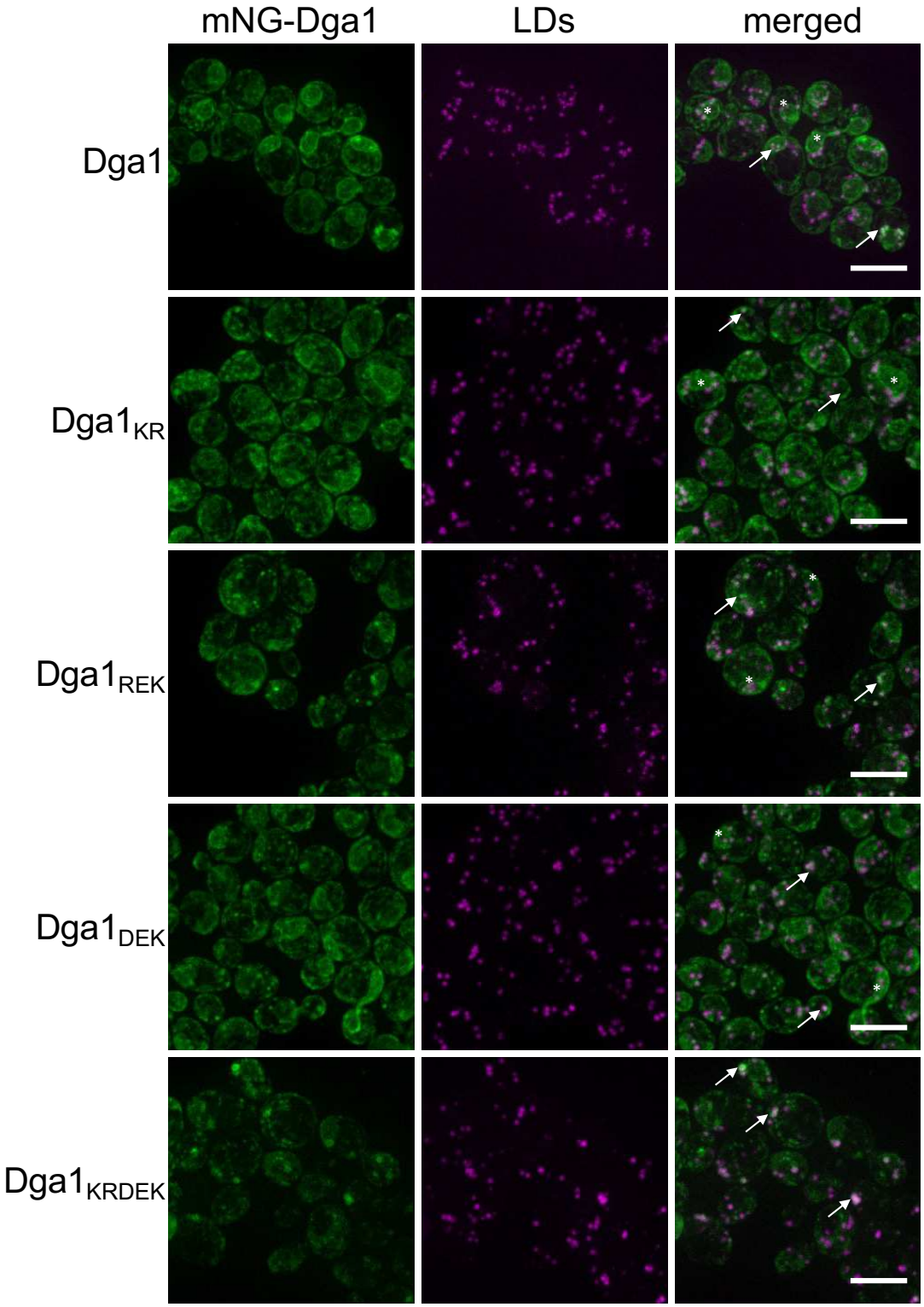

Figure 4.10 **Dga1$_{KRDEK}$ exhibits reduced ER localization during active growth.** Z-projections of cells expressing indicated mNeonGreen-Dga1 variants (mNG-Dga1, green) and treated with LD stain MDH (LDs, magenta) after 6 hours of growth. White arrows indicate mNeonGreen-Dga1 encircled LDs. White asterisks denote clear nER localization. Scale bar is 10 μm.

The subcellular distribution of the mNeonGreen-Dga1$_{1\text{-}398}$, mNeonGreen-Dga1$_{\Delta 389\text{-}410}$, mNeonGreen-Dga1$_{1\text{-}408}$, and mNeonGreen-Dga1$_{KRDEK}$ variants was characterized and compared to the wildtype acyltransferase. Cells with clear continuous nER localization as in Figure 4.11 displayed a strong mNeonGreen signal around the nER, with no breaks in the fluorescence. Cells with breaks in the nER mNeonGreen fluorescence were scored as containing patchy nER localization, while cells lacking any clear mNeonGreen nER signal were counted as no nER.

The wildtype acyltransferase exhibited a strong nER signal, with 90.5% of the cells found in a continuous nER localization pattern. Approximately 3.1% of cells exhibited a patchy distribution, and only 6.4% of cells did not have any clear mNeonGreen-Dga1 nER localization. The mNeonGreen-Dga1$_{1\text{-}398}$ truncation was localized with a continuous nER localization in the minority of cells, a significant difference from the wildtype distribution (8.4%, $p = 6.7E^{-15}$) (Figure 4.11). Cells expressing the truncation were primarily scored (50.0%) as a patchy nER mNeonGreen distribution, with no nER localization 41.6% of the time. The proportion of cells demonstrating both distribution patterns was significantly different from that of the wildtype ($p = 1.0E^{-06}$ and $p = 1.1E^{-05}$, respectively). mNeonGreen-Dga1$_{\Delta 389\text{-}410}$ retains the conserved ^{411}DAELKIVG^{418} and putative ER retention signal. This truncation exhibited a significantly different distribution from the wildtype, with a continuous nER localization pattern in 24.3% of cells, 50.1% of cells retaining a patchy nER distribution, and 25.6% scored as no nER localization ($p = 1.7E^{-08}$, $p = 1.1E^{-07}$, $p = 0.001$, respectively). The distribution of this acyltransferase was also significantly different from the mNeonGreen-Dga1$_{1\text{-}398}$ localization, with a higher proportion of cells continuously found throughout the nER and a lower proportion exhibiting no nER

localization ($p = 1.9E^{-05}$ and $p = 0.003$, respectively). mNeonGreen-Dga1$_{1-408}$, as mentioned, demonstrated an nER pattern similar to the wildtype acyltransferase with the majority (69.4%) of cells with a continuous nER distribution, 23.3% of cells scored as patchy nER, and only 7.3% of cells exhibiting no nER localization (Figure 4.9, Figure 4.11). However, the proportions of cells showing a continuous nER and patchy nER distribution were significantly different than the wildtype ($p = 0.0002$ and $p = 3.7E^{-05}$, respectively).

mNeonGreen-Dga1$_{KRDEK}$, the only construct in this characterization that retained acyltransferase activity (3.4.6), also exhibited a remarkably different localization pattern to wildtype mNeonGreen-Dga1. The majority of cells were characterized as having none or patchy nER localization, with 46.7% and 38.1% of the cells scoring as such. Only 15.2% of the cells contained a continuous mNeonGreen signal throughout the nER. This distribution pattern was significantly different from the wildtype ($p = 3.0E^{-11}$, $p = 2.9E^{-05}$, $p = 0.0001$, respectively) and closely resembled the distribution pattern of the inactive truncation mNeonGreen-Dga1$_{1-398}$ (Figure 4.9, Figure 4.10, Figure 4.11).

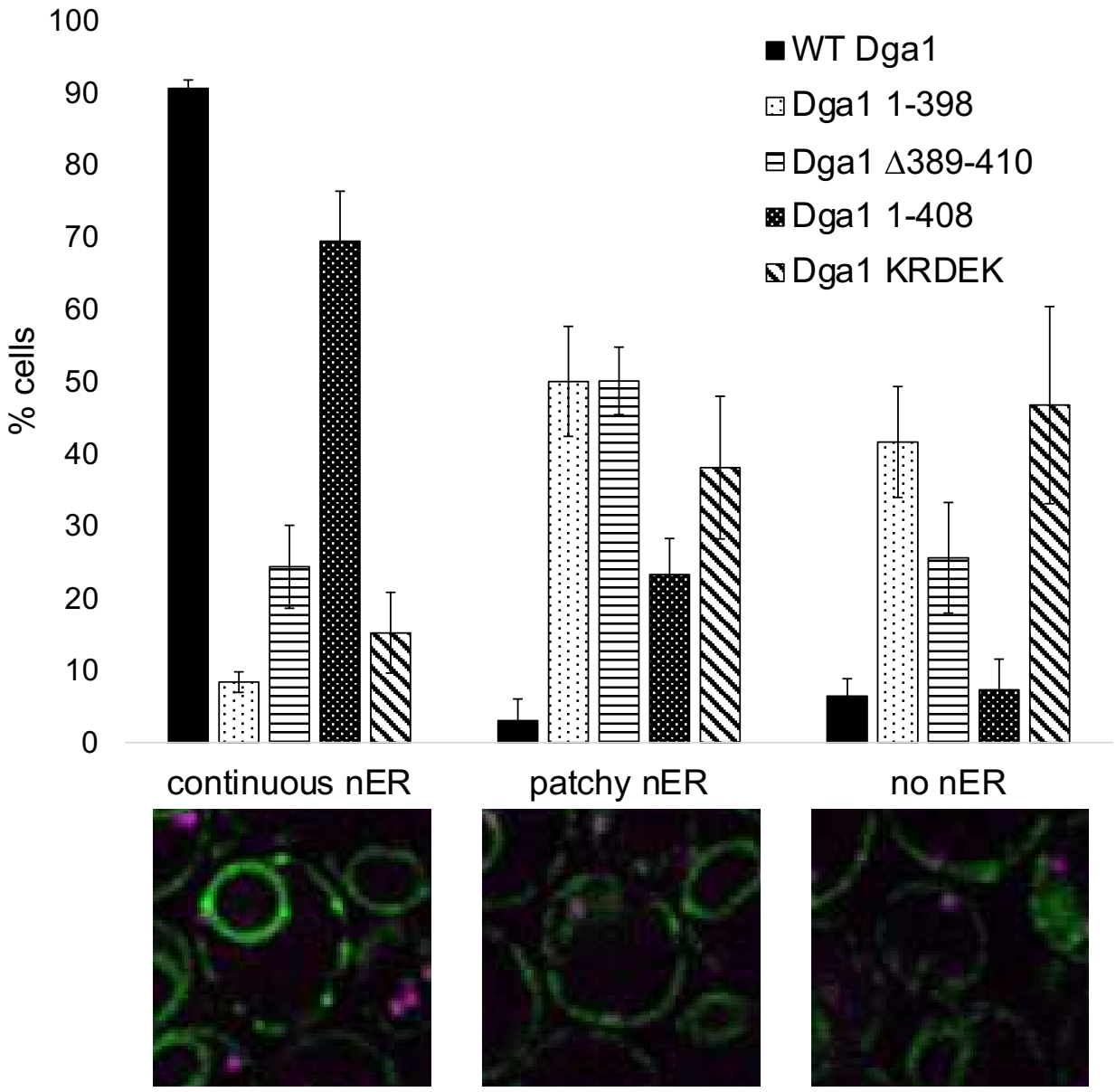

Figure 4.11 **Characterization of nER localization of Dga1 mutants during active growth.** Cells were scored per representative single plane images obtained after 6 hours of growth. Images show mNeonGreen-Dga1 (green) and LD stain MDH (magenta). WT Dga1 n = 220, $Dga1_{1\text{-}398}$ n = 218, $Dga1_{\Delta 389\text{-}410}$ n = 252, $Dga1_{1\text{-}408}$ n = 236, $Dga1_{KRDEK}$ n = 219.

The different Dga1 constructs demonstrate specific patterns of localization (Table 4.4). The charged to alanine mutants $Dga1_{KR}$, $Dga1_{REK}$, and $Dga1_{DEK}$ as well as the ten amino acid truncation ($Dga1_{1\text{-}408}$) retain a very similar localization pattern to the wildtype

acyltransferase. The protein is readily found in the nER and circles the LD as the wildtype does. However, the other truncations ($Dga1_{1-318}$, $Dga1_{1-398}$, and $Dga1_{\Delta 389-410}$) and the alanine mutant $Dga1_{KRDEK}$ exhibit a significantly decreased nER localization pattern, though all but the mutant lacking the putative LD targeting domain ($Dga1_{1-318}$) are found on the LD as the wildtype (Table 4.4). The localization pattern of the acyltransferase variants is distinctly associated with the interaction strength of the variant with Ole1, and not the acyltransferase catalytic activity of the protein. To investigate whether the Ole1-Dga1 interaction strength also correlated with subcellular distribution after the cells had stopped actively growing, we imaged these truncations during stationary phase as well.

Table 4.4 A comparison of Dga1 mutant characteristics and subcellular localization during active growth.

Construct	Interacts with Ole1[a]	Catalytically active	nER localization	LD localization
Dga1	*****	Yes	Yes	Yes
$Dga1_{1-318}$	*	No	No	No
$Dga1_{1-398}$	*	No	No	Yes
$Dga1_{\Delta 389-410}$	*	No	No	Yes
$Dga1_{1-408}$	***	No	Yes	Yes
$Dga1_{KR}$	***	Yes	Yes	Yes
$Dga1_{REK}$	*****	Yes	Yes	Yes
$Dga1_{DEK}$	***	Yes	Yes	Yes
$Dga1_{KRDEK}$	*	Yes	No	Yes

[a] * = 20% of the interaction strength between Ole1 and the full length Dga1

4.3.4. Localization of Dga1 variants is greatly altered during stationary phase

As Dga1 is the main TAG synthesizing acyltransferase in stationary phase, we were interested in the effect of the truncations on Dga1 distribution after 30 hours of growth. As mentioned, the full-length mNeonGreen-Dga1 is localized both to the ER and LDs during stationary phase. A deletion of the carboxyl-terminus, including the potential LD binding domain (mNeonGreen-Dga1$_{1\text{-}318}$), localizes primarily in one large distinct punctum within the cell (Figure 4.12). The puncta are unassociated with LDs.

mNeonGreen-Dga1$_{1\text{-}398}$ is also found principally in distinct puncta that are independent from the LD, with rare localization to the cER. LD association of mNeonGreen-Dga1$_{1\text{-}398}$ was not observed (Figure 4.12). mNeonGreen-Dga1$_{\Delta 389\text{-}410}$, similar to mNeonGreen-Dga1$_{1\text{-}398}$, was found in one distinct punctum within the cell and within the cER. The protein was not detected on LDs or within the nER (Figure 4.12).

In contrast, mNeonGreen-Dga1$_{1\text{-}408}$ was found readily throughout the nER and cER (Figure 4.12). A subpopulation of cells exhibited a similar distribution of mNeonGreen to the other truncations, with one distinct mNeonGreen punctum independent of the LD. The primary subcellular distribution, however, was within the ER. mNeonGreen-Dga1$_{1\text{-}408}$ was also found on the LD during stationary phase (Figure 4.12).

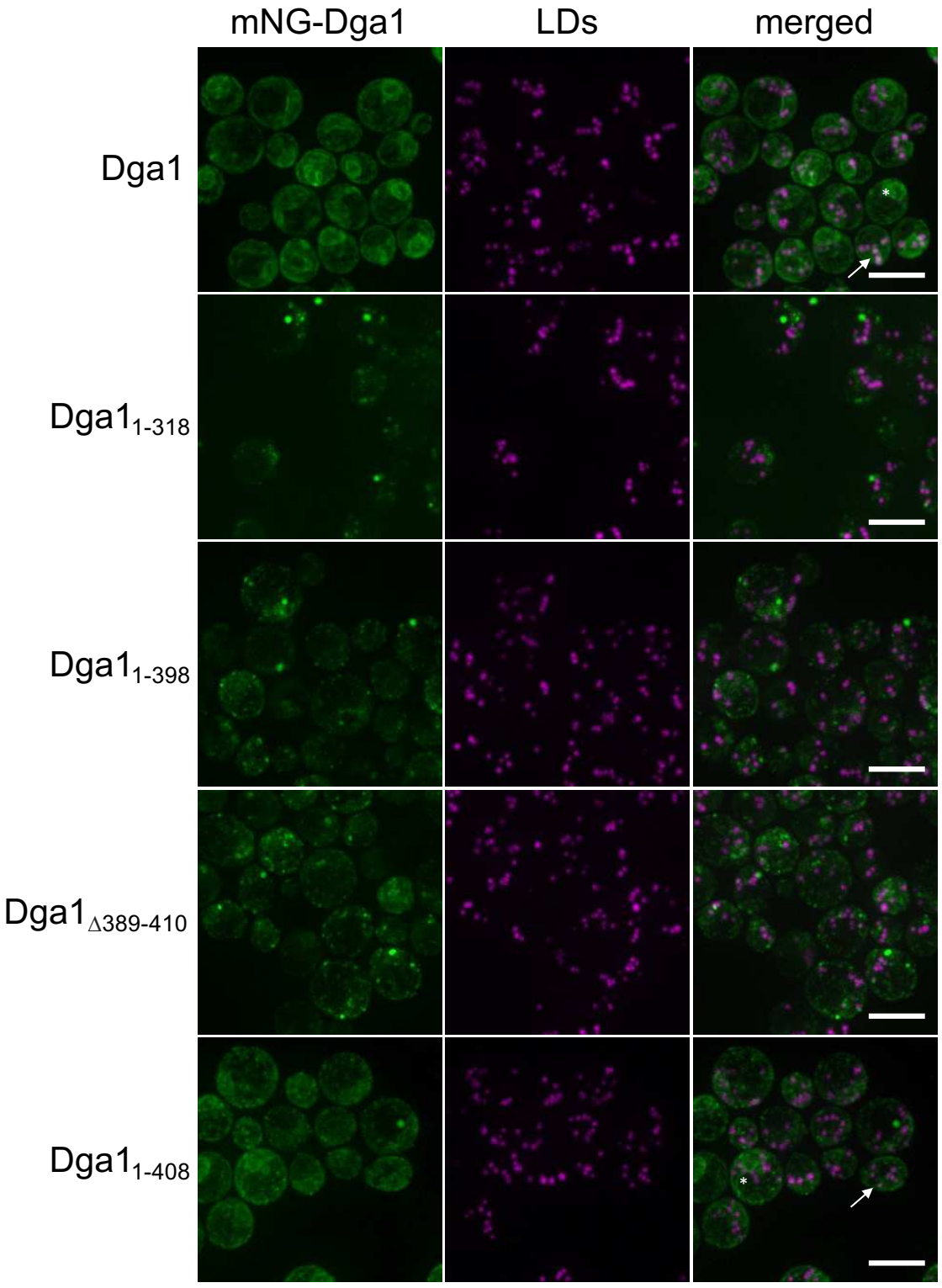

Figure 4.12 **Carboxyl-terminal truncations of Dga1 at stationary phase of cell growth.** Z-projections of cells expressing indicated mNeonGreen-Dga1 truncations (green) and treated with LD stain MDH (magenta) after 30 hours of growth. White arrows indicate mNeonGreen-Dga1 encircled LDs. White asterisks denote clear nER localization. Scale bar is 10 μm.

Alanine mutants of the acyltransferase primarily exhibited a subcellular localization reminiscent of the full-length Dga1. mNeonGreen-Dga1$_{KR}$, mNeonGreen-Dga1$_{REK}$, and mNeonGreen-Dga1$_{DEK}$ were localized throughout the nER and cER readily. All three acyltransferase variants were found on the LD in stationary phase (Figure 4.13).

The stationary phase distribution of mNeonGreen-Dga1$_{KRDEK}$ resembled the localization of truncation mutants that lack interaction with Ole1 (Figure 4.12, Figure 4.13). The protein was rarely found within the ER and many cells contained one large mNeonGreen punctum. mNeonGreen-Dga1$_{KRDEK}$ was also not detected on the surface of LDs during stationary phase (Figure 4.13).

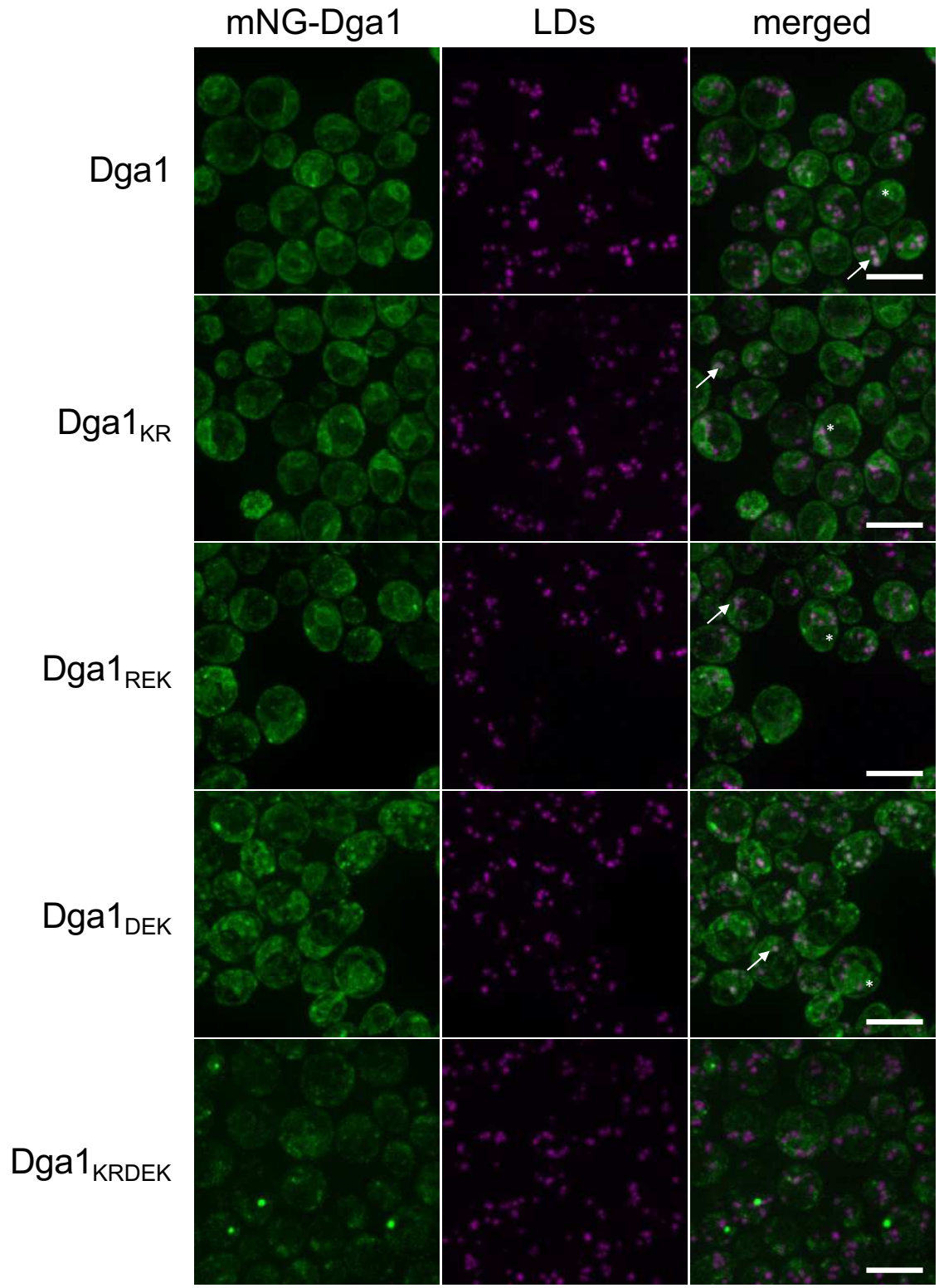

Figure 4.13 **Dga1$_{KRDEK}$ exhibits little to no ER or LD localization during stationary phase.** Z-projections of cells expressing indicated mNeonGreen-Dga1 variants (green) and treated with LD stain MDH (magenta) after 30 hours of growth. White arrows indicate mNeonGreen-Dga1 encircled LDs. White asterisks denote clear nER localization. Scale bar is 10 μm.

The Dga1 variants exhibit altered subcellular localization both in logarithmic phase and in stationary phase. During the stationary growth phase, the variants that retain an interaction with Ole1 ($Dga1_{1\text{-}408}$, $Dga1_{KR}$, $Dga1_{REK}$, $Dga1_{DEK}$) are found within the nER and on the LDs (Table 4.5). The cells rarely, if ever, exhibit one distinct punctum. The truncations and mutant that do not interact strongly with Ole1, however, are not widely distributed in the ER. The mNeonGreen signal from these variants is mainly found localized to one bright punctum per cell and is not associated with LDs (Table 4.5). The alanine mutant retained acyltransferase activity while the truncations were catalytically inactive, so catalytic capability does not correlate with localization pattern. The primary characteristic that all non-nER localized Dga1 variants share is little to no interaction with Ole1, so we were next interested in whether Ole1 and Dga1 display similar localization patterns and whether the interaction with the ER-resident desaturase was the mechanism retaining the acyltransferase in the nER.

Table 4.5 A comparison of Dga1 mutant characteristics and subcellular localization during the stationary phase of growth.

Construct	Interacts with Ole1[a]	Catalytically active	nER localization	LD localization	Single punctum in cells
Dga1	*****	Yes	Yes	Yes	No
$Dga1_{1\text{-}318}$	*	No	No	No	Yes
$Dga1_{1\text{-}398}$	*	No	No	No	Yes
$Dga1_{\Delta 389\text{-}410}$	*	No	No	No	Yes
$Dga1_{1\text{-}408}$	***	No	Yes	Yes	Rarely
$Dga1_{KR}$	***	Yes	Yes	Yes	No
$Dga1_{REK}$	*****	Yes	Yes	Yes	No
$Dga1_{DEK}$	***	Yes	Yes	Yes	No
$Dga1_{KRDEK}$	*	Yes	No	No	Yes

[a] * = 20% of the interaction strength between Ole1 and the full length Dga1

4.3.5. Dga1 localization pattern mirrors Ole1

We analyzed the localization patterns of Ole1-mCherry and mNeonGreen-Dga1 during active growth. Indeed, both Ole1-mCherry and mNeonGreen-Dga1 are found strongly localized to the perinuclear ER and cortical ER. Dga1 was found circling LDs, as observed previously, and Ole1 was excluded from LD localization as the ER marker in Figure 4.7. We next investigated whether Ole1 was indeed tethering Dga1 to the ER with a Δole1 mutant.

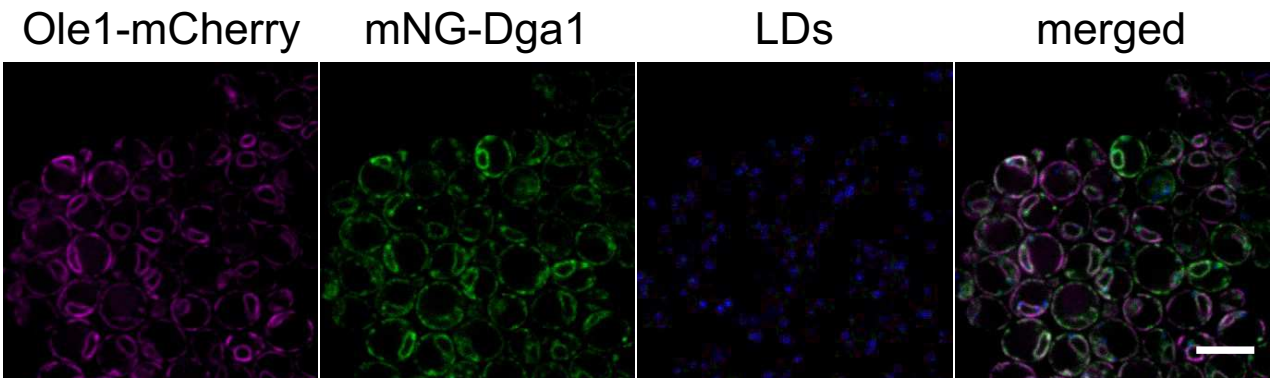

Figure 4.14 **Ole1 and Dga1 exhibit similar subcellular localization during active growth.** Single plane image of cells expressing Ole1-mCherry (magenta) and mNeonGreen-Dga1 (mNG-Dga1, green), treated with LD stain MDH (LDs, blue) after 6 hours of growth.

4.3.6. Ole1 deletion does not affect Dga1 distribution

We determined the localization pattern of the full length mNeonGreen-Dga1 in a wildtype strain that retained Ole1 and compared to mNeonGreen-Dga1 distribution in a mutant strain lacking Ole1 (Δole1). Subcellular distribution of the protein was analyzed both during active growth and stationary phase. As a deletion of Ole1 is lethal to cells, we supplemented the media for both strains with 0.05% C18:1 and 0.5% Tween-80. In both strains, mNeonGreen-Dga1 was found to localize readily to the nER, cER, and LDs. During active growth, the protein localized similarly regardless of presence or absence of Ole1. The same was seen during stationary phase. After 30 hours of growth in medium supplemented with oleic acid, mNeonGreen-Dga1 was found in the nER, cER, and LDs regardless of Ole1. In both strains, the mNeonGreen signal was much brighter than when cells are cultured in the absence of oleic acid.

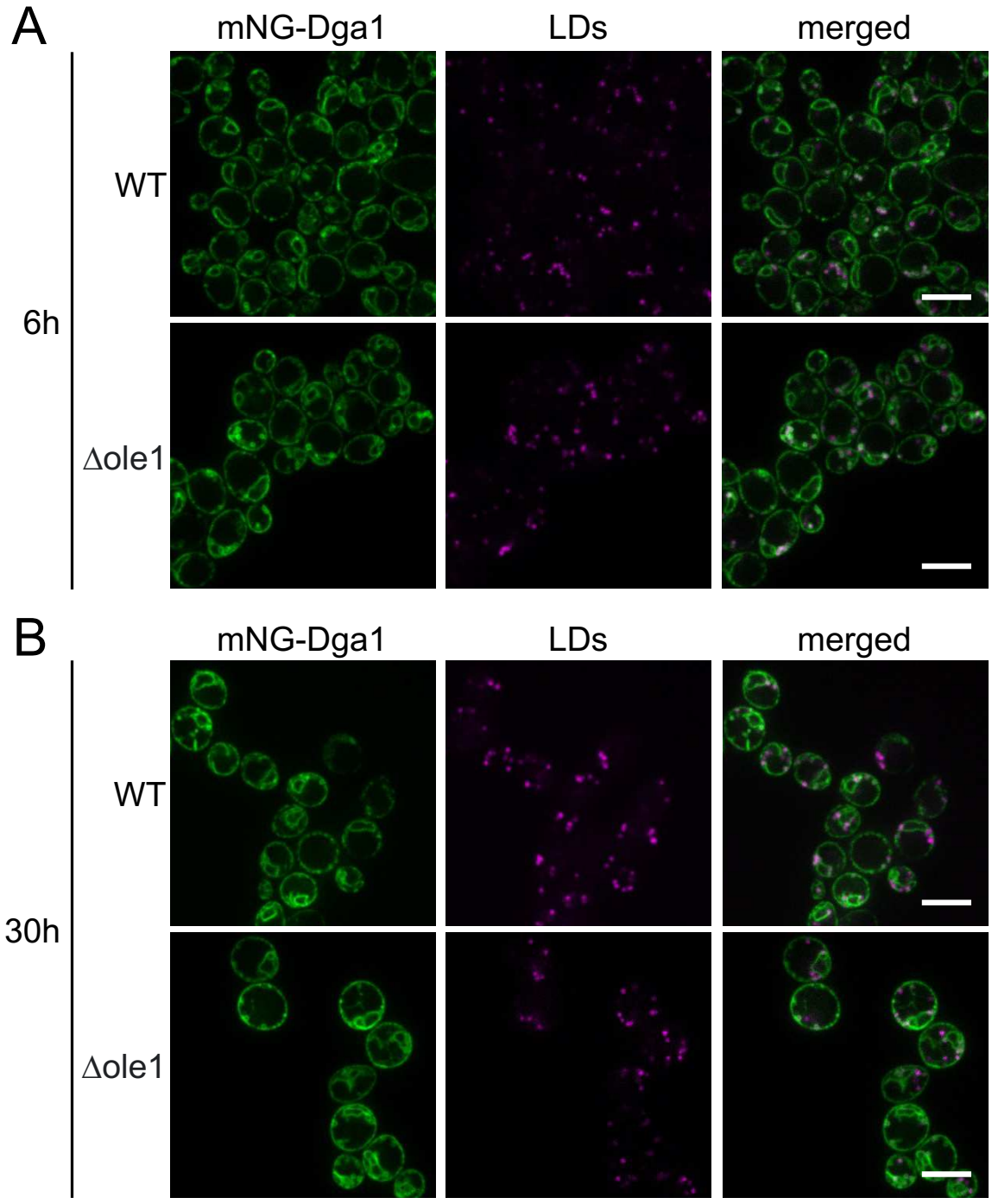

Figure 4.15 **Dga1 localization in an Δ*ole1* mutant is not altered.** A. Single plane images of cells expressing mNeonGreen-Dga1 (mNG-Dga1, green) and treated with LD stain MDH (LDs, magenta) with (WT) and without (Δ*ole1*) endogenous Ole1. Images were obtained after 6 hours (6h) of growth in media supplemented with oleic acid and Tween-80. B. Single plane images of cells expressing mNeonGreen-Dga1 (green) and treated with LD stain MDH (magenta) with (WT) and without (Δ*ole1*) endogenous Ole1. Images were obtained after 30 hours (30h) of growth in media supplemented with oleic acid and Tween-80.

4.4. Conclusions

This study has demonstrated that native Dga1 localizes to the nER, cER, and LD readily during both active growth and stationary phase. Previous investigations of the Dga1 subcellular distribution have used a *GAL* inducible promoter or overexpression vectors and have found that the acyltransferase moves fully to the LD and is retained there until growth resumes. This work has revealed that when Dga1 is present at native levels, the acyltransferase will transfer from the ER to the LD but does not ever fully leave the ER. As mentioned in 4.3.1, the ratio of protein to neutral lipid on the LD is much higher during active growth than stationary phase. We propose that this is due to the accumulation of lipid that is characteristic of *S. cerevisiae* in stationary phase, but true biochemical analyses are needed to confirm whether the absolute amount of Dga1 on the LD decreases as cells transition from active growth to stationary phase.

This work has revealed that the distribution of Dga1 variants correlates more so with the Dga1-Ole1 interaction strength than catalytic capability of the acyltransferase. The variants lacking an interaction with Ole1 ($Dga1_{1\text{-}318}$, $Dga1_{1\text{-}398}$, $Dga1_{\Delta 389\text{-}410}$, $Dga1_{KRDEK}$) do not distribute throughout the nER and cER as the wildtype protein. Variants that retain a strong interaction with the desaturase ($Dga1_{1\text{-}408}$, $Dga1_{KR}$, $Dga1_{REK}$, $Dga1_{DEK}$) have a localization pattern that resembles that of both Dga1 and Ole1, with widespread dissemination throughout the nER and cER. This data suggests that the interaction between the acyltransferase and desaturase serves to retain Dga1 throughout the ER. Analysis of whether this interaction impedes Dga1 movement to the ER will determine whether the interaction promotes or inhibits LD expansion.

The Stone lab has previously determined that a potential amphipathic helix at the carboxyl-terminus of MmDGAT2 is responsible for DGAT2 targeting to the LD monolayer (55). We generated a Dga1 truncation ($Dga1_{1\text{-}318}$) that lacks this putative LD targeting domain ($Dga1_{321\text{-}342}$) and demonstrated that it no longer localizes to and encircles LDs, though it is still retained in the membrane (3.4.3). This suggests that these residues are responsible, at least in part, for the direction of the acyltransferase to the LD monolayer. It should be noted that this truncation lacks activity and contains a deletion of almost 25% of the protein, and these factors could be impacting the acyltransferase folding and LD localization as well. Further analysis of the nature of this region and whether it localizes to the LD independent of Dga1 would allow us to conclusively determine whether $Dga1_{321\text{-}342}$ is an LD targeting domain.

The highly conserved carboxyl-terminus of Dga1 has been proposed to be an ER retention signal (47). We analyzed the distribution of $Dga1_{\Delta 389\text{-}410}$, which no longer includes the residues responsible for interaction between Ole1 and Dga1 but contains the conserved ^{411}DAELKIVG^{418} and determined that it does not retain the majority of the protein in the nER. Accordingly, the $Dga1_{DEK}$ mutant, which contains a carboxyl-terminal ^{411}AAALAIVG^{418}, is distributed throughout the nER and cER in a similar manner to the full-length protein. A mutation of only the charged residues leaves room for the argument that the highly conserved Leu^{414} is the pivotal residue for ER maintenance (69). However, a deletion of the last ten amino acids ($Dga1_{1\text{-}408}$) including the conserved Leu^{414} does not abolish localization of the acyltransferase to the nER and cER. ER localization of the protein is not abolished until both regions of Dga1 responsible for the Ole1-Dga1 interaction maintenance are mutated ($Dga1_{KRDEK}$). Taken together, this suggests that

while the carboxyl-terminus is essential for activity (48), it is not responsible for ER retention. Dissection of the distribution of these mutants between the ER and Golgi would serve to conclude whether this region is indeed responsible for ER retrieval from the Golgi.

Cells expressing Dga1 truncation mutants mNeonGreen-Dga1$_{1\text{-}398}$ and mNeonGreen-Dga1$_{\Delta 389\text{-}410}$ contained bright and distinct puncta within the cER. This was a phenomenon not observed readily with the other strains, including a strain expressing mNeonGreen-Dga1$_{KRDEK}$. These puncta do not appear to be associated with LDs, though they could be associated with smaller, nascent LDs or lipid lenses that escape detection by the neutral lipid stain. Indeed, Dga1 and Lro1 have been shown to concentrate in puncta with seipin and other proteins essential for proper LD formation upon LD induction (4). Both Dga1$_{1\text{-}398}$ and Dga1$_{\Delta 389\text{-}410}$ do not interact strongly with Ole1 and are seen less readily throughout the nER. It is possible the puncta observed are the truncations colocalizing with sites of LD generation more readily than the full-length proteins due to lack of tethering to the nER and desaturasome by the desaturase.

Analysis of Dga1 localization during stationary phase revealed a subcellular distribution to the nER, cER, and LD for the wildtype acyltransferase and those mutants that interact strongly with Ole1 (Dga1$_{1\text{-}408}$, Dga1$_{KR}$, Dga1$_{REK}$, Dga1$_{DEK}$). The variants that do not interact with Ole1 (Dga1$_{1\text{-}318}$, Dga1$_{1\text{-}398}$, Dga1$_{\Delta 389\text{-}410}$, Dga1$_{KRDEK}$) localized primarily to one distinct punctum within cells. It is yet unknown what structure this punctum represents, though it does greatly resemble the autophagosome during starvation (15). Lipid synthesis and autophagic flux are intimately linked, as proper autophagy progression is reliant on both LDs and an active desaturase (70–72). Indeed, LDs are a

macroautophagy target in stationary phase (17, 73). The observed structure could be a concentration of mNeonGreen in an autophagosome due to catabolism of LDs containing the variants that localize to the LD readily over the ER during active growth ($Dga1_{1\text{-}398}$, $Dga1_{\Delta 389\text{-}410}$, $Dga1_{KRDEK}$). However, the distinct puncta were also present in cells expressing mNeonGreen-$Dga1_{1\text{-}318}$, which does not localize to the LD and thus the observed structure could not be strictly autophagosomes catabolizing LDs. While Dga1 is a target of the ERAD proteasomal degradation pathway distinct from autophagy, ubiquitinated proteins can be targeted for autophagic degradation if aggregated (74). Therefore, it is also possible that interaction with Ole1 prevents aggregation of the acyltransferase variants, providing protection from autophagic degradation. Future work to understand the nature of the structure observed in these stationary cells is needed before conclusions can be drawn.

This ER distribution of Dga1 greatly resembles that of Ole1, the only desaturase in *S. cerevisiae* and an ER-resident polytopic membrane protein that has been found to interact strongly with the acyltransferase. Indeed, Dga1 mutants and truncations that do not interact strongly with Ole1 are not detected to the same extent within the nER, independent of whether the constructs retain acyltransferase activity or not. Though this suggested that the Ole1-Dga1 interaction retains Dga1 within the ER, imaging of the acyltransferase localization in the absence of Ole1 revealed that Dga1 does not require the desaturase to localize throughout the ER (Figure 4.15). However, it should be noted that the supplementation with oleic acid, a molecule classically used to induce LD formation, seems to have increased the amount of mNeonGreen-Dga1 within both strains. Thus, the requirement for supplementation of UFA in a Δole1 strain makes

determination of true Dga1 localization difficult. Future work should aim to determine the impact of Ole1 presence on Dga1 localization in a system that does not rely on UFA addition for growth; strains with a temperature sensitive Ole1 mutant or degron-tagged Ole1 would be good candidates for this determination.

Ultimately, this work implicates the diacylglycerol acyltransferase – desaturase interaction in subcellular distribution of Dga1. While we have demonstrated that the Ole1-Dga1 interaction promotes proper LD budding from the ER (Figure 4.1, arrow 1), this study supports the contention that the desaturasome serves to retain the acyltransferase in the ER, which may decrease Dga1 transfer to the LD monolayer and modulate LD growth (Figure 4.1, arrow 2). Determination of whether the desaturase is indeed the protein tethering Dga1 to the ER or if another ER-resident protein within the desaturasome is responsible will expand the understanding of the regulatory mechanisms controlling Dga1 localization and LD growth.

Chapter 5 – Conclusions

5.1. Reflections

This project began as a response to metabolic engineering work from the Stuart lab demonstrating that the unsaturated fatty acyl-CoA generated by Ole1 is not readily available to exogenous enzymes. Initially, I was interested in whether Ole1 interacts with the *Saccharomyces cerevisiae* acyltransferases, channeling the newly unsaturated acyl-CoA to endogenous lipid production and sequestering the acyl chains from use by the exogenously expressed proteins. The scope of this study expanded greatly from there, all with one overarching goal: a determination of the protein-protein interaction (PPI) network in phospholipid and storage lipid synthesis in the yeast *S. cerevisiae*.

5.1.1. Identification of the lipid biosynthetic interactome

The lipidome is dynamic and will rapidly change in composition depending on the physiological state of the cell. Organization of lipid biosynthetic enzymes into metabolons, interaction networks with transient and dynamic composition, could indeed direct acyl chains to precise fates according to metabolic requirements (1). This work has discovered novel interactions between the *S. cerevisiae* desaturase and proteins catalyzing PA, PL, and storage lipid synthesis. In PA synthesis, Ole1 interacts with the acyltransferases Gpt2 and Slc1, which may explain the preference for Gpt2 to incorporate unsaturated acyl chains into LPA and the characteristic enrichment for an unsaturated acyl chain in the *sn-2* position of certain phospholipids (PLs) and triacylglycerol (TAG) (2, 3). Slc1 also interacts with Gpt2 over Sct1, implying the Gpt2-generated LPA is preferentially

accessible to the LPAAT. Channeling unsaturated acyl chains into PA synthesis would create a building block for *de novo* PLs and TAG that generate a more disordered membrane and neutral lipid lens.

The control of membrane fluidity relies on a regulation of unsaturated acyl chain incorporation into PLs. Certain species of downstream phospholipid are preferentially di-unsaturated; the majority of *de novo* PE and PC contain two unsaturated acyl chains (4). In our map of the desaturase interactome, Ole1, Slc1, and Cds1 are proximal to Cho1, the enzyme responsible for synthesis of the PE precursor PS, and Cho2, the initial enzyme in PC synthesis from PE. This data taken together suggests the preferential channeling of unsaturated acyl-CoA into PE and PC is a result of protein-protein interactions between Ole1 and these phospholipid biosynthetic enzymes.

It has become clear that budding of the lipid droplet (LD) from the ER necessitates not only unsaturated acyl chain incorporation into PL at the LD initiation site, but into TAG as well (5, 6). Both TAG and the other neutral lipid in yeast, sterol ester (SE), are synthesized specifically with unsaturated acyl donors – 60% of the TAG generated in *Saccharomyces cerevisiae* are made of only palmitolyl and oleoyl moieties, and SE is preferentially acylated by unsaturated acyl chains (3, 7). This work has revealed interactions between Ole1, Slc1, Cds1, and all four final acyltransferases in neutral lipid synthesis. A complex of Ole1, Gpt2, Slc1, and Dga1 could indeed produce a TAG profile wherein the majority of the species contain only unsaturated acyl chains. The existence of Cds1 within the same supercomplex as Ole1 and neutral lipid synthesizing enzymes could provide a rapidly synthesized set of PLs imparting the requisite fluidity to permit LD budding from the ER. Taken together, this PPI network analysis implies the existence of

a lipid biosynthetic complex, wherein unsaturated acyl-CoA is channeled into PA that will form the PL monolayer as well as TAG.

This analysis of the desaturasome has provided an attractive explanation for why cells can respond rapidly in response to physiological concerns and direct flux of unsaturated acyl-CoA preferentially toward PE, PC, and TAG. While control of membrane fluidity is obviously essential for the membrane integrity of unicellular organisms unable to regulate temperature, regulation of the fluidity of subcellular membranes is essential for proper progression of cellular processes in higher eukaryotes. The incorporation of unsaturated moieties in PL and TAG are necessary to permit budding of the LD from the ER and promote lipid deposition, and desaturase activity is required for progression of autophagy (5, 6, 8, 9). In contrast, the characteristic enrichment for saturated lipids in the plasma membrane is crucial for cell growth, ion homeostasis, and immune system functioning (10). Understanding the mechanisms controlling the proper partitioning of unsaturated acyl chains thus lends an understanding to the mechanisms controlling lipid accumulation, autophagy initiation, and immune function. This work initially intended to have applications in metabolic engineering, but it has expanded to provide a foundation of knowledge crucial to understanding the role of the lipid biosynthetic interactome in disorders of lipid dysregulation and cancer.

5.1.2. Dissection of the desaturase – diacylglycerol acyltransferase interaction

Incorporation of unsaturated acyl chains into TAG is critical to the regulation of lipid accumulation, compelling a more in-depth analysis of the interaction between Ole1 and

Dga1. Mutations of charged residues in the carboxyl-terminus of Dga1 ($Dga1_{KRDEK}$) reduced the Ole1-Dga1 interaction without removing catalytic capability of the acyltransferase. Though the $Dga1_{KRDEK}$ mutant can incorporate exogenous unsaturated FA into TAG, the LDs it produces are smaller in size, indicating a struggle to initiate LD budding from the ER. The mutant also generated significantly fewer LDs per cell during active growth than the wildtype enzyme, though cells examined in stationary phase of growth revealed an increased accumulation of LDs. This implicates the Ole1-Dga1 interaction in coordination of Dga1 at LD initiation sites and promotion of LD emergence from the ER.

To this point in the investigation, the evidence pointed to the Ole1-Dga1 interaction promoting TAG synthesis and LD emergence. However, the transfer of the TAG synthase to the LD surface, an essential step to LD growth and TAG deposition (11–13), could potentially be inhibited by the interaction of Dga1 with the ER resident Ole1. We observed that Dga1 and Ole1 localize in similar subcellular patterns during active growth, with a widespread nuclear ER and cortical ER distribution for both proteins. Dga1 circles LDs, while Ole1 does not, which indicates the detected interaction is primarily seen within the ER. Distribution of the non-interacting $Dga1_{KRDEK}$ mutant within the ER was significantly decreased, though LD localization was still observed. When we attempted to confirm the role of Ole1 in the ER retention of Dga1, the results were inconclusive. This work suggests that the Ole1-Dga1 interaction does indeed play a role in determining subcellular distribution of the acyltransferase, though Ole1's role as the ER tether has yet to be confirmed.

A better appreciation of this interaction provides a strong foundation to the understanding of lipid deposition disorders in humans, with a better understanding of nonalcoholic fatty liver disease (NAFLD) in particular. NAFLD is a significant cause of chronic liver disease worldwide and is initiated by an increased deposition of TAG within hepatocytes (14, 15). Desaturase activity is positively associated with TAG synthesis in the liver, and both SCD1 and DGAT2 inhibitors have shown promise in clinical trials for NAFLD (6, 15, 16). It is clear both the desaturase and the diacylglycerol acyltransferase play a role in NAFLD progression. This study has presented evidence that an interaction between stearoyl-CoA desaturase and diacylglycerol acyltransferase shuttles unsaturated acyl-CoA to TAG production, promoting LD biogenesis from the ER. After LD budding, this interaction may maintain Dga1 within the ER and prevent aberrant TAG accumulation in an inhibitory fashion. It is therefore possible that the desaturasome serves as an important regulatory step in the maintenance of lipid homeostasis, instead of purely promoting TAG deposition in LDs. This work has revealed the desaturase-diacylglycerol acyltransferase interaction as a modulator of fat deposition in lipid droplets and provided a foundational understanding to its role in NAFLD progression.

5.2. Recommendations

These studies have made great strides in identifying the desaturasome and determining its composition. It has opened future avenues for investigation that have been discussed throughout this work that are worth reiterating here.

Metabolons can control flux through certain pathways through substrate channeling via protein-protein interactions (17). Though we have shown that proteins within

phospholipid and neutral lipid synthesis interact, we have not to this date determined that these PPIs are channeling substrate. Future work will need to explore the biochemical nature of these interactions, and whether they shuttle pathway intermediates to certain fates. To analyze the Ole1-Slc1 interaction, we have created a strain lacking all neutral lipid acyltransferases and the minor LPAAT Ale1 (Δdga1Δlro1Δare1Δare2Δale1). Isolation of microsomes from this strain would contain Ole1 and Slc1 and could be used to probe whether the Ole1-Slc1 interaction channels unsaturated acyl-CoA with *in vitro* competition assays and an analysis of PA produced. Classifying whether the complex we have identified is indeed a metabolon will lend insight to the role of this complex in phospholipid and neutral lipid flux determination.

Ole1, Slc1, and Cds1 all interact with Cho1, but the cellular PS is enriched for saturated acyl moieties, particularly the PS species located at the plasma membrane (18). The MYTH technique, while a powerful tool to determine transient interactions between membrane proteins, cannot resolve whether proteins are interacting in particular subcellular compartments. Mapping the partitioning of these interactions via either the bimolecular fluorescence complementation or fluorescence resonance energy transfer techniques will determine whether these proteins are found in complex with each other at specific locations within the cell (19, 20). For instance, Cho1 is located within the ER but concentrates in the mitochondrial associated ER membrane (MAM) (21). As di-unsaturated PS is preferentially converted to di-unsaturated PE by mitochondrially located Psd1, it is possible a complex including Ole1, Gpt2, Slc1, Cds1, and Cho1 is concentrated within the MAM and channels di-unsaturated PA to CDP-DAG and PS (22). Cho1 activity is also concentrated within the plasma membrane associated ER (PAM),

but the PS species comprising the plasma membrane contains a larger proportion of saturated acyl chains than those found in the ER (18, 23). This may indicate that Ole1 and Cho1 interact less readily within the PAM, leading to the production of a more saturated PS profile. Determining the composition of the desaturasome at various organelle contact sites could reveal the mechanism controlling subcellular lipid distribution as well.

It is additionally important to note that the methods used in this work have the ability to detect interactions in a binary fashion. While it is true that Ole1, Slc1, and Cds1 all interact with proteins in lipid biosynthesis like Gpt2 or Cho1, it cannot be discerned whether all of these enzymes exist within the same supercomplex. A set of co-immunoprecipitations with multiple proteins tagged endogenously with separate epitope tags would be able to determine whether a complex of Ole1, Gpt2, Slc1, Cds1, and Cho1 indeed exists, or whether these proteins interact independently of one another. Elucidating whether these proteins exist in ternary complexes would lend strength to the argument that the desaturasome is a metabolon, directing unsaturated acyl chains to specific fates.

We have demonstrated that the Ole1-Dga1 interaction plays a role in cellular distribution of the acyltransferase and that a loss of the interaction impedes proper LD initiation. It is yet unclear whether the loss of interaction additionally alters TAG composition; it is probable that the determination may be difficult from FAME preparation of the TAG obtained from bulk cells, as TAG contains three acyl chains and would require a dramatic difference in acyl chain incorporation at the *sn-3* position to reveal the interaction significance on TAG composition. A competition assay using microsomes from

Δdga1Δlro1Δare1Δare2 cells expressing either Dga1 or $Dga1_{KRDEK}$ may better elucidate whether the Ole1-Dga1 interaction does indeed control the incorporation of unsaturated acyl chains into TAG by Dga1. Understanding the biochemical nature of this interaction will solve the question that has been asked since the SCD1-DGAT2 interaction discovery in 2006: is this desaturase-acyltransferase interaction truly generating a more unsaturated TAG profile?

One last direction to be explored that has come from this work is the idea of Ole1 as a Dga1 ER tether. Our analysis of mNeonGreen-Dga1 localization in a strain lacking Ole1 showed a large increase in mNeonGreen signal in both the wildtype and Δole1 strains due to the requirement for UFA supplementation in the absence of an active desaturase in *Saccharomyces*. Future investigations should consider titration of UFA to determine a concentration that will support growth without altering Dga1 levels. An alternative would utilize a degron-tagged Ole1 in a strain expressing mNeonGreen-Dga1 and visualize the localization of Dga1 in the ER compared to the LD over time (24). If Ole1 does indeed serve to tether Dga1 to the ER, this interaction may play a major role in lipid homeostasis and TAG synthase inhibition within the cell.

Ultimately, this project has revealed crucial evidence for the argument of a lipid synthesizing metabolon in *Saccharomyces cerevisiae*. We have contributed fundamentally to the determination of a protein interactome that may channel unsaturated acyl-CoA to specific fates within the cell. This work has the potential to not only serve as a foundation to better understand metabolic engineering of lipid products in *Saccharomyces cerevisiae*, but to frame the understanding of lipid dysregulatory disorders as a function of protein-protein interactions.

Works Cited

Chapter 1

1. Fahy, E., Cotter, D., Sud, M., and Subramaniam, S. (2011) Lipid classification, structures and tools. *Biochim. Biophys. Acta BBA - Mol. Cell Biol. Lipids*. **1811**, 637–647
2. Natter, K., Leitner, P., Faschinger, A., Wolinski, H., McCraith, S., and Fields, S. (2005) The Spatial Organization of Lipid Synthesis in the Yeast *Saccharomyces cerevisiae* Derived from Large Scale Green Fluorescent Protein Tagging and High Resolution Microscopy. *Mol. Cell. Proteomics*. **4**, 662–672
3. Ji, J., and Greenberg, M. L. (2022) Cardiolipin function in the yeast *S. cerevisiae* and the lessons learned for Barth syndrome. *J. Inherit. Metab. Dis.* **45**, 60–71
4. Klug, L., and Daum, G. (2014) Yeast lipid metabolism at a glance. *FEMS Yeast Res.* **14**, 369–388
5. Czabany, T., Wagner, A., Zweytick, D., Lohner, K., Leitner, E., Ingolic, E., and Daum, G. (2008) Structural and Biochemical Properties of Lipid Particles from the Yeast *Saccharomyces cerevisiae*. *J. Biol. Chem.* **283**, 17065–17074
6. Sibirny, A. A. (2016) Yeast peroxisomes: structure, functions and biotechnological opportunities. *FEMS Yeast Res.* **16**, fow038
7. Wu, H., Carvalho, P., and Voeltz, G. K. (2018) Here, There and Everywhere: The Importance of ER Membrane Contact Sites. *Science*. **361**, 1–27
8. Zheng, Z., and Zou, J. (2001) The Initial Step of the Glycerolipid Pathway. *J. Biol. Chem.* **276**, 41710–41716
9. Ståhl, U., Stålberg, K., Stymne, S., and Ronne, H. (2008) A family of eukaryotic lysophospholipid acyltransferases with broad specificity. *FEBS Lett.* **582**, 305–309
10. Pichler, H., Gaigg, B., Hrastnik, C., Achleitner, G., Kohlwein, S. D., Zellnig, G., Perktold, A., and Daum, G. (2001) A subfraction of the yeast endoplasmic reticulum associates with the plasma membrane and has a high capacity to synthesize lipids. *Eur. J. Biochem.* **268**, 2351–2361
11. Gulshan, K., Shahi, P., and Moye-Rowley, W. S. (2010) Compartment-specific Synthesis of Phosphatidylethanolamine Is Required for Normal Heavy Metal Resistance. *Mol. Biol. Cell*. **21**, 443–455
12. Hasslacher, M., Ivessa, A., Paltauf, F., and Kohlwein, S. D. (1993) Acetyl-CoA carboxylase from yeast is an essential enzyme and is regulated by factors that control phospholipid metabolism. *J. Biol. Chem.* **268**, 10946–10952
13. Kühn, L., Castorph, H., and Schweizer, E. (1972) Gene Linkage and Gene-Enzyme Relations in the Fatty-Acid-Synthetase System of *Saccharomyces cerevisiae*. *Eur. J. Biochem.* **24**, 492–497
14. Chirala, S. S., Zhong, Q., Huang, W., and Al-Feel, W. (1994) Analysis of FAS3/ACC regulatory region of *Saccharomyces cerevisiae*: identification of a functional UAS|N0 and sequences responsible for fatty acid mediated repression. *Nucleic Acids Res.* **22**, 412–418

15. Blank, H. M., Perez, R., He, C., Maitra, N., Metz, R., Hill, J., Lin, Y., Johnson, C. D., Bankaitis, V. A., Kennedy, B. K., Aramayo, R., and Polymenis, M. (2017) Translational control of lipogenic enzymes in the cell cycle of synchronous, growing yeast cells. *EMBO J.* **36**, 487–502
16. Woods, A., Munday, M. R., Scott, J., Yang, X., Carlson, M., and Carling, D. (1994) Yeast SNF1 is functionally related to mammalian AMP-activated protein kinase and regulates acetyl-CoA carboxylase *in vivo*. *J. Biol. Chem.* **269**, 19509–19515
17. Witters, L. A., and Watts, T. D. (1990) Yeast acetyl-CoA carboxylase: *In vitro* phosphorylation by mammalian and yeast protein kinases. *Biochem. Biophys. Res. Commun.* **169**, 369–376
18. Pham, T., Walden, E., Huard, S., Pezacki, J., Fullerton, M. D., and Baetz, K. (2022) Fine-tuning acetyl-CoA carboxylase 1 activity through localization: functional genomics reveals a role for the lysine acetyltransferase NuA4 and sphingolipid metabolism in regulating Acc1 activity and localization. *Genetics*. **221**, 1–19
19. Kamiryo, T., Parthasarathy, S., and Numa, S. (1976) Evidence that acyl coenzyme A synthetase activity is required for repression of yeast acetyl coenzyme A carboxylase by exogenous fatty acids. *Proc. Natl. Acad. Sci.* **73**, 386–390
20. Suresh, H. G., da Silveira dos Santos, A. X., Kukulski, W., Tyedmers, J., Riezman, H., Bukau, B., and Mogk, A. (2015) Prolonged starvation drives reversible sequestration of lipid biosynthetic enzymes and organelle reorganization in *Saccharomyces cerevisiae*. *Mol. Biol. Cell*. **26**, 1601–1615
21. Black, P. N., and DiRusso, C. C. (2007) Yeast acyl-CoA synthetases at the crossroads of fatty acid metabolism and regulation. *Biochim. Biophys. Acta - Mol. Cell Biol. Lipids*. **1771**, 286–298
22. Knoll, J., Levin, D. E., and Gordon, I. (1994) *Saccharomyces cerevisiae* Contains Four Fatty Acid Activation (FAA) Genes: An Assessment of Their Role in Regulating Protein N-Myristoylation and Cellular Lipid Metabolism. *J. Cell Biol.* **127**, 12
23. Currie, E., Guo, X., Christiano, R., Chitraju, C., Kory, N., Harrison, K., Haas, J., Walther, T. C., and Farese, R. V. (2014) High confidence proteomic analysis of yeast LDs identifies additional droplet proteins and reveals connections to dolichol synthesis and sterol acetylation. *J. Lipid Res.* **55**, 1465–1477
24. Hettema, E. H., van Roermund, C. W., Distel, B., van den Berg, M., Vilela, C., Rodrigues-Pousada, C., Wanders, R. J., and Tabak, H. F. (1996) The ABC transporter proteins Pat1 and Pat2 are required for import of long-chain fatty acids into peroxisomes of *Saccharomyces cerevisiae*. *EMBO J.* **15**, 3813–3822
25. Watkins, P. A., Lu, J.-F., Steinberg, S. J., Gould, S. J., Smith, K. D., and Braiterman, L. T. (1998) Disruption of the *Saccharomyces cerevisiae* FAT1 Gene Decreases Very Long-chain Fatty Acyl-CoA Synthetase Activity and Elevates Intracellular Very Long-chain Fatty Acid Concentrations. *J. Biol. Chem.* **273**, 18210–18219

26. van Roermund, C. W. T., IJlst, L., Majczak, W., Waterham, H. R., Folkerts, H., Wanders, R. J. A., and Hellingwerf, K. J. (2012) Peroxisomal Fatty Acid Uptake Mechanism in *Saccharomyces cerevisiae*. *J. Biol. Chem.* **287**, 20144–20153
27. Færgeman, N. J., Black, P. N., Zhao, X. D., Knudsen, J., and DiRusso, C. C. (2001) The Acyl-CoA Synthetases Encoded within FAA1 and FAA4 in *Saccharomyces cerevisiae* Function as Components of the Fatty Acid Transport System Linking Import, Activation, and Intracellular Utilization. *J. Biol. Chem.* **276**, 37051–37059
28. Tamura, Y., Yoshida, Y., Sato, R., and Kumaoka, H. (1976) Fatty acid desaturase system of yeast microsomes. *Arch. Biochem. Biophys.* **175**, 284–294
29. Stukey, J. E., McDonough, V. M., and Martin, C. E. (1989) Isolation and characterization of OLE1, a gene affecting fatty acid desaturation from *Saccharomyces cerevisiae*. *J. Biol. Chem.* **264**, 16537–16544
30. Lou, Y., and Shanklin, J. (2010) Evidence That the Yeast Desaturase Ole1p Exists as a Dimer *in vivo*. *J. Biol. Chem.* **285**, 19384–19390
31. Aloi, E., Guzzi, R., and Bartucci, R. (2019) Unsaturated lipid bilayers at cryogenic temperature: librational dynamics of chain-labeled lipids from pulsed and CW-EPR. *Phys. Chem. Chem. Phys.* **21**, 18699–18705
32. Martinez-Seara, H., Róg, T., Pasenkiewicz-Gierula, M., Vattulainen, I., Karttunen, M., and Reigada, R. (2007) Effect of Double Bond Position on Lipid Bilayer Properties: Insight through Atomistic Simulations. *J. Phys. Chem. B*. **111**, 11162–11168
33. Mykhaylyk, O. O., and Martin, C. M. (2009) Effect of unsaturated acyl chains on structural transformations in triacylglycerols. *Eur. J. Lipid Sci. Technol.* **111**, 227–235
34. Martinez-Seara, H., Róg, T., Karttunen, M., Vattulainen, I., and Reigada, R. (2009) Why is the *sn* -2 Chain of Monounsaturated Glycerophospholipids Usually Unsaturated whereas the *sn* -1 Chain Is Saturated? Studies of 1-Stearoyl-2-oleoyl- *sn* -glycero-3-phosphatidylcholine (SOPC) and 1-Oleoyl-2-stearoyl- *sn* -glycero-3-phosphatidylcholine (OSPC) Membranes with and without Cholesterol. *J. Phys. Chem. B*. **113**, 8347–8356
35. Toke, D. A., and Martin, C. E. (1996) Isolation and Characterization of a Gene Affecting Fatty Acid Elongation in *Saccharomyces cerevisiae*. *J. Biol. Chem.* **271**, 18413–18422
36. Schneiter, R., Tatzer, V., Gogg, G., Leitner, E., and Kohlwein, S. D. (2000) Elo1p-Dependent Carboxy-Terminal Elongation of C14:1Δ9 to C16:1Δ11 Fatty Acids in *Saccharomyces cerevisiae*. *J. Bacteriol.* **182**, 3655–3660
37. Oh, C.-S., Toke, D. A., Mandala, S., and Martin, C. E. (1997) ELO2 and ELO3, Homologues of the *Saccharomyces cerevisiae* ELO1 Gene, Function in Fatty Acid Elongation and Are Required for Sphingolipid Formation. *J. Biol. Chem.* **272**, 17376–17384
38. Martin, C. E., Oh, C.-S., and Jiang, Y. (2007) Regulation of long chain unsaturated fatty acid synthesis in yeast. *Biochim. Biophys. Acta - Mol. Cell Biol. Lipids*. **1771**, 271–285

39. Casanovas, A., Sprenger, R. R., Tarasov, K., Ruckerbauer, D. E., Hannibal-Bach, H. K., Zanghellini, J., Jensen, O. N., and Ejsing, C. S. (2015) Quantitative Analysis of Proteome and Lipidome Dynamics Reveals Functional Regulation of Global Lipid Metabolism. *Chem. Biol.* **22**, 412–425
40. Wei, Y., Siewers, V., and Nielsen, J. (2017) Cocoa butter-like lipid production ability of non-oleaginous and oleaginous yeasts under nitrogen-limited culture conditions. *Appl. Microbiol. Biotechnol.* **101**, 3577–3585
41. Tuller, G., Nemec, T., Hrastnik, C., and Daum, G. (1999) Lipid composition of subcellular membranes of an FY1679-derived haploid yeast wild-type strain grown on different carbon sources. *Yeast*. **15**, 1555–1564
42. DeRisi, J. L., Iyer, V. R., and Brown, P. O. (1997) Exploring the Metabolic and Genetic Control of Gene Expression on a Genomic Scale. *Science*. **278**, 680–686
43. Zhang, S., Skalsky, Y., and Garfinkel, D. J. (1999) MGA2 or SPT23 Is Required for Transcription of the Δ9 Fatty Acid Desaturase Gene, OLE1, and Nuclear Membrane Integrity in *Saccharomyces cerevisiae*. *Genetics*. **151**, 473–483
44. Surma, M. A., Klose, C., Peng, D., Shales, M., Mrejen, C., Stefanko, A., Braberg, H., Gordon, D. E., Vorkel, D., Ejsing, C. S., Farese, R., Simons, K., Krogan, N. J., and Ernst, R. (2013) A Lipid E-MAP Identifies Ubx2 as a Critical Regulator of Lipid Saturation and Lipid Bilayer Stress. *Mol. Cell*. **51**, 519–530
45. Athenstaedt, K., and Daum, G. (1997) Biosynthesis of phosphatidic acid in lipid particles and endoplasmic reticulum of *Saccharomyces cerevisiae*. *J. Bacteriol.* **179**, 7611–7616
46. Han, G.-S., Wu, W.-I., and Carman, G. M. (2006) The *Saccharomyces cerevisiae* Lipin Homolog Is a Mg2+-dependent Phosphatidate Phosphatase Enzyme*. *J. Biol. Chem.* **281**, 9210–9218
47. Nikawa, J., Kodaki, T., and Yamashita, S. (1987) Primary structure and disruption of the phosphatidylinositol synthase gene of *Saccharomyces cerevisiae*. *J. Biol. Chem.* **262**, 4876–4881
48. Letts, V. A., Klig, L. S., Bae-Lee, M., Carman, G. M., and Henry, S. A. (1983) Isolation of the yeast structural gene for the membrane-associated enzyme phosphatidylserine synthase. *Proc. Natl. Acad. Sci.* **80**, 7279–7283
49. Clancey, C. J., Chang, S. C., and Dowhan, W. (1993) Cloning of a gene (PSD1) encoding phosphatidylserine decarboxylase from *Saccharomyces cerevisiae* by complementation of an Escherichia coli mutant. *J. Biol. Chem.* **268**, 24580–24590
50. Trotter, P. J., and Voelker, D. R. (1995) Identification of a Non-mitochondrial Phosphatidylserine Decarboxylase Activity (PSD2) in the Yeast *Saccharomyces cerevisiae*. *J. Biol. Chem.* **270**, 6062–6070
51. Kodaki, T., and Yamashita, S. (1987) Yeast phosphatidylethanolamine methylation pathway. Cloning and characterization of two distinct methyltransferase genes. *J. Biol. Chem.* **262**, 15428–15435

52. Morash, S. C., McMaster, C. R., Hjelmstad, R. H., and Bell, R. M. (1994) Studies employing *Saccharomyces cerevisiae* cpt1 and ept1 null mutants implicate the CPT1 gene in coordinate regulation of phospholipid biosynthesis. *J. Biol. Chem.* **269**, 28769–28776
53. Kim, K., Kim, K.-H., Storey, M. K., Voelker, D. R., and Carman, G. M. (1999) Isolation and Characterization of the *Saccharomyces cerevisiae* EKI1 Gene Encoding Ethanolamine Kinase. *J. Biol. Chem.* **274**, 14857–14866
54. Henry, S. A., Kohlwein, S. D., and Carman, G. M. (2012) Metabolism and Regulation of Glycerolipids in the Yeast *Saccharomyces cerevisiae*. *Genetics*. **190**, 317–349
55. Oelkers, P., Tinkelenberg, A., Erdeniz, N., Cromley, D., Billheimer, J. T., and Sturley, S. L. (2000) A Lecithin Cholesterol Acyltransferase-like Gene Mediates Diacylglycerol Esterification in Yeast. *J. Biol. Chem.* **275**, 15609–15612
56. Oelkers, P., Cromley, D., Padamsee, M., Billheimer, J. T., and Sturley, S. L. (2002) The DGA1 Gene Determines a Second Triglyceride Synthetic Pathway in Yeast. *J. Biol. Chem.* **277**, 8877–8881
57. Tauchi-Sato, K., Ozeki, S., Houjou, T., Taguchi, R., and Fujimoto, T. (2002) The Surface of Lipid Droplets Is a Phospholipid Monolayer with a Unique Fatty Acid Composition. *J. Biol. Chem.* **277**, 44507–44512
58. Jacquier, N., Choudhary, V., Mari, M., Toulmay, A., Reggiori, F., and Schneiter, R. (2011) Lipid droplets are functionally connected to the endoplasmic reticulum in *Saccharomyces cerevisiae*. *J. Cell Sci.* **124**, 2424–2437
59. Choudhary, V., Ojha, N., Golden, A., and Prinz, W. A. (2015) A conserved family of proteins facilitates nascent lipid droplet budding from the ER. *J. Cell Biol.* **211**, 261–271
60. Wilfling, F., Wang, H., Haas, J. T., Krahmer, N., Gould, T. J., Uchida, A., Cheng, J.-X., Graham, M., Christiano, R., Fröhlich, F., Liu, X., Buhman, K. K., Coleman, R. A., Bewersdorf, J., Farese, R. V., and Walther, T. C. (2013) Triacylglycerol Synthesis Enzymes Mediate Lipid Droplet Growth by Relocalizing from the ER to Lipid Droplets. *Dev. Cell*. **24**, 384–399
61. Yu, C., Kennedy, N. J., Chang, C. C. Y., and Rothblatt, J. A. (1996) Molecular Cloning and Characterization of Two Isoforms of *Saccharomyces cerevisiae* Acyl-CoA:Sterol Acyltransferase. *J. Biol. Chem.* **271**, 24157–24163
62. Bratschi, M. W., Burrowes, D. P., Kulaga, A., Cheung, J. F., Alvarez, A. L., Kearley, J., and Zaremberg, V. (2009) Glycerol-3-Phosphate Acyltransferases Gat1p and Gat2p Are Microsomal Phosphoproteins with Differential Contributions to Polarized Cell Growth. *Eukaryot. Cell*. **8**, 1184–1196
63. Zaremberg, V., and McMaster, C. R. (2002) Differential Partitioning of Lipids Metabolized by Separate Yeast Glycerol-3-phosphate Acyltransferases Reveals That Phospholipase D Generation of Phosphatidic Acid Mediates Sensitivity to Choline-containing Lysolipids and Drugs. *J. Biol. Chem.* **277**, 39035–39044

64. Debelyy, M. O., Waridel, P., Quadroni, M., Schneiter, R., and Conzelmann, A. (2017) Chemical crosslinking and mass spectrometry to elucidate the topology of integral membrane proteins. *PLOS ONE*. **12**, e0186840
65. Pagac, M., Vazquez, H. M., Bochud, A., Roubaty, C., Knöpfli, C., Vionnet, C., and Conzelmann, A. (2012) Topology of the microsomal glycerol-3-phosphate acyltransferase Gpt2p/Gat1p of *Saccharomyces cerevisiae*: Topology of GPATs in yeast. *Mol. Microbiol.* **86**, 1156–1166
66. Athenstaedt, K., Weys, S., Paltauf, F., and Daum, G. (1999) Redundant Systems of Phosphatidic Acid Biosynthesis via Acylation of Glycerol-3-Phosphate or Dihydroxyacetone Phosphate in the Yeast *Saccharomyces cerevisiae*. *J. Bacteriol.* **181**, 1458–1463
67. Wang, X., Li, S., Wang, H., Shui, W., and Hu, J. (2017) Quantitative proteomics reveal proteins enriched in tubular endoplasmic reticulum of *Saccharomyces cerevisiae*. *eLife*. **6**, e23816
68. Marr, N., Foglia, J., Terebiznik, M., Athenstaedt, K., and Zaremberg, V. (2012) Controlling Lipid Fluxes at Glycerol-3-phosphate Acyltransferase Step in Yeast. *J. Biol. Chem.* **287**, 10251–10264
69. De Smet, C. H., Vittone, E., Scherer, M., Houweling, M., Liebisch, G., Brouwers, J. F., and de Kroon, A. I. P. M. (2012) The yeast acyltransferase Sct1p regulates fatty acid desaturation by competing with the desaturase Ole1p. *Mol. Biol. Cell*. **23**, 1146–1156
70. Kiegerl, B., Tavassoli, M., Smart, H., Shabits, B. N., Zaremberg, V., and Athenstaedt, K. (2019) Phosphorylation of the lipid droplet localized glycerol-3-phosphate acyltransferase Gpt2 prevents a futile triacylglycerol cycle in yeast. *Biochim. Biophys. Acta BBA - Mol. Cell Biol. Lipids*. **1864**, 158509
71. Benghezal, M., Roubaty, C., Veepuri, V., Knudsen, J., and Conzelmann, A. (2007) SLC1 and SLC4 Encode Partially Redundant Acyl-Coenzyme A 1-Acylglycerol-3-phosphate O-Acyltransferases of Budding Yeast. *J. Biol. Chem.* **282**, 30845–30855
72. Chen, Q., Kazachkov, M., Zheng, Z., and Zou, J. (2007) The yeast acylglycerol acyltransferase LCA1 is a key component of Lands cycle for phosphatidylcholine turnover. *FEBS Lett.* **581**, 5511–5516
73. Jain, S., Stanford, N., Bhagwat, N., Seiler, B., Costanzo, M., Boone, C., and Oelkers, P. (2007) Identification of a Novel Lysophospholipid Acyltransferase in *Saccharomyces cerevisiae*. *J. Biol. Chem.* **282**, 30562–30569
74. Tamaki, H., Shimada, A., Ito, Y., Ohya, M., Takase, J., Miyashita, M., Miyagawa, H., Nozaki, H., Nakayama, R., and Kumagai, H. (2007) LPT1 Encodes a Membrane-bound O-Acyltransferase Involved in the Acylation of Lysophospholipids in the Yeast *Saccharomyces cerevisiae*. *J. Biol. Chem.* **282**, 34288–34298
75. Pagac, M., de la Mora, H. V., Duperrex, C., Roubaty, C., Vionnet, C., and Conzelmann, A. (2011) Topology of 1-Acyl-sn-glycerol-3-phosphate Acyltransferases SLC1 and ALE1 and Related Membrane-bound O-Acyltransferases (MBOATs) of *Saccharomyces cerevisiae*. *J. Biol. Chem.* **286**, 36438–36447

76. Robertson, R. M., Yao, J., Gajewski, S., Kumar, G., Martin, E. W., Rock, C. O., and White, S. W. (2017) A two-helix motif positions the lysophosphatidic acid acyltransferase active site for catalysis within the membrane bilayer. *Nat. Struct. Mol. Biol.* **24**, 666–671
77. Blobel, G. (1980) Intracellular protein topogenesis. *Proc. Natl. Acad. Sci.* **77**, 1496–1500
78. Yamashita, A., Nakanishi, H., Suzuki, H., Kamata, R., Tanaka, K., Waku, K., and Sugiura, T. (2007) Topology of acyltransferase motifs and substrate specificity and accessibility in 1-acyl-sn-glycero-3-phosphate acyltransferase 1. *Biochim. Biophys. Acta BBA - Mol. Cell Biol. Lipids*. **1771**, 1202–1215
79. Oelkers, P., and Pokhrel, K. (2016) Four Acyltransferases Uniquely Contribute to Phospholipid Heterogeneity in *Saccharomyces cerevisiae*. *Lipid Insights*. 10.4137/LPI.S40597
80. Shui, G., Guan, X. L., Gopalakrishnan, P., Xue, Y., Goh, J. S. Y., Yang, H., and Wenk, M. R. (2010) Characterization of Substrate Preference for Slc1p and Cst26p in *Saccharomyces cerevisiae* Using Lipidomic Approaches and an LPAAT Activity Assay. *PLoS ONE*. **5**, e11956
81. Patton-Vogt, J., and de Kroon, A. I. P. M. (2020) Phospholipid turnover and acyl chain remodeling in the yeast ER. *Biochim. Biophys. Acta BBA - Mol. Cell Biol. Lipids*. **1865**, 158462
82. Shen, H., Heacock, P. N., Clancey, C. J., and Dowhan, W. (1996) The CDS1 Gene Encoding CDP-diacylglycerol Synthase In *Saccharomyces cerevisiae* Is Essential for Cell Growth. *J. Biol. Chem.* **271**, 789–795
83. Tamura, Y., Harada, Y., Nishikawa, S., Yamano, K., Kamiya, M., Shiota, T., Kuroda, T., Kuge, O., Sesaki, H., Imai, K., Tomii, K., and Endo, T. (2013) Tam41 Is a CDP-Diacylglycerol Synthase Required for Cardiolipin Biosynthesis in Mitochondria. *Cell Metab.* **17**, 709–718
84. Romanauska, A., and Köhler, A. (2018) The Inner Nuclear Membrane Is a Metabolically Active Territory that Generates Nuclear Lipid Droplets. *Cell*. **174**, 700-715.e18
85. Bochud, A., and Conzelmann, A. (2015) The active site of yeast phosphatidylinositol synthase Pis1 is facing the cytosol. *Biochim. Biophys. Acta BBA - Mol. Cell Biol. Lipids*. **1851**, 629–640
86. Fei, W., Wang, H., Fu, X., Bielby, C., and Yang, H. (2009) Conditions of endoplasmic reticulum stress stimulate lipid droplet formation in *Saccharomyces cerevisiae*. *Biochem. J.* **424**, 61–67
87. Huh, W.-K., Falvo, J. V., Gerke, L. C., Carroll, A. S., Howson, R. W., Weissman, J. S., and O'Shea, E. K. (2003) Global analysis of protein localization in budding yeast. *Nature*. **425**, 686–691
88. Leber, A., Hrastnik, C., and Daum, G. (1995) Phospholipid-synthesizing enzymes in Golgi membranes of the yeast, *Saccharomyces cerevisiae*. *FEBS Lett.* **377**, 271–274
89. Atkinson, K., Fogel, S., and Henry, S. A. (1980) Yeast mutant defective in phosphatidylserine synthesis. *J. Biol. Chem.* **255**, 6653–6661
90. Hamamatsu, S., Shibuya, I., Takagi, M., and Ohta, A. (1994) Loss of phosphatidylserine synthesis results in aberrant solute sequestration and vacuolar morphology in *Saccharomyces cerevisiae*. *FEBS Lett.* **348**, 33–36

91. Achleitner, G., Gaigg, B., Krasser, A., Kainersdorfer, E., Kohlwein, S. D., Perktold, A., Zellnig, G., and Daum, G. (1999) Association between the endoplasmic reticulum and mitochondria of yeast facilitates interorganelle transport of phospholipids through membrane contact. *Eur. J. Biochem.* **264**, 545–553
92. Gaigg, B., Simbeni, R., Hrastnik, C., Paltauf, F., and Daum, G. (1995) Characterization of a microsomal subfraction associated with mitochondria of the yeast, *Saccharomyces cerevisiae*. Involvement in synthesis and import of phospholipids into mitochondria. *Biochim. Biophys. Acta BBA - Biomembr.* **1234**, 214–220
93. Zinser, E., Sperka-Gottlieb, C. D., Fasch, E. V., Kohlwein, S. D., Paltauf, F., and Daum, G. (1991) Phospholipid synthesis and lipid composition of subcellular membranes in the unicellular eukaryote *Saccharomyces cerevisiae*. *J. Bacteriol.* **173**, 2026–2034
94. Horvath, S. E., Wagner, A., Steyrer, E., and Daum, G. (2011) Metabolic link between phosphatidylethanolamine and triacylglycerol metabolism in the yeast *Saccharomyces cerevisiae*. *Biochim. Biophys. Acta BBA - Mol. Cell Biol. Lipids*. **1811**, 1030–1037
95. Bürgermeister, M., Birner-Grünberger, R., Nebauer, R., and Daum, G. (2004) Contribution of different pathways to the supply of phosphatidylethanolamine and phosphatidylcholine to mitochondrial membranes of the yeast *Saccharomyces cerevisiae*. *Biochim. Biophys. Acta BBA - Mol. Cell Biol. Lipids*. **1686**, 161–168
96. Renne, M. F., Bao, X., Hokken, M. W., Bierhuizen, A. S., Hermansson, M., Sprenger, R. R., Ewing, T. A., Ma, X., Cox, R. C., Brouwers, J. F., Smet, C. H. D., Ejsing, C. S., and Kroon, A. I. de (2022) Molecular species selectivity of lipid transport creates a mitochondrial sink for di-unsaturated phospholipids. *EMBO J.* **41**, e106837
97. Horvath, S. E., Böttinger, L., Vögtle, F.-N., Wiedemann, N., Meisinger, C., Becker, T., and Daum, G. (2012) Processing and Topology of the Yeast Mitochondrial Phosphatidylserine Decarboxylase 1. *J. Biol. Chem.* **287**, 36744–36755
98. Onguka, O., Calzada, E., Ogunbona, O. B., and Claypool, S. M. (2015) Phosphatidylserine Decarboxylase 1 Autocatalysis and Function Does Not Require a Mitochondrial-specific Factor. *J. Biol. Chem.* **290**, 12744–12752
99. Friedman, J. R., Kannan, M., Toulmay, A., Jan, C. H., Weissman, J. S., Prinz, W. A., and Nunnari, J. (2018) Lipid Homeostasis Is Maintained by Dual Targeting of the Mitochondrial PE Biosynthesis Enzyme to the ER. *Dev. Cell*. **44**, 261-270.e6
100. Sam, P. N., Calzada, E., Acoba, M. G., Zhao, T., Watanabe, Y., Nejatfard, A., Trinidad, J. C., Shutt, T. E., Neal, S. E., and Claypool, S. M. (2021) Impaired phosphatidylethanolamine metabolism activates a reversible stress response that detects and resolves mutant mitochondrial precursors. *iScience*. **24**, 102196

101. Gok, M. O., Speer, N. O., Henne, W. M., and Friedman, J. R. (2022) ER-localized phosphatidylethanolamine synthase plays a conserved role in lipid droplet formation. *Mol. Biol. Cell*. **33**, ar11
102. Wu, W.-I., and Voelker, D. R. (2001) Characterization of Phosphatidylserine Transport to the Locus of Phosphatidylserine Decarboxylase 2 in Permeabilized Yeast. *J. Biol. Chem.* **276**, 7114–7121
103. Kitamura, H., Wu, W.-I., and Voelker, D. R. (2002) The C2 Domain of Phosphatidylserine Decarboxylase 2 Is Not Required for Catalysis but Is Essential for *in vivo*Function. *J. Biol. Chem.* **277**, 33720–33726
104. Day, K. J., Casler, J. C., and Glick, B. S. (2018) Budding Yeast Has a Minimal Endomembrane System. *Dev. Cell*. **44**, 56-72.e4
105. Iadarola, D. M., Joshi, A., Caldwell, C. B., and Gohil, V. M. (2021) Choline restores respiration in Psd1-deficient yeast by replenishing mitochondrial phosphatidylethanolamine. *J. Biol. Chem.* **296**, 100539
106. Riekhof, W. R., Wu, W.-I., Jones, J. L., Nikrad, M., Chan, M. M., Loewen, C. J. R., and Voelker, D. R. (2014) An Assembly of Proteins and Lipid Domains Regulates Transport of Phosphatidylserine to Phosphatidylserine Decarboxylase 2 in *Saccharomyces cerevisiae*. *J. Biol. Chem.* **289**, 5809–5819
107. Kuroda, T., Tani, M., Moriguchi, A., Tokunaga, S., Higuchi, T., Kitada, S., and Kuge, O. (2011) FMP30 is required for the maintenance of a normal cardiolipin level and mitochondrial morphology in the absence of mitochondrial phosphatidylethanolamine synthesis: Role of FMP30 in mitochondria. *Mol. Microbiol.* **80**, 248–265
108. Boumann, H. A., Chin, P. T. K., Heck, A. J. R., de Kruijff, B., and de Kroon, A. I. P. M. (2004) The Yeast Phospholipid N-Methyltransferases Catalyzing the Synthesis of Phosphatidylcholine Preferentially Convert Di-C16:1 Substrates Both *in vivo* and *in vitro*. *J. Biol. Chem.* **279**, 40314–40319
109. Karanasios, E., Barbosa, A. D., Sembongi, H., Mari, M., Han, G.-S., Reggiori, F., Carman, G. M., and Siniossoglou, S. (2013) Regulation of lipid droplet and membrane biogenesis by the acidic tail of the phosphatidate phosphatase Pah1p. *Mol. Biol. Cell*. **24**, 2124–2133
110. Karanasios, E., Han, G.-S., Xu, Z., Carman, G. M., and Siniossoglou, S. (2010) A phosphorylation-regulated amphipathic helix controls the membrane translocation and function of the yeast phosphatidate phosphatase. *Proc. Natl. Acad. Sci.* **107**, 17539–17544
111. Choi, H.-S., Su, W.-M., Han, G.-S., Plote, D., Xu, Z., and Carman, G. M. (2012) Pho85p-Pho80p Phosphorylation of Yeast Pah1p Phosphatidate Phosphatase Regulates Its Activity, Location, Abundance, and Function in Lipid Metabolism♦. *J. Biol. Chem.* **287**, 11290–11301

112. Choudhary, V., El Atab, O., Mizzon, G., Prinz, W. A., and Schneiter, R. (2020) Seipin and Nem1 establish discrete ER subdomains to initiate yeast lipid droplet biogenesis. *J. Cell Biol.* **219**, e201910177
113. Choudhary, V., Jacquier, N., and Schneiter, R. (2011) The topology of the triacylglycerol synthesizing enzyme Lro1 indicates that neutral lipids can be produced within the luminal compartment of the endoplasmatic reticulum: Implications for the biogenesis of lipid droplets. *Commun. Integr. Biol.* **4**, 781–784
114. Dahlqvist, A., Ståhl, U., Lenman, M., Banas, A., Lee, M., Sandager, L., Ronne, H., and Stymne, S. (2000) Phospholipid:diacylglycerol acyltransferase: An enzyme that catalyzes the acyl-CoA-independent formation of triacylglycerol in yeast and plants. *Proc. Natl. Acad. Sci.* **97**, 6487–6492
115. Sandager, L., Gustavsson, M. H., Ståhl, U., Dahlqvist, A., Wiberg, E., Banas, A., Lenman, M., Ronne, H., and Stymne, S. (2002) Storage Lipid Synthesis Is Non-essential in Yeast. *J. Biol. Chem.* **277**, 6478–6482
116. Barbosa, A. D., Lim, K., Mari, M., Edgar, J. R., Gal, L., Sterk, P., Jenkins, B. J., Koulman, A., Savage, D. B., Schuldiner, M., Reggiori, F., Wigge, P. A., and Siniossoglou, S. (2019) Compartmentalized Synthesis of Triacylglycerol at the Inner Nuclear Membrane Regulates Nuclear Organization. *Dev. Cell*. **50**, 755-766.e6
117. Schneiter, R., and Choudhary, V. (2022) Seipin collaborates with the ER membrane to control the sites of lipid droplet formation. *Curr. Opin. Cell Biol.* **75**, 102070
118. Wurie, H. R., Buckett, L., and Zammit, V. A. (2012) Diacylglycerol acyltransferase 2 acts upstream of diacylglycerol acyltransferase 1 and utilizes nascent diglycerides and *de novo* synthesized fatty acids in HepG2 cells: DGAT2 acts upstream of DGAT1. *FEBS J.* **279**, 3033–3047
119. Gao, Q., Binns, D. D., Kinch, L. N., Grishin, N. V., Ortiz, N., Chen, X., and Goodman, J. M. (2017) Pet10p is a yeast perilipin that stabilizes lipid droplets and promotes their assembly. *J. Cell Biol.* **216**, 3199–3217
120. Markgraf, D. F., Klemm, R. W., Junker, M., Hannibal-Bach, H. K., Ejsing, C. S., and Rapoport, T. A. (2014) An ER Protein Functionally Couples Neutral Lipid Metabolism on Lipid Droplets to Membrane Lipid Synthesis in the ER. *Cell Rep.* **6**, 44–55
121. Meyers, A., Weiskittel, T. M., and Dalhaimer, P. (2017) Lipid Droplets: Formation to Breakdown. *Lipids*. **52**, 465–475
122. McFie, P. J., Jin, Y., Banman, S. L., Beauchamp, E., Berthiaume, L. G., and Stone, S. J. (2014) Characterization of the interaction of diacylglycerol acyltransferase-2 with the endoplasmic reticulum and lipid droplets. *Biochim. Biophys. Acta BBA - Mol. Cell Biol. Lipids*. **1841**, 1318–1328
123. Xu, N., Zhang, S. O., Cole, R. A., McKinney, S. A., Guo, F., Haas, J. T., Bobba, S., Farese, R. V., and Mak, H. Y. (2012) The FATP1–DGAT2 complex facilitates lipid droplet expansion at the ER–lipid droplet interface. *J. Cell Biol.* **198**, 895–911

124. Liu, Q., Siloto, R. M. P., Snyder, C. L., and Weselake, R. J. (2011) Functional and Topological Analysis of Yeast Acyl-CoA:Diacylglycerol Acyltransferase 2, an Endoplasmic Reticulum Enzyme Essential for Triacylglycerol Biosynthesis. *J. Biol. Chem.* **286**, 13115–13126
125. Khaddaj, R., Mari, M., Cottier, S., Reggiori, F., and Schneiter, R. (2022) The surface of lipid droplets constitutes a barrier for endoplasmic reticulum-resident integral membrane proteins. *J. Cell Sci.* **135**, jcs256206
126. Stone, S. J., Levin, M. C., and Farese, R. V. (2006) Membrane Topology and Identification of Key Functional Amino Acid Residues of Murine Acyl-CoA:Diacylglycerol Acyltransferase-2. *J. Biol. Chem.* **281**, 40273–40282
127. Binder, H., and Gawrisch, K. (2001) Effect of Unsaturated Lipid Chains on Dimensions, Molecular Order and Hydration of Membranes. *J. Phys. Chem. B*. **105**, 12378–12390
128. Yang, H., Bard, M., Bruner, D. A., Gleeson, A., Deckelbaum, R. J., Aljinovic, G., Pohl, T. M., Rothstein, R., and Sturley, S. L. (1996) Sterol Esterification in Yeast: A Two-Gene Process. *Science*. **272**, 1353–1356
129. Zweytick, D., Leitner, E., Kohlwein, S. D., Yu, C., Rothblatt, J., and Daum, G. (2000) Contribution of Are1p and Are2p to steryl ester synthesis in the yeast *Saccharomyces cerevisiae*: Are1p and Are2p of the yeast *Saccharomyces cerevisiae*. *Eur. J. Biochem.* **267**, 1075–1082
130. Jensen-Pergakes, K., Guo, Z., Giattina, M., Sturley, S. L., and Bard, M. (2001) Transcriptional Regulation of the Two Sterol Esterification Genes in the Yeast *Saccharomyces cerevisiae*. *J. Bacteriol.* **183**, 4950–4957
131. Ejsing, C. S., Sampaio, J. L., Surendranath, V., Duchoslav, E., Ekroos, K., Klemm, R. W., Simons, K., and Shevchenko, A. (2009) Global analysis of the yeast lipidome by quantitative shotgun mass spectrometry. *Proc. Natl. Acad. Sci.* **106**, 2136–2141
132. Schneiter, R., Brügger, B., Sandhoff, R., Zellnig, G., Leber, A., Lampl, M., Athenstaedt, K., Hrastnik, C., Eder, S., Daum, G., Paltauf, F., Wieland, F. T., and Kohlwein, S. D. (1999) Electrospray Ionization Tandem Mass Spectrometry (ESI-MS/MS) Analysis of the Lipid Molecular Species Composition of Yeast Subcellular Membranes Reveals Acyl Chain-Based Sorting/Remodeling of Distinct Molecular Species En Route to the Plasma Membrane. *J. Cell Biol.* **146**, 741–754
133. Wagner, S., and Paltauf, F. (1994) Generation of glycerophospholipid molecular species in the yeast *Saccharomyces cerevisiae*. Fatty acid pattern of phospholipid classes and selective acyl turnover at *sn-1* and *sn-2* positions. *Yeast*. **10**, 1429–1437
134. Holub, B. J., and Kuksis, A. (1969) Molecular species of phosphatidyl ethanolamine from egg yolk. *Lipids*. **4**, 466–472
135. Boumann, H. A., Damen, M. J. A., Versluis, C., Heck, A. J. R., de Kruijff, B., and de Kroon, A. I. P. M. (2003) The Two Biosynthetic Routes Leading to Phosphatidylcholine in Yeast Produce Different Sets of Molecular Species. Evidence for Lipid Remodeling. *Biochemistry*. **42**, 3054–3059

136. De Smet, C. H., Cox, R., Brouwers, J. F., and de Kroon, A. I. P. M. (2013) Yeast cells accumulate excess endogenous palmitate in phosphatidylcholine by acyl chain remodeling involving the phospholipase B Plb1p. *Biochim. Biophys. Acta BBA - Mol. Cell Biol. Lipids*. **1831**, 1167–1176
137. Le Guédard, M., Bessoule, J.-J., Boyer, V., Ayciriex, S., Velours, G., Kulik, W., Ejsing, C. S., Shevchenko, A., Coulon, D., Lessire, R., and Testet, E. (2009) PSI1 is responsible for the stearic acid enrichment that is characteristic of phosphatidylinositol in yeast: Psi1p directs stearic acid into PI in yeast. *FEBS J.* **276**, 6412–6424
138. Řezanka, T., Kolouchová, I., Čejková, A., Cajthaml, T., and Sigler, K. (2013) Identification of regioisomers and enantiomers of triacylglycerols in different yeasts using reversed- and chiral-phase LC–MS. *J. Sep. Sci.* **36**, 3310–3320
139. Haley, J. E., and Jack, R. C. L. (1974) Stereospecific Analysis of Triacylglycerols and Major Phosphoglycerides from *Lipomyces Lipoferus*. *Lipids*. **9**, 3
140. Nuber, S., Nam, A. Y., Rajsombath, M. M., Cirka, H., Hronowski, X., Wang, J., Hodgetts, K., Kalinichenko, L. S., Müller, C. P., Lambrecht, V., Winkler, J., Weihofen, A., Imberdis, T., Dettmer, U., Fanning, S., and Selkoe, D. J. (2021) A Stearoyl–Coenzyme A Desaturase Inhibitor Prevents Multiple Parkinson Disease Phenotypes in A -Synuclein Mice. *Ann. Neurol.* **89**, 74–90
141. Zoni, V., Khaddaj, R., Campomanes, P., Thiam, A. R., Schneiter, R., and Vanni, S. (2021) Pre-existing bilayer stresses modulate triglyceride accumulation in the ER versus lipid droplets. *eLife*. **10**, e62886
142. Zimmerberg, J., and Kozlov, M. M. (2006) How proteins produce cellular membrane curvature. *Nat. Rev. Mol. Cell Biol.* **7**, 9–19
143. Israelachvili, J. N., Marčelja, S., and Horn, R. G. (1980) Physical principles of membrane organization. *Q. Rev. Biophys.* **13**, 121–200
144. Manford, A. G., Stefan, C. J., Yuan, H. L., MacGurn, J. A., and Emr, S. D. (2012) ER-to-Plasma Membrane Tethering Proteins Regulate Cell Signaling and ER Morphology. *Dev. Cell*. **23**, 1129–1140
145. Ben M'barek, K., Ajjaji, D., Chorlay, A., Vanni, S., Forêt, L., and Thiam, A. R. (2017) ER Membrane Phospholipids and Surface Tension Control Cellular Lipid Droplet Formation. *Dev. Cell*. **41**, 591-604.e7
146. Grillitsch, K., Connerth, M., Köfeler, H., Arrey, T. N., Rietschel, B., Wagner, B., Karas, M., and Daum, G. (2011) Lipid particles/droplets of the yeast *Saccharomyces cerevisiae* revisited: Lipidome meets Proteome. *Biochim. Biophys. Acta BBA - Mol. Cell Biol. Lipids*. **1811**, 1165–1176
147. Bartz, R., Li, W.-H., Venables, B., Zehmer, J. K., Roth, M. R., Welti, R., Anderson, R. G. W., Liu, P., and Chapman, K. D. (2007) Lipidomics reveals that adiposomes store ether lipids and mediate phospholipid traffic. *J. Lipid Res.* **48**, 837–847

148. Chitraju, C., Trötzmüller, M., Hartler, J., Wolinski, H., Thallinger, G. G., Lass, A., Zechner, R., Zimmermann, R., Köfeler, H. C., and Spener, F. (2012) Lipidomic analysis of lipid droplets from murine hepatocytes reveals distinct signatures for nutritional stress. *J. Lipid Res.* **53**, 2141–2152
149. Renne, M. F., and de Kroon, A. I. P. M. (2018) The role of phospholipid molecular species in determining the physical properties of yeast membranes. *FEBS Lett.* **592**, 1330–1345
150. Mollinedo, F. (2012) Lipid raft involvement in yeast cell growth and death. *Front. Oncol.* 10.3389/fonc.2012.00140
151. Raghupathy, R., Anilkumar, A. A., Polley, A., Singh, P. P., Yadav, M., Johnson, C., Suryawanshi, S., Saikam, V., Sawant, S. D., Panda, A., Guo, Z., Vishwakarma, R. A., Rao, M., and Mayor, S. (2015) Transbilayer Lipid Interactions Mediate Nanoclustering of Lipid-Anchored Proteins. *Cell*. **161**, 581–594
152. West, M., Zurek, N., Hoenger, A., and Voeltz, G. K. (2011) A 3D analysis of yeast ER structure reveals how ER domains are organized by membrane curvature. *J. Cell Biol.* **193**, 333–346
153. Quon, E., Sere, Y. Y., Chauhan, N., Johansen, J., Sullivan, D. P., Dittman, J. S., Rice, W. J., Chan, R. B., Di Paolo, G., Beh, C. T., and Menon, A. K. (2018) Endoplasmic reticulum-plasma membrane contact sites integrate sterol and phospholipid regulation. *PLOS Biol.* **16**, e2003864
154. Loewen, C. J. R., Young, B. P., Tavassoli, S., and Levine, T. P. (2007) Inheritance of cortical ER in yeast is required for normal septin organization. *J. Cell Biol.* **179**, 467–483
155. Toulmay, A., and Prinz, W. A. (2012) A conserved membrane-binding domain targets proteins to organelle contact sites. *J. Cell Sci.* **125**, 49–58
156. Loewen, C. J. R., Roy, A., and Levine, T. P. (2003) A conserved ER targeting motif in three families of lipid binding proteins and in Opi1p binds VAP. *EMBO J.* **22**, 2025–2035
157. Thomas, F. B., Omnus, D. J., Bader, J. M., Chung, G. H., Kono, N., and Stefan, C. J. (2022) Tricalbin proteins regulate plasma membrane phospholipid homeostasis. *Life Sci. Alliance*. **5**, e202201430
158. Ercan, E., Momburg, F., Engel, U., Temmerman, K., Nickel, W., and Seedorf, M. (2009) A Conserved, Lipid-Mediated Sorting Mechanism of Yeast Ist2 and Mammalian STIM Proteins to the Peripheral ER. *Traffic*. **10**, 1802–1818
159. Posor, Y., Jang, W., and Haucke, V. (2022) Phosphoinositides as membrane organizers. *Nat. Rev. Mol. Cell Biol.* **23**, 797–816
160. Tarassov, K., Messier, V., Landry, C. R., Radinovic, S., Serna Molina, M. M., Shames, I., Malitskaya, Y., Vogel, J., Bussey, H., and Michnick, S. W. (2008) An *in vivo* Map of the Yeast Protein Interactome. *Science*. **320**, 1465–1470
161. Kornmann, B., Currie, E., Collins, S. R., Schuldiner, M., Nunnari, J., Weissman, J. S., and Walter, P. (2009) An ER-Mitochondria Tethering Complex Revealed by a Synthetic Biology Screen. *Science*. **325**, 477–481

162. Kopec, K. O., Alva, V., and Lupas, A. N. (2010) Homology of SMP domains to the TULIP superfamily of lipid-binding proteins provides a structural basis for lipid exchange between ER and mitochondria. *Bioinformatics*. **26**, 1927–1931
163. Kojima, R., Endo, T., and Tamura, Y. (2016) A phospholipid transfer function of ER-mitochondria encounter structure revealed *in vitro*. *Sci. Rep.* **6**, 30777
164. Nguyen, T. T., Lewandowska, A., Choi, J.-Y., Markgraf, D. F., Junker, M., Bilgin, M., Ejsing, C. S., Voelker, D. R., Rapoport, T. A., and Shaw, J. M. (2012) Gem1 and ERMES Do Not Directly Affect Phosphatidylserine Transport from ER to Mitochondria or Mitochondrial Inheritance. *Traffic*. **13**, 880–890
165. Murley, A., Sarsam, R. D., Toulmay, A., Yamada, J., Prinz, W. A., and Nunnari, J. (2015) Ltc1 is an ER-localized sterol transporter and a component of ER–mitochondria and ER–vacuole contacts. *J. Cell Biol.* **209**, 539–548
166. Lahiri, S., Chao, J. T., Tavassoli, S., Wong, A. K. O., Choudhary, V., Young, B. P., Loewen, C. J. R., and Prinz, W. A. (2014) A Conserved Endoplasmic Reticulum Membrane Protein Complex (EMC) Facilitates Phospholipid Transfer from the ER to Mitochondria. *PLoS Biol.* **12**, e1001969
167. Park, J.-S., Thorsness, M. K., Policastro, R., McGoldrick, L. L., Hollingsworth, N. M., Thorsness, P. E., and Neiman, A. M. (2016) Yeast Vps13 promotes mitochondrial function and is localized at membrane contact sites. *Mol. Biol. Cell*. **27**, 2435–2449
168. Li, P., Lees, J. A., Lusk, C. P., and Reinisch, K. M. (2020) Cryo-EM reconstruction of a VPS13 fragment reveals a long groove to channel lipids between membranes. *J. Cell Biol.* **219**, e202001161
169. Aaltonen, M. J., Friedman, J. R., Osman, C., Salin, B., di Rago, J.-P., Nunnari, J., Langer, T., and Tatsuta, T. (2016) MICOS and phospholipid transfer by Ups2–Mdm35 organize membrane lipid synthesis in mitochondria. *J. Cell Biol.* **213**, 525–534
170. Man, W. C., Miyazaki, M., Chu, K., and Ntambi, J. (2006) Colocalization of SCD1 and DGAT2: implying preference for endogenous monounsaturated fatty acids in triglyceride synthesis. *J. Lipid Res.* **47**, 1928–1939
171. Wolinski, H., Kolb, D., Hermann, S., Koning, R. I., and Kohlwein, S. D. (2011) A role for seipin in lipid droplet dynamics and inheritance in yeast. *J. Cell Sci.* **124**, 3894–3904
172. Santos-Rosa, H., Leung, J., Grimsey, N., Peak-Chew, S., and Siniossoglou, S. (2005) The yeast lipin Smp2 couples phospholipid biosynthesis to nuclear membrane growth. *EMBO J.* **24**, 1931–1941
173. Joshi, A. S., Nebenfuehr, B., Choudhary, V., Satpute-Krishnan, P., Levine, T. P., Golden, A., and Prinz, W. A. (2018) Lipid droplet and peroxisome biogenesis occur at the same ER subdomains. *Nat. Commun.* **9**, 2940
174. Choudhary, V., and Schneiter, R. (2020) Lipid droplet biogenesis from specialized ER subdomains. *Microb. Cell*. **7**, 218–221

175. Castro, I. G., Shortill, S. P., Dziurdzik, S. K., Cadou, A., Ganesan, S., Valenti, R., David, Y., Davey, M., Mattes, C., Thomas, F. B., Avraham, R. E., Meyer, H., Fadel, A., Fenech, E. J., Ernst, R., Zaremberg, V., Levine, T. P., Stefan, C., Conibear, E., and Schuldiner, M. (2022) Systematic analysis of membrane contact sites in *Saccharomyces cerevisiae* uncovers modulators of cellular lipid distribution. *eLife*. **11**, e74602
176. Dumesnil, C., Vanharanta, L., Prasanna, X., Omrane, M., Carpentier, M., Bhapkar, A., Enkavi, G., Salo, V. T., Vattulainen, I., Ikonen, E., and Thiam, A. R. (2023) Cholesterol esters form supercooled lipid droplets whose nucleation is facilitated by triacylglycerols. *Nat. Commun.* **14**, 915
177. Akita, C., Kawaguchi, T., and Kaneko, F. (2006) Structural Study on Polymorphism of Cis-Unsaturated Triacylglycerol: Triolein. *J. Phys. Chem. B*. **110**, 4346–4353
178. Barneda, D., and Christian, M. (2017) Lipid droplet growth: regulation of a dynamic organelle. *Curr. Opin. Cell Biol.* **47**, 9–15
179. Jin, Y., McFie, P. J., Banman, S. L., Brandt, C., and Stone, S. J. (2014) Diacylglycerol Acyltransferase-2 (DGAT2) and Monoacylglycerol Acyltransferase-2 (MGAT2) Interact to Promote Triacylglycerol Synthesis. *J. Biol. Chem.* **289**, 28237–28248
180. Cottier, S., and Schneiter, R. (2022) Lipid droplets form a network interconnected by the endoplasmic reticulum through which their proteins equilibrate. *J. Cell Sci.* **135**, jcs258819
181. Chorlay, A., Monticelli, L., Veríssimo Ferreira, J., Ben M'barek, K., Ajjaji, D., Wang, S., Johnson, E., Beck, R., Omrane, M., Beller, M., Carvalho, P., and Rachid Thiam, A. (2019) Membrane Asymmetry Imposes Directionality on Lipid Droplet Emergence from the ER. *Dev. Cell*. **50**, 25-42.e7
182. Krahmer, N., Guo, Y., Wilfling, F., Hilger, M., Lingrell, S., Heger, K., Newman, H. W., Schmidt-Supprian, M., Vance, D. E., Mann, M., Farese, R. V., and Walther, T. C. (2011) Phosphatidylcholine Synthesis for Lipid Droplet Expansion Is Mediated by Localized Activation of CTP:Phosphocholine Cytidylyltransferase. *Cell Metab.* **14**, 504–515
183. Choudhary, V., Golani, G., Joshi, A. S., Cottier, S., Schneiter, R., Prinz, W. A., and Kozlov, M. M. (2018) Architecture of Lipid Droplets in Endoplasmic Reticulum Is Determined by Phospholipid Intrinsic Curvature. *Curr. Biol.* **28**, 915-926.e9
184. Hedin, S. G. (1906) Trypsin and Antitrypsin. *Biochem. J.* **1**, 474–483
185. Karimizadeh, E., Sharifi-Zarchi, A., Nikaein, H., Salehi, S., Salamatian, B., Elmi, N., Gharibdoost, F., and Mahmoudi, M. (2019) Analysis of gene expression profiles and protein-protein interaction networks in multiple tissues of systemic sclerosis. *BMC Med. Genomics*. **12**, 199
186. Islam, M. M., Wallin, R., Wynn, R. M., Conway, M., Fujii, H., Mobley, J. A., Chuang, D. T., and Hutson, S. M. (2007) A Novel Branched-chain Amino Acid Metabolon. *J. Biol. Chem.* **282**, 11893–11903
187. Seychell, B. C., and Beck, T. (2021) Molecular basis for protein–protein interactions. *Beilstein J. Org. Chem.* **17**, 1–10

188. Jones, S., and Thornton, J. M. (1996) Principles of protein-protein interactions. *Proc Natl Acad Sci USA*
189. Xu, D., Tsai, C. J., and Nussinov, R. (1998) Mechanism and evolution of protein dimerization. *Protein Sci. Publ. Protein Soc.* **7**, 533–544
190. Nooren, I. M. A. (2003) NEW EMBO MEMBER'S REVIEW: Diversity of protein-protein interactions. *EMBO J.* **22**, 3486–3492
191. Srere, P. A. (1985) The metabolon. *Trends Biochem. Sci.* **10**, 109–110
192. Srere, P. A. (1987) Complexes of sequential metabolic enzymes. *Annu. Rev. Biochem.* **56**, 89–124
193. Pareek, V., Sha, Z., He, J., Wingreen, N. S., and Benkovic, S. J. (2021) Metabolic channeling: predictions, deductions, and evidence. *Mol. Cell*. **81**, 3775–3785
194. Møller, B. L. (2010) Dynamic Metabolons. *Science*. **330**, 1328–1329
195. Zhang, Y., and Fernie, A. R. (2021) Metabolons, enzyme–enzyme assemblies that mediate substrate channeling, and their roles in plant metabolism. *Plant Commun.* **2**, 100081
196. Debnam, P. M., Shearer, G., Blackwood, L., and Kohl, D. H. (1997) Evidence for Channeling of Intermediates in the Oxidative Pentose Phosphate Pathway by Soybean and Pea Nodule Extracts, Yeast Extracts, and Purified Yeast Enzymes. *Eur. J. Biochem.* **246**, 283–290
197. Brandina, I., Graham, J., Lemaitre-Guillier, C., Entelis, N., Krasheninnikov, I., Sweetlove, L., Tarassov, I., and Martin, R. P. (2006) Enolase takes part in a macromolecular complex associated to mitochondria in yeast. *Biochim. Biophys. Acta BBA - Bioenerg.* **1757**, 1217–1228
198. Araiza-Olivera, D., Chiquete-Felix, N., Rosas-Lemus, M., Sampedro, J. G., Peña, A., Mujica, A., and Uribe-Carvajal, S. (2013) A glycolytic metabolon in *Saccharomyces cerevisiae* is stabilized by F-actin. *FEBS J.* **280**, 3887–3905
199. Sumegi, B., Sherry, A. D., Malloy, C. R., and Srere, P. A. (1993) Evidence for orientation-conserved transfer in the TCA cycle in *Saccharomyces cerevisiae*: carbon-13 NMR studies. *Biochemistry*. **32**, 12725–12729
200. Xu, Y., Caldo, K. M. P., Jayawardhane, K., Ozga, J. A., Weselake, R. J., and Chen, G. (2019) A transferase interactome that may facilitate channeling of polyunsaturated fatty acid moieties from phosphatidylcholine to triacylglycerol. *J. Biol. Chem.* **294**, 14838–14844
201. Shabits, B. N. (2017) *Proteomic analysis of yeast membranes enriched in acyltransferases Gpt2p and Sct1p provides insight into their roles and regulation*. Ph.D. thesis, University of Calgary
202. Cooper, D. E., Young, P. A., Klett, E. L., and Coleman, R. A. (2015) Physiological Consequences of Compartmentalized Acyl-CoA Metabolism. *J. Biol. Chem.* **290**, 20023–20031
203. Lee, J., and Ridgway, N. D. (2020) Substrate channeling in the glycerol-3-phosphate pathway regulates the synthesis, storage and secretion of glycerolipids. *Biochim. Biophys. Acta BBA - Mol. Cell Biol. Lipids*. **1865**, 158438

Chapter 2

1. Fahy, E., Cotter, D., Sud, M., and Subramaniam, S. (2011) Lipid classification, structures and tools. *Biochim. Biophys. Acta BBA - Mol. Cell Biol. Lipids*. **1811**, 637–647
2. van Roermund, C. W. T., IJlst, L., Majczak, W., Waterham, H. R., Folkerts, H., Wanders, R. J. A., and Hellingwerf, K. J. (2012) Peroxisomal Fatty Acid Uptake Mechanism in *Saccharomyces cerevisiae*. *J. Biol. Chem.* **287**, 20144–20153
3. Daum, G., Lees, N. D., Bard, M., and Dickson, R. (1998) Biochemistry, cell biology and molecular biology of lipids of *Saccharomyces cerevisiae*. *Yeast*. **14**, 1471–1510
4. Markgraf, D. F., Klemm, R. W., Junker, M., Hannibal-Bach, H. K., Ejsing, C. S., and Rapoport, T. A. (2014) An ER Protein Functionally Couples Neutral Lipid Metabolism on Lipid Droplets to Membrane Lipid Synthesis in the ER. *Cell Rep.* **6**, 44–55
5. Ploier, B., Korber, M., Schmidt, C., Koch, B., Leitner, E., and Daum, G. (2015) Regulatory link between steryl ester formation and hydrolysis in the yeast *Saccharomyces cerevisiae*. *Biochim. Biophys. Acta BBA - Mol. Cell Biol. Lipids*. **1851**, 977–986
6. Tehlivets, O., Scheuringer, K., and Kohlwein, S. D. (2007) Fatty acid synthesis and elongation in yeast. *Biochim. Biophys. Acta - Mol. Cell Biol. Lipids*. **1771**, 255–270
7. Trotter, P. J. (2001) The Genetics of Fatty Acid Metabolism in *Saccharomyces cerevisiae*. *Annu. Rev. Nutr.* **21**, 97–119
8. Casanovas, A., Sprenger, R. R., Tarasov, K., Ruckerbauer, D. E., Hannibal-Bach, H. K., Zanghellini, J., Jensen, O. N., and Ejsing, C. S. (2015) Quantitative Analysis of Proteome and Lipidome Dynamics Reveals Functional Regulation of Global Lipid Metabolism. *Chem. Biol.* **22**, 412–425
9. Wei, Y., Siewers, V., and Nielsen, J. (2017) Cocoa butter-like lipid production ability of non-oleaginous and oleaginous yeasts under nitrogen-limited culture conditions. *Appl. Microbiol. Biotechnol.* **101**, 3577–3585
10. Zheng, Z., and Zou, J. (2001) The Initial Step of the Glycerolipid Pathway. *J. Biol. Chem.* **276**, 41710–41716
11. Athenstaedt, K., and Daum, G. (1997) Biosynthesis of phosphatidic acid in lipid particles and endoplasmic reticulum of *Saccharomyces cerevisiae*. *J. Bacteriol.* **179**, 7611–7616
12. Ståhl, U., Stålberg, K., Stymne, S., and Ronne, H. (2008) A family of eukaryotic lysophospholipid acyltransferases with broad specificity. *FEBS Lett.* **582**, 305–309
13. Tuller, G., Nemec, T., Hrastnik, C., and Daum, G. (1999) Lipid composition of subcellular membranes of an FY1679-derived haploid yeast wild-type strain grown on different carbon sources. *Yeast*. **15**, 1555–1564
14. Henry, S. A., Kohlwein, S. D., and Carman, G. M. (2012) Metabolism and Regulation of Glycerolipids in the Yeast *Saccharomyces cerevisiae*. *Genetics*. **190**, 317–349

15. Morash, S. C., McMaster, C. R., Hjelmstad, R. H., and Bell, R. M. (1994) Studies employing *Saccharomyces cerevisiae* cpt1 and ept1 null mutants implicate the CPT1 gene in coordinate regulation of phospholipid biosynthesis. *J. Biol. Chem.* **269**, 28769–28776
16. Kim, K., Kim, K.-H., Storey, M. K., Voelker, D. R., and Carman, G. M. (1999) Isolation and Characterization of the *Saccharomyces cerevisiae* EKI1 Gene Encoding Ethanolamine Kinase. *J. Biol. Chem.* **274**, 14857–14866
17. Hu, Z., He, B., Ma, L., Sun, Y., Niu, Y., and Zeng, B. (2017) Recent Advances in Ergosterol Biosynthesis and Regulation Mechanisms in *Saccharomyces cerevisiae*. *Indian J. Microbiol.* **57**, 270–277
18. Basson, M. E., Thorsness, M., and Rine, J. (1986) *Saccharomyces cerevisiae* contains two functional genes encoding 3-hydroxy-3-methylglutaryl-coenzyme A reductase. *Proc. Natl. Acad. Sci. U. S. A.* **83**, 5563–5567
19. Bard, M., and Downing, J. F. (1981) Genetic and Biochemical Aspects of Yeast Sterol Regulation Involving 3-Hydroxy-3-methylglutaryl Coenzyme A Reductase. *Microbiology*. **125**, 415–420
20. Trocha, P. J., and Sprinson, D. B. (1976) Location and regulation of early enzymes of sterol biosynthesis in yeast. *Arch. Biochem. Biophys.* **174**, 45–51
21. Natter, K., Leitner, P., Faschinger, A., Wolinski, H., McCraith, S., and Fields, S. (2005) The Spatial Organization of Lipid Synthesis in the Yeast *Saccharomyces cerevisiae* Derived from Large Scale Green Fluorescent Protein Tagging and High Resolution Microscopy. *Mol. Cell. Proteomics*. **4**, 662–672
22. Hayakawa, H., Sobue, F., Motoyama, K., Yoshimura, T., and Hemmi, H. (2017) Identification of enzymes involved in the mevalonate pathway of Flavobacterium johnsoniae. *Biochem. Biophys. Res. Commun.* **487**, 702–708
23. Jordá, T., and Puig, S. (2020) Regulation of Ergosterol Biosynthesis in *Saccharomyces cerevisiae*. *Genes*. **11**, 795
24. Parks, L. W., and Casey, W. M. (1995) Physiological implications of sterol biosynthesis in yeast. *Annu. Rev. Microbiol.* **49**, 95–116
25. Zinser, E., Paltauf, F., and Daum, G. (1993) Sterol composition of yeast organelle membranes and subcellular distribution of enzymes involved in sterol metabolism. *J. Bacteriol.* **175**, 2853–2858
26. Schneiter, R., Brügger, B., Sandhoff, R., Zellnig, G., Leber, A., Lampl, M., Athenstaedt, K., Hrastnik, C., Eder, S., Daum, G., Paltauf, F., Wieland, F. T., and Kohlwein, S. D. (1999) Electrospray Ionization Tandem Mass Spectrometry (ESI-MS/MS) Analysis of the Lipid Molecular Species Composition of Yeast Subcellular Membranes Reveals Acyl Chain-Based Sorting/Remodeling of Distinct Molecular Species En Route to the Plasma Membrane. *J. Cell Biol.* **146**, 741–754
27. Dupont, S., Lemetais, G., Ferreira, T., Cayot, P., Gervais, P., and Beney, L. (2012) Ergosterol biosynthesis: A fungal pathway for life on land? *Evolution*. **66**, 2961–2968

28. Aguilera, F., Peinado, R. A., Millán, C., Ortega, J. M., and Mauricio, J. C. (2006) Relationship between ethanol tolerance, H+-ATPase activity and the lipid composition of the plasma membrane in different wine yeast strains. *Int. J. Food Microbiol.* **110**, 34–42
29. Inoue, T., Iefuji, H., Fujii, T., Soga, H., and Satoh, K. (2000) Cloning and Characterization of a Gene Complementing the Mutation of an Ethanol-sensitive Mutant of *Sake* Yeast. *Biosci. Biotechnol. Biochem.* **64**, 229–236
30. Oelkers, P., Cromley, D., Padamsee, M., Billheimer, J. T., and Sturley, S. L. (2002) The DGA1 Gene Determines a Second Triglyceride Synthetic Pathway in Yeast. *J. Biol. Chem.* **277**, 8877–8881
31. Zweytick, D., Leitner, E., Kohlwein, S. D., Yu, C., Rothblatt, J., and Daum, G. (2000) Contribution of Are1p and Are2p to steryl ester synthesis in the yeast *Saccharomyces cerevisiae*: Are1p and Are2p of the yeast *Saccharomyces cerevisiae*. *Eur. J. Biochem.* **267**, 1075–1082
32. Leber, R., Zinser, E., Paltauf, F., Daum, G., and Zellnig, G. (1994) Characterization of lipid particles of the yeast, *Saccharomyces cerevisiae*. *Yeast*. **10**, 1421–1428
33. Klose, C., Surma, M. A., Gerl, M. J., Meyenhofer, F., Shevchenko, A., and Simons, K. (2012) Flexibility of a Eukaryotic Lipidome – Insights from Yeast Lipidomics. *PLoS ONE*. **7**, e35063
34. Wimalarathna, R., Tsai, C.-H., and Shen, C.-H. (2011) Transcriptional control of genes involved in yeast phospholipid biosynthesis. *J. Microbiol.* **49**, 265–273
35. Loewen, C. J. R., Gaspar, M. L., Jesch, S. A., Delon, C., Ktistakis, N. T., Henry, S. A., and Levine, T. P. (2004) Phospholipid Metabolism Regulated by a Transcription Factor Sensing Phosphatidic Acid. *Science*. **304**, 1644–1647
36. Stukey, J. E., McDonough, V. M., and Martin, C. E. (1989) Isolation and characterization of OLE1, a gene affecting fatty acid desaturation from *Saccharomyces cerevisiae*. *J. Biol. Chem.* **264**, 16537–16544
37. Stukey, J. E., McDonough, V. M., and Martin, C. E. (1990) The OLE1 Gene of *Saccharomyces cerevisiae* Encodes the delta9 Fatty Acid Desaturase and Can Be Functionally Replaced by the Rat Stearoyl-CoA Desaturase Gene. *J. Biol. Chem.* **265**, 20144–20149
38. Zhang, S., Skalsky, Y., and Garfinkel, D. J. (1999) MGA2 or SPT23 Is Required for Transcription of the ⌬9 Fatty Acid Desaturase Gene, OLE1, and Nuclear Membrane Integrity in *Saccharomyces cerevisiae*. *Genetics*. **151**, 473–483
39. Hoppe, T., Matuschewski, K., Rape, M., Schlenker, S., Ulrich, H. D., and Jentsch, S. (2000) Activation of a Membrane-Bound Transcription Factor by Regulated Ubiquitin/Proteasome-Dependent Processing. *Cell*. **102**, 577–586
40. Nakagawa, Y., Sakumoto, N., Kaneko, Y., and Harashima, S. (2002) Mga2p Is a Putative Sensor for Low Temperature and Oxygen to Induce OLE1 Transcription in *Saccharomyces cerevisiae*. *Biochem. Biophys. Res. Commun.* **291**, 707–713

41. Martin, C. E., Oh, C.-S., and Jiang, Y. (2007) Regulation of long chain unsaturated fatty acid synthesis in yeast. *Biochim. Biophys. Acta - Mol. Cell Biol. Lipids*. **1771**, 271–285
42. Gonzalez, C. I., and Martin, C. E. (1996) Fatty Acid-responsive Control of mRNA Stability. *J. Biol. Chem.* **271**, 25801–25809
43. Braun, S. (2002) Role of the ubiquitin-selective CDC48UFD1/NPL4 chaperone (segregase) in ERAD of OLE1 and other substrates. *EMBO J.* **21**, 615–621
44. DeRisi, J. L., Iyer, V. R., and Brown, P. O. (1997) Exploring the Metabolic and Genetic Control of Gene Expression on a Genomic Scale. *Science*. **278**, 680–686
45. Boumann, H. A., Damen, M. J. A., Versluis, C., Heck, A. J. R., de Kruijff, B., and de Kroon, A. I. P. M. (2003) The Two Biosynthetic Routes Leading to Phosphatidylcholine in Yeast Produce Different Sets of Molecular Species. Evidence for Lipid Remodeling. *Biochemistry*. **42**, 3054–3059
46. Gietz, R. D., and Schiestl, R. H. (1991) Applications of high efficiency lithium acetate transformation of intact yeast cells using single-stranded nucleic acids as carrier. *Yeast*. **7**, 253–263
47. Thomas, B. J., and Rothstein, R. (1989) Elevated recombination rates in transcriptionally active DNA. *Cell*. **56**, 619–630
48. Gibson, D. G., Young, L., Chuang, R.-Y., Venter, J. C., Hutchison, C. A., and Smith, H. O. (2009) Enzymatic assembly of DNA molecules up to several hundred kilobases. *Nat. Methods*. **6**, 343–345
49. Pare, J. M., LaPointe, P., and Hobman, T. C. (2013) Hsp90 cochaperones p23 and FKBP4 physically interact with hAgo2 and activate RNA interference–mediated silencing in mammalian cells. *Mol. Biol. Cell*. **24**, 2303–2310
50. Mellacheruvu, D., Wright, Z., Couzens, A. L., Lambert, J.-P., St-Denis, N., Li, T., Miteva, Y. V., Hauri, S., Sardiu, M. E., Low, T. Y., Halim, V. A., Bagshaw, R. D., Hubner, N. C., al-Hakim, A., Bouchard, A., Faubert, D., Fermin, D., Dunham, W. H., Goudreault, M., Lin, Z.-Y., Badillo, B. G., Pawson, T., Durocher, D., Coulombe, B., Aebersold, R., Superti-Furga, G., Colinge, J., Heck, A. J. R., Choi, H., Gstaiger, M., Mohammed, S., Cristea, I. M., Bennett, K. L., Washburn, M. P., Raught, B., Ewing, R. M., Gingras, A.-C., and Nesvizhskii, A. I. (2013) The CRAPome: a Contaminant Repository for Affinity Purification Mass Spectrometry Data. *Nat. Methods*. **10**, 730–736
51. Robinson, M. D., Grigull, J., Mohammad, N., and Hughes, T. R. (2002) FunSpec: a web-based cluster interpreter for yeast. *BMC Bioinformatics*
52. Bindea, G., Mlecnik, B., Hackl, H., Charoentong, P., Tosolini, M., Kirilovsky, A., Fridman, W.-H., Pagès, F., Trajanoski, Z., and Galon, J. (2009) ClueGO: a Cytoscape plug-in to decipher functionally grouped gene ontology and pathway annotation networks. *Bioinformatics*. **25**, 1091–1093
53. Cherry, J. M., Hong, E. L., Amundsen, C., Balakrishnan, R., Binkley, G., Chan, E. T., Christie, K. R., Costanzo, M. C., Dwight, S. S., Engel, S. R., Fisk, D. G., Hirschman, J. E., Hitz, B. C., Karra,

K., Krieger, C. J., Miyasato, S. R., Nash, R. S., Park, J., Skrzypek, M. S., Simison, M., Weng, S., and Wong, E. D. (2012) *Saccharomyces* Genome Database: the genomics resource of budding yeast. *Nucleic Acids Res.* **40**, D700–D705

54. Oughtred, R., Chatr-aryamontri, A., Breitkreutz, B.-J., Chang, C. S., Rust, J. M., Theesfeld, C. L., Heinicke, S., Breitkreutz, A., Chen, D., Hirschman, J., Kolas, N., Livstone, M. S., Nixon, J., O'Donnell, L., Ramage, L., Winter, A., Reguly, T., Sellam, A., Stark, C., Boucher, L., Dolinski, K., and Tyers, M. (2016) BioGRID: A Resource for Studying Biological Interactions in Yeast. *Cold Spring Harb. Protoc.* **2016**, pdb.top080754
55. Tarassov, K., Messier, V., Landry, C. R., Radinovic, S., Serna Molina, M. M., Shames, I., Malitskaya, Y., Vogel, J., Bussey, H., and Michnick, S. W. (2008) An *in vivo* Map of the Yeast Protein Interactome. *Science*. **320**, 1465–1470
56. Johnsson, N., and Varshavsky, A. (1994) Split ubiquitin as a sensor of protein interactions *in vivo*. *Proc. Natl. Acad. Sci. U. S. A.* **91**, 10340–10344
57. Stagljar, I., Korostensky, C., Johnsson, N., and te Heeson, S. (1998) A genetic system based on split-ubiquitin for the analysis of interactions between membrane proteins *in vivo*. *Proc. Natl. Acad. Sci.* **95**, 5187–5192
58. Snider, J., Kittanakom, S., Curak, J., and Stagljar, I. (2010) Split-Ubiquitin Based Membrane Yeast Two-Hybrid (MYTH) System: A Powerful Tool For Identifying Protein-Protein Interactions. *J. Vis. Exp.* 10.3791/1698
59. Brodsky, J. L., and McCracken, A. A. (1999) ER protein quality control and proteasome-mediated protein degradation. *Semin. Cell Dev. Biol.* **10**, 507–513
60. Debelyy, M. O., Waridel, P., Quadroni, M., Schneiter, R., and Conzelmann, A. (2017) Chemical crosslinking and mass spectrometry to elucidate the topology of integral membrane proteins. *PLOS ONE*. **12**, e0186840
61. Bochud, A., and Conzelmann, A. (2015) The active site of yeast phosphatidylinositol synthase Pis1 is facing the cytosol. *Biochim. Biophys. Acta BBA - Mol. Cell Biol. Lipids*. **1851**, 629–640
62. Choudhary, V., Jacquier, N., and Schneiter, R. (2011) The topology of the triacylglycerol synthesizing enzyme Lro1 indicates that neutral lipids can be produced within the luminal compartment of the endoplasmatic reticulum: Implications for the biogenesis of lipid droplets. *Commun. Integr. Biol.* **4**, 781–784
63. Liu, Q., Siloto, R. M. P., Snyder, C. L., and Weselake, R. J. (2011) Functional and Topological Analysis of Yeast Acyl-CoA:Diacylglycerol Acyltransferase 2, an Endoplasmic Reticulum Enzyme Essential for Triacylglycerol Biosynthesis. *J. Biol. Chem.* **286**, 13115–13126
64. Man, W. C., Miyazaki, M., Chu, K., and Ntambi, J. M. (2006) Membrane Topology of Mouse Stearoyl-CoA Desaturase 1. *J. Biol. Chem.* **281**, 1251–1260
65. Bai, Y., McCoy, J. G., Levin, E. J., Sobrado, P., Rajashankar, K. R., Fox, B. G., and Zhou, M. (2015) X-ray structure of a mammalian stearoyl-CoA desaturase. *Nature*. **524**, 252–256

66. De Smet, C. H., Vittone, E., Scherer, M., Houweling, M., Liebisch, G., Brouwers, J. F., and de Kroon, A. I. P. M. (2012) The yeast acyltransferase Sct1p regulates fatty acid desaturation by competing with the desaturase Ole1p. *Mol. Biol. Cell*. **23**, 1146–1156
67. Shabits, B. N. (2017) *Proteomic analysis of yeast membranes enriched in acyltransferases Gpt2p and Sct1p provides insight into their roles and regulation*. Ph.D. thesis, University of Calgary
68. Haley, J. E., and Jack, R. C. L. (1974) Stereospecific Analysis of Triacylglycerols and Major Phosphoglycerides from *Lipomyces Lipoferus*. *Lipids*. **9**, 3
69. Řezanka, T., Kolouchová, I., Čejková, A., Cajthaml, T., and Sigler, K. (2013) Identification of regioisomers and enantiomers of triacylglycerols in different yeasts using reversed- and chiral-phase LC–MS. *J. Sep. Sci.* **36**, 3310–3320
70. Zoni, V., Khaddaj, R., Campomanes, P., Thiam, A. R., Schneiter, R., and Vanni, S. (2021) Pre-existing bilayer stresses modulate triglyceride accumulation in the ER versus lipid droplets. *eLife*. **10**, e62886
71. Krahmer, N., Guo, Y., Wilfling, F., Hilger, M., Lingrell, S., Heger, K., Newman, H. W., Schmidt-Supprian, M., Vance, D. E., Mann, M., Farese, R. V., and Walther, T. C. (2011) Phosphatidylcholine Synthesis for Lipid Droplet Expansion Is Mediated by Localized Activation of CTP:Phosphocholine Cytidylyltransferase. *Cell Metab.* **14**, 504–515
72. Chorlay, A., Monticelli, L., Veríssimo Ferreira, J., Ben M'barek, K., Ajjaji, D., Wang, S., Johnson, E., Beck, R., Omrane, M., Beller, M., Carvalho, P., and Rachid Thiam, A. (2019) Membrane Asymmetry Imposes Directionality on Lipid Droplet Emergence from the ER. *Dev. Cell*. **50**, 25-42.e7
73. Manford, A. G., Stefan, C. J., Yuan, H. L., MacGurn, J. A., and Emr, S. D. (2012) ER-to-Plasma Membrane Tethering Proteins Regulate Cell Signaling and ER Morphology. *Dev. Cell*. **23**, 1129–1140
74. Thomas, F. B., Omnus, D. J., Bader, J. M., Chung, G. H., Kono, N., and Stefan, C. J. (2022) Tricalbin proteins regulate plasma membrane phospholipid homeostasis. *Life Sci. Alliance*. **5**, e202201430
75. Murley, A., Sarsam, R. D., Toulmay, A., Yamada, J., Prinz, W. A., and Nunnari, J. (2015) Ltc1 is an ER-localized sterol transporter and a component of ER–mitochondria and ER–vacuole contacts. *J. Cell Biol.* **209**, 539–548
76. Man, W. C., Miyazaki, M., Chu, K., and Ntambi, J. (2006) Colocalization of SCD1 and DGAT2: implying preference for endogenous monounsaturated fatty acids in triglyceride synthesis. *J. Lipid Res.* **47**, 1928–1939
77. Achleitner, G., Gaigg, B., Krasser, A., Kainersdorfer, E., Kohlwein, S. D., Perktold, A., Zellnig, G., and Daum, G. (1999) Association between the endoplasmic reticulum and mitochondria of yeast facilitates interorganelle transport of phospholipids through membrane contact. *Eur. J. Biochem.* **264**, 545–553

78. Gaigg, B., Simbeni, R., Hrastnik, C., Paltauf, F., and Daum, G. (1995) Characterization of a microsomal subfraction associated with mitochondria of the yeast, *Saccharomyces cerevisiae*. Involvement in synthesis and import of phospholipids into mitochondria. *Biochim. Biophys. Acta BBA - Biomembr.* **1234**, 214–220
79. Cottier, S., and Schneiter, R. (2022) Lipid droplets form a network interconnected by the endoplasmic reticulum through which their proteins equilibrate. *J. Cell Sci.* **135**, jcs258819
80. Wilfling, F., Wang, H., Haas, J. T., Krahmer, N., Gould, T. J., Uchida, A., Cheng, J.-X., Graham, M., Christiano, R., Fröhlich, F., Liu, X., Buhman, K. K., Coleman, R. A., Bewersdorf, J., Farese, R. V., and Walther, T. C. (2013) Triacylglycerol Synthesis Enzymes Mediate Lipid Droplet Growth by Relocalizing from the ER to Lipid Droplets. *Dev. Cell*. **24**, 384–399

Chapter 3

1. Tehlivets, O., Scheuringer, K., and Kohlwein, S. D. (2007) Fatty acid synthesis and elongation in yeast. *Biochim. Biophys. Acta - Mol. Cell Biol. Lipids*. **1771**, 255–270
2. Wagner, S., and Paltauf, F. (1994) Generation of glycerophospholipid molecular species in the yeast *Saccharomyces cerevisiae*. Fatty acid pattern of phospholipid classes and selective acyl turnover at *sn-1* and *sn-2* positions. *Yeast*. **10**, 1429–1437
3. Stukey, J. E., McDonough, V. M., and Martin, C. E. (1990) The OLE1 Gene of *Saccharomyces cerevisiae* Encodes the delta9 Fatty Acid Desaturase and Can Be Functionally Replaced by the Rat Stearoyl-CoA Desaturase Gene. *J. Biol. Chem.* **265**, 20144–20149
4. Nagle, J. F., and Tristram-Nagle, S. (2000) Structure of lipid bilayers. *Biochim. Biophys. Acta*. **1469**, 159–195
5. Zheng, Z., and Zou, J. (2001) The Initial Step of the Glycerolipid Pathway. *J. Biol. Chem.* **276**, 41710–41716
6. Benghezal, M., Roubaty, C., Veepuri, V., Knudsen, J., and Conzelmann, A. (2007) SLC1 and SLC4 Encode Partially Redundant Acyl-Coenzyme A 1-Acylglycerol-3-phosphate O-Acyltransferases of Budding Yeast. *J. Biol. Chem.* **282**, 30845–30855
7. Riekhof, W. R., Wu, J., Jones, J. L., and Voelker, D. R. (2007) Identification and Characterization of the Major Lysophosphatidylethanolamine Acyltransferase in *Saccharomyces cerevisiae*. *J. Biol. Chem.* **282**, 28344–28352
8. Athenstaedt, K., and Daum, G. (1997) Biosynthesis of phosphatidic acid in lipid particles and endoplasmic reticulum of *Saccharomyces cerevisiae*. *J. Bacteriol.* **179**, 7611–7616
9. Jain, S., Stanford, N., Bhagwat, N., Seiler, B., Costanzo, M., Boone, C., and Oelkers, P. (2007) Identification of a Novel Lysophospholipid Acyltransferase in *Saccharomyces cerevisiae*. *J. Biol. Chem.* **282**, 30562–30569
10. Ejsing, C. S., Sampaio, J. L., Surendranath, V., Duchoslav, E., Ekroos, K., Klemm, R. W., Simons, K., and Shevchenko, A. (2009) Global analysis of the yeast lipidome by quantitative shotgun mass spectrometry. *Proc. Natl. Acad. Sci.* **106**, 2136–2141

11. Carman, G. M., and Henry, S. A. (1999) Phospholipid biosynthesis in the yeast *Saccharomyces cerevisiae* and interrelationship with other metabolic processes. *Prog. Lipid Res.* **38**, 361–399
12. Han, G.-S., Wu, W.-I., and Carman, G. M. (2006) The *Saccharomyces cerevisiae* Lipin Homolog Is a Mg2+-dependent Phosphatidate Phosphatase Enzyme*. *J. Biol. Chem.* **281**, 9210–9218
13. Oelkers, P., Cromley, D., Padamsee, M., Billheimer, J. T., and Sturley, S. L. (2002) The DGA1 Gene Determines a Second Triglyceride Synthetic Pathway in Yeast. *J. Biol. Chem.* **277**, 8877–8881
14. Dahlqvist, A., Ståhl, U., Lenman, M., Banas, A., Lee, M., Sandager, L., Ronne, H., and Stymne, S. (2000) Phospholipid:diacylglycerol acyltransferase: An enzyme that catalyzes the acyl-CoA-independent formation of triacylglycerol in yeast and plants. *Proc. Natl. Acad. Sci.* **97**, 6487–6492
15. Sorger, D., and Daum, G. (2002) Synthesis of Triacylglycerols by the Acyl-Coenzyme A:Diacyl-Glycerol Acyltransferase Dga1p in Lipid Particles of the Yeast *Saccharomyces cerevisiae*. *J. Bacteriol.* **184**, 519–524
16. Yang, H., Bard, M., Bruner, D. A., Gleeson, A., Deckelbaum, R. J., Aljinovic, G., Pohl, T. M., Rothstein, R., and Sturley, S. L. (1996) Sterol Esterification in Yeast: A Two-Gene Process. *Science*. **272**, 1353–1356
17. Srere, P. A. (1987) Complexes of sequential metabolic enzymes. *Annu. Rev. Biochem.* **56**, 89–124
18. Wheeldon, I., Minteer, S. D., Banta, S., Barton, S. C., Atanassov, P., and Sigman, M. (2016) Substrate channelling as an approach to cascade reactions. *Nat. Chem.* **8**, 299–309
19. Sweetlove, L. J., and Fernie, A. R. (2018) The role of dynamic enzyme assemblies and substrate channelling in metabolic regulation. *Nat. Commun.* **9**, 2136
20. Shuib, S., Ibrahim, I., Mackeen, M. M., Ratledge, C., and Hamid, A. A. (2018) First evidence for a multienzyme complex of lipid biosynthesis pathway enzymes in Cunninghamella bainieri. *Sci. Rep.* **8**, 3077
21. Gangar, A., Karande, A. A., and Rajasekharan, R. (2001) Isolation and Localization of a Cytosolic 10 S Triacylglycerol Biosynthetic Multienzyme Complex from Oleaginous Yeast. *J. Biol. Chem.* **276**, 10290–10298
22. Xu, Y., Caldo, K. M. P., Jayawardhane, K., Ozga, J. A., Weselake, R. J., and Chen, G. (2019) A transferase interactome that may facilitate channeling of polyunsaturated fatty acid moieties from phosphatidylcholine to triacylglycerol. *J. Biol. Chem.* **294**, 14838–14844
23. Regmi, A., Shockey, J., Kotapati, H. K., and Bates, P. D. (2020) Oil-Producing Metabolons Containing DGAT1 Use Separate Substrate Pools from those Containing DGAT2 or PDAT1[OPEN]. *Plant Physiol.* **184**, 720–737
24. Shockey, J., Regmi, A., Cotton, K., Adhikari, N., Browse, J., and Bates, P. D. (2016) Identification of Arabidopsis GPAT9 (At5g60620) as an Essential Gene Involved in Triacylglycerol Biosynthesis1[OPEN]. *Plant Physiol.* **170**, 163–179

25. Jin, Y., McFie, P. J., Banman, S. L., Brandt, C., and Stone, S. J. (2014) Diacylglycerol Acyltransferase-2 (DGAT2) and Monoacylglycerol Acyltransferase-2 (MGAT2) Interact to Promote Triacylglycerol Synthesis. *J. Biol. Chem.* **289**, 28237–28248
26. Renne, M. F., and de Kroon, A. I. P. M. (2018) The role of phospholipid molecular species in determining the physical properties of yeast membranes. *FEBS Lett.* **592**, 1330–1345
27. Czabany, T., Wagner, A., Zweytick, D., Lohner, K., Leitner, E., Ingolic, E., and Daum, G. (2008) Structural and Biochemical Properties of Lipid Particles from the Yeast *Saccharomyces cerevisiae*. *J. Biol. Chem.* **283**, 17065–17074
28. Ntambi, J. M., Miyazaki, M., Stoehr, J. P., Lan, H., Kendziorski, C. M., Yandell, B. S., Song, Y., Cohen, P., Friedman, J. M., and Attie, A. D. (2002) Loss of stearoyl–CoA desaturase-1 function protects mice against adiposity. *Proc. Natl. Acad. Sci. U. S. A.* **99**, 11482–11486
29. Shi, X., Li, J., Zou, X., Greggain, J., Rødkær, S. V., Færgeman, N. J., Liang, B., and Watts, J. L. (2013) Regulation of lipid droplet size and phospholipid composition by stearoyl-CoA desaturase. *J. Lipid Res.* **54**, 2504–2514
30. Lou, Y., Schwender, J., and Shanklin, J. (2014) FAD2 and FAD3 Desaturases Form Heterodimers That Facilitate Metabolic Channeling *in vivo*. *J. Biol. Chem.* **289**, 17996–18007
31. Man, W. C., Miyazaki, M., Chu, K., and Ntambi, J. (2006) Colocalization of SCD1 and DGAT2: implying preference for endogenous monounsaturated fatty acids in triglyceride synthesis. *J. Lipid Res.* **47**, 1928–1939
32. Murphy, D. J., Mukherjee, K. D., and Woodrow, I. E. (1984) Functional association of a monoacylglycerophosphocholine acyltransferase and the oleoylglycerophosphocholine desaturase in microsomes from developing leaves. *Eur. J. Biochem.* **139**, 373–379
33. Bai, Y., McCoy, J. G., Levin, E. J., Sobrado, P., Rajashankar, K. R., Fox, B. G., and Zhou, M. (2015) X-ray structure of a mammalian stearoyl-CoA desaturase. *Nature*. **524**, 252–256
34. Wang, L., Qian, H., Nian, Y., Han, Y., Ren, Z., Zhang, H., Hu, L., Prasad, B. V. V., Laganowsky, A., Yan, N., and Zhou, M. (2020) Structure and mechanism of human diacylglycerol O-acyltransferase-1. *Nature*. **581**, 329–332
35. McFie, P. J., Banman, S. L., Kary, S., and Stone, S. J. (2011) Murine Diacylglycerol Acyltransferase-2 (DGAT2) Can Catalyze Triacylglycerol Synthesis and Promote Lipid Droplet Formation Independent of Its Localization to the Endoplasmic Reticulum. *J. Biol. Chem.* **286**, 28235–28246
36. McFie, P. J., Banman, S. L., and Stone, S. J. (2018) Diacylglycerol acyltransferase-2 contains a c-terminal sequence that interacts with lipid droplets. *Biochim. Biophys. Acta BBA - Mol. Cell Biol. Lipids*. **1863**, 1068–1081
37. Güldener, U., Heck, S., Fielder, T., Beinhauer, J., and Hegemann, J. H. (1996) A new efficient gene disruption cassette for repeated use in budding yeast. *Nucleic Acids Res.* **24**, 2519–2524

38. Gibson, D. G., Young, L., Chuang, R.-Y., Venter, J. C., Hutchison, C. A., and Smith, H. O. (2009) Enzymatic assembly of DNA molecules up to several hundred kilobases. *Nat. Methods*. **6**, 343–345
39. Sandager, L., Gustavsson, M. H., Ståhl, U., Dahlqvist, A., Wiberg, E., Banas, A., Lenman, M., Ronne, H., and Stymne, S. (2002) Storage Lipid Synthesis Is Non-essential in Yeast. *J. Biol. Chem.* **277**, 6478–6482
40. Gietz, R. D., and Schiestl, R. H. (1991) Applications of high efficiency lithium acetate transformation of intact yeast cells using single-stranded nucleic acids as carrier. *Yeast*. **7**, 253–263
41. Stagljar, I., Korostensky, C., Johnsson, N., and te Heeson, S. (1998) A genetic system based on split-ubiquitin for the analysis of interactions between membrane proteins *in vivo*. *Proc. Natl. Acad. Sci.* **95**, 5187–5192
42. Foiani, M., Marini, F., Gamba, D., Lucchini, G., and Plevani, P. (1994) The B subunit of the DNA polymerase alpha-primase complex in *Saccharomyces cerevisiae* executes an essential function at the initial stage of DNA replication. *Mol. Cell. Biol.* **14**, 923–933
43. Siloto, R. M. P., Truksa, M., He, X., McKeon, T., and Weselake, R. J. (2009) Simple Methods to Detect Triacylglycerol Biosynthesis in a Yeast-Based Recombinant System. *Lipids*. **44**, 963–973
44. McNeil, B. A., and Stuart, D. T. (2018) Optimization of C16 and C18 fatty alcohol production by an engineered strain of *Lipomyces starkeyi*. *J. Ind. Microbiol. Biotechnol.* **45**, 1–14
45. Exner, T., Beretta, C. A., Gao, Q., Afting, C., Romero-Brey, I., Bartenschlager, R., Fehring, L., Poppelreuther, M., and Füllekrug, J. (2019) Lipid droplet quantification based on iterative image processing. *J. Lipid Res.* **60**, 1333–1344
46. Man, W. C., Miyazaki, M., Chu, K., and Ntambi, J. M. (2006) Membrane Topology of Mouse Stearoyl-CoA Desaturase 1. *J. Biol. Chem.* **281**, 1251–1260
47. Braun, S. (2002) Role of the ubiquitin-selective CDC48UFD1/NPL4 chaperone (segregase) in ERAD of OLE1 and other substrates. *EMBO J.* **21**, 615–621
48. Liu, Q., Siloto, R. M. P., Snyder, C. L., and Weselake, R. J. (2011) Functional and Topological Analysis of Yeast Acyl-CoA:Diacylglycerol Acyltransferase 2, an Endoplasmic Reticulum Enzyme Essential for Triacylglycerol Biosynthesis. *J. Biol. Chem.* **286**, 13115–13126
49. Kamisaka, Y., Tomita, N., Kimura, K., Kainou, K., and Uemura, H. (2007) *DGA1* (diacylglycerol acyltransferase gene) overexpression and leucine biosynthesis significantly increase lipid accumulation in the Δ *snf2* disruptant of *Saccharomyces cerevisiae*. *Biochem. J.* **408**, 61–68
50. Albuquerque, C. P., Smolka, M. B., Payne, S. H., Bafna, V., Eng, J., and Zhou, H. (2008) A Multidimensional Chromatography Technology for In-depth Phosphoproteome Analysis. *Mol. Cell. Proteomics MCP*. **7**, 1389–1396
51. Pan, X., Siloto, R. M. P., Wickramarathna, A. D., Mietkiewska, E., and Weselake, R. J. (2013) Identification of a Pair of Phospholipid:Diacylglycerol Acyltransferases from Developing Flax

(*Linum usitatissimum L.*) Seed Catalyzing the Selective Production of Trilinolenin. *J. Biol. Chem.* **288**, 24173–24188

52. Choudhary, V., El Atab, O., Mizzon, G., Prinz, W. A., and Schneiter, R. (2020) Seipin and Nem1 establish discrete ER subdomains to initiate yeast lipid droplet biogenesis. *J. Cell Biol.* **219**, e201910177
53. Markgraf, D. F., Klemm, R. W., Junker, M., Hannibal-Bach, H. K., Ejsing, C. S., and Rapoport, T. A. (2014) An ER Protein Functionally Couples Neutral Lipid Metabolism on Lipid Droplets to Membrane Lipid Synthesis in the ER. *Cell Rep.* **6**, 44–55
54. Xu, N., Zhang, S. O., Cole, R. A., McKinney, S. A., Guo, F., Haas, J. T., Bobba, S., Farese, R. V., and Mak, H. Y. (2012) The FATP1–DGAT2 complex facilitates lipid droplet expansion at the ER–lipid droplet interface. *J. Cell Biol.* **198**, 895–911
55. Petschnigg, J., Wolinski, H., Kolb, D., Zellnig, G., Kurat, C. F., Natter, K., and Kohlwein, S. D. (2009) Good Fat, Essential Cellular Requirements for Triacylglycerol Synthesis to Maintain Membrane Homeostasis in Yeast. *J. Biol. Chem.* **284**, 30981–30993
56. Zoni, V., Khaddaj, R., Campomanes, P., Thiam, A. R., Schneiter, R., and Vanni, S. (2021) Pre-existing bilayer stresses modulate triglyceride accumulation in the ER versus lipid droplets. *eLife*. **10**, e62886
57. Shabits, B. N. (2017) *Proteomic analysis of yeast membranes enriched in acyltransferases Gpt2p and Sct1p provides insight into their roles and regulation*. Ph.D. thesis, University of Calgary
58. Ruggiano, A., Mora, G., Buxó, L., and Carvalho, P. (2016) Spatial control of lipid droplet proteins by the ERAD ubiquitin ligase Doa10. *EMBO J.* **35**, 1644–1655
59. Brandt, C., McFie, P. J., and Stone, S. J. (2016) Diacylglycerol acyltransferase-2 and monoacylglycerol acyltransferase-2 are ubiquitinated proteins that are degraded by the 26S proteasome. *Biochem. J.* **473**, 3621–3637
60. Romanauska, A., and Köhler, A. (2021) Reprogrammed lipid metabolism protects inner nuclear membrane against unsaturated fat. *Dev. Cell*. **56**, 2562-2578.e3

Chapter 4

1. Czabany, T., Wagner, A., Zweytick, D., Lohner, K., Leitner, E., Ingolic, E., and Daum, G. (2008) Structural and Biochemical Properties of Lipid Particles from the Yeast *Saccharomyces cerevisiae*. *J. Biol. Chem.* **283**, 17065–17074
2. Tauchi-Sato, K., Ozeki, S., Houjou, T., Taguchi, R., and Fujimoto, T. (2002) The Surface of Lipid Droplets Is a Phospholipid Monolayer with a Unique Fatty Acid Composition. *J. Biol. Chem.* **277**, 44507–44512
3. Cottier, S., and Schneiter, R. (2022) Lipid droplets form a network interconnected by the endoplasmic reticulum through which their proteins equilibrate. *J. Cell Sci.* **135**, jcs258819

4. Choudhary, V., El Atab, O., Mizzon, G., Prinz, W. A., and Schneiter, R. (2020) Seipin and Nem1 establish discrete ER subdomains to initiate yeast lipid droplet biogenesis. *J. Cell Biol.* **219**, e201910177
5. Choudhary, V., Ojha, N., Golden, A., and Prinz, W. A. (2015) A conserved family of proteins facilitates nascent lipid droplet budding from the ER. *J. Cell Biol.* **211**, 261–271
6. Khandelia, H., Duelund, L., Pakkanen, K. I., and Ipsen, J. H. (2010) Triglyceride Blisters in Lipid Bilayers: Implications for Lipid Droplet Biogenesis and the Mobile Lipid Signal in Cancer Cell Membranes. *PLoS ONE*. **5**, e12811
7. Dumesnil, C., Vanharanta, L., Prasanna, X., Omrane, M., Carpentier, M., Bhapkar, A., Enkavi, G., Salo, V. T., Vattulainen, I., Ikonen, E., and Thiam, A. R. (2023) Cholesterol esters form supercooled lipid droplets whose nucleation is facilitated by triacylglycerols. *Nat. Commun.* **14**, 915
8. Wang, S., Idrissi, F.-Z., Hermansson, M., Grippa, A., Ejsing, C. S., and Carvalho, P. (2018) Seipin and the membrane-shaping protein Pex30 cooperate in organelle budding from the endoplasmic reticulum. *Nat. Commun.* **9**, 2939
9. Choudhary, V., Golani, G., Joshi, A. S., Cottier, S., Schneiter, R., Prinz, W. A., and Kozlov, M. M. (2018) Architecture of Lipid Droplets in Endoplasmic Reticulum Is Determined by Phospholipid Intrinsic Curvature. *Curr. Biol.* **28**, 915-926.e9
10. Gao, Q., Binns, D. D., Kinch, L. N., Grishin, N. V., Ortiz, N., Chen, X., and Goodman, J. M. (2017) Pet10p is a yeast perilipin that stabilizes lipid droplets and promotes their assembly. *J. Cell Biol.* **216**, 3199–3217
11. Xu, N., Zhang, S. O., Cole, R. A., McKinney, S. A., Guo, F., Haas, J. T., Bobba, S., Farese, R. V., and Mak, H. Y. (2012) The FATP1–DGAT2 complex facilitates lipid droplet expansion at the ER–lipid droplet interface. *J. Cell Biol.* **198**, 895–911
12. Wilfling, F., Wang, H., Haas, J. T., Krahmer, N., Gould, T. J., Uchida, A., Cheng, J.-X., Graham, M., Christiano, R., Fröhlich, F., Liu, X., Buhman, K. K., Coleman, R. A., Bewersdorf, J., Farese, R. V., and Walther, T. C. (2013) Triacylglycerol Synthesis Enzymes Mediate Lipid Droplet Growth by Relocalizing from the ER to Lipid Droplets. *Dev. Cell*. **24**, 384–399
13. Petschnigg, J., Wolinski, H., Kolb, D., Zellnig, G., Kurat, C. F., Natter, K., and Kohlwein, S. D. (2009) Good Fat, Essential Cellular Requirements for Triacylglycerol Synthesis to Maintain Membrane Homeostasis in Yeast. *J. Biol. Chem.* **284**, 30981–30993
14. Hariri, H., Speer, N., Bowerman, J., Rogers, S., Fu, G., Reetz, E., Datta, S., Feathers, J. R., Ugrankar, R., Nicastro, D., and Henne, W. M. (2019) Mdm1 maintains endoplasmic reticulum homeostasis by spatially regulating lipid droplet biogenesis. *J. Cell Biol.* **218**, 1319–1334
15. Li, D., Yang, S.-G., He, C.-W., Zhang, Z.-T., Liang, Y., Li, H., Zhu, J., Su, X., Gong, Q., and Xie, Z. (2020) Excess diacylglycerol at the endoplasmic reticulum disrupts endomembrane homeostasis and autophagy. *BMC Biol.* **18**, 107

16. Grabner, G. F., Xie, H., Schweiger, M., and Zechner, R. (2021) Lipolysis: cellular mechanisms for lipid mobilization from fat stores. *Nat. Metab.* **3**, 1445–1465
17. Fairman, G., and Ouimet, M. (2022) Lipophagy pathways in yeast are controlled by their distinct modes of induction. *Yeast*. **39**, 429–439
18. Meyers, A., Weiskittel, T. M., and Dalhaimer, P. (2017) Lipid Droplets: Formation to Breakdown. *Lipids*. **52**, 465–475
19. Listenberger, L. L., Han, X., Lewis, S. E., Cases, S., Farese, R. V., Ory, D. S., and Schaffer, J. E. (2003) Triglyceride accumulation protects against fatty acid-induced lipotoxicity. *Proc. Natl. Acad. Sci.* **100**, 3077–3082
20. Sandager, L., Gustavsson, M. H., Ståhl, U., Dahlqvist, A., Wiberg, E., Banas, A., Lenman, M., Ronne, H., and Stymne, S. (2002) Storage Lipid Synthesis Is Non-essential in Yeast. *J. Biol. Chem.* **277**, 6478–6482
21. Stone, S. J., Myers, H. M., Watkins, S. M., Brown, B. E., Feingold, K. R., Elias, P. M., and Farese, R. V. (2004) Lipopenia and Skin Barrier Abnormalities in DGAT2-deficient Mice. *J. Biol. Chem.* **279**, 11767–11776
22. Xu, S., Zhang, X., and Liu, P. (2018) Lipid droplet proteins and metabolic diseases. *Biochim. Biophys. Acta BBA - Mol. Basis Dis.* **1864**, 1968–1983
23. Choudhary, V., Jacquier, N., and Schneiter, R. (2011) The topology of the triacylglycerol synthesizing enzyme Lro1 indicates that neutral lipids can be produced within the luminal compartment of the endoplasmatic reticulum: Implications for the biogenesis of lipid droplets. *Commun. Integr. Biol.* **4**, 781–784
24. Oelkers, P., Cromley, D., Padamsee, M., Billheimer, J. T., and Sturley, S. L. (2002) The DGA1 Gene Determines a Second Triglyceride Synthetic Pathway in Yeast. *J. Biol. Chem.* **277**, 8877–8881
25. Oelkers, P., Tinkelenberg, A., Erdeniz, N., Cromley, D., Billheimer, J. T., and Sturley, S. L. (2000) A Lecithin Cholesterol Acyltransferase-like Gene Mediates Diacylglycerol Esterification in Yeast. *J. Biol. Chem.* **275**, 15609–15612
26. Wang, L., Qian, H., Nian, Y., Han, Y., Ren, Z., Zhang, H., Hu, L., Prasad, B. V. V., Laganowsky, A., Yan, N., and Zhou, M. (2020) Structure and mechanism of human diacylglycerol O-acyltransferase-1. *Nature*. **581**, 329–332
27. Stone, S. J., Levin, M. C., Zhou, P., Han, J., Walther, T. C., and Farese, R. V. (2009) The Endoplasmic Reticulum Enzyme DGAT2 Is Found in Mitochondria-associated Membranes and Has a Mitochondrial Targeting Signal That Promotes Its Association with Mitochondria. *J. Biol. Chem.* **284**, 5352–5361
28. Dahlqvist, A., Ståhl, U., Lenman, M., Banas, A., Lee, M., Sandager, L., Ronne, H., and Stymne, S. (2000) Phospholipid:diacylglycerol acyltransferase: An enzyme that catalyzes the acyl-CoA-independent formation of triacylglycerol in yeast and plants. *Proc. Natl. Acad. Sci.* **97**, 6487–6492

29. Owen, M. R., Corstorphine, C. C., and Zammit, V. A. (1997) Overt and latent activities of diacylglycerol acyltransferase in rat liver microsomes: possible roles in very-low-density lipoprotein triacylglycerol secretion. *Biochem. J.* **323**, 17–21
30. Wurie, H. R., Buckett, L., and Zammit, V. A. (2011) Evidence That Diacylglycerol Acyltransferase 1 (DGAT1) Has Dual Membrane Topology in the Endoplasmic Reticulum of HepG2 Cells. *J. Biol. Chem.* **286**, 36238–36247
31. Sorger, D., and Daum, G. (2002) Synthesis of Triacylglycerols by the Acyl-Coenzyme A:Diacyl-Glycerol Acyltransferase Dga1p in Lipid Particles of the Yeast *Saccharomyces cerevisiae*. *J. Bacteriol.* **184**, 519–524
32. Jacquier, N., Choudhary, V., Mari, M., Toulmay, A., Reggiori, F., and Schneiter, R. (2011) Lipid droplets are functionally connected to the endoplasmic reticulum in *Saccharomyces cerevisiae*. *J. Cell Sci.* **124**, 2424–2437
33. Kuerschner, L., Moessinger, C., and Thiele, C. (2008) Imaging of Lipid Biosynthesis: How a Neutral Lipid Enters Lipid Droplets. *Traffic*. **9**, 338–352
34. McFie, P. J., Banman, S. L., Kary, S., and Stone, S. J. (2011) Murine Diacylglycerol Acyltransferase-2 (DGAT2) Can Catalyze Triacylglycerol Synthesis and Promote Lipid Droplet Formation Independent of Its Localization to the Endoplasmic Reticulum. *J. Biol. Chem.* **286**, 28235–28246
35. McFie, P. J., Jin, Y., Banman, S. L., Beauchamp, E., Berthiaume, L. G., and Stone, S. J. (2014) Characterization of the interaction of diacylglycerol acyltransferase-2 with the endoplasmic reticulum and lipid droplets. *Biochim. Biophys. Acta BBA - Mol. Cell Biol. Lipids*. **1841**, 1318–1328
36. Ganesan, S., Tavassoli, M., Shabits, B. N., and Zaremberg, V. (2020) Tubular ER Associates With Diacylglycerol-Rich Structures During Lipid Droplet Consumption. *Front. Cell Dev. Biol.* **8**, 700
37. Grillitsch, K., Connerth, M., Köfeler, H., Arrey, T. N., Rietschel, B., Wagner, B., Karas, M., and Daum, G. (2011) Lipid particles/droplets of the yeast *Saccharomyces cerevisiae* revisited: Lipidome meets Proteome. *Biochim. Biophys. Acta BBA - Mol. Cell Biol. Lipids*. **1811**, 1165–1176
38. Jin, Y., McFie, P. J., Banman, S. L., Brandt, C., and Stone, S. J. (2014) Diacylglycerol Acyltransferase-2 (DGAT2) and Monoacylglycerol Acyltransferase-2 (MGAT2) Interact to Promote Triacylglycerol Synthesis. *J. Biol. Chem.* **289**, 28237–28248
39. Nuber, S., Nam, A. Y., Rajsombath, M. M., Cirka, H., Hronowski, X., Wang, J., Hodgetts, K., Kalinichenko, L. S., Müller, C. P., Lambrecht, V., Winkler, J., Weihofen, A., Imberdis, T., Dettmer, U., Fanning, S., and Selkoe, D. J. (2021) A Stearoyl–Coenzyme A Desaturase Inhibitor Prevents Multiple Parkinson Disease Phenotypes in A -Synuclein Mice. *Ann. Neurol.* **89**, 74–90
40. Lv, X., Liu, J., Qin, Y., Liu, Y., Jin, M., Dai, J., Chua, B. T., Yang, H., and Li, P. (2019) Identification of gene products that control lipid droplet size in yeast using a high-throughput quantitative image analysis. *Biochim. Biophys. Acta BBA - Mol. Cell Biol. Lipids*. **1864**, 113–127

41. Zoni, V., Khaddaj, R., Campomanes, P., Thiam, A. R., Schneiter, R., and Vanni, S. (2021) Pre-existing bilayer stresses modulate triglyceride accumulation in the ER versus lipid droplets. *eLife*. **10**, e62886
42. Li, C., Li, L., Lian, J., Watts, R., Nelson, R., Goodwin, B., and Lehner, R. (2015) Roles of Acyl-CoA:Diacylglycerol Acyltransferases 1 and 2 in Triacylglycerol Synthesis and Secretion in Primary Hepatocytes. *Arterioscler. Thromb. Vasc. Biol.* **35**, 1080–1091
43. Man, W. C., Miyazaki, M., Chu, K., and Ntambi, J. (2006) Colocalization of SCD1 and DGAT2: implying preference for endogenous monounsaturated fatty acids in triglyceride synthesis. *J. Lipid Res.* **47**, 1928–1939
44. Bai, Y., McCoy, J. G., Levin, E. J., Sobrado, P., Rajashankar, K. R., Fox, B. G., and Zhou, M. (2015) X-ray structure of a mammalian stearoyl-CoA desaturase. *Nature*. **524**, 252–256
45. Natter, K., Leitner, P., Faschinger, A., Wolinski, H., McCraith, S., and Fields, S. (2005) The Spatial Organization of Lipid Synthesis in the Yeast *Saccharomyces cerevisiae* Derived from Large Scale Green Fluorescent Protein Tagging and High Resolution Microscopy. *Mol. Cell. Proteomics*. **4**, 662–672
46. Markgraf, D. F., Klemm, R. W., Junker, M., Hannibal-Bach, H. K., Ejsing, C. S., and Rapoport, T. A. (2014) An ER Protein Functionally Couples Neutral Lipid Metabolism on Lipid Droplets to Membrane Lipid Synthesis in the ER. *Cell Rep.* **6**, 44–55
47. Cao, H. (2011) Structure-Function Analysis of Diacylglycerol Acyltransferase Sequences from 70 Organisms. *BMC Res. Notes*. **4**, 249
48. Liu, Q., Siloto, R. M. P., Snyder, C. L., and Weselake, R. J. (2011) Functional and Topological Analysis of Yeast Acyl-CoA:Diacylglycerol Acyltransferase 2, an Endoplasmic Reticulum Enzyme Essential for Triacylglycerol Biosynthesis. *J. Biol. Chem.* **286**, 13115–13126
49. Stone, S. J., Levin, M. C., and Farese, R. V. (2006) Membrane Topology and Identification of Key Functional Amino Acid Residues of Murine Acyl-CoA:Diacylglycerol Acyltransferase-2. *J. Biol. Chem.* **281**, 40273–40282
50. Shockey, J. M., Gidda, S. K., Chapital, D. C., Kuan, J.-C., Dhanoa, P. K., Bland, J. M., Rothstein, S. J., Mullen, R. T., and Dyer, J. M. (2006) Tung Tree DGAT1 and DGAT2 Have Nonredundant Functions in Triacylglycerol Biosynthesis and Are Localized to Different Subdomains of the Endoplasmic Reticulum. *Plant Cell*. **18**, 2294–2313
51. Binder, H., and Gawrisch, K. (2001) Effect of Unsaturated Lipid Chains on Dimensions, Molecular Order and Hydration of Membranes. *J. Phys. Chem. B*. **105**, 12378–12390
52. Lewis, B. A., and Engelman, D. M. (1983) Lipid bilayer thickness varies linearly with acyl chain length in fluid phosphatidylcholine vesicles. *J. Mol. Biol.* **166**, 211–217
53. Robertson, R. M., Yao, J., Gajewski, S., Kumar, G., Martin, E. W., Rock, C. O., and White, S. W. (2017) A two-helix motif positions the lysophosphatidic acid acyltransferase active site for catalysis within the membrane bilayer. *Nat. Struct. Mol. Biol.* **24**, 666–671

54. Tunyasuvunakool, K., Adler, J., Wu, Z., Green, T., Zielinski, M., Žídek, A., Bridgland, A., Cowie, A., Meyer, C., Laydon, A., Velankar, S., Kleywegt, G. J., Bateman, A., Evans, R., Pritzel, A., Figurnov, M., Ronneberger, O., Bates, R., Kohl, S. A. A., Potapenko, A., Ballard, A. J., Romera-Paredes, B., Nikolov, S., Jain, R., Clancy, E., Reiman, D., Petersen, S., Senior, A. W., Kavukcuoglu, K., Birney, E., Kohli, P., Jumper, J., and Hassabis, D. (2021) Highly accurate protein structure prediction for the human proteome. *Nature*. **596**, 590–596
55. McFie, P. J., Banman, S. L., and Stone, S. J. (2018) Diacylglycerol acyltransferase-2 contains a c-terminal sequence that interacts with lipid droplets. *Biochim. Biophys. Acta BBA - Mol. Cell Biol. Lipids*. **1863**, 1068–1081
56. Brandt, C., McFie, P. J., and Stone, S. J. (2016) Diacylglycerol acyltransferase-2 and monoacylglycerol acyltransferase-2 are ubiquitinated proteins that are degraded by the 26S proteasome. *Biochem. J.* **473**, 3621–3637
57. Prévost, C., Sharp, M. E., Kory, N., Lin, Q., Voth, G. A., Farese, R. V., and Walther, T. C. (2018) Mechanism and Determinants of Amphipathic Helix-Containing Protein Targeting to Lipid Droplets. *Dev. Cell*. **44**, 73-86.e4
58. Ruggiano, A., Mora, G., Buxó, L., and Carvalho, P. (2016) Spatial control of lipid droplet proteins by the ERAD ubiquitin ligase Doa10. *EMBO J.* **35**, 1644–1655
59. Gietz, R. D., and Schiestl, R. H. (1991) Applications of high efficiency lithium acetate transformation of intact yeast cells using single-stranded nucleic acids as carrier. *Yeast*. **7**, 253–263
60. Thomas, B. J., and Rothstein, R. (1989) Elevated recombination rates in transcriptionally active DNA. *Cell*. **56**, 619–630
61. Zhu, J., Zhang, Z.-T., Tang, S.-W., Zhao, B.-S., Li, H., Song, J.-Z., Li, D., and Xie, Z. (2019) A Validated Set of Fluorescent-Protein-Based Markers for Major Organelles in Yeast (*Saccharomyces cerevisiae*). *mBio*. **10**, e01691-19
62. Goldstein, A. L., and McCusker, J. H. (1999) Three new dominant drug resistance cassettes for gene disruption in*Saccharomyces cerevisiae*. *Yeast*. **15**, 1541–1553
63. Hailey, D. W., Dams, T. N., and Muller, E. G. D. (2002) Fluorescence resonance energy transfer using color variants of green fluorescent protein. in *Methods in Enzymology*, pp. 34–49, Elsevier, **351**, 34–49
64. Gueldener, U., Heinisch, J., Koehler, G. J., Voss, D., and Hegemann, J. H. (2002) A second set of loxP marker cassettes for Cre-mediated multiple gene knockouts in budding yeast. *Nucleic Acids Res.* **30**, e23
65. Crooks, G. E., Hon, G., Chandonia, J.-M., and Brenner, S. E. (2004) WebLogo: A Sequence Logo Generator. *Genome Res.* **14**, 1188–1190

66. Waterhouse, A. M., Procter, J. B., Martin, D. M. A., Clamp, M., and Barton, G. J. (2009) Jalview Version 2—a multiple sequence alignment editor and analysis workbench. *Bioinformatics*. **25**, 1189–1191
67. Schindelin, J., Arganda-Carreras, I., Frise, E., Kaynig, V., Longair, M., Pietzsch, T., Preibisch, S., Rueden, C., Saalfeld, S., Schmid, B., Tinevez, J.-Y., White, D. J., Hartenstein, V., Eliceiri, K., Tomancak, P., and Cardona, A. (2012) Fiji: an open-source platform for biological-image analysis. *Nat. Methods*. **9**, 676–682
68. Shaner, N. C., Lambert, G. G., Chammas, A., Ni, Y., Cranfill, P. J., Baird, M. A., Sell, B. R., Allen, J. R., Day, R. N., Israelsson, M., Davidson, M. W., and Wang, J. (2013) A bright monomeric green fluorescent protein derived from Branchiostoma lanceolatum. *Nat. Methods*. **10**, 407–409
69. Liu, Q., Siloto, R. M. P., Lehner, R., Stone, S. J., and Weselake, R. J. (2012) Acyl-CoA:diacylglycerol acyltransferase: Molecular biology, biochemistry and biotechnology. *Prog. Lipid Res.* **51**, 350–377
70. Shpilka, T., Welter, E., Borovsky, N., Amar, N., Mari, M., Reggiori, F., and Elazar, Z. (2015) Lipid droplets and their component triglycerides and steryl esters regulate autophagosome biogenesis. *EMBO J.* **34**, 2117–2131
71. Ogasawara, Y., Kira, S., Mukai, Y., Noda, T., and Yamamoto, A. (2016) Ole1, fatty acid desaturase, is required for Atg9 delivery and isolation membrane expansion during autophagy in *Saccharomyces cerevisiae*. *Biol. Open*. **6**, 35–40
72. Ogasawara, Y., Itakura, E., Kono, N., Mizushima, N., Arai, H., Nara, A., Mizukami, T., and Yamamoto, A. (2014) Stearoyl-CoA Desaturase 1 Activity Is Required for Autophagosome Formation. *J. Biol. Chem.* **289**, 23938–23950
73. van Zutphen, T., Todde, V., de Boer, R., Kreim, M., Hofbauer, H. F., Wolinski, H., Veenhuis, M., van der Klei, I. J., and Kohlwein, S. D. (2014) Lipid droplet autophagy in the yeast *Saccharomyces cerevisiae*. *Mol. Biol. Cell*. **25**, 290–301
74. Lu, K., den Brave, F., and Jentsch, S. (2017) Pathway choice between proteasomal and autophagic degradation. *Autophagy*. **13**, 1799–1800

Chapter 5

1. Lee, J., and Ridgway, N. D. (2020) Substrate channeling in the glycerol-3-phosphate pathway regulates the synthesis, storage and secretion of glycerolipids. *Biochim. Biophys. Acta BBA - Mol. Cell Biol. Lipids*. **1865**, 158438
2. Wagner, S., and Paltauf, F. (1994) Generation of glycerophospholipid molecular species in the yeast *Saccharomyces cerevisiae*. Fatty acid pattern of phospholipid classes and selective acyl turnover at *sn-1* and *sn-2* positions. *Yeast*. **10**, 1429–1437

3. Řezanka, T., Kolouchová, I., Čejková, A., Cajthaml, T., and Sigler, K. (2013) Identification of regioisomers and enantiomers of triacylglycerols in different yeasts using reversed- and chiral-phase LC–MS. *J. Sep. Sci.* **36**, 3310–3320
4. Ejsing, C. S., Sampaio, J. L., Surendranath, V., Duchoslav, E., Ekroos, K., Klemm, R. W., Simons, K., and Shevchenko, A. (2009) Global analysis of the yeast lipidome by quantitative shotgun mass spectrometry. *Proc. Natl. Acad. Sci.* **106**, 2136–2141
5. Zoni, V., Khaddaj, R., Campomanes, P., Thiam, A. R., Schneiter, R., and Vanni, S. (2021) Pre-existing bilayer stresses modulate triglyceride accumulation in the ER versus lipid droplets. *eLife*. **10**, e62886
6. Nuber, S., Nam, A. Y., Rajsombath, M. M., Cirka, H., Hronowski, X., Wang, J., Hodgetts, K., Kalinichenko, L. S., Müller, C. P., Lambrecht, V., Winkler, J., Weihofen, A., Imberdis, T., Dettmer, U., Fanning, S., and Selkoe, D. J. (2021) A Stearoyl–Coenzyme A Desaturase Inhibitor Prevents Multiple Parkinson Disease Phenotypes in A -Synuclein Mice. *Ann. Neurol.* **89**, 74–90
7. Casanovas, A., Sprenger, R. R., Tarasov, K., Ruckerbauer, D. E., Hannibal-Bach, H. K., Zanghellini, J., Jensen, O. N., and Ejsing, C. S. (2015) Quantitative Analysis of Proteome and Lipidome Dynamics Reveals Functional Regulation of Global Lipid Metabolism. *Chem. Biol.* **22**, 412–425
8. Ogasawara, Y., Kira, S., Mukai, Y., Noda, T., and Yamamoto, A. (2016) Ole1, fatty acid desaturase, is required for Atg9 delivery and isolation membrane expansion during autophagy in *Saccharomyces cerevisiae*. *Biol. Open*. **6**, 35–40
9. Ogasawara, Y., Itakura, E., Kono, N., Mizushima, N., Arai, H., Nara, A., Mizukami, T., and Yamamoto, A. (2014) Stearoyl-CoA Desaturase 1 Activity Is Required for Autophagosome Formation. *J. Biol. Chem.* **289**, 23938–23950
10. Mollinedo, F. (2012) Lipid raft involvement in yeast cell growth and death. *Front. Oncol.* 10.3389/fonc.2012.00140
11. Wilfling, F., Wang, H., Haas, J. T., Krahmer, N., Gould, T. J., Uchida, A., Cheng, J.-X., Graham, M., Christiano, R., Fröhlich, F., Liu, X., Buhman, K. K., Coleman, R. A., Bewersdorf, J., Farese, R. V., and Walther, T. C. (2013) Triacylglycerol Synthesis Enzymes Mediate Lipid Droplet Growth by Relocalizing from the ER to Lipid Droplets. *Dev. Cell*. **24**, 384–399
12. McFie, P. J., Jin, Y., Banman, S. L., Beauchamp, E., Berthiaume, L. G., and Stone, S. J. (2014) Characterization of the interaction of diacylglycerol acyltransferase-2 with the endoplasmic reticulum and lipid droplets. *Biochim. Biophys. Acta BBA - Mol. Cell Biol. Lipids*. **1841**, 1318–1328
13. Xu, N., Zhang, S. O., Cole, R. A., McKinney, S. A., Guo, F., Haas, J. T., Bobba, S., Farese, R. V., and Mak, H. Y. (2012) The FATP1–DGAT2 complex facilitates lipid droplet expansion at the ER–lipid droplet interface. *J. Cell Biol.* **198**, 895–911
14. Le, M. H., Le, D. M., Baez, T. C., Wu, Y., Ito, T., Lee, E. Y., Lee, K., Stave, C. D., Henry, L., Barnett, S. D., Cheung, R., and Nguyen, M. H. (2023) Global incidence of non-alcoholic fatty liver

disease: a systematic review and meta-analysis of 63 studies and 1,201,807 persons. *J. Hepatol.* 10.1016/j.jhep.2023.03.040

15. Negi, C. K., Babica, P., Bajard, L., Bienertova-Vasku, J., and Tarantino, G. (2022) Insights into the molecular targets and emerging pharmacotherapeutic interventions for nonalcoholic fatty liver disease. *Metabolism*. **126**, 154925
16. Fu, Y., Zhou, Y., Shen, L., Li, X., Zhang, H., Cui, Y., Zhang, K., Li, W., Chen, W., Zhao, S., Li, Y., and Ye, W. (2022) Diagnostic and therapeutic strategies for non-alcoholic fatty liver disease. *Front. Pharmacol.* **13**, 973366
17. Srere, P. A. (1987) Complexes of sequential metabolic enzymes. *Annu. Rev. Biochem.* **56**, 89–124
18. Schneiter, R., Brügger, B., Sandhoff, R., Zellnig, G., Leber, A., Lampl, M., Athenstaedt, K., Hrastnik, C., Eder, S., Daum, G., Paltauf, F., Wieland, F. T., and Kohlwein, S. D. (1999) Electrospray Ionization Tandem Mass Spectrometry (ESI-MS/MS) Analysis of the Lipid Molecular Species Composition of Yeast Subcellular Membranes Reveals Acyl Chain-Based Sorting/Remodeling of Distinct Molecular Species En Route to the Plasma Membrane. *J. Cell Biol.* **146**, 741–754
19. Ma, L., Yang, F., and Zheng, J. (2014) Application of fluorescence resonance energy transfer in protein studies. *J. Mol. Struct.* **1077**, 87–100
20. Feng, S., Sekine, S., Pessino, V., Li, H., Leonetti, M. D., and Huang, B. (2017) Improved split fluorescent proteins for endogenous protein labeling. *Nat. Commun.* **8**, 370
21. Gaigg, B., Simbeni, R., Hrastnik, C., Paltauf, F., and Daum, G. (1995) Characterization of a microsomal subfraction associated with mitochondria of the yeast, *Saccharomyces cerevisiae*. Involvement in synthesis and import of phospholipids into mitochondria. *Biochim. Biophys. Acta BBA - Biomembr.* **1234**, 214–220
22. Renne, M. F., Bao, X., Hokken, M. W., Bierhuizen, A. S., Hermansson, M., Sprenger, R. R., Ewing, T. A., Ma, X., Cox, R. C., Brouwers, J. F., Smet, C. H. D., Ejsing, C. S., and Kroon, A. I. de (2022) Molecular species selectivity of lipid transport creates a mitochondrial sink for di-unsaturated phospholipids. *EMBO J.* **41**, e106837
23. Pichler, H., Gaigg, B., Hrastnik, C., Achleitner, G., Kohlwein, S. D., Zellnig, G., Perktold, A., and Daum, G. (2001) A subfraction of the yeast endoplasmic reticulum associates with the plasma membrane and has a high capacity to synthesize lipids. *Eur. J. Biochem.* **268**, 2351–2361
24. Bondeson, D. P., Mullin-Bernstein, Z., Oliver, S., Skipper, T. A., Atack, T. C., Bick, N., Ching, M., Guirguis, A. A., Kwon, J., Langan, C., Millson, D., Paolella, B. R., Tran, K., Wie, S. J., Vazquez, F., Tothova, Z., Golub, T. R., Sellers, W. R., and Ianari, A. (2022) Systematic profiling of conditional degron tag technologies for target validation studies. *Nat. Commun.* **13**, 5495

Appendix – Lab procedures

Using the Emulsiflex to lyse yeast

This protocol can be used to obtain cell lysate from yeast. Lysis buffer can be adjusted depending on downstream applications for cell lysate. This is an effective method to isolate large amounts of cell lysate for a membrane isolation.

Must be trained on Emulsiflex prior to use by Dr. LaPointe
After training, ask for access to Emulsiflex calendar. Sign up on the google calendar prior to usage.

Culture preparation:

1. Grow cells to an OD_{600} under 2. Any higher, and cells may become difficult to lyse.
2. If more cells needed, grow up 2L.
3. After centrifugation to collect, wash cells once in H_2O.
4. Resuspend in at least 50mL lysis buffer.

Emulsiflex lysis:

1. Chiller on.
2. Machine on.
3. Nitrogen on – not the regulator, use the handle on the tank.
4. H_2O in to flush.
5. Pressurize in lysis buffer to 5,000 psi.
6. Pressurize in sample to 20,000 psi.
7. 8 passes to lyse cells (can check cultures at this point under light microscope to confirm efficient lysis).
8. Flush with H_2O to clean.
9. Clean the canister, O-ring, beveled top – take off the machine and wipe.
10. Flush again with H_2O.
11. Wipe the tube.

12. Force H_2O through.
13. Flush with 70% EtOH.
14. Force 70% EtOH through.
15. Run 70% EtOH into the system, place the cap back on.
16. Make sure nitrogen, machine, and chiller are all off.
17. Sign off on the log.

Lysis buffer, pH 7.2

100mM NaCl

50mM Tris-HCl

1mM EDTA

1mM EGTA

1mM PMSF

Leupeptin

Pepstatin

Crosslinking antibody to beads

This protocol can be used to prepare beads reversibly crosslinked to antibody for a coimmunoprecipitation. The method was designed to prevent antibody carryover into sample destined for analysis by LC-MS/MS.

1. Wash 200uL protein G beads 3x in PBS. Centrifuge no quicker than 500g when working with beads.
2. Separate beads to 100uL no antibody (noAb), 100uL with antibody (+Ab).
3. Store 100uL noAb at 4°C until final wash step.
4. Mix anti-Myc antibody with +Ab beads in PBS (1uL antibody per 30uL beads).
5. Incubate 1 hour at room temperature, with agitation.
6. Wash 2x with 10 volumes 100mM sodium borate.
7. Crosslink in 20mM DMP, 30 minutes at room temperature.
8. Wash 2x with 1mL 200mM ethanolamine, incubate 1 hour at room temperature with agitation.
9. Wash both noAb and +Ab 3x with buffer cells were lysed in, resuspend each in 100uL, store at 4°C for up to one week.

PBS

1L H_2O
NaCl, 8g
KCl, 0.2g
Na_2HPO_4, 1.44g
KH_2PO4, 0.24g

Dimethyl pimelimidate (DMP), 20mM

1mL 100mM sodium borate, pH 9
0.0052g DMP

Sodium borate, 100mM, pH 9

100mL H_2O
3.8137g sodium borate

Membrane Isolation

This protocol can be used to isolate solubilized membrane proteins from yeast lysate. Cells can be lysed using preferred method, but the method will dictate volume of lysate and thus rotor/ultracentrifuge used. Type/amount of detergent can be optimized. This method was designed to isolate and concentrate membrane proteins for a coimmunoprecipitation to determine strong interactors with the protein of interest.

*PMSF is unstable in aqueous solution. Re-add to solution every 30 minutes until membranes are pelleted.

1. Prepare lysate as desired (bead beating, Emulsiflex, or frozen pellet grinding). Be sure to include a non-tagged strain as control if needed.
2. Centrifuge at 3,000g for 20 minutes, 4^{o}C to clear lysate. Add 50uL of cell lysate to 50uL 2x SB.
3. Balance samples using a scale – it's essential to balance properly before ultracentrifugation.
4. Centrifuge at ~106,000g for 1 hour, 4^{o}C to pellet membranes (Ti45, 30k rpm or TLA110, 45k rpm). Aim for at least 40mL of sample to reduce risk of tube collapse with the Ti45 rotor.
5. Add 50uL of 106k g supernatant to 50uL 2x SB.
6. Wash pellet with lysis buffer. Move pellet to pre-chilled douncer with 5mL lysis buffer + 0.5% Triton-X 100. Dounce 5-10 times on ice, until pellet is resuspended. Incubate resuspended membranes for 45 minutes on ice with agitation. Add 50uL of 100k g pellet to 50uL 2x SB.
7. Centrifuge at 106,000g for 1 hour, 4^{o}C to remove aggregates. Keep supernatant – this contains your membrane proteins. The pellet is aggregated protein.

Measure protein concentration via DC protein assay:

1. Prep reagent A'
    a. 30uL reagent S
    b. 1.5mL reagent A
2. Assay:

a. 100uL A'
b. 800uL B
c. 20uL sample diluted 1:10 (or standard)

3. Standards (from 5mg/mL BSA):
    a. 1.5mg/mL (30uL BSA in 70uL H_2O)
    b. 1mg/mL (20uL BSA in 80uL H_2O)
    c. 0.75mg/mL (10uL 1.5mg/mL BSA in 10uL H_2O)
    d. 0.5mg/mL (20uL 1mg/mL BSA in 20uL H_2O)
    e. 0.25mg/mL (10uL 0.5mg/mL BSA in 10uL H_2O)
4. Add reagents in order: sample or standard, 100uL A', vortex, 800uL B, vortex.
5. Incubate for 15 minutes at room temperature.
6. Read within 1 hour at 750nm.

Lysis buffer, pH 7.2

100mM NaCl

50mM Tris-HCl

1mM EDTA

1mM EGTA

1mM PMSF

Leupeptin

Pepstatin

Microsome Isolation

This protocol can be used to obtain microsomes from yeast while preserving protein-protein interactions. Spheroplasting is used to remove the cell wall, before a relatively gentle lysis using a douncer. Potassium phosphate buffer can be replaced as needed, depending on downstream applications for microsomes. This method is designed to isolate microsomes for a substrate channeling assay.

1. Collect cells by centrifugation. Aim for an OD600 under 1-2, as spheroplasting is easier when the cells are still dividing.
2. Wash with water.
3. Wash with 20mL 1M sorbitol.
4. Collect cells and resuspend in 20mL lyticase buffer. Add DTT to 30mM.
5. Incubate at 30^{o}C for 15 minutes.
6. Collect cells, resuspend in lyticase (200uL of 10mg/mL per 5mL buffer) and lyticase buffer. Add DTT fresh to 2mM.
7. Incubate for 10 minutes at 37^{o}C with very gentle agitation. Check spheroplast efficiency under a light microscope by adding water to the slide. If the cells burst, they are spheroplasts. Repeat until 80% or so of the cells burst when checked.
8. Centrifuge to collect cells. Resuspend in lyticase buffer and protease inhibitors.
9. Lyse by 10 passes in a pre-chilled douncer on ice. Rest 2-3 minutes, and repeat 10 passes.
10. Add 1 volume TBS.
11. Centrifuge at 3000g for 5 minutes at 4^{o}C to clear lysate.
12. Centrifuge supernatant for 15 minutes at 20,000g to pellet mitochondria.
13. Ultracentrifuge at ~106k g for 1 hour at 4^{o}C to pellet membranes (Ti45, 30k rpm or TLA110, 45k rpm). Aim for at least 40mL of sample to reduce risk of tube collapse with the Ti45 rotor.
14. Discard supernatant and wash the pelleted membranes in 0.1M potassium phosphate buffer, pH 7.2.
15. Resuspend the pellet in ~2-5mL 0.1M potassium phosphate buffer, pH 7.2. Use 10 passes in a pre-chilled douncer on ice. These are your microsomes.

Measure protein concentration via DC protein assay:

1. Prep reagent A'
    a. 30uL reagent S
    b. 1.5mL reagent A
2. Assay:
    a. 100uL A'
    b. 800uL B
    c. 20uL sample diluted 1:10 (or standard)
3. Standards (from 5mg/mL BSA):
    a. 1.5mg/mL (30uL BSA in 70uL H_2O)
    b. 1mg/mL (20uL BSA in 80uL H_2O)
    c. 0.75mg/mL (10uL 1.5mg/mL BSA in 10uL H_2O)
    d. 0.5mg/mL (20uL 1mg/mL BSA in 20uL H_2O)
    e. 0.25mg/mL (10uL 0.5mg/mL BSA in 10uL H_2O)
4. Add reagents in order: sample or standard, 100uL A', vortex, 800uL B, vortex.
5. Incubate for 15 minutes at room temperature.
6. Read within 1 hour at 750nm.

Lyticase buffer (200mL) pH 6

Sorbitol, 1M (100mL 2M)

Trisodium citrate, 100mM (5.1612g)

EDTA, 10mM (4mL 500mM)

Potassium phosphate buffer (0.1M, pH 7.2, 1L)

K_2HPO_4 (71.7mL 1M or 12.48g)

KH_2PO_4 (28.3mL 1M or 3.85g)

CoIP from membrane isolation

This protocol can be used to determine interactors with the membrane protein of interest. Investigations for interactors with soluble proteins can be performed using this method, but PMSF will need to be added to solution every 30 minutes to prevent proteolysis.

* Try to use same day as membrane preparation, if possible. This will allow you to capture weaker interactions.
* Volumes can be scaled up as needed, just be sure to prepare the correct amount of beads and lysate.

1. Add 5-10mg of protein to each incubation, to a final volume of 1mL.
2. Aliquot 50uL of beads to each sample.
3. Incubate at 4°C with agitation for 2 hours.
4. Centrifuge at 500g for 5 minutes at 4°C.
5. Wash with 1mL wash buffer 2x.
6. Resuspend in wash buffer, move to new tubes.
7. Wash again, remove all wash buffer.
8. Add 50uL 2x SB, 50uL lysis buffer, vortex 15s.
9. Heat to 65°C for 10 minutes.
10. Vortex 30s and centrifuge 10 minutes at full speed to collect beads.
11. Remove 80uL to new tube. This can be stored at -20°C overnight. Add 8uL DTT fresh.
12. Prepare a 10% SDS gel from filtered buffers. Run into resolving gel 1cm (about 20 minutes at 160V) in buffer that's been filtered.
13. Stain overnight using colloidal Coomassie in covered Tupperware, agitating at room temperature, destaining in the morning in ddH_2O.
14. Cut out lanes and deliver to proteomics facility in microfuge tubes.

Wash Buffer

Lysis Buffer

0.5% Triton X-100

Colloidal Coomassie

- ddH_2O to 1L
- Ammonium sulfate, 100g
- Coomassie blue G-250, 1.2g
- Orthophosphoric acid to 10% (118mL of 85%)
- MeOH, 200mL
- * don’t filter sterilize

Beta-galactosidase assay

This protocol can be used to determine LacZ reporter gene activity in yeast cells. The method was developed to relatively quantify interactions between membrane proteins in the membrane yeast-two hybrid assay, though it could also have applications in a typical yeast two-hybrid assay.

1. Take OD600 of all cultures and record. If OD_{600} > 0.8, dilute 100uL of culture in 900uL media and re-take OD_{600}. Multiply new OD by 10 and record.
2. Move 1mL of cells to new, labeled tubes, and centrifuge at full speed 3min to collect. If OD_{600} > 3, take 500uL of cells.
3. Pour off media and use p200 to remove as much as you can, being careful to not disturb the cell pellet. Resuspend in 500uL Z-buffer.
4. Add 50uL 0.1% SDS and 50uL chloroform. Vortex 15s to lyse cells.
5. Add 100uL ONPG. Move quickly here, as the reaction starts as soon as you add the substrate.
6. Let colour develop, 2-5 minutes, in water bath set to 37^{o}C. Remove from water bath, add 500uL sodium carbonate (Na_2CO_3) to quench.
7. Centrifuge reactions 5 minutes at full speed. Take upper 900uL to cuvette and record OD_{420}. If OD_{420} > 1, dilute 1:10 as you did the cultures, and re-take OD_{420}.
8. Data analysis:
    a. Use this formula to determine beta-gal units: ((1000)x(OD420))/((Length of time incubated at 37C in minutes)x(Volume of cells in mL)x(OD600))
    b. Take average and standard deviation of your replicates. Drop out any outliers.
    c. Assess statistical significance of differences between samples using a two-tailed t-test, assuming equal variance.
    d. Normalize averages and standard deviation to the positive control (Alg5-NubI).
    e. Plot normalized averages on a bar graph, including error bars. This will give you relative beta-gal activity in an easy-to-visualize form:

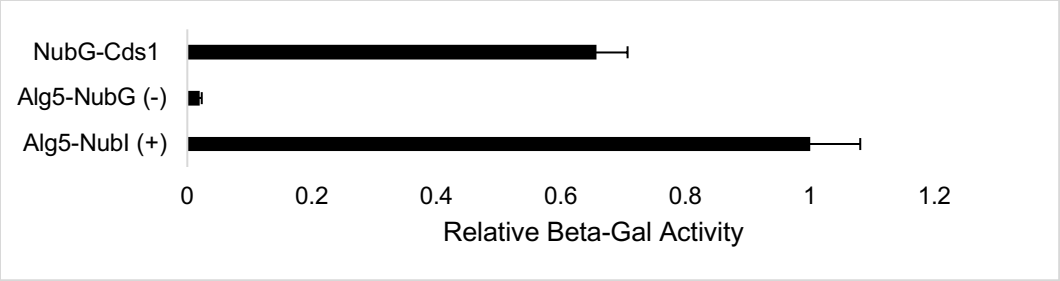

Z-buffer

1L ddH_2O

60mM Na_2HPO_4, 16.1g

40mM NaH_2PO_4, 5.5g

10mM KCl, 0.750g

1mM $MgSO_4$, 0.246g

pH 7

ONPG (4mg/mL)

10mL 0.1M potassium phosphate buffer pH 7

0.04g ONPG

Na_2CO_3

50mL ddH_2O

5.3g Na_2CO_3

Fatty acid toxicity assay

This protocol is used to prepare plates for fatty acid toxicity assay plating. It is an effective method, used in conjunction with H1246 cells, to determine if acyltransferase mutants are still active.

1. Prepare 0.005% fatty acid plates.
    a. -ura media
    b. Add Tween 80 to 0.1%. Stir until no longer cloudy.
    c. Prepare FFA in ethyl acetate to 1% (w/v).
        i. 11.2uL FFA per 1mL ethyl acetate
    d. Add to -ura + Tween 80 plates to a concentration of 0.005%.
        i. Dilute 1:200 – for every 100mL media, add 0.5mL 1% FFA
    e. Add a corresponding amount of ethyl acetate to control plates
2. Allow to solidify, store at 4°C. I find these plates perform better after a night or two in the fridge.

Analysis of acyl chains incorporated into TAG

This procedure was designed to isolate the TAG generated by different Dga1 mutants by TLC, extract the TAG from a TLC plate, and generate FAME for eventual GC analysis.

Lipid extraction

1. Inoculate media with H1246 strain containing Dga1 mutants of interest to grow overnight.
2. Measure OD_{600} the next morning, dilute to OD_{600} 0.1-0.2, and grow 6 hours to exponential phase in YEPD.
3. Collect 1-2 OD_{600} equivalent of cells and wash in PBS. Freeze at -80^{o}C overnight or snap freeze in liquid nitrogen prior to extraction.
4. Add 200uL acid-washed beads.
5. Add 500uL chloroform:methanol (2:1) to sample. Bead beat (8x 90 seconds on, 30 seconds off).
6. Centrifuge 10,000g for 5 minutes.
7. Transfer supernatant to new tubes, being sure to leave the cell debris.
8. Evaporate supernatant in speedvac.
9. Repeat from step 5, adding supernatant to same tube, 5 times total.
10. Evaporate samples overnight or until supernatant is fully evaporated, leaving a yellow tinted film.
11. Dissolve lipid extracts in 50uL chloroform.

TLC for neutral lipid separation

1. Add mobile phase (hexane:diethyl ether:acetic acid [70:30:1]) to TLC chamber and equilibrate for at least 30 minutes.
2. Prepare TLC plate by activating in an oven if necessary.
3. Draw sample line in pencil and label sample lanes. Be sure to be gentle as to not disturb the mobile phase.
4. Spot 5-20uL of sample on plate alongside 1-5ug of tristearin control. Allow to evaporate fully before adding more sample or developing.
5. Develop plate to within 1 centimeter of top. Allow to dry for 30 minutes to an hour.

6. Stain plate with 0.03% Coomassie R-250 solution in 20% methanol for 15 minutes, destain for 10 minutes. Allow to dry for 30 minutes to an hour.
7. Image plate.

TAG extraction from TLC plate

1. Scrape TAG bands into individual tubes containing 45uL water.
2. Add 160uL chloroform and vortex for 2 minutes.
3. Add 320uL methanol and vortex for 20 minutes. Add 320uL water, centrifuge 2,000g for 2 minutes, and take lower organic phase (about 160uL) as that contains the TAG.

FAME analysis

1. Take TAG in organic phase, add to 3mL methanolic HCl in glass tubes, and incubate at 50^{o}C overnight.
2. Add 1mL hexane and 1mL water. Vortex and centrifuge at 2,000 rpm for 5 minutes to allow for phase separation.
3. Take upper organic phase and dry down in speedvac. Resuspend in 200uL hexane and deliver to lipidomics facility using vial inserts.

Coimmunoprecipitation

This procedure was designed to analyse the interaction of Ole1 and Dga1 in a more direct format. As we expect the interaction is fairly transient, a reversable crosslinker is employed to capture the interaction in the affinity purification. This coIP is designed to detect interactions via a western blot.

1. Inoculate media with strains containing Ole1-myc and HA-Dga1 to grow overnight.
2. Measure OD_{600} the next morning, dilute to OD_{600} 0.1-0.2, and grow 6 hours to exponential phase in YEPD.
3. Collect all cells and wash in PBS two times. Incubate with 2mM DSP in PBS 15 minutes at room temperature with gentle agitation.
4. Quench by addition of 25mM Tris and incubate for 15 minutes at room temperature with gentle agitation.
5. Collect all cells and wash in TBS two times. Resuspend in 300uL lysis buffer, add acid-washed beads, and lyse using bead beater (4x1 minute on, 30 seconds off at 4^{o}C).
6. Add 500uL lysis buffer, mix by pipetting, and remove to new tube.
7. Clear lysate by 4 min centrifugation at 5000g at 4 degrees. Move lysate to new tube and measure protein concentration.
8. Add 200-500ug of protein to each tube.
9. Prepare beads by collecting at 500g for 1 min and washing with 1mL PBS 5x. Incubate with 5uL ascites fluid in 1mL lysis buffer at room temperature for 1-2 hours. Wash with lysis buffer. Resuspend in lysis buffer and add 100uL beads to each sample. Incubate 2 hours at 4^{o}C with gentle agitation.
10. Collect samples with a 2 minute centrifugation at 500g in 4^{o}C. Remove supernatant and wash with lysis buffer x2. Repeat wash and remove samples to new tubes. Work quickly and collect supernatant sample for western blot analysis. Do not allow beads to dry out or remaining proteins may stick to beads, leading to nonspecific interaction detection.
11. Remove all lysis buffer. It is ok for beads to dry out at this point. Resuspend in 1:1 2x SDS sample buffer and lysis buffer with DTT added fresh. Vortex 15 seconds and incubate at 37^{o}C for 30 minutes to elute proteins and reverse crosslink.
12. Resolve samples via 10-12% SDS PAGE. Transfer samples to PVDF membrane at 200mA for 90 minutes. Block membranes overnight in 10% skim milk powder in TBST at 4^{o}C with gentle agitation.

13. Proceed with western blot using the appropriate antibodies conjugated to HRP directly. As the antibody used in the affinity purification is not crosslinked to the beads, it will be detected if a two step western blot procedure is used. Be aware that the conjugated HRP antibody will require a 1:1000 dilution for proper detection.
14. To prevent protein loss by membrane stripping to remove antibody, inactivate HRP with 10% acetic acid in a 37°C water bath for 30 minutes. Flush thoroughly with ddH_2O and block overnight. Probe with the appropriate antibody for a loading control and proceed with western blot as usual.

Lysis buffer

PBS
Leupeptin
Pepstatin
PMSF
0.5% Triton-X 100

Dithiobis(succinimidyl proprionate) (DSP) 100mM

400mg DSP
1mL DMSO

Western blot visualisation by ECL

Solution I

2mL 1M Tris-HCl pH 8.5
200uL 250mM luminol
88uL 90mM p-coumaric acid
water to 20mL

Solution II

2mL 1M Tris-HCl pH 8.5
13uL hydrogen peroxide
water to 20mL